SLMAP3 Governs Embryogenesis Through Mechanisms That Involve Centrosomal Dynamics as Exemplified in Developing Muscle

Ana Dias

Thesis submitted in partial fulfillment of the requirements for the

Doctorate in Philosophy Degree in Cellular and Molecular Medicine

Department of Cellular and Molecular Medicine

Faculty of Medicine

University of Ottawa

Preface

This is a manuscript-based thesis, with the manuscripts entitled "*Tail Anchored Membrane Protein SLMAP3 is essential for the Targeting of Centrosomal Proteins to the Nuclear Envelope for Skeletal Myogenesis*" (published)[1]; "*SLMAP3 is crucial for organogenesis through mechanisms involving primary cilia formation*" (in press - Open Biology)[2]; "*Deletion of Sarcolemmal Membrane-Associated Protein Isoform 3 (SLMAP3) in Cardiac Progenitors Delays Embryonic Growth of Myocardium without Affecting Hippo Pathway*" (published)[3]; and "*SLMAP, Paralogs and Adaptors: Roles in Homeostasis, Physiology and Diseases*" (review being submitted)[4].

In the manuscripts where I am 1st author, I performed most of the experiments, analysis and wrote the initial draft. In the manuscript as 2nd author, my contributions involved the cell biology of H9C2 cardiomyoblasts cells and I engineered shRNAs to target all SLMAP isoforms in a lentivirus system to study cell cycle dynamics, and contributed to writing the initial draft. The fourth manuscript is a comprehensive review article on SLMAP and its paralogs TRAF3IP3/T3JAM and CCDC136/NAG6 and the adaptors SIKE1 and FGFR1OP2/Wit3.0. I wrote the initial draft, which is now being edited by Dr. Balwant Tuana.

Abstract

SLMAP3 is a tail-anchored membrane protein that targets the microtubule-organizing center (MTOC), subcellular membranes, and is a component of the evolutionary conserved Striatin-Interacting Phosphatase and Kinase (STRIPAK) Complex. In this complex, SLMAP3 was demonstrated to inhibit Hippo signaling, leading to the expression of genes for cell proliferation in *Drosophila* and human cells. Here I investigated the *in vivo* roles of SLMAP by employing a mouse model that we generated with global ablation of the SLMAP3. These mice presented major deficits in organ development, leading to embryonic/perinatal lethality consistent with those reported for aberrant Planar Cell Polarity (PCP). These mice also exhibited polycystic kidneys, which is a common manifestation of ciliopathies, and abnormal embryonic muscle fibers with perturbation in distribution of their nuclei. RNA-seq indicated a repression of the myogenic program in SLMAP3 null embryos, and CRISPR/Cas9 mediated knockout of SLMAP3 in myoblasts resulted in defective differentiation and a clearly impaired recruitment of centrosomal proteins to the nuclear envelope, a process crucial for myogenesis. The loss of SLMAP3 affected the cell cycle dynamics including senescence in myoblasts. Cellular senescence was also observed in heart cardiomyoblasts with depletion of all SLMAP isoforms. Further, mouse embryonic fibroblasts (MEFs) isolated from SLMAP3$^{-/-}$ embryos had reduced primary cilia formation, which was accompanied by decreased protein levels of DVL3, a PCP member. SLMAP3 loss had no impact on Hippo pathway, and my data here reveals an entirely new mode for SLMAP action in development involving the MTOC, Cilia, PCP components and cell cycle dynamics.

Keywords: SLMAP3, Primary Cilium, MTOC, STRIPAK, PCP, Embryonic Development.

Table of Contents

List of Figures

Chapter One

Chapter Two

Chapter Three

Chapter Four

Chapter Five

Chapter Six

List of Tables

Chapter 2

Chapter 3

Chapter 5

List of Abbreviations

ACVS	Animal Care and Veterinary Service
ALMS	Alström syndrome
ATCC	American Type Culture Collection
BBS	Bardet–Biedl syndrome
CC	Coiled-Coil
CE	Convergent Extension
cGAS	Cyclic GMP-AMP synthase
CIHR	Canadian Institute of Health Research
CNM	Centronuclear Myopathy
CRISPR	Clustered Regularly Interspaced Short Palindromic Repeats
Cyto	Cytoplasm
DCM	Dilated Cardiomyopathy
DKO	Double Knockout
DMEM	Dulbecco's Modified Eagle Medium
DON	Deoxynivalenol
DSS	Disease-Specific Survival
E-C	Excitation-Contraction
EDMD	Emery Dreifuss Muscular Dystrophy
ER	Endoplasmic Reticulum
ERES	Endoplasmic Reticulum Exit Sites
ERM	Ezrin, Radixin and Moesin
EV71	Enterovirus 71
FA	Focal Adhesion
F-actin	Filament of Actin
FBS	Fetal Bovine Serum
FHA	Forkhead Associated Domain
FHF	First Heart Field
FPKM	Fragments Per Kilobase Per Million Mapped Fragments
Ft-Ds-Fj	Fat-Dachsous-Four-jointed
GCK	Germinal Center Kinases
GEO	Gene Expression Omnibus
GLP-1RA	Glucagon-Like Peptide-1 Receptor Agonist
H&E	Hematoxylin and eosin
HCD	Higher Energy Collision Dissociation
HCM	Hypertrophic Cardiomyopathy
HPLC	High Performance Liquid Chromatography
ICC	Intrahepatic Cholangiocarcinoma
IP-MS	Immunoprecipitation Followed by Mass Spectrometry
IVS	Intraventricular Septum
JBTS	Joubert syndrome
KASH	Klarsicht, ANC-1, Syne Homology
KD	Knockdown
KO	Knockout
KXA	Ketamine–Xylazine–Acepromazine
LC-MS/MS	Liquid Chromatography with Tandem Mass Spectrometry

LINC	Linker of Nucleoskeleton and Cytoskeleton
LMS	Leiomyosarcomas
LV	Left Ventricle
LVPW	Left Ventricle Posterior Wall
MAVS	Mitochondrial Antiviral-Signalling Protein
MEF	Mouse Embryonic Fibroblasts
MHC	Myosin Heavy Chain
MKS	Meckel syndrome
MOI	Multiplicity of Infection
MS/MS	Tandem Mass Spectrometry
MTOC	Microtubule Organizing Center
NCBI	National Center for Biotechnology Information
NE	Nuclear Envelope
NKT	Natural Killer T Cell
NTC	Non-Targeting Control
PBS	Phosphate Buffered Saline
PCP	Planar Cell Polarity
PCR	Polymerase Chain Reaction
PE	Peripodial Epithelium
pen-strep	Penicillin-Streptomycin
Peri	Perinuclear
PI	Propidium Iodide
PVDF	Polyvinylidene Fluoride
QA/QC	Quality Assurance/Quality Control
RLR	RIG-I-Like Receptor
RPPA	Reverse Phase Protein Array
RRID	Research Resource Identifiers
RRR	Residual Ridge Resorption
RTK	Receptor Tyrosine Kinase
RT-qPCR	Real Time-Quantitative PCR
SA-β-Gal	Senescence-Associated-β-Galactosidase
SDS-PAGE	Sodium Dodecyl-Sulfate Polyacrylamide Gel Electrophoresis
SEM	Standard Error of Mean
sgRNA	Single Guide RNA
SHF	Secondary Heart Field
shRNA	short hairpin RNA
SIN	Septation Initiation Network
SIP	SIN Inhibitory Phosphatase
SLMAP	Sarcolemmal Membrane-Associated Protein 3
SNP	Single Nucleotide Polymorphism
STING	Stimulator of Interferon Genes
STRIPAK	Striatin-Interacting Phosphatase and Kinase
TBST	Tris-Buffered Saline
TLR4	Toll-Like Receptor 4
TM	Transmembrane Domain
TnC	Troponin C

TSEA	Tissue Specific Expression Analysis
WT	Wild Type
WTS	warts
Yki	yorkie

Acknowledgements

Firstly, I would like to express my deepest gratitude to my supervisor Dr. Balwant Tuana, who recruited me while I was still in Brazil. His constant support for my success and understanding of the difficulties faced by international students in pursuing a doctorate abroad and in a second language were vital for me to conduct this project. I am also thankful for his mentoring and guidance during all these years to help me to become a better researcher.

I would like to thank the members of my thesis advisory committee: Dr. Douglas Gray, Dr. Antonio Colavita and Dr. Michael Downey. They patiently followed my progress during these years and all the feedback received helped me to guide this project. I am grateful for the amazing lab colleagues that I had. Maysoon Salih was always ready to teach me new techniques, and the discussions I had with Taha Rehmani about SLMAP and STRIPAK functions were important to conduct this study. I am grateful to all facilities involved in this project, including, but not limited to, the Cell Biology and Image Acquisition, Louise Pelletier Histology, Flow Cytometry and Virometry, Genome Editing and Molecular Biology core facilities at University of Ottawa, the StemCore and Bioinformatics facilities at the Ottawa Hospital Research Institute, and the Animal Care and Animal Service facility. Every training, suggestions and discussions contributed to my growth as a researcher.

My boyfriend Christoph Klein, who has already passed through the bumps of the PhD journey, was also very important during these years, being my family in Canada. Finally, I would like to express my profound appreciation to my family, especially my parents Sonia Gonçalves Dias and Edilson da Silva Dias. They have always encouraged me to pursue education, despite all the difficulties we faced in the past living in Brazil. Because of that, I dedicate this thesis to them.

Chapter One - Introduction

1. Introduction

Our laboratory was the first to identify, isolate and investigate the potential roles of SLMAP, and the studies here are an extension of that quest. In the following sections I provide a brief description of SLMAP3 structure and functions in the context of the STRIPAK complex and Hippo signaling. The section also includes a summary of the functions of SIKE1 and FGFR1OP2, which I have proposed to be SLMAP3 adaptors. I then provide an overview of the MTOC formation in the nuclear envelope (NE) during the differentiation of myoblasts. This is followed by an overview of PCP and primary cilium and how they are connected.

This thesis is presented in the form of manuscripts, which have been organized into four chapters. The first one (Chapter Two) is the investigation of the impact of cell specific knockout of SLMAP3 in cardiac progenitors. The second (Chapter Three) is about the role of SLMAP3 in the MTOC formation in the NE during the skeletal myogenesis, which is a follow up from our initial proposal of SLMAP3 being a centrosomal protein[5]. The third (Chapter Four) is the study of the phenotypes discovered with the global knockout of SLMAP3, which my data indicated to stem from a ciliopathy with a link to PCP. Finally, the fourth (Chapter Five) is a literature review of the roles of SLMAP, its paralogs TRAF3IP3/T3JAM and CCDC136/NAG6 and the SLMAP adaptors SIKE1 and FGFR1OP2/Wit3.0 in homeostasis and diseases. The four manuscripts together advance our understanding of SLMAP3 functions, demonstrating its importance for not only muscle development but also mouse embryogenesis through novel mechanisms independent from any Hippo involvement.

1.1. Structure of SLMAP Proteins

The *slmap* gene was first cloned and characterized by our lab[6]. It encodes multiple protein isoforms with molecular weights of approximately 37 kDa, 45 kDa and 80-95 kDa designated SLMAP1, SLMAP2 and SLMAP3, respectively[5–8]. In humans, *slmap* gene is spread over 25 exons (reference transcript Ensembl ENST00000671191.1), with exons 2 to 11 always present in the largest isoforms (SLMAP3), whereas exons 12 to 15 and 18 to 24 are alternatively spliced, generating a great variety of SLMAP isoforms. Exon 2 contains the start codon for SLMAP3 isoforms, whereas exon 17 has the start codon for SLMAP1 and SLMAP2.

While SLMAP3 is ubiquitously expressed, SLMAP1 and SLMAP2 display tissue and developmental stage specific expression[5,7]. All these isoforms have leucine enriched coiled-coil domains, which are involved with protein-protein interaction and homodimerization[9,10], and one of two possible C-terminal transmembrane domain that are alternatively spliced and target SLMAP to subcellular organelles, including endoplasmic reticulum (ER), mitochondria and perinuclear membranes[5,7,11]. The N-terminus of SLMAP3 contains the forkhead associated domain (FHA) that was shown to target the protein to the centrosomal microtubule organizing center (MTOC)[5], and the FHA domain of its homolog Csc1p in *Schizosaccharomyces pombe* also targets the protein to the spindle pole body[12], suggesting an evolutionary conserved function. Further, the FHA domain present in SLMAP is known to bind to phosphothreonine residues[13,14]. SLMAP3 structure is depicted in **Figure 1**.

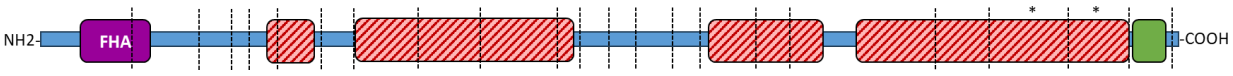

Figure 1. **SLMAP3 (Uniprot Q14BN4-1) domains based on the structure obtained from SMART[15,16]**. The FHA domain is in purple, the coiled-coil domains are represented in red diagonal stripes, and the transmembrane domain in the C-terminus, which can be alternatively spliced, is in green. Each section delimited by lines represents a coding exon. Exons containing leucine zippers that we previously predicted[5] are shown with *.

1.2. SLMAP3, STRIPAK Complex and Hippo Signaling

The STRIPAK complex (depicted in Figure 4, Chapter Five) was identified in mammals fifteen year ago by affinity purification coupled to mass spectrometry studies aiming to identify the interactors of the phosphatase PP2A[17,18], although it was first observed in *Saccharomyces cerevisiae* over two decades ago as the Far complex[19]. Indeed, STRIPAK is evolutionary conserved[20], although a functional repurposing of the complex during evolution has been suggested[21]. In mammals, the complex consists of phosphatase subunits PP2A-C and PP2A-A, the kinases from the germinal center kinase families II, III and IV, and adaptors proteins including SLMAP, and its paralog TRAF3IP3/T3JAM, and the paralogs SIKE1 and FGFR1OP2[17,18,22–26]. An initial role for STRIPAK was the negative regulation of the Hippo signaling axis[24,25,27–29], although other functions have been proposed, such as polarization of the Golgi apparatus[30] and regulation of cortical actomyosin[31].

The Hippo pathway, originally described in *Drosophila*, controls a series of processes, including cell fate, survival, proliferation and organ growth. The signaling cascade consists of the germinal center kinase II family members MST1/2 and their adaptor protein SAV1 that induce the phosphorylation and activation of the NDR kinases members LATS1/2 and their adaptor protein Mob1. LATS1/2 then phosphorylate the transcriptional coactivators YAP and TAZ, which causes their cytoplasmic sequestration and degradation[32] (signaling axis depicted in Figure 8a, Chapter Three). The functions of Hippo pathway can be observed with the overexpression of Yki (YAP homolog) or mutation of Wts (LATS homolog) in the *Drosophila* wing disc, which results in pronounced growth of this structure[33,34]. This overgrowth effect is also observable in mouse, where the knockout of MST1/2 leads to liver hypertrophy and hepatocellular carcinoma[35,36].

The negative regulation of the Hippo pathway by the STRIPAK depends on SLMAP3, which binds to phosphothreonine residues in the linker region of MST1/2 by its FHA domain, recruiting the kinases to the complex to be dephosphorylated by PP2A[28,29]. The impact of SLMAP3 depletion in *Drosophila* has been demonstrated in the eye imaginal disc, a tissue that generates retinal progenitor cells or peripodial epithelium (PE)[37]. SLMAP3 was shown to be required for the PE fate by suppressing Hippo pathway and consequently keeping YAP active[37]. The repression of Hippo pathway by SLMAP3 was also demonstrated to be important for the *Drosophila* flight muscle morphogenesis[38].

1.3. SLMAP Adaptors: SIKE and FGFR1OP2/Wit3.0

SIKE1 is a coiled-coil protein member of STRIPAK that bridges SLMAP3 to the complex[10]. It was first described as an inhibitor of the IKKε and TBK1, being able to block IRF3 response upon TRL3 or virus stimulation[39,40]. In hearts, the inhibition of TBK1 by SIKE1 has a cardioprotective effect because it reduces AKT-mTOR signaling, a driver of pathological cardiac hypertrophy[41]. Despite these described roles, in mice the global knockout of SIKE1, which has ubiquitous expression[42], results in viable and fertile animals[43]. It is possible that SIKE1 has overlapping functions with its paralog FGFR1OP2.

FGFR1OP2 is also a coiled-coil protein with ubiquitous expression[44], but differently from SIKE1, the knockout of FGFR1OP2 in mice results in lethality[45]. Still, how FGFR1OP2 functions during embryonic development is unknown. Previous reports demonstrated that it is upregulated in edentulous mucosa after tooth extraction to enhance wound closure[46–48]. FGFR1OP2 has also been linked to cancer. Fused FGFR1OP2-FGFR1 was found in two patients with myeloproliferative syndrome and in KG-1 cell line derived from an acute myeloid leukemia[49–51].

It is believed that that the coiled-coil domains of the FGFR1OP2 contributes to the dimerization of the fused protein, resulting in a constitutive active FGFR1, which induces the uncontrolled proliferation of the cancer cells[49].

1.4. The NE-MTOC in muscles

The formation of MTOC on sites other than the centrosome, the so called non-centrosomal MTOC, is a hallmark of differentiation[52]. This can be seen in epithelial cells, where microtubules nucleate from the apical region of the cells[52] while in neurons the MTOC seems to localize in dendritic branch points with Golgi outposts being a proposed site of microtubule nucleation[52,53], and in striated muscles where MTOC proteins is present in the NE[54–57]. In muscle, the NE-MTOC is linked to nuclear positioning[58]. Nuclear mispositioning in myofibers has been related to Emery Dreifuss Muscular Dystrophy (EDMD) and Centronuclear Myopathy (CNM)[58,59], which are known to cause muscular weakness and atrophy[60,61]. Genes linked to EDMD include emerin, SUN1, SUN2, Lamin A/C, and Nesprin-1, Nesprin-2, which are members of the Linker of Nucleoskeleton and Cytoskeleton (LINC) complex[61–63]. CNM is caused by mutations in DNM2, MTM1, RYR1, BIN1 and TTN[64], but how they govern nuclear positioning remains to be elucidated. DNM2 has been associated with vesicle trafficking, microtubule stabilization and centrosome functions, but the precise mechanism controlling the nuclear positioning has yet to be demonstrated[58].

During myogenesis, the LINC complex member Nesprin-1α has been proposed as a key protein that participates in the nuclear positioning and MTOC switch by recruiting to the NE the motor complexes dynein and kinesin-1[65–69], which provide mobility of the nuclei in the myofiber, and AKAP6, which complexes with pericentrin and AKAP9[70–72], these that can anchor γ-TurC

complex[73] to start the microtubule nucleation from the NE. The formed microtubules then can function as rails for the motor proteins to allow the nuclear trafficking[58].

In addition to the MTOC proteins, PCM1 is also recruited to the NE[74,75], suggesting that centriolar satellites follow the changes in localization of the MTOC proteins. Further, the endoplasmic reticulum exit sites (ERES) and the Golgi apparatus are also reorganized to perinuclear regions[76–78], and the latter forms the structure known as Golgi-belt like ring structure, which is mediated by interaction with AKAP9[70]. The Golgi itself also gains microtubule nucleation activity[70,79,80]. The changes of both ERES and Golgi suggests that the reorganization of the secretory pathways is also important during myogenesis, exemplified by the trafficking of M-cadherin to the plasma membrane to allow cell fusion[78].

1.5. The Wnt non-canonical Planar Cell Polarity Pathway

The Wnt non-canonical pathway Planar Cell Polarity (PCP) was first described in *Drosophila melanogaster* to explain the polarized organization of bristles and hairs[81,82]. Considering the findings in *Drosophila*, the generation of planar cell polarity is based on two different modules, the "core" PCP and the Fat-Dachsous-Four-jointed (Ft-Ds-Fj) system, both that have asymmetric distribution of their components in the cells, which allows the formation of a polarized pattern that propagates in the tissue[81,82]. The "core" PCP consists of Frizzled receptors and their cytosolic interactors Dishevelled and Diversin in one side of the cell, whereas on the opposite side resides Vangl and its cytosolic interactor Prickle. The membrane protein Celsr localizes at both sides[81,82]. The second system consists in the asymmetrical localization of the cadherins Ft and Ds in the cell edges, which are regulated by the Golgi kinase Fj[81]. Although these

are the main components of PCP, many others including Ptk7[83], ROR1/2[84] and Scrib[85] are closely associated with this pathway.

PCP regulates the morphogenic process known as convergent extension (CE), which takes places in tissues of both mesenchymal and epithelial nature[86]. CE consists of narrowing of the tissue in one axis by cell intercalation and elongation in another. This process occurs during embryonic development, being important for processes such as gastrulation, body axis elongation[86], neural tube closure, extension of kidney tubules[82], skeletal growth[87] and gut elongation[88]. PCP controls CE by F-actin cytoskeleton remodelling[86]. The proposed signaling for this process involves the binding of Wnt ligands, such as Wnt5a or Wnt11, to Frizzled receptors, which leads to the intracellular recruitment of DVL proteins to these receptors[89,90]. DVL proteins with the adaptor Daam1 then induces the activation of small GTPases, RhoA and Rac1, ultimately resulting in the activation the kinases ROCK and JNK, respectively to remodel the actin cytoskeleton[89,90] (pathway in Figure 2b, Chapter Six). Further, DVL can also lead to Vangl/Prickle inhibition, promoting the asymmetric PCP signaling[90].

In humans, mutations in the PCP components Scrib and Celsr1 have been linked to craniorachischisis, the most severe case of completely open neural tube[91]. In mouse, mutations in Dvl1, Dvl2, Fzd3, Fzd6, Ptk7 and Vangl2 also causes craniorachischisis[92]. Mutations in Vangl2 and Celsr1 in mice leads to underdeveloped lungs and abnormal kidneys[93–95], while suppression of Wnt5a causes skeletal defects[96], underdeveloped lungs[97] and short intestines[98]; and the knockout of ROR1/2 results in lung and skeleton defects[99,100]. These reports exemplify the importance of the PCP axis for proper embryonic development. It is notable that we found SLMAP to localize and specifically concentrate at adjacent membrane regions in pluripotential P19 cells in culture

and it was absent from cell membrane that were not in contact with other cells[6]. Whether SLMAP can interact with and participate in distribution of PCP components remains to be explored.

1.6. Primary Cilium, Ciliopathies and the link with PCP

Cilium is a cellular protrusion surrounded by plasma membrane that emanates from the basal body, a structure that is derived from the mother centriole (example shown in Figure 2b, Chapter Six). It is divided into motile and non-motile, the latter also known as primary cilium. Examples of motile cilium include that present in cells from the embryonic node, where it controls the left-right axis patterning, and the flagellum required for sperm motility. Multiciliated cells with motile cilia are present in the fallopian tubes, respiratory track and brain ventricles, where they are responsible for fluid propulsion[101–103].

The primary cilium is present in almost all vertebrate cells and functions as an antenna, being a hub of cellular signaling such as Hedgehog, Wnt, Receptor Tyrosine Kinase, G protein-coupled receptors and TGF-β/BMP, which are important for embryonic development[104]. Some specialized cells have modified primary cilium, as is the case of olfactory receptor neurons that have multiple non-motile cilia, and retinal photoreceptor cells that have one non-motile cilia that is a component of the outer segment[102].

The cilium formation is dependent on cell cycle, as its base, the basal body, is formed by the mother centriole, which is in the spindle pole during cell division[101–103]. During interphase, ciliogenesis can take place by two mechanisms. One is the intracellular pathway, where vesicles derived from the Golgi attaches to the distal end of the mother centriole, where they fuse, followed by the docking of this assembly in the cell surface. This pathway is observed in mesenchymal cells such as fibroblasts. The second mode of cilium biogenesis is the extracellular pathway, where the

mother centriole first docks in the cell surface, followed by the extension of the ciliary membrane and axoneme. This pathway is found in kidney epithelial cells[105].

Another organizational tier of cilium is the centriolar satellites, which are granular protein complexes present around the centrosomal and basal body, but also found in the cytoplasm[75]. The base of centriolar satellite is composed by PCM1, but other proteins such as HOOK3, BBS4, OFD1, CEP170, CEP290 and PCNT are also present in these structures[75,106,107]. Centriolar satellites control the composition of centrosome and cilia by recruiting and sequestering proteins from these organelles[106]. Vesicles from the ER-Golgi and the BBSome/IFT system also contribute to the cilium formation and composition[105,108].

It is estimated that mutations in 247 genes are linked to ciliopathies[105]. Ciliopathies can be classified as first-order, when the mutation is present in genes that encode proteins that are part of the cilium/basal body, whereas second-order is when the genes encode proteins that localizes elsewhere in the cell and affect the functioning of the cilia, as for example proteins involved with vesicular trafficking or transcription factors required for expression of ciliary proteins[105]. Ciliopathies have a large variety of clinical manifestations, ranging from a single organ being affected to a syndromic disorder, and these differences are attributed to the heterogenous composition of the primary cilium across different cells and during different developmental stages[105]. Examples of ciliopathies include Alström syndrome (ALMS), Bardet–Biedl syndrome (BBS), Meckel syndrome (MKS) and Joubert syndrome (JBTS), which affect the brain, kidney, skeleton and eyes[108].

Some studies have investigated the link between primary cilium and Wnt signaling, particularly how ciliary proteins affect DVLs. In HEK-293T cells, the overexpression of the ciliary proteins NPHP2 and NHPH4 increased the degradation of DVL1, DVL2 and DVL3[109,110], and

depletion of BBS4 resulted in increase in DVL1 protein levels[111]. In contrast, NPHP8 (Rpgrip1l), which is required for defining the number of ciliated cells and cilia length, is necessary for the stability of DVL2 and DVL3 in MDCK cells and for their localization in the base of the primary cilium[112]. These studies show that ciliary proteins can have both negative and positive impact on DVL proteins, and consequently on Wnt signaling. In fact, additional studies have suggested an antagonistic role of the cilium on Wnt canonical pathway[113]. Suppression of the ciliary proteins as NPHP4, BBS4, BBS6, KIF3A, IFT88 and OFD1 positively impacted the Wnt canonical axis[110,111,114], while the overexpression of NHPH2 (inversin) antagonized this signaling[109].

Cilia were also found important for the planar polarity of cells[113]. It was demonstrated that RPGRIP1L (NPHP8), BBS4, BBS6 and IFT88 are required for the correct orientation and organization of stereociliary bundle of the cells from the organ of Corti[112,115,116]. Further, the PCP member Vangl2 was also shown to genetically interact with BBS1 and BBS6 in mice and to localize in the cilium base of IMCD3 kidney cells[116]. Likewise, PCP proteins were found to be important for ciliary patch orientation in ependymal cells and the positioning of primary cilium in radial glial progenitor cells, and for cell-cell polarity organization in both cell types[117]. In addition, in the mucociliary epithelium from *Xenopus laevis* DVL proteins were shown to regulate the docking of the basal body to the cell cortex, in a mechanism dependent on RhoA GTPase, and in this way contributing to the planar polarization of basal body in the epithelial cells and directional cilia beating[118]. These studies suggest that primary cilium and PCP are closely connected, with one affecting the other.

1.7. Hypothesis and Objectives

Given that SLMAP3 is a component of the MTOC and a STRIPAK member, I hypothesized that "*SLMAP3 regulates organogenesis through mechanisms that influence Hippo axis, MTOC, Cilia and PCP signaling*". The objectives were:

1. Examination of the *in vivo* role for SLMAP3 in mouse development;
2. Investigation of SLMAP3 function in MTOC, cell cycle dynamics and Hippo signaling;
3. Study of SLMAP3 in primary cilia biology and PCP signaling.

These objectives have been completed and the results are reported in a series of manuscripts that define SLMAP3 as a critical player with a new mode of action in development and organogenesis.

Chapter Two - Deletion of Sarcolemmal Membrane-Associated Protein Isoform 3 (SLMAP3) in Cardiac Progenitors Delays Embryonic Growth of Myocardium without Affecting Hippo Pathway

Manuscript Publication and Copyright

Dear Authors,

We are pleased to inform you that your article "Deletion of Sarcolemmal Membrane-Associated Protein Isoform 3 (SLMAP3) in Cardiac Progenitors Delays Embryonic Growth of Myocardium without Affecting Hippo Pathway" has been published in IJMS as part of the Special Issue Ion Movements and Membrane Proteins and is available online:

Website: https://www.mdpi.com/1422-0067/25/5/2888
PDF Version: https://www.mdpi.com/1422-0067/25/5/2888/pdf
The meta data of your article, the manuscript files and a publication certificate are available here (only available to corresponding authors after login):
https://susy.mdpi.com/user/manuscripts/review_info/b14b1df041109ae60599c6fb9daaad45
Special Issue: https://www.mdpi.com/journal/ijms/special_issues/4035DLUPX3

International Journal of
Molecular Sciences

MDPI

Article

Deletion of Sarcolemmal Membrane-Associated Protein Isoform 3 (SLMAP3) in Cardiac Progenitors Delays Embryonic Growth of Myocardium without Affecting Hippo Pathway

Taha Rehmani, Ana Paula Dias, Marsel Kamal, Maysoon Salih and Balwant S. Tuana *

Deletion of Sarcolemmal Membrane-Associated Protein Isoform 3 (SLMAP3) in Cardiac Progenitors Delays Embryonic Growth of Myocardium without Affecting Hippo Pathway

Taha Rehmani, Ana Paula Dias, Marsel Kamal, Maysoon Salih and Balwant S. Tuana*
Department of Cellular and Molecular Medicine, Faculty of Medicine, University of Ottawa

*Correspondence: btuana@uottawa.ca

Abstract

The slmap gene is alternatively spliced to generate many isoforms that are abundant in developing myocardium. The largest protein isoform SLMAP3 is ubiquitously expressed and has been linked to cardiomyopathy, Brugada syndrome and Hippo signaling. To examine any role in cardiogenesis, mice homozygous for floxed slmap allele were crossed with Nkx2.5-cre mice to nullify its expression in cardiac progenitors. Targeted deletion of the slmap gene resulted in the specific knockout (KO) of the SLMAP3 (~91 KDa) isoform without any changes in the expression of the SLMAP2 (~43 kDa) or the SLMAP1 (~35 kDa) isoforms which continued to accumulate to similar levels as seen in Wt embryonic hearts. The loss of SLMAP3 from cardiac progenitors resulted in decreased size of the developing embryonic hearts evident at E9.5 to E16.5 with four small chambers and significantly thinner left ventricles. The proliferative capacity assessed with the phosphorylation of histone 3 or with Ki67 in E12.5 hearts was not significantly altered due to SLMAP3 deficiency. The size of embryonic cardiomyocytes, marked with anti-Troponin C, revealed significantly smaller cells, but their hypertrophic response (AKT1 and MTOR1) was not significantly affected by the specific loss of SLMAP3 protein. Further, no changes in phosphorylation of MST1/2 or YAP were detected in SLMAP3-KO embryonic myocardium, ruling out any impact on Hippo signaling. Rat embryonic cardiomyocytes express the three SLMAP isoforms and their knockdown (KD) with sh-RNA, resulted in decreased proliferation and enhanced senescence but without any impact on Hippo signaling. Collectively, these data show that SLMAP is critical for normal cardiac development with potential for the various isoforms to serve compensatory roles. Our data imply novel mechanisms for SLMAP action in cardiac growth independent of Hippo signaling.

Keywords: SLMAP3; STRIPAK complex; Hippo signaling; cardiac morphogenesis

1. Introduction

During embryogenesis, the first functional organ is the heart, derived from mesoderm and endoderm due to the expression of cardiogenic transcription factors Nkx2.5, Mef2, GATA, Tbx and Hand that work in tandem to differentiate precardiac cells and to control the expression of cardiac genes to mediate cardiac morphogenesis [1]. Cardiac morphogenesis or cardiogenesis is the stage-by-stage development of the heart during embryogenesis beginning at embryonic day 7.5 (E7.5) in mice, where cardiogenic mesoderm cells coalesce at splanchnic mesoderm to form the cardiac crescent. Cells within the cardiac crescent are divided into a collection of cells known as the first heart field (FHF), which migrate to venous poles to form the linear heart tube (E8.5) [2,3]. A subgroup of cells derived from FHF known as secondary heart field (SHF) migrate caudally to further develop the linear heart tube into the looping heart (E9.5). The FHF cells differentiate and proliferate to form the left atria and ventricle, and the SHF cells migrate anteriorly and posteriorly; the anterior SHF cells give rise to the right ventricle and aorta, while the posterior SHF cells generate the atria and the pulmonary artery in maturing embryos, thus generating the immature

four-chambered heart (E10.5), which septate to form mature four-chamber heart by E14.5 [4,5]. During the late stages of cardiac development, immature cardiomyocytes grow and increase cardiac function due to a series of structural, metabolic, and transcriptional modifications in a process referred to as cardiomyocyte maturation [6]. Cardiomyocytes will exit the cell cycle shortly after birth; therefore, cardiac growth is sustained through cardiomyocyte maturation to maintain the growing supply of nutrients and oxygen demands of the growing body [7]. Impacting cardiac development at the morphogenesis or maturation stage can increase the risk of developing congenital heart disease and predisposing individuals to later-stage cardiomyopathies. Therefore, understanding the mechanisms that govern cardiac maturation and/or morphogenesis is of much interest.

We have defined the sarcolemmal membrane-associated proteins SLMAP1 (~35 kDa), SLMAP2 (~45 kDa), and SLMAP3 (~80–95 kDa) (Figure 1) that are expressed in myocardium as early as E9 and continue to be accumulated in cardiomyocytes during their maturation and postnatal development [8,9]. The SLMAPs target subcellular organelles including nuclear envelope, endoplasmic/sarcoplasmic reticulum, mitochondria, and the microtubule organizing center (MTOC) [10,11]. The SLMAPs have been shown to associate with cardiac myosin, colocalize with α-actinin and calcium release channels, as well as being found in close apposition to the sarcolemma [9]. Aberrant SLMAP expression has been shown to cause heart failure due to gene mutations present in Brugada patients [12]. Studies indicate that SLMAPs may play roles in regulating the diverse organelles, influence electrophysiology, metabolism, and cardiac function [13–15]. However, the role of SLMAPs in the growth and maturation of myocardium remains unknown. The slmap gene is alternatively spliced to generate numerous isoforms that are expressed in a tissue-specific manner, with SLMAP1 and SLMAP2 being abundant in cardiomyocytes [16]. The C-terminus of all SLMAP isoforms comprises an alternatively spliced transmembrane domain, TM1 or TM2, which can target different subcellular membranes, while the extended coiled coil leucine zipper domain and the n-terminal sequences diversify the polypeptide structure for cytoplasmic interactions [10,17]. For example, the SLMAP3 isoform which is ubiquitously expressed carries an n-terminal forkhead-associated (FHA) domain (Figure 1) that can mediate phosphoprotein–protein interactions [11,18] and has been shown to negatively regulate Hippo signaling via the STRIPAK (Striatin-interacting phosphatases and kinases) complex. The Hippo pathway is important for organogenesis through effects on cell proliferation and apoptosis [19]. SLMAP-STRIPAK interactions can inhibit phosphorylation and enhance nuclear translocation of transcriptional co-activators YAP/TAZ and influence TEAD-mediated gene expression [20–22]. Hippo signaling has been linked to cardiac development and maturation and can directly impact the size and function of the myocardium [23–27]. SLMAP3 has been reported to regulate the proliferation of cancer cells through Hippo signaling [28]; whether it can impact this pathway to influence growth and development *in vivo* remains to be examined. Here, we have engineered the specific removal of SLMAP3 from cardiac progenitors to examine its role in cardiogenesis in mice and its impact on the Hippo pathway.

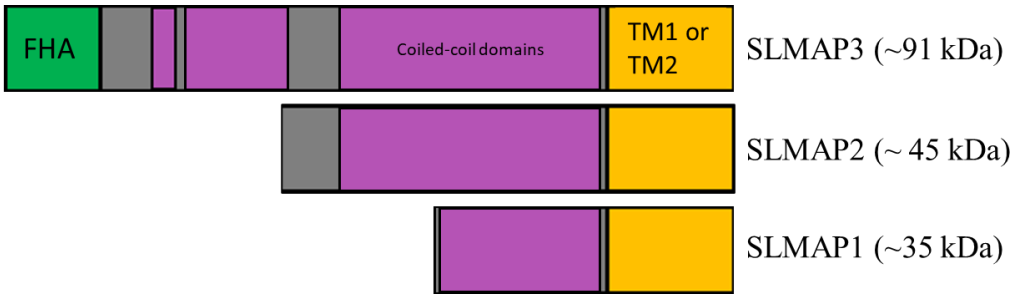

Figure 1. Sarcolemmal membrane-associated protein isoforms and protein domains. SLMAP gene alternatively splices to generate three main protein isoforms, SLMAP1 (~35 kDa), SLMAP2 (~45 kDa), and SLMAP3 (~95 kDa). FHA (green) symbolizes forkhead-associated domain. Coiled-coil domains (purple) identify the coiled-coil leucine zipper domains. TM1 or TM2 (orange) symbolizes the alternatively spliced transmembrane domain 1 or 2.

2. Results

2.1. The Specific Loss of SLMAP3 Isoform in Cardiac Progenitors' Delays Cardiogenesis

We examined the prenatal knockout of the SLMAP gene by crossing floxed SLMAP mice with Nkx2.5-Cre [29] to assess the role of SLMAP during early cardiogenesis. Western blot analysis of E18.5 heart lysates with anti-SLMAP displayed significant loss in SLMAP3 protein levels in (−66.05% ± −15.10%, $\rho < 0.05$, $n = 3$) heterozygous embryonic hearts (KD) and (−97.36% ± −11.39%, $\rho < 0.05$, $n = 3$) homozygous (KO) embryonic hearts. No significant changes were noted in the expression levels of SLMAP1 or SLMAP2, indicating the generation of mice with the specific loss of SLMAP3 in fetal myocardium (Figure 2A). We excised embryos at different developmental stages and examined cardiac development (E9.5, E12.5, and E16.5) by cross-section histology with H&E to visualize Wt and SLMAP3-KO myocardium (Figure 2B). Microscopic analysis indicated that prenatal SLMAP3-KO hearts were significantly smaller at each developmental stage E9.5 (−25.16% ± −11.10%, $\rho < 0.05$, $n = 3$), E12.5 (−29.36% ± −7.86%, $\rho < 0.05$, $n = 3$) and E16.5 (−40.27%, ± −6.51%, $\rho < 0.05$, $n = 3$) compared to Wt littermates (Figure 2C). Further, the atria and ventricles appeared to be thinner in SLMAP3-KO, and measurements of the left ventricular walls indicated they were significantly thinner in E9.5 (−48.65% ± −6.61%, $\rho < 0.05$, $n = 3$), E12.5 (−33.49% ± −5.44 %, $\rho < 0.05$, $n = 3$), and E16.5 (−41.12%, ± −1.39%, $\rho < 0.05$, $n = 3$) vs. Wt embryonic hearts (Figure 2C). There is also a noticeable delay in septation in SLMAP3-KO hearts at E12.5 since the atrioventricular cushions have not fused (Figure 2B; black arrow); however, these differences in cardiac chamber formation or septation appeared to be rectified by E16.5 (Figure 2B). Thus, appropriate expression levels of SLMAP3 protein are important to support normal cardiac growth during early cardiogenesis.

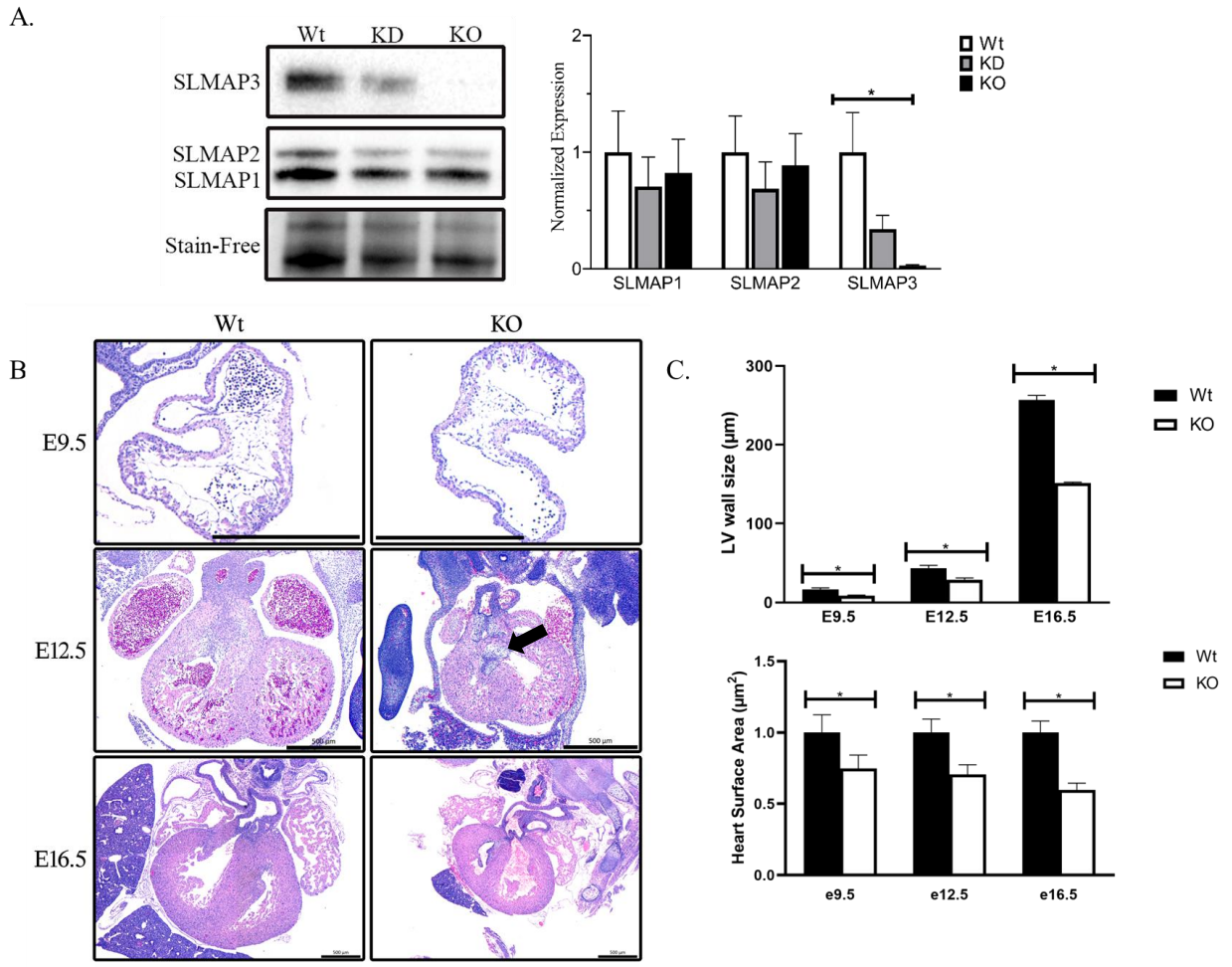

Figure 2. Embryonic heart development in mice with cell-targeted deletion of SLMAP3. (**A**) Western blot displaying SLMAP isoform expression in Wt, KD, and KO in E18.5 mouse heart lysates. Bar graphs represent normalized expression of SLMAP isoforms using Stain-Free™ total protein as a loading control quantified by via densitometry n = 6. * $\rho < 0.05$. (**B**) Representative sections of Wt and KO hearts at E9.5, E12.5, and E16.5 with H&E stain to visualize nucleus (blue) and myocardium (pink) which displayed developing cardiac structures: ventricles, atria, outflow tract, and septa. Black arrow highlights delay during atrioventricular cushion fusion at E12.5 in SLMAP3-KO. Lens magnification = 5×. Scale bar = 0.5 mm. (**C**) Bar graph shows quantification of measurement of left ventricle wall thickness (upper graph) and heart surface area (lower graph) at indicated embryonic ages in Wt and KO hearts. * $\rho < 0.05$.

2.2. STRIPAK and Hippo Signaling Was Unaltered in SLMAP3-Deficient Embryonic Myocardium

Given the dramatic effects of SLMAP3 loss on the growth delay of embryonic heart development and its proposed role as a negative regulator of Hippo signaling via STRIPAK [22,30], we examined any impact on striatin, PP2A-A, PP2A-C, Striatin-3, and the activity of Hippo components in E16.5 Wt and SLMAP3-KO hearts by Western blotting. Striatin (−2.56% ± −22.05%, $\rho = 0.93$, $n = 4$), striatin-3 (−0.21% ± −19.46%, $\rho = 0.89$, $n = 4$), PP2A-A (−16.34% ± −16.23%, $\rho = 0.54$, $n = 4$), and PP2A-C (23.58% ± 11.65%, $\rho = 0.20$, $n = 4$) were not significantly

affected in KO hearts when compared to Wt (Figure 3A). To assess Hippo signaling, we analyzed the phosphorylation of MST1 and YAP; however, the phospho-to-total ratio of MST1 (−6.61% ± −23.56%, ρ = 0.63, *n* = 4) and phospho-to- total ratio of YAP (−8.43% ± −12.25%, ρ = 0.64, *n* = 4) was unaltered in SLMAP3-KO hearts (Figure 3B). Further, qPCR examination for expression of *c-myc* and *CTGF*, which are known downstream gene targets of Wnt and Hippo signaling, showed no significant changes due to SLMAP3 deficiency (ρ = 0.72). Thus, specific deletion of the SLMAP3 isoform in cardiac progenitors delays cardiogenesis but not through any changes in Hippo signaling.

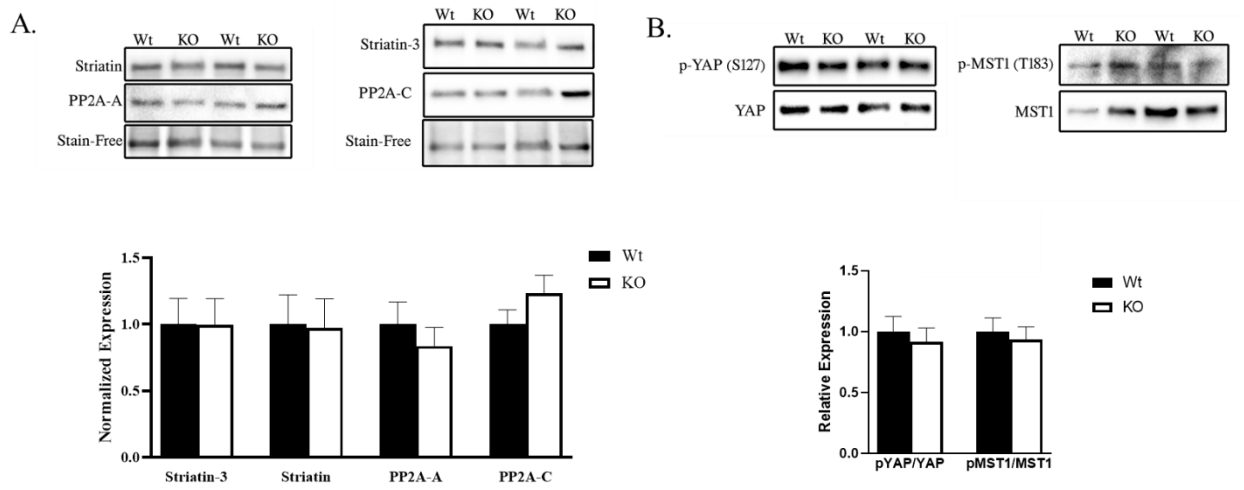

Figure 3. STRIPAK and Hippo signaling in developing myocardium from SLMAP3-depleted cardioprogenitors. (**A**) Western blot showing the expression of STRIPAK components (striatin, striatin-3, PP2A-A, and PP2A-C) in Wt and KO E16.5 hearts. Bar graphs represent normalized expressions of indicated protein to total proteins visualized by Stain-Free™ technology. n = 3. (**B**) Western blot showing phospho to total MST1 and YAP in E16.5 hearts. Bar graphs represent relative expression of phospho-YAP(S127) to total YAP and phospho-MST1 (T183) to total MST1 quantified by densitometry. n = 3.

2.3. Cardiomyocyte Proliferation Is Not Affected by SLMAP3-KO during Cardiogenesis

Cardiac growth is regulated by cardiomyocyte proliferation and hypertrophy through mechanisms involving Hippo and other pathways including FGF, Notch, and Wnt signaling [31]. The evaluation of proliferation with immunofluorescence microscopy for the proliferation markers pH3 and Ki67 in embryos, co-stained with the cardiomyocyte marker Troponin C (TnC) in E12.5 Wt and SLMAP3-KO mouse hearts is shown in Figure 4. The pH3 detects cell division at the G2/M phase (Figure 4A), while Ki67 tags cells at the G1 to G2/M phase of the cell cycle (Figure 4B), providing a cardiomyocyte proliferation index that indicated no significant differences in $pH3^{+}$- or $Ki67^{+}$-positive cardiomyocytes in SLMAP3-KO vs. Wt embryos (Figure 4C). Therefore, the delay in early cardiac development due to the specific loss of SLMAP3 in cardiac progenitors is not due to any changes in their proliferation.

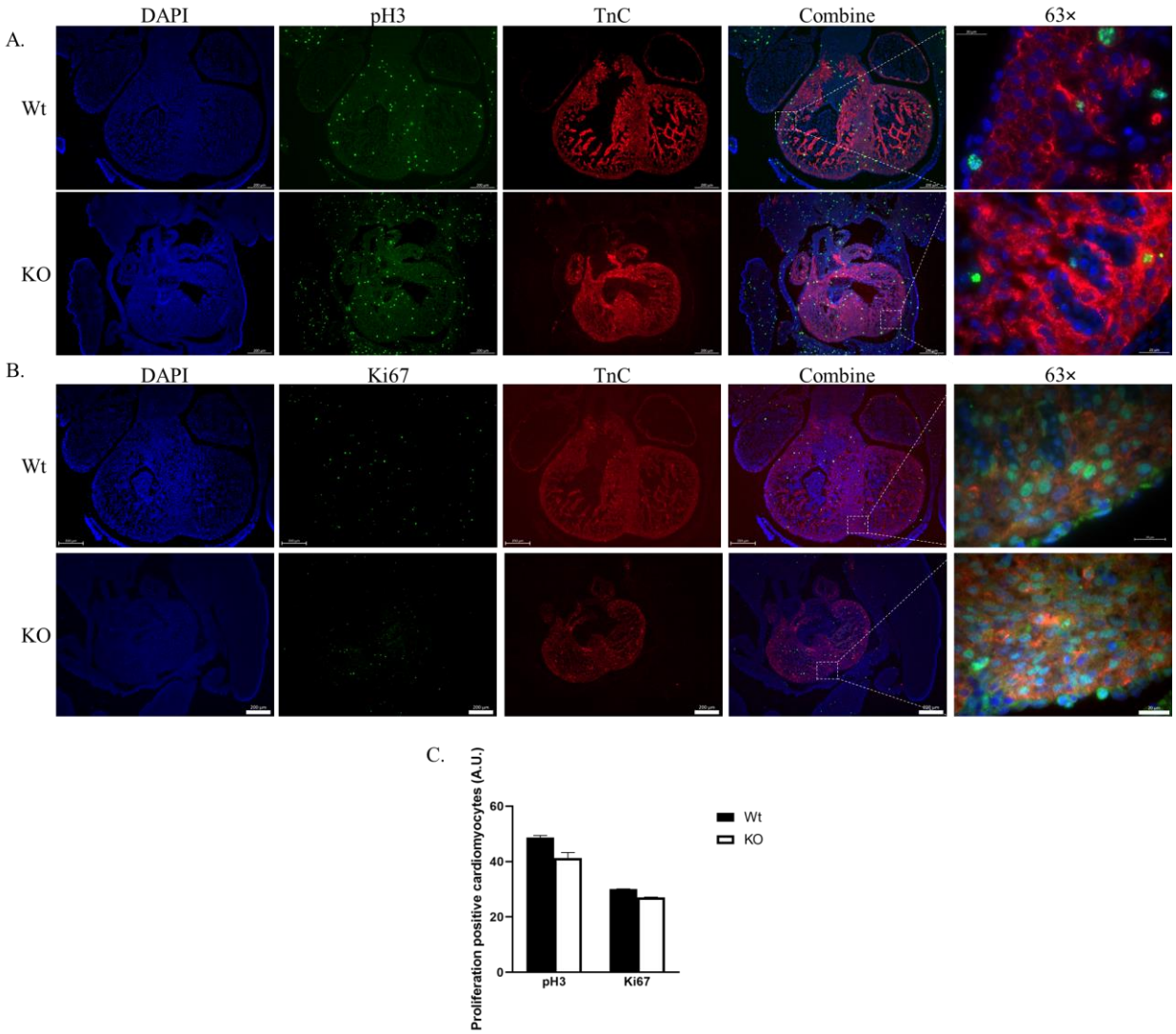

Figure 4. Proliferation of cardiomyocytes in SLMAP3-KO embryonic hearts. Immunofluorescent images of sectioned Wt and KO hearts at E12.5. stained for proliferative marker Histone 3 (**A**) or Antigen Kiel 67 (**B**), nucleus (DAPI; blue), (pH3; green), and anti-troponin C (TnC; red). Lens magnification = 5× or 63×. Representative Scale bar = 0.2 mm at 5× or 0.02 mm at 63×. (**C**) Bar graph representing pH3 or Ki67 proliferation events within TnC^{+}-positive cells. n = 3.

2.4. Cardiomyocyte Size Is Reduced in SLMAP3-KO Embryonic Hearts

Since changes in proliferation could not account for the smaller embryonic hearts, we investigated if the size of cardiomyocytes was affected by the loss of SLMAP3 by assessing right ventricle and left ventricle cardiomyocytes in E12.5 heart sections, and the magnified images obtained with H&E and TnC staining is shown (Figure 5A). We identified the perimeter of cardiomyocytes with H&E (black dashed line, white arrow) and cardiomyocytes with TnC (grey arrow) to calculate the area that represents the cardiomyocyte size. Our analysis on left ventricular cardiomyocytes appeared to be significantly smaller in KO (−19.43% ± −7.55%, $\rho < 0.05$, $n = 3$) when compared to Wt (Figure 5B). The cardiomyocytes also appeared to be disorganized in

SLMAP-KO E12.5 hearts where the nuclei of neighboring cardiomyocytes cluster together with changes in cardiomyocyte shape and orientation (Figure 5A, grey arrows). Cardiomyocyte hypertrophy is linked to the upregulation of AKT1 and MTOR1 [32], which affect cell survival and growth. The activity of AKT1 and MTOR1 assessed in Western blots indicated that the phospho-to-total ratios of AKT1 (1.45% ± 26.50%, ρ = 0.97, n = 3) and mTOR (−12.87% ± −51.12%, ρ = 0.64, n = 3) were not significantly altered in E16.5 SLMAP3-KO hearts compared to Wt (Figure 5C). Thus, the specific loss of SLMAP3 during cardiogenesis leads to significant changes in the size and structure of cardiomyocytes but without any impact on the hypertrophic program.

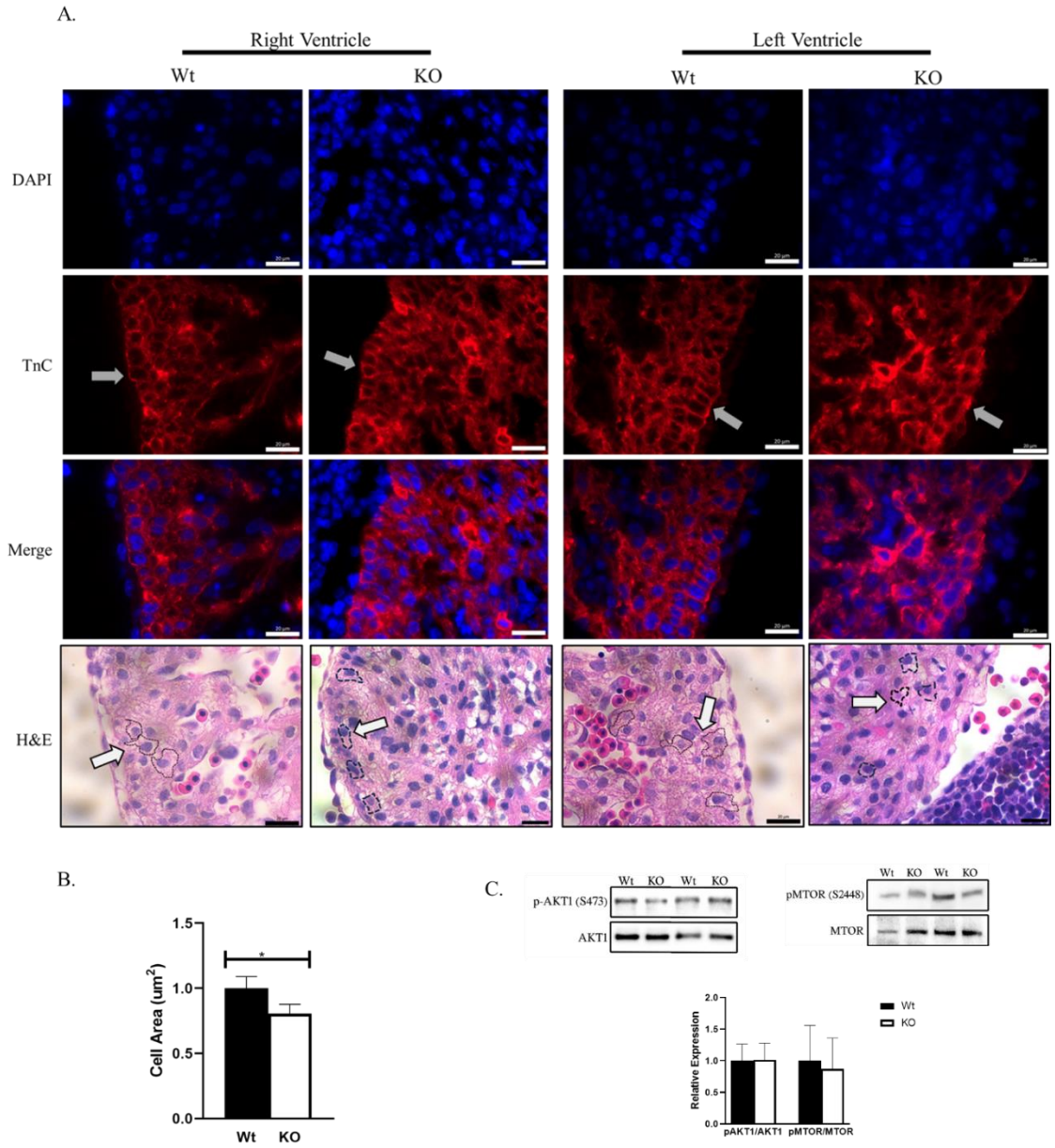

Figure 5. Cell size and hypertrophy in Nkx2.5/SLMAP3-KO mice. (**A**) Images of sectioned Wt and KO hearts at E12.5 showing cradiomyocytes from right and left ventricles stained for the nucleus (DAPI; blue) and cardiac anti-troponin C (TnC; red) or H&E (pink; myocardium). Black

dash lined indicates the perimeter and shape of a cardiomyocyte marked by white arrow. Lens magnification = 63×. Scale bar = 0.02 mm. (**B**) Bar graph shows quantification of left ventricular cardiomyocyte area in Wt and KO E12.5 embryonic hearts. *; $\rho < 0.05$, n = 3. (**C**) Western blot showing expression of phospho-to-total ratios of AKT1 and mTOR in E16.5 Wt and KO hearts. Bar graphs represent quantification of relative expression of phospho-mTOR (S2448) to total mTOR and phospho-AKT1 (S473) to total AKT1 with densitometry of the Western blots. n = 3.

2.5. SLMAP3-KO Hearts Grow to Normal Size and Function in Postnatal Development

Despite the significant delay in the growth of the embryonic myocardium, the cardiac-specific SLMAP3-KO neonatal pups were born normally without any obvious cardiac phenotypes at birth and survived into adulthood similar to Wt. We sectioned P0 and P7 SLMAP3-KO and Wt hearts and stained them with H&E to visualize cardiac structure. At postnatal day 0 (P0); the left ventricle size of KO hearts (−14.19% ± −7.55%, $\rho = 0.10$, $n = 3$) was almost similar to Wt hearts (Figure 6A). At P7, the H&E stain revealed no differences in the left ventricle wall size in KO hearts (−0.08% ± −0.7 8%, $\rho = 0.97$, $n = 3$) (Figure 6A). Further, examination of adult SLMAP3-KO with ECHO at 10 weeks of age indicated no significant differences in cardiac structure or function (Figure 6B) with an equivalent survival age to Wt.

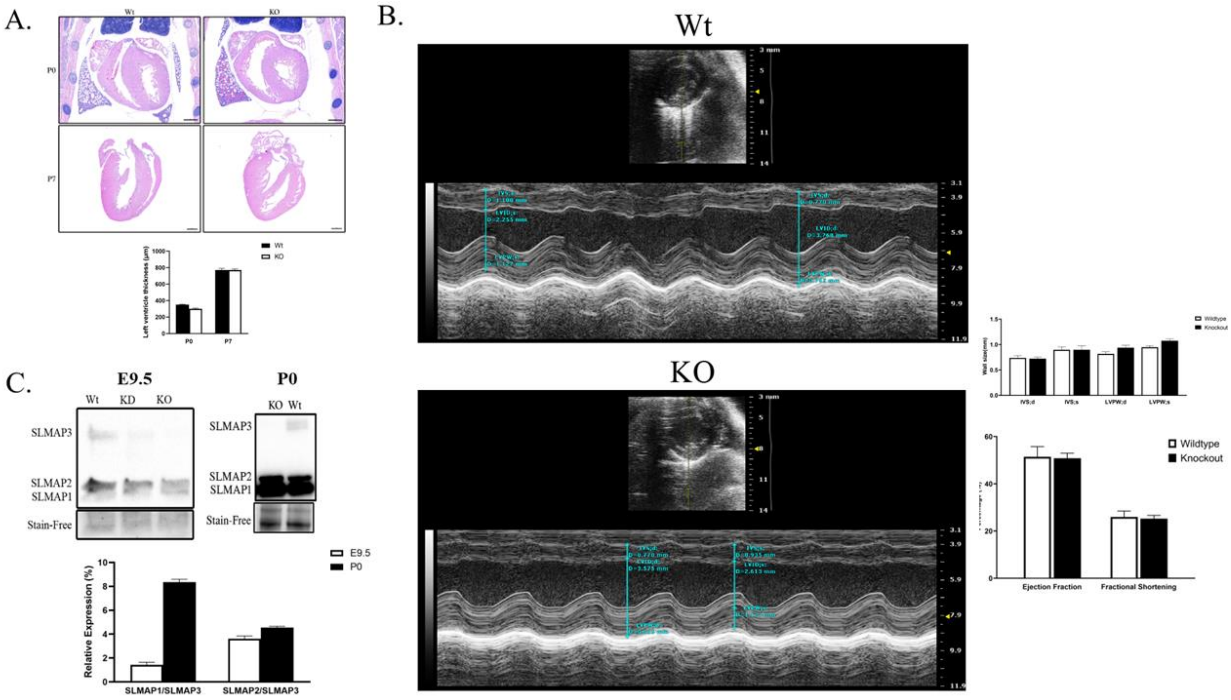

Figure 6. Analysis of postnatal hearts from Nkx2.5-Cre/SLMAP3-null mice. (**A**) Representative histological staining of Wt and KO Nkx2.5-Cre/SLMAP3-null myocardium at P0 and P7 with H&E. Scale bar = 0.5 mm. (**B**) Representative short axis echocardiography m-mode images of 10-week-old Wt and KO. Bar graphs show quantification of ejection fraction, fractional shortening, and left ventricle wall thickness. LV; left ventricle. IVS, LVPW; intraventricular septum, LV posterior wall. d,s; diastole, systole. n = 6. (**C**) Western blot displaying expression of SLMAP isoforms (SLMAP1, SLMAP2 and SLMAP3) in Wt and KO hearts at E9.5 and P0. Bar

graph is the quantification of relative expression of SLMAP1 or SLMAP2 compared to SLMAP3 in E9.5 and P0 Wt hearts. n = 3.

We quantified the expression of SLMAP isoforms in SLMAP3-KO hearts, and Western blot analysis indicated no changes in SLMAP1 and SLMAP2 protein levels in KO vs. Wt at E9.5 or P0, and SLMAP3 protein was not detected in the KO at either stage. However, the relative expression of SLMAP1/SLMAP3 and SLMAP2/SLMAP3 in the wild-type myocardium was 6.07× and 1.42× greater in P0 hearts when compared to E9.5 (Figure 6C). The data indicate that as the myocardium develops, there is a substantial increase in the expression of the smaller SLMAP isoforms compared to SLMAP3, and the loss of SLMAP3 did not influence their expression levels in embryonic or postnatal myocardium.

2.6. Depletion of SLMAP Isoforms in Rat Embryonic Cardiomyocytes (H9C2 Cells) Impacts Their Growth

To examine whether all three isoforms expressed in the heart are important for the growth of the embryonic myocardium, we investigated the expression of SLMAPs in the rat embryonic cardiomyocyte cell line H9C2. Western blot analysis indicated that H9C2 cells express the three SLMAP isoforms-SLMAP-1, 2, and 3 (Figure 7A), identical in molecular size to that seen in mouse embryonic hearts (Figure 6C). H9C2 cells transduced with shRNA-S4 (S4) or shRNA-S5 (S5) displayed a decrease in SLMAP expression when compared to the control scrambled shRNA-Sc (Sc), although only S5 drastically reduced the expression of all three SLMAP isoforms and was employed in all subsequent studies (Figure 7A). Notably, the depletion of all SLMAP isoforms in H9C2 cells resulted in a decrease in growth rate (Figure 7B). Further, the depletion of SLMAP isoforms lead to an increase in X-gal-positive cells in the Senescence-Associated-β-Galactosidase (SA-β-Gal) Assay (Figure 7C), and a decrease in proliferation, as indicated by the reduced number of Ki67-positive cells (Figure 7D). Western blots of transduced H9C2 lysates indicated that the depletion of SLMAPs had no impact on the phosphorylation of YAP in these embryonic cardiomyocytes (Figure 7E). Thus, SLMAP isoforms appear to play an important role in the growth of embryonic cardiomyocytes, independently of Hippo signaling.

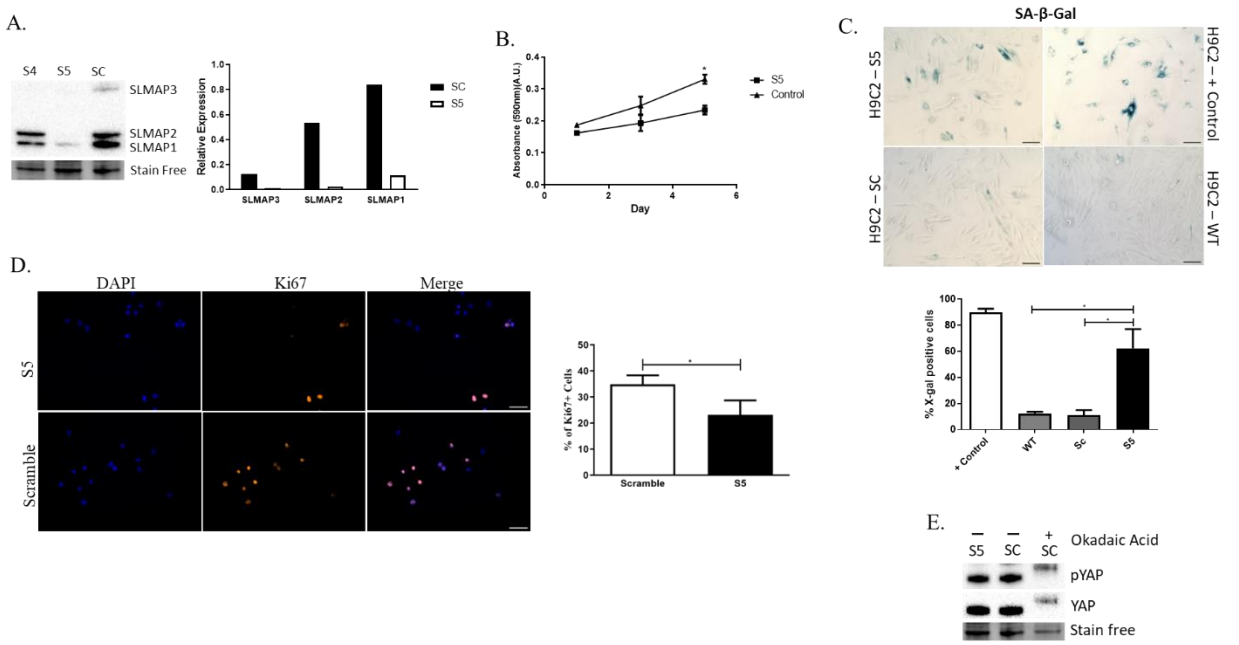

Figure 7. Loss of SLMAP expression in embryonic cardiomyocytes impacts growth and senescence. (**A**) Western blot displaying expression of SLMAP1, SLMAP2, and SLMAP3 in sh-RNA transduced H9C2 cells and bar graph showing quantification of expression of SLMAPs in Sc, S4, and S5 cells normalized to total proteins visualized by Stain-Free™. (**B**) Line graph displaying crystal violet absorbance measurements on days 1, 3, and 5 after seeding transduced H9C2 to compare growth rates. * $\rho < 0.05$. (**C**) Senescence analysis on Wt positive (+) control, Wt, and transduced (Sc, S5) H9C2 cells with SA-β-Gal assay. Bar graph represents percentage (%) of X-gal-positive cells. * $\rho < 0.05$. Scale bar = 100 µm. (**D**) Immunofluorescence staining with DAPI (Blue; nucleus) and Ki67 (orange) in transduced H9C2 cells. Bar graph represents mean percentage of $Ki67^{+}$ cells. * $\rho < 0.05$. Scale bar = 100 µm. (**E**) Western blot evaluating phospho to total YAP in transduced H9C2 and Sc-H9C2 cells treated with okadaic acid as a positive control.

3. Discussion

Here, we report that the specific loss of SLMAP3 isoform in cardiac progenitors by gene targeting with Nkx2.5-cre mice leads to a growth delay in the formation of the heart during early cardiogenesis. The developmental delay in cardiac formation was not due to changes in the proliferation or hypertrophic response in embryonic cardiomyocytes, although a difference in cell size was evident at E12.5 due to SLMAP3 deletion. Intriguingly, the early delay in cardiogenesis was completely reversed at birth and the postnatal development and function of the heart was unaffected in these mice in the absence of any SLMAP3. While the expression of SLMAP3 protein was completely nullified in cardiac progenitors, due to Nkx2.5-cre, the expression of the more abundant SLMAP1 and SLMAP2 remained unchanged and continued to accumulate normally during embryonic and postnatal development to levels that were similar to those in wildtype mouse hearts. Whether SLMAP1 and SLMAP2 can compensate for a loss of SLMAP3 function needs to be considered because of the very close structural similarities between these isoforms, which are derived by alternative splicing mechanisms from a single gene (Figure 1). In this regard, SLMAP3 is clearly distinguishable from the other SLMAPs due to its extended N-terminal sequences which encompass an FHA domain that was shown to bind MST1/2 kinases and regulate Hippo to impact

proliferation of 293 T cells [30]. The *in vivo* data here did not support a role for SLMAP3 in the proliferation of embryonic cardiomyocytes or the regulation of MST or YAP phosphorylation, since SLMAP3 deletion had no impact on these parameters during cardiogenesis. The loss of SLMAP3 did not affect Hippo signaling in the postnatal heart either, and the myocardium appeared normal in terms of its structure and function in adulthood. These data are consistent with our studies on the targeted deletion of the SLMAP3 isoform in postnatal myocardium [33]. Our previous data have shown that SLMAP is expressed early during cardiogenesis, and thus could influence the growth and maturation of cardiomyocytes. Perhaps the deletion of the other SLMAP isoforms is necessary to observe the critical nature of SLMAP in developing myocardium. Cardiac development begins at E7.5 in mice with the formation of the cardiac crescent, when the cardiac homeobox transcription factor Nkx2.5 is highly expressed within cardiac progenitor cells [34]. Nkx2.5-Cre mice are often employed to study genes during early cardiogenesis [29,35], and the deletion of SLMAP3 expression at this stage within FHF and SHF did not apparently impact cardiomyocyte differentiation/migration; however, there was a growth delay in septation with underdeveloped cardiac chambers in these mice hearts at E12.5 but without any obvious structural abnormalities. In order to interrogate the potential role of the other SLMAP isoforms, we employed rat embryonic cardiomyocytes (H9C2 cells) that were found to express SLMAP1, SLMAP2, and SLMAP3 with similar molecular characteristics to those in mouse embryonic heart tissue. Our constructed sh-RNAs-targeting SLMAPs resulted in a significant decrease in the expression of the three SLMAP isoforms accompanied by a profound deficit in growth and proliferation as well as enhanced cellular senescence in these embryonic cardiomyocytes. It is notable that depletion of the three SLMAPs in H9C2 cells had no impact on the main components of Hippo signaling. Thus, the mechanisms of SLMAP action that impact the embryonic growth of cardiomyocytes are independent of any regulation through Hippo signaling. The data support the contention that SLMAP isoforms are collectively critical for embryonic cardiomyocyte growth and that they can potentially compensate for each other since the specific embryonic KO of the SLMAP3 isoform in early heart development was non-lethal. It is conceivable that the more abundant SLMAP1 and SLMAP2 proteins may substitute for the loss of SLMAP3 during cardiogenesis. Given that the knockdown of all three SLMAP isoforms in H9C2 cardiomyocytes lead to defective growth and cellular senescence, it would be meaningful to delete SLMAP1 and SLMAP2 in cardiac progenitors *in vivo* to gauge the contribution of SLMAP to heart development, although the H9C2 data would suggest that it would be lethal. The size of cardiomyocytes was noticeably smaller in embryonic hearts due to Nkx2.5-Cre-mediated SLMAP3 loss, but there was no change in hypertrophic signaling (AKT/mTOR), and nor was there any change in cardiomyocyte numbers. We aim to employ additional stereological analysis by isolating embryonic cardiomyocytes and further staining to decipher the mechanisms that may impact their size and shape at the cellular level.

It is notable that unique structural elements in SLMAP3 (i.e., FHA domain) target the MTOC [11], which has been shown to be critical for mitosis and differentiation [36]. The microtubules and the cytoskeleton serve important roles in cell shape and function, and their contributions to cardiomyocyte growth and size/shape *in vivo* remain elusive. The data here further point to a unique structural mechanism for SLMAP actions through their interactions with subcellular organelles, microtubules, and the cytoskeleton to guide cardiac development.

4. Materials and Methods

4.1. Generating and Genotyping the SLMAP Knockout Model

The Nkx2.5-Cre mice [29] were generously donated by Dr. Kyoung-Han Kim and backcrossed with wildtype B6C3F1 mice to generate the B6C3F1 Nkx2.5-cre mice. The generation of our flox-SLMAP, breeding strategies, and PCR genotyping were performed as described previously [33]. Briefly, B6C3F1 flox-SLMAP mice were crossed with B6C3F1 Nkx2.5-cre mice to generate heterozygous floxed-SLMAP;Nkx2.5-cre or knockdown (KD) mice. Crossing KD mice with each other generates homozygous floxed-SLMAP;Nkx2.5-cre or knockout (KO) mice. Mice harboring heterozygous or homozygous Nkx2.5-cre were followed for one year and did not exhibit any abnormalities. Thus, chronic expression of cre did not result in any phenotypes.

For embryo studies, pregnant mothers that were plug-checked (day of plug was E0.5) and carrying our experimental embryos at the desired stage were anesthetized with a standard ketamine–xylazine–acepromazine (KXA) drug cocktail during embryo isolation and euthanized after they were harvested. The embryos were dissected in ice cold 1x PBS and whole embryos or prenatal hearts were fixed in 10% neutral buffered formalin for 48–96 h or snap-frozen in liquid nitrogen for proteomic analysis. Caudal tissues or tails were used for genotyping.

Mice were handled in accordance with the guidelines set by Canadian Council on Animal Care, Guide to the Care and Use of Experimental Animals, 2 vols. (Ottawa, Ont.: CCAC, 1980–1993) and Animals for Research Act, R.S.O. 1990, c.A. 22. All animal protocols and procedures were approved by the Animal Care Committee of the University of Ottawa.

4.2. Protein Isolation and Western Blotting

Hearts of embryonic (E9.5–E18.5) or P0 mice were collected after explanting from mothers and immediately frozen at −80 °C. Each heart was later washed with ice-cold 1× phosphate buffered saline (PBS) and homogenized using a Fisher handheld Maximizer homogenizer (Thermo Fisher Scientific, Waltham, MA, USA) in ice-cold lysis buffer (1 mM ethylene glycol tetraacetic acid (EGTA), 1 mM ethylenediaminetetraacetic (EDTA), 20 mM Tris base, 1% Triton, 150 mM sodium chloride, 1× complete mini EDTA-free protease inhibitor cocktail (Roche, Basel, Switzerland), and 1× PhosSTOP (Roche). The suspension was centrifuged for 15 min at 12,000× *g* to separate the proteins from the cell debris. The supernatant-containing protein was stored at −80 °C. Protein concentration was calculated using the BSA method.

For Western blotting experiments, 10 µg of protein was loaded in each well of a 4–15% gradient SDS-PAGE gel. The gels were transferred overnight on a polyvinylidene fluoride (PVDF) membrane (Bio-Rad) in a buffer containing 25 mM Tris, 190 mM Glycine, and 20% methanol. All membranes were blocked at room temperature for 1 h in Tris-buffered saline (TBST) containing 1 M Tris, 290 mM NaCl, 0.1% Tween 20, pH 7.4, and 5% bovine serum albumin. Primary antibodies (listed in Table 1) were incubated overnight at 4 °C with 5% bovine serum albumin (BSA). Membranes were washed 3 times for 5 min each in TBST prior to adding the appropriate horseradish peroxidase-labeled secondary antibody (Jackson ImmunoResearch, West Grove, PA, USA) in a 1:10,000 dilution in TBST with 5% nonfat dry milk. Membranes were shaken slowly at room temperature for 1 h while incubating with secondary antibody, followed by 3 washes for 5 min each with TBST. Membranes were treated with a BioRad Western blotting kit (Bio-Rad, Hercules, CA, USA) and developed using ChemiDoc machines (Bio-Rad, Hercules, CA, USA). Bands were quantified by densitometry using Image Lab software v.6.0.0 (Bio-Rad). Membranes were stripped (25 mM glycine, 10% SDS, and pH 2.2 in dH_2O) and reprobed with different antibodies. When using stain-free technology, stain-free gels (Bio-Rad) and low-fluorescence PVDF membranes (Bio-Rad) were used.

Table 1. List of antibodies used in this study. All antibodies used in this study are listed with the corresponding distributor, catalog number, and dilution used for Western blot (WB) or immunofluorescence (IF). Novus Biological (Centennial, CO, USA), BD Transduction Laboratories (Franklin Lakes, NJ, USA), Bethyl Laboratories (Montgomery, TX, USA), Santa Cruz (Dallas, TX, USA), Cell Signaling Technology (Danvers, MA, USA), Abcam (Cambridge, U.K.)

Antibody	Manufacturer	Dilution
SLMAP	Novus Biologicals (NBP1-81397)	1:1000(WB)
Striatin-1	BD Transduction Laboratories (610838)	1:1000 (WB)
Striatin-3	Novus Biological (NBP-74572)	1:1000 (WB)
STRIP1	Bethyl Laboratories (A304-644A)	1:1000 (WB)
PP2A-C α/β subunit	Santa Cruz Biotechnology (sc-80665)	1:200 (WB)
PP2A-A α subunit	Millipore Sigma (07-250)	1:600 (WB)
Phospho-YAP (S127)	Cell Signaling Technology (13008S)	1:1000 (WB)
YAP	Cell Signaling Technology (14074S)	1:1000 (WB)
pH3	Abcam (ab5176)	1:200 (IF)
Ki67	Abcam (ab15580)	1:200 (IF)
Troponin C (TnC)	Santa Cruz (sc-52265)	1:200 (IF)
pAKT1	Cell Signaling Technology (9018S)	1:1000 (WB)
AKT1	Cell Signaling Technology (9272)	1:1000 (WB)
pMTOR1	Cell Signaling Technology (5536)	1:1000 (WB)
MTOR1	Cell Signaling Technology (2972)	1:1000 (WB)

4.3. Echocardiography

All echocardiographic analysis was performed using the VEVO 2100 system (FUJIFILM VisualSonics), identically to our previous publication [33].

4.4. Histological and Immunofluorescent Analysis

Embryonic and postnatal mouse hearts were fixed using 10% Neutral Buffered Formalin (Thermo Fisher Scientific). After fixing for 48 h, hearts were sectioned 4 μm longitudinally per section. Paraffin-embedded slides were rehydrated through well-established protocols for rehydration with citrate buffer for antigen retrieval [37]. For histological analysis, sectioned hearts were stained with hematoxylin and eosin (H&E) stain to visualize the myocardium and nuclei. For immunofluorescence, rehydrated slides were subjected to 1 h of 5% BSA in PBS-T (1x PBS, 0.01% Triton X-100) of blocking. After rinsing with PBS, we diluted antibodies according to Table 1 in

blocking solution and incubated them overnight at 4 °C. Samples were then washed 3x for 5 min with PBS, and then secondary Alexa-555 (Thermo Fisher Scientific, USA) or Alexa 647 (Thermo Fisher Scientific, USA) were incubated for 1 h at room temperature. We used VectaShield Plus DAPI (MJS Biolynx, CA, USA) mounting medium with 1.5 mm coverslips (Fisher Scientific, USA) sealed with nail polish and imaged when completely dried. Images were captured on Zeiss AxioImager M2 and analyzed using ImageJ v1.8.

Cardiomyocyte size was measured by staining sectioned E12.5 hearts with H&E or immunofluorescence for troponin C (TnC). We marked the perimeter of cardiomyocytes based on the staining and used ImageJ v1.8 to calculate the area of cardiomyocytes which would reflect their size.

4.5. Creation of Short-Hairpin RNA (sh-RNA) Lentivirus for Depletion of SLMAP3

To stably deplete SLMAP3 expression in H9C2 cells, we designed two shRNAs targeting mouse SLMAP sequences from exon 22 (Ensembl reference transcript ENSMUST00000139075.8), which were conserved in rat SLMAP gene. The targeting sequences are 5′-GCAATCAATCACAGATGAGCTCAAA and 5′-GCTGCTGCGAGAGAAAGGAAATAAT, which were called S4 and S5, respectively. The control scramble target sequence is 5′-AGGATAAGCGTCAACGAATAGGTGA, referred to as SC, and was generated by inputting the S5 plasmid sequence into GenScript Sequence Scramble tool [38]. The shRNAs were designed in a lentivirus vector with the VectorBuilder design tool [39]. VectorBuilder cloned and delivered the plasmids in *Escherichia coli* (VB UltraStable). Plasmids were isolated via PureYield Plasmid Midprep System protocol (Promega Cooperation, Technical Manual #TM253) and transfected in Lenti-X 293 T cells with the packing and envelope plasmids psPAX2 [40] and pMD2.G [41] via polyethyleneimine (PEI), following an established protocol [42]. The supernatants of Lenti-X 293 T cells containing lentiviruses were harvested 48 and 72 h after transfection and filtered with 0.45 µm sterile syringe filter. The viral particles were concentrated via Lenti-X-Concentrator (Clontech, Mountain View, CA, USA, catalog number PT4421-2), and the titer was quantified with the PCR Lentivirus Titer Kit (abm, New York, NY, USA, catalog number LV900).

4.6. Maintenance and Transduction of H9C2 Rat Cardiomyocyte Cell Line

H9C2 cell line was originally acquired from ATCC and gifted by the Megeney Laboratory at University of Ottawa. H9C2 cells were kept at 37 °C with 5% carbon dioxide in high humidity. H9C2 media consisted of high-glucose (4.5 g/L) Dulbecco modified essential media (DMEM) (Multicell, Woonsocket, RI, USA, Catalogue #319-005-CL) containing 1.00% pen-strep, 1.00% non-essential amino acids (Gibco, Carlsbad, CA, USA, Reference #11140-050). The H9C2 cell line was tested in the lab for mycoplasma contamination and tested negative in all instances. The lentiviral reverse transduction was performed following Addgene protocol [43]. H9C2 cells were plated at 25,000 cells per cm^2 of growth area and transduced with S4, S5, and Sc at multiplicity of infection (MOI) of 150. Selection for successfully transduced cells was carried out by incorporating puromycin into cell media (3 µg/mL) for 3 days. For induction of YAP phosphorylation to be used as a positive control, H9C2 cells were treated with 1.5 µM okadaic acid for 1 h. Protein lysate was isolated soon after that.

4.7. Senescence Analysis on H9C2

Cellular senescence was analyzed via Senescence Beta-Galactosidase Staining Kit according to the protocol outlined by the manufacturer (Cell Signaling Technology, (Danvers, CO, USA, Cat. #9860). All the cells were plated in triplicate, and cells were quantified in 3 fields of each. Total and positive X-gal cells were counted blindly to avoid any bias. For positive control, we induced cellular senescence in H9C2 WT cells by 600 μm H_2O_2 treatment for 2 h in two consecutive days.

4.8. H9C2 Growth Curve Analysis

Cells were plated at 9000 cells per cm2 and left overnight to attach. Cells were fixed with 4% paraformaldehyde in 1X PBS, pH 7.4 (warmed to 37 °C) for 20 min followed by distilled water wash. Samples were incubated with 0.1% crystal violet for 20 min at room temperature followed by 4 distilled water washes. Samples were left to air dry at room temperature for a minimum of 2 h followed by 10% acetic acid incubation for 20 min at room temperature, while shaking, to dissolve the crystal violet. Quantification was performed by measuring absorbance of samples at 590 nm relative to each other using Synergy Hybrid Multi-Mode Microplate Reader (BioTek Instruments, Highland Park, VT, USA). Procedure was performed 3 times corresponding to the day of the experiment (days 1, 3, and 5) for each sample.

4.9. Statistical Analyses

The statistical analysis was performed using GraphPad Prism software version 8 for Windows (GraphPad Software). All comparisons between wildtype and knockout groups were analyzed using non-paired two-tailed Student's T-test. If three groups were analyzed, we used one-way ANOVA with post hoc Tukey test to determine significance. All values and points on graphs represent mean values obtained from multiple experiments. All error bars presented in graphs are represented using the standard error of the mean. All sample size values (n) represent replicates.

Author Contributions: T.R.: project conceptualization, methodology, validation, formal analysis, investigation, resources, data visualization and manuscript writing; A.P.D.: project conceptualization, investigation, data visualization and manuscript writing; M.K.: investigation, data visualization; M.S.: investigation, resources and methodology; B.S.T.: project conceptualization, supervision, manuscript review and funding acquisition. All authors have read and agreed to the published version of the manuscript.

Funding: This research was funded by the Canadian Institute of Health Research project grant, grant number 220996-151999, to B.S.T.

Institutional Review Board Statement: Mice were handled in accordance with the guidelines set by Canadian Council on Animal Care, Guide to the Care and Use of Experimental Animals, 2 vols. (Ottawa, Ont.: CCAC, 1980-1993) and Animals for Research Act, R.S.O. 1990, c.A. 22. All animal protocols and procedures were approved by the Animal Care Committee of the University of Ottawa.

Informed Consent Statement: Not applicable.

Data Availability Statement: Data are contained within the article.

Acknowledgments: We would like to thank Kyoung-Han Kim and Lynn Megeney for providing the Nkx2.5-Cre mice and H9C2 cell line. We are thanking all the facilities involved in this study: Cell Biology and Image Acquisition Core (RRID: SCR_021845) and the Louise Pelletier Histology Core Facility (RRID: SCR_021737).

Conflicts of Interest: The authors declare no conflicts of interest.

5. Reference

1. Schleich, J.-M.; Abdulla, T.; Summers, R.; Houyel, L. An overview of cardiac morphogenesis. *Arch. Cardiovasc. Dis.* **2013**, *106*, 612–623. https://doi.org/10.1016/j.acvd.2013.07.001.
2. Kelly, R.G.; Buckingham, M.E.; Moorman, A.F. Heart Fields and Cardiac Morphogenesis. *Cold Spring Harb. Perspect. Med.* **2014**, *4*, a015750. https://doi.org/10.1101/cshperspect.a015750.
3. van den Berg, G.; Abu-Issa, R.; de Boer, B.A.; Hutson, M.R.; de Boer, P.A.; Soufan, A.T.; Ruijter, J.M.; Kirby, M.L.; van den Hoff, M.J.; Moorman, A.F. A caudal proliferating growth center contributes to both poles of the forming heart tube. *Circ. Res*. **2009**, *104*, 179–188.
4. Colombo, S.; de Sena-Tomás, C.; George, V.; Werdich, A.A.; Kapur, S.; MacRae, C.A.; Targoff, K.L. Nkx genes establish second heart field cardiomyocyte progenitors at the arterial pole and pattern the venous pole through Isl1 repression. *Development* **2018**, *145*, dev161497.
5. Hoff, M.J.v.D.; Kruithof, B.P.; Moorman, A.F.; Markwald, R.R.; Wessels, A. Formation of Myocardium after the Initial Development of the Linear Heart Tube. *Dev. Biol.* **2001**, *240*, 61–76. https://doi.org/10.1006/dbio.2001.0449.
6. Yotti, R.; Seidman, C.E.; Seidman, J.G. Advances in the Genetic Basis and Pathogenesis of Sarcomere Cardiomyopathies. *Annu. Rev. Genom. Hum. Genet.* **2019**, *20*, 129–153. https://doi.org/10.1146/annurev-genom-083118-015306.
7. Guo, Y.; Pu, W. Cardiomyocyte Maturation: New Phase in Development. *Circ. Res*. **2020**, *126*, 1086–1106.
8. Wigle, J.; Demchyshyn, L.; Pratt, M.; Staines, W.; Salih, M.; Tuana, B. Molecular cloning, expression, and chromosomal assignment of sarcolemmal-associated proteins. A family of acidic amphipathic alpha-helical proteins associated with the membrane. *J. Biol. Chem*. **1997**, *272*, 32384–32394.
9. Guzzo, R.M.; Salih, M.; Moore, E.D.; Tuana, B.S. Molecular properties of cardiac tail-anchored membrane protein SLMAP are consistent with structural role in arrangement of excitation-contraction coupling apparatus. *Am. J. Physiol. Heart Circ. Physiol.* **2005**, *288*, H1810–H1819. https://doi.org/10.1152/ajpheart.01015.2004.
10. Byers, J.T.; Guzzo, R.M.; Salih, M.; Tuana, B.S. Hydrophobic profiles of the tail anchors in SLMAP dictate subcellular targeting. *BMC Cell Biol.* **2009**, *10*, 48. https://doi.org/10.1186/1471-2121-10-48.
11. Guzzo, R.M.; Sevinc, S.; Salih, M.; Tuana, B.S. A novel isoform of sarcolemmal membrane-associated protein (SLMAP) is a component of the microtubule organizing centre. *J. Cell Sci.* **2004**, *117*, 2271–2281. https://doi.org/10.1242/jcs.01079.
12. Ishikawa, T.; Sato, A.; Marcou, C.; Tester, D.; Ackerman, M.; Crotti, L.; Schwartz, P.; On, Y.; Park, J.; Nakamura, K.; et al. A novel disease gene for Brugada syndrome: Sarcolemmal membrane-associated protein gene mutations impair intracellular trafficking of hNav1.5. *Circ. Arrhythm. Electrophysiol*. **2012**, *5*, 1098–1107.
13. Nader, M.; Westendorp, B.; Hawari, O.; Salih, M.; Stewart, A.F.R.; Leenen, F.H.H.; Tuana, B.S. Tail-anchored membrane protein SLMAP is a novel regulator of cardiac function at the sarcoplasmic reticulum. *Am. J. Physiol. Circ. Physiol.* **2012**, *302*, H1138–H1145. https://doi.org/10.1152/ajpheart.00872.2011.
14. Mlynarova, J.; Trentin-Sonoda, M.; da Silva, F.G.; Major, J.L.; Salih, M.; Carneiro-Ramos, M.S.; Tuana, B.S. SLMAP3 isoform modulates cardiac gene expression and function. *PLoS ONE* **2019**, *14*, e0214669. https://doi.org/10.1371/journal.pone.0214669.

15. Wielowieyski, P.; Sevinc, S.; Guzzo, R.; Salih, M.; Wigle, J.; Tuana, B. Alternative splicing, expression, and genomic structure of the 3' region of the gene encoding the sarcolemmal-associated proteins (SLAPs) defines a novel class of coiled-coil tail-anchored membrane proteins. *J. Biol. Chem*. **2000**, *275*, 38474–38481.
16. Consortium, U. UniProt: A worldwide hub of protein knowledge. *Nucleic Acids Res*. **2019**, *47*, D506–D515.
17. Guzzo, R.M.; Wigle, J.; Salih, M.; Moore, E.D.; Tuana, B.S. Regulated expression and temporal induction of the tail-anchored sarcolemmal-membrane-associated protein is critical for myoblast fusion. *Biochem. J.* **2004**, *381*, 599–608. https://doi.org/10.1042/bj20031723.
18. Mahajan, A.; Yuan, C.; Lee, H.; Chen, E.S.-W.; Wu, P.-Y.; Tsai, M.-D. Structure and Function of the Phosphothreonine-Specific FHA Domain. *Sci. Signal.* **2008**, *1*, re12. https://doi.org/10.1126/scisignal.151re12.
19. Yu, F.; Zhao, B.; Guan, K. Hippo Pathway in Organ Size Control, Tissue Homeostasis, and Cancer. *Cell* **2015**, *163*, 811–828.
20. Goudreault, M.; D'Ambrosio, L.M.; Kean, M.J.; Mullin, M.J.; Larsen, B.G.; Sanchez, A.; Chaudhry, S.; Chen, G.I.; Sicheri, F.; Nesvizhskii, A.I.; et al. A PP2A Phosphatase High Density Interaction Network Identifies a Novel Striatin-interacting Phosphatase and Kinase Complex Linked to the Cerebral Cavernous Malformation 3 (CCM3) Protein. *Mol. Cell. Proteom.* **2009**, *8*, 157–171. https://doi.org/10.1074/mcp.m800266-mcp200.
21. Jeong, B.-C.; Bae, S.J.; Ni, L.; Zhang, X.; Bai, X.-C.; Luo, X. Cryo-EM structure of the Hippo signaling integrator human STRIPAK. *Nat. Struct. Mol. Biol.* **2021**, *28*, 290–299. https://doi.org/10.1038/s41594-021-00564-y.
22. Couzens, A.L.; Knight, J.D.R.; Kean, M.J.; Teo, G.; Weiss, A.; Dunham, W.H.; Lin, Z.-Y.; Bagshaw, R.D.; Sicheri, F.; Pawson, T.; et al. Protein Interaction Network of the Mammalian Hippo Pathway Reveals Mechanisms of Kinase-Phosphatase Interactions. *Sci. Signal.* **2013**, *6*, rs15. https://doi.org/10.1126/scisignal.2004712.
23. von Gise, A.; Lin, Z.; Schlegelmilch, K.; Honor, L.B.; Pan, G.M.; Buck, J.N.; Ma, Q.; Ishiwata, T.; Zhou, B.; Camargo, F.D.; et al. YAP1, the nuclear target of Hippo signaling, stimulates heart growth through cardiomyocyte proliferation but not hypertrophy. *Proc. Natl. Acad. Sci. USA* **2012**, *109*, 2394–2399. https://doi.org/10.1073/pnas.1116136109.
24. Heallen, T.; Zhang, M.; Wang, J.; Bonilla-Claudio, M.; Klysik, E.; Johnson, R.L.; Martin, J.F. Hippo Pathway Inhibits Wnt Signaling to Restrain Cardiomyocyte Proliferation and Heart Size. *Science* **2011**, *332*, 458–461. https://doi.org/10.1126/science.1199010.
25. Xin, M.; Kim, Y.; Sutherland, L.B.; Murakami, M.; Qi, X.; McAnally, J.; Porrello, E.R.; Mahmoud, A.I.; Tan, W.; Shelton, J.M.; et al. Hippo pathway effector Yap promotes cardiac regeneration. *Proc. Natl. Acad. Sci. USA* **2013**, *110*, 13839–13844. https://doi.org/10.1073/pnas.1313192110.
26. Xin, M.; Kim, Y.; Sutherland, L.B.; Qi, X.; McAnally, J.; Schwartz, R.J.; Richardson, J.A.; Bassel-Duby, R.; Olson, E.N. Regulation of Insulin-Like Growth Factor Signaling by Yap Governs Cardiomyocyte Proliferation and Embryonic Heart Size. *Sci. Signal.* **2011**, *4*, ra70. https://doi.org/10.1126/scisignal.2002278.
27. Heallen, T.; Morikawa, Y.; Leach, J.; Tao, G.; Willerson, J.T.; Johnson, R.L.; Martin, J.F. Hippo signaling impedes adult heart regeneration. *Development* **2013**, *140*, 4683–4690. https://doi.org/10.1242/dev.102798.
28. Zheng, Y.; Liu, B.; Wang, L.; Lei, H.; Prieto, K.D.P.; Pan, D. Homeostatic Control of Hpo/MST Kinase Activity through Autophosphorylation-Dependent Recruitment of the

STRIPAK PP2A Phosphatase Complex. *Cell Rep.* **2017**, *21*, 3612–3623. https://doi.org/10.1016/j.celrep.2017.11.076.
29. Stanley, E.G.; Biben, C.; Elefanty, A.; Barnett, L.; Koentgen, F.; Robb, L.; Harvey, R.P. Efficient Cre-mediated deletion in cardiac progenitor cells conferred by a 3'UTR-ires-Cre allele of the homeobox gene Nkx2-5. **2002**, *46*, 431–439.
30. Bae, S.; Ni, L.; Osinski, A.; Tomchick, D.; Brautigam, C.; Luo, X. SAV1 promotes Hippo kinase activation through antagonizing the PP2A phosphatase STRIPAK. *eLife* **2017**, *6*, 30278.
31. Brade, T.; Pane, L.S.; Moretti, A.; Chien, K.R.; Laugwitz, K.-L. Embryonic Heart Progenitors and Cardiogenesis. *Cold Spring Harb. Perspect. Med.* **2013**, *3*, a013847. https://doi.org/10.1101/cshperspect.a013847.
32. Aoyagi, T.; Matsui, T. Phosphoinositide-3 Kinase Signaling in Cardiac Hypertrophy and Heart Failure. *Curr. Pharm. Des.* **2011**, *17*, 1818–1824. https://doi.org/10.2174/138161211796390976.
33. Rehmani, T.; Mlynarova, J.; Byers, J.; Salih, M.; Tuana, B.S. Specific Deletion of the FHA Domain Containing SLMAP3 Isoform in Postnatal Myocardium Has No Impact on Structure or Function. *Cardiogenetics* **2021**, *11*, 164–184. https://doi.org/10.3390/cardiogenetics11040018.
34. George, V.; Colombo, S.; Targoff, K.L. An early requirement for nkx2.5 ensures the first and second heart field ventricular identity and cardiac function into adulthood. *Dev. Biol.* **2015**, *400*, 10–22. https://doi.org/10.1016/j.ydbio.2014.12.019.
35. Cambier, L.; Plate, M.; Sucov, H.M.; Pashmforoush, M. Nkx2-5 regulates cardiac growth through modulation of Wnt signaling by R-spondin3. *Development* **2014**, *141*, 2959–2971. https://doi.org/10.1242/dev.103416.
36. Becker, R.; Leone, M.; Engel, F.B. Microtubule Organization in Striated Muscle Cells. *Cells* **2020**, *9*, 1395. https://doi.org/10.3390/cells9061395.
37. Available online: https://www.novusbio.com/support-by-application/Fluorescent-IHC-Staining-of-FFPE-Tissue (accessed on November 1st ,2019).
38. Available online: https://www.genscript.com/tools/create-scrambled-sequence-reference (accessed on October 31st ,2022).
39. Available online: https://en.vectorbuilder.com/design/pLV_shRNA_U6.html-reference (accessed on November 1st ,2022).
40. Available online: https://www.addgene.org/12260/ (accessed on November 1st ,2022).
41. Available online: https://www.addgene.org/12259/ (accessed on November 1st ,2022).
42. Available online: https://www.addgene.org/protocols/lentivirus-production/ (accessed on November 1st ,2022).
43. Available online: https://www.addgene.org/protocols/generating-stable-cell-lines/-reference (accessed on November 1st ,2022)

Chapter Three - Tail Anchored Membrane Protein SLMAP3 is essential for the Targeting of Centrosomal Proteins to the Nuclear Envelope for Skeletal Myogenesis

Manuscript Publication and Copyright

From: Royal Society Publishing <alerts@royalsocietypublishing.org>
Sent: Tuesday, October 8, 2024 7:05 PM
To: Balwant Tuana <btuana@uottawa.ca>
Subject: Author Services Notification - Open Biology

Attention : courriel externe | external email

Dear Balwant Tuana,

Your paper "Tail-anchored membrane protein SLMAP3 is essential for targeting centrosomal proteins to the nuclear envelope in skeletal myogenesis" has now been published online and is available to read and download at https://royalsocietypublishing.org/doi/10.1098/rsob.240094. Please send this to your co-authors as this notification has only been sent to the corresponding author.

We want to make the experience of publishing with us better. We value your feedback and invite you to complete this short, five minute survey https://forms.royalsociety.org/s/rsauthors/ about your publishing experience. When you complete the survey, you can enter an annual prize draw to win £100 and a Royal Society print of your choice.

If your paper has been published under an open access licence you are now free to distribute your paper as you wish. See https://royalsociety.org/journals/open-access for details.

If your paper has been published under our standard licence, you may now link to the published article from other websites or repositories. You may not post the final PDF on other sites. You can deposit a final, accepted manuscript version (post-print) in an institutional or not-for-profit repository. Please visit https://royalsociety.org/journals/ethics-policies for information.

The following link provides free access to your paper. You may send this link to colleagues that may be interested. If your paper is not published under an open access model, this free access link may NOT be used for commercial purposes or posted on openly accessible websites.

To activate your access, please click on the following link:
https://www.royalsocietypublishing.org/eprint/C7GBF7IWXMIPB88X9NIU/full

Thank you for publishing with us - we look forward to the opportunity to work with you again in the future.

Yours sincerely
Royal Society Publishing team

OPEN BIOLOGY

royalsocietypublishing.org/journal/rsob

Research

Cite this article: Dias AP, Rehmani T, Salih M, Tuana B. 2024 Tail-anchored membrane protein SLMAP3 is essential for targeting centrosomal proteins to the nuclear envelope in skeletal myogenesis. *Open Biol.* **14**: 240094.
https://doi.org/10.1098/rsob.240094

Received: 23 April 2024
Accepted: 10 July 2024

Tail-anchored membrane protein SLMAP3 is essential for targeting centrosomal proteins to the nuclear envelope in skeletal myogenesis

Ana Paula Dias, Taha Rehmani, Maysoon Salih and Balwant Tuana

Department of Cellular and Molecular Medicine, University of Ottawa, Ottawa, Canada K1H 8M5

THE ROYAL SOCIETY PUBLISHING

Tail-Anchored Membrane Protein SLMAP3 is Essential for Targeting Centrosomal Proteins to the Nuclear Envelope in Skeletal Myogenesis

Ana Paula Dias[1], Taha Rehmani[1], Maysoon Salih[1], Balwant Tuana[1*]
[1]Department of Cellular and Molecular Medicine, University of Ottawa, Ottawa, K1H 8M5, Canada

[*]Correspondence: btuana@uottawa.ca

Summary

The positioning and communication between the nucleus and centrosomes are essential in cell division, differentiation and tissue formation. During skeletal myogenesis, the nuclei become evenly spaced with the switch of the microtubule-organizing centre (MTOC) from the centrosome to the nuclear envelope (NE). We report that the tail-anchored sarcolemmal membrane associated protein 3 (SLMAP3), a component of the MTOC and NE, is crucial for myogenesis because its deletion in mice leads to a reduction in the NE-MTOC formation, mislocalization of the nuclei, dysregulation of the myogenic programme and abnormal embryonic myofibres. SLMAP3$^{-/-}$ myoblasts also displayed a similar disorganized distribution of nuclei with an aberrant NE-MTOC and defective myofiber formation and differentiation programming. We identified novel interactors of SLMAP3, including pericentrin, PCM1 (pericentriolar material 1), AKAP9 (A-kinase anchoring protein 9), kinesin-1 members Kif5B (kinesin family member 5B), KLC1 (kinesin light chain 1), KLC2 (kinesin light chain 2) and nuclear lamins, and observed that the distribution of centrosomal proteins at the NE together with Nesprin-1 was significantly altered by the loss of SLMAP3 in differentiating myoblasts. SLMAP3 is believed to negatively regulate Hippo signalling, but its loss was without impact on this pathway in developing muscle. These results reveal that SLMAP3 is essential for skeletal myogenesis through unique mechanisms involving the positioning of nuclei, NE-MTOC dynamics and gene programming.

Keywords: SLMAP3, skeletal myogenesis, non-centrosomal microtubule organizing center, Golgi, LINC complex, centrosome, nuclear envelope.

1. Introduction

Mechanisms that guide the positioning of the nucleus are critical for cell migration, division and tissue formation. The linker of nucleoskeleton and cytoskeleton (LINC) complex comprising klarsicht/ANC-1/Syne-1 homology (KASH) and Sad1/UNC-84 (SUN) proteins are believed to bridge the nuclear membrane to transmit mechanical information from the cytoskeleton to influence nuclear positioning as well as impact the nuclear lamina and chromatin organization [1,2]. Skeletal muscle formation is a fascinating example of the radical cellular cytoskeleton reorganizations that cells can undergo, where the proliferative progenitor myoblast cells differentiate and fuse, forming a syncytium that is called myotube [3]. In this process, a cytoskeletal remodelling takes place before myoblast fusion [4–6], where microtubule-organizing centre (MTOC) proteins from the centrosome relocate to the nuclear envelope (NE) [4,7–9], in a process dependent on the LINC complex member Nesprin-1 [10]. It is hypothesized that this MTOC switch is important for the proper localization of nuclei in developing myotubes [11,12]. Nuclear mispositioning in myofibres has been associated with muscular dysfunctions, including Emery–Dreifuss muscular dystrophy (EDMD) and centronuclear myopathy (CNM) [11,12], which are characterized by muscle weakness and wasting [13,14]. Following the MTOC switch in

differentiating myoblast, the Golgi apparatus relocalizes in perinuclear regions (PEs), forming a Golgi belt-like ring structure [4,5,8,15], and itself also becomes an MTOC [16–18]. The endoplasmic reticulum (ER) exit sites (ERES) are remodelled together with the Golgi [5,15,19]. The remodelling of Golgi and ERES suggests that the secretory pathway surrounding the nucleus must be also important for the skeletal muscle function, such as the proper transport of M-cadherin to cellular membrane and contribute to myoblast fusion [19]. Centrosomal proteins including pericentrin, PCM1 and AKAP9 have been reported to be important for the centrosome-NE MTOC switch and Golgi remodelling [10,18,20,21].

Previously, we defined the sarcolemmal membrane associated protein 3 (SLMAP3) as a component of the centrosome, where it localizes via its N-terminal sequences encompassing the forkhead-associated domain (FHA) [22]. SLMAP3 can also target the perinuclear membrane via its hydrophobic C-terminal tail anchor [23,24]. SLMAP3 has also been found in the striatin-interacting phosphatase and kinase (STRIPAK) complex [25,26] and linked to the Hippo signalling by inhibiting MST kinase, and consequently activating Yes1 associated transcriptional regulator (YAP) and transcriptional coactivator with PDZ-binding motif (TAZ) to induce proliferation [27–30]. To elucidate the role of SLMAP3 *in vivo*, we devised a strategy to specifically delete the SLMAP3 isoform in embryonic and post-natal heart muscle, but these mice exhibited normal physiology most likely due to the presence of the other SLMAP isoforms in cardiomyocytes [31,32]. Splicing mechanisms generate many SLMAP isoforms that are expressed in a developmental and tissue-specific manner [33,34]. Here we report the generation of global SLMAP3 knockout($^{-/-}$) mice, which displayed stunted growth characteristics with widespread organ deficits leading to lethality. SLMAP3$^{-/-}$ embryos presented abnormal skeletal muscle and molecular analysis indicated downregulation of genes involved in skeletal muscle development. Furthermore, the deletion of the SLMAP gene in mouse myoblasts, which express only SLMAP3, caused aberrant differentiation and myotube formation. A major impact on the distribution and positioning of the nuclei and a defective centrosome-NE MTOC switch was evident *in vivo*, and cultured myotubes devoid of SLMAP3. The loss of SLMAP3 also led to a reduction in the Golgi apparatus remodelling to PEs in myoblasts. We identified SLMAP3 in a novel complex with components of the MTOC, kinesin-1 motor proteins and nuclear lamins. AKAP9, pericentrin and PCM1, as well as Kinesin-1 members Kif5B, KLC1 and KLC2, are known to contribute to the proper positioning of nuclei in developing myotubes [20,35–37]. The ability of SLMAP3 to localize and assemble with components from the various organelles implies that it can influence their functions and organization in cell biology. The impact on genes associated with muscle development and new interactions of SLMAP3 reveal an essential role for this protein through mechanisms linking centrosomal and nuclear organization and activity.

2. Results

2.1. SLMAP3 is present in the centrosome and perinuclear membrane of skeletal myoblasts

The *slmap* gene encodes multiple protein isoforms, which display C-terminus transmembrane domain (TM) and coiled-coil (CC) domains along their structure [22,33,34] (electronic supplementary material, figure S1*a*). The TM domain anchors SLMAP to ER, mitochondria and perinuclear membranes [23,23,24], whereas the CC domains are responsible for protein–protein interaction, including its own self-assembly [24,38,39]. The SLMAP3 isoform additionally has an N-terminus containing an FHA (electronic supplementary material, figure S1*a*), which is necessary to target the centrosome [22,40]. SLMAP3 is ubiquitously expressed whereas the other isoforms are expressed in a tissue-specific manner, with muscle subtypes

exhibiting diverse isoforms [33,34]. SLMAP3 localization in skeletal myoblasts was examined by transducing C2C12 cells with adenovirus carrying SLMAP3 tagged with green fluorescent protein (GFP-SLMAP3) and inducing their differentiation in low serum medium for 3 days (electronic supplementary material, figure S1*b*). In undifferentiated and differentiated myoblasts (stained for MyoG), GFP-SLMAP3 localized in the centrosome (arrows) and NE (arrowhead). Upon differentiation, GFP-SLMAP3 localization in the NE becomes more evident and correlates with pericentrin localization at this structure (electronic supplementary material, figure S1*b*). The cytoplasmic localization of GFP-SLMAP3 corresponds to the ER, which was stained for calnexin, with Pearson`s $r = 0.705$ and Mander' s coefficients $M1 = 0.991$ and $M2 = 0.963$ (electronic supplementary material, figure S1*c*). The Golgi staining with anti-GM130 showed poor colocalization of GFP-SLMAP3 with this organelle (Pearson`s $r = 0.241$). These data demonstrate that in skeletal myoblasts SLMAP3 localizes in the centrosome, NE and in the ER, but not in the Golgi apparatus.

2.2. Genes downregulated in SLMAP3$^{-/-}$ mice embryos enrich for muscle developmental processes

Since the *in vivo* function of SLMAP remains elusive, we have generated a floxed mouse line for global ablation of SLMAP3 using the Cre-Lox system. The loxP sites were inserted flanking exon 3 of the *slmap* gene (reference ENSMUST00000139075.8; figure 1*a*) as described [31], and these mice were crossed with CMV-Cre mice to create the SLMAP3$^{-/-}$ animals (figure 1*b*). The resulting mice exhibit late embryonic/perinatal lethality due to underdeveloped essential organs, such as lungs, and display other phenotypes including short tail and limbs (figure 1*c*) and reduced body weight (figure 1*d*).

For a better characterization of SLMAP3$^{-/-}$ embryonic phenotype, we performed RNA sequencing of whole E11.5 embryos from SLMAP3$^{-/-}$ and wild-type (WT) animals (electronic supplementary material, table S1). The significant genes with log2 fold change below or equal to −0.75 were selected as query for the tissue-specific expression analysis (TSEA) tool [41,42] and for gene ontology enrichment analysis on g:Profiler [43]. TSEA results indicate the strongest enrichment of muscle tissues, with statistical significance reached in all specificity index thresholds (pSI; figure 1*e*), and the topmost significant enriched biological processes detected on g:Profiler are associated with muscle development (figure 1*f*). The data are also available in the Gene Expression Omnibus (GEO) genomics data repository with the accession number GSE230748.

2.3. SLMAP3 exists in association with MTOC proteins and nuclear lamins

To investigate SLMAP3 interactors *in vivo*, we performed immunoprecipitation followed by mass spectrometry (IP–MS) with protein lysates from E12.5 mouse brain, an organ where only the SLMAP3 isoform is expressed (figure 2*a*). We identified SLMAP3 in a new complex with AKAP9, PCNT, PCM1, Kinesin-1 subunits (Kif5B, KLC1 and KLC2) and lamin B as well as the expected STRIPAK component striatin (STRN) (electronic supplementary material, table S2). The IP–MS data were validated by IP with anti-SLMAP and western blot with anti-STRN and anti-lamin B1, both of which were detected in the IP–MS (figure 2*b*). The SLMAP3 interactors were used for gene ontology enrichment analysis on g:Profiler. The top cellular components enriched include cytoskeleton (GO:0005856) and supramolecular complex (GO:0099080), but also

centrosome (GO:0005813), microtubule cytoskeleton (GO:0015630) and MTOC (GO:0005815; figure 2*c*). The proteins enriching these cellular components are shown in figure 2*d*. These proteomics data are available via ProteomeXchange with identifier PXD041687, and the exclusive unique spectrum counts of the interactors are given in electronic supplementary material, table S2.

It is notable that SMAP3 is a component of the MTOC and localizes to the NE and its newly identified interactors (PCNT, PCM1, AKAP9, kinesin-1 and lamin B) also reside at these locations, providing credence to the IP–MS data. These proteins play important roles during skeletal muscle development, by participating in nuclear positioning and in centrosomal MTOC switch to the NE [11,12]. Considering the downregulation of genes associated with muscle development and the identification of the aforementioned proteins in complex with SLMAP3, we speculated that depletion of SLMAP3 impairs muscle development by affecting the function of MTOC.

2.4. SLMAP3$^{-/-}$ myoblasts display differentiation and myotube formation defects

To elucidate the role of SLMAP3 in skeletal muscle development, we generated SLMAP3 $^{-/-}$ C2C12 myoblasts with CRISPR/Cas9, as these cells represent an excellent model of myogenesis. Two guide RNAs were designed to target exon 3 of SLMAP (reference ENSMUST00000139075.8) next to the predicted start codon (electronic supplementary material, figure S2*a*), keeping the same strategy of exon 3 disruption as in our Cre-Lox SLMAP3$^{-/-}$ mouse. A monoclonal colony of each guide was selected for further experiments, designated KO1 and KO2 (colony 90 and 14, respectively), with depletion of the SLMAP3 protein assayed by western blots (electronic supplementary material, figure S2*b*) and immunofluorescence staining of SLMAP3 in KO2 (electronic supplementary material, figure S2*c*). Skeletal myogenesis is regulated by the myogenic regulatory factors (MRFs) comprising the basic helix‐loop‐helix transcription factors MyoD, Myf5, MyoG and MRF4 [3]. To assess any impact of SLMAP3 loss on the differentiation of C2C12 myoblasts, we investigated the expression of these MRFs. Real-time quantitative polymerase chain reaction (RT-qPCR) indicated downregulation of MyoD and MyoG (figure 3*a*), with MyoD and MyoG expression reduced ~9-fold and ~19-fold, respectively, due to SLMAP3 loss (figure 3*b*,*c*), which is similar to what we observed in SLMAP$^{-/-}$ embryos. These results indicate that deletion of SLMAP3 in C2C12 myoblasts recapitulates transcriptional changes observed in SLMAP3$^{-/-}$ embryos and represents an excellent model to investigate further the mechanisms of SLMAP3 action in myogenesis.

Given the changes in the MRF transcripts in SLMAP3−/− C2C12 myoblasts, we proceeded to differentiation assays. For this, we incubated cells with 2% horse serum medium and collected protein lysates on days 0, 2 and 4 of differentiation for western blot analysis. The results show that both SLMAP3−/− C2C12 cells have drastically reduced expression of MyoG and myosin heavy chain (MHC) proteins, although no changes in MyoD levels were observed on day 0 and day 2 of differentiation (figure 3*d*), despite the reduced transcripts observed in the RT-qPCR (figure 3*a*). On day 4, the KO cells still had significant MyoD expression, which is reflective of a defect in differentiation. A significantly reduced fusion index during differentiation of SLMAP3$^{-/-}$ myoblasts was also notable by day 4 (figure 3*e*), and on day 8 of differentiation, it was reduced by ~93% in KO1 and ~40% in KO2 (figure 3*e*). These findings indicate that SLMAP3 is important for the proper skeletal myoblast differentiation and fusion via mechanisms involving the temporal expression of key myogenic factors such as MyoG and MyoD.

2.5. Depletion of STRN3, a STRIPAK component, does not affect myoblast differentiation

SLMAP3 is found in complex with STRIPAK together with STRN3, the latter that acts as a regulatory B‴ subunit of PP2A phosphatase [25,26]. Similarly to SLMAP3, STRN3 knockout results in embryonic lethality with complete penetrance [44]. Due to the partnership between SLMAP3 and STRN3 in the STRIPAK, and because of the lethal phenotype with their knockout, we questioned if depletion of STRN3 would also affect skeletal myoblasts. Two shRNAs targeting STRN3 and a shRNA scramble (SC) control were designed and packaged in lentivirus and used to transduce C2C12 myoblasts. Both the shRNAs reduced STRN3 protein levels, but shRNA STRN3#2 completely abolished its expression (figure 3*f*). Induction of myoblast differentiation with low serum levels showed that the C2C12-shRNA STRN3#2 cells did not have reduced expression of MyoD, MyoG or MHC (figure 3*g*), nor any impairment of myotube formation (figure 3*h*) after 5 days of differentiation compared to the C2C12-shRNA SC control. These findings suggest that SLMAP3 action in myoblast differentiation is distinctly unique from that of STRN3.

2.6. Differentiating SLMAP3$^{-/-}$ myoblasts present defective MTOC recruitment to the NE and reduced Golgi-belt like ring structure formation

Given that SLMAP3 can reside at the centrosome in association with its identified interactors AKAP9, PCNT, PCM1 and kinesin-1 subunits, we hypothesized that it contributes to the function of these proteins in myogenesis. To investigate this, we analysed the MTOC switch from the centrosome to the NE during the differentiation of SLMAP3$^{-/-}$ C2C12 cells.

Firstly, we performed the differentiation of SLMAP3$^{-/-}$ C2C12 myoblasts for 5 days and analysed the localization of pericentrin, AKAP6 and Kif5b proteins by immunofluorescence. AKAP6 was reported to be a key player in the MTOC switch of centrosomal proteins to the NE [18,21]. Because these proteins were described to localize in the NE after MyoG expression [21], we only analysed MyoG+ cells. With CellProfiler software, we used the MyoG staining to mask the cells and quantify their pericentrin, AKAP6 and Ki5fb mean intensity staining in concentric bands of 1 μm around the nucleus, which were designated NE, perinuclear (Peri) and cytoplasm (Cyto). It is notable that pericentrin, AKAP6 and Kif5b have the NE recruitment impaired in SLMAP3$^{-/-}$ MyoG+ C2C12 cells (electronic supplementary material, figure S3*a–c*, respectively). The mean intensity of pericentrin, AKAP6 and Kif5b in the NE was 5.5-fold, 3.5-fold and 2.47-fold higher in the WT compared to the KO cells. Also, the differences in the mean intensity between NE and Cyto for their staining in SLMAP3$^{-/-}$ MyoG+ C2C12 cells were reduced compared to WT controls, suggesting a reduced recruitment of these proteins to the NE.

If pericentrin, AKAP6 and Kif5b recruitment to the NE is affected, then a defective remodelling of the Golgi apparatus to Pes is also expected. AKAP6 was reported to be recruited to the NE by the interaction with the LINC complex member Nesprin-1 α [18,21,45]. AKAP6 binds to AKAP9, which in turn is important for Golgi recruitment [18]. To assess the Golgi remodelling, we measured the intensity of the staining Golgi around the nucleus of MyoG+ cells, with the modification of having the first band starting 0.5 μm further from the NE, and then calling the resulting bands as Peri, Cyto1 and Cyto2. The recruitment of Golgi apparatus to PEs was reduced in SLMAP3$^{-/-}$ myoblasts as well, with a higher difference between the mean intensity in the Peri and Cyto2 bands in the WT compared to the KO cells (figure 4*a*).

To test if the reduced recruitment of centrosomal proteins to the NE of SLMAP3$^{-/-}$ myoblasts was because of either a delayed differentiation or an anchorage defect, we performed

the pericentrin, AKAP6 and Kif5b analysis again, but in MHC+ cells after 8 days of differentiation. Remarkably, their recruitment to the NE was still significantly impaired in SLMAP3$^{-/-}$ MHC+ cells (figure 4*b–d*). To further validate this finding, we analysed pericentrin recruitment to the NE in MHC+ cells in two other colonies generated by each sgRNA, and the same phenotype was observed (electronic supplementary material, figure S3*d*). To rule out the possibility of reduced expression of these proteins due to the differentiation defects, we performed western blot with C2C12 lysates after 8 days of differentiation, and the expressions of AKAP6 and Kif5b were not significantly different from that of the control WT cells (figure 4*e*). Additionally, after 8 days of differentiation, the MHC expression in C2C12 KO2 cells was no longer significantly reduced compared to the WT (figure 4*e*). Therefore, the reduced presence of AKAP6, Kif5b and most likely pericentrin in the NE is due to protein mislocalization and not changes in their protein levels.

Although depletion of STRN3 did not affect C2C12 differentiation or myotube formation, we tested if this protein had any impact on the recruitment of MTOC proteins to the NE. After 5 days of differentiation, the STRN3-depleted cells did not present defective pericentrin recruitment to the NE (figure 4*f*).

These findings suggest SLMAP3 has a unique mode of action in muscle formation through a structural mechanism involving the anchorage of centrosomal proteins to the NE, and consequently, for the Golgi remodelling in PEs and myoblast differentiation, a function that is distinct from STRN3.

2.7. Differentiating SLMAP3$^{-/-}$ myoblasts display defective microtubule growth from the NE

Analysis of microtubule cytoskeleton in both SLMAP3$^{-/-}$ and WT cells before differentiation does not indicate any obvious differences between them (figure 5*a*). Also, microtubule nucleation assay with α-tubulin and AKAP9 staining shows centrosomal microtubule nucleation in both undifferentiated SLMAP3$^{-/-}$ and WT cells (figure 5*b*). However, it is observable that microtubule nucleation from the centrosome in SLMAP3$^{-/-}$ cells is stronger compared to WT myoblasts (arrows in figure 5*b*). This could be because in the WT cells, there was already a level of decentralization of MTOC activity from the centrosome to the NE (arrowhead in figure 5*b*). In SLMAP3$^{-/-}$ fibroblasts, the microtubule cytoskeleton and Golgi (electronic supplementary material, figure S4*a*) and microtubule growth from the centrosome (electronic supplementary material, figure S4*b*) do not have any obvious abnormalities. Additionally, microtubule nucleation remains in the centrosome of fibroblasts rather than decentralized to the Golgi (electronic supplementary material, figure S4*c*). This is consistent with our findings in undifferentiated C2C12 myoblasts, where centrosomal MTOC activity is not reduced in cells lacking SLMAP3.

Next, we asked how the microtubule growth would appear in SLMAP3$^{-/-}$ C2C12 cells after differentiation, considering their defective MTOC switch to the NE. The initial visualization of the microtubule cytoskeleton in myotubes after 5 days of differentiation shows that parallel arrays of microtubules along the myotube structure are present in both SLMAP3$^{-/-}$ and WT myoblasts (figure 5*c*). To visualize the sites of microtubule growth, we performed a microtubule nucleation assay. It is visible that the microtubule growth in SLMAP3$^{-/-}$ myotubes takes place in the cytoplasm (figure 5*d*). By performing this same assay but with Golgin-97 staining, it became evident that those sites of microtubule nucleation in the cytoplasm correspond to the dispersed Golgi (figure 5*e*). The quantification of the mean intensity of α-tubulin staining in the NE was

also significantly reduced in SLMAP3$^{-/-}$ MyoG+ cells (figure 5*f*), suggesting reduced microtubule nucleation from the NE in differentiation.

These results suggest two things: firstly, the nucleation of the microtubules from the NE in SLMAP3$^{-/-}$ myotubes is compromised, consistent with our findings of the defective MTOC switch; secondly, the microtubule nucleation from the centrosome before differentiation and from the Golgi after differentiation is unaffected. Thus, in the context of skeletal myogenesis, SLMAP3 is important for microtubule nucleation specifically from the NE.

2.8. Skeletal Muscle of SLMAP3$^{-/-}$ embryos display defective recruitment of pericentrin to the NE and nuclear mispositioning

Given the downregulation of genes involved in muscle development in SLMAP3$^{-/-}$ embryos and the defects in differentiation, myotube formation and MTOC switch, we analyed sections of hind limbs at E16.5, a time when secondary myogenesis is taking place and sustained mostly by myoblast fusion [3]. It is notable that the overall muscle in the SLMAP3$^{-/-}$ embryos, visualized by haematoxylin and eosin (H&E) staining, is smaller compared to WT (figure 6*a*). We manually quantified the fibre length across the muscle using Fiji software and found that the fibre length in SLMAP3$^{-/-}$ embryos was reduced by approximately 40% when compared to WT (figure 6*a*). Although we could not identify significant changes in the diameter and in the number of nuclei per fibre of the SLMAP3$^{-/-}$, we found that the inter-nuclear distance within the fibres was approximately half of the distance in WT embryonic muscle (figure 6*a*). In one SLMAP3$^{-/-}$ embryo, multiple muscle fibres show agglomeration of nuclei (figure 6*a*), compared with the even spread seen in WT. These findings suggest that the mechanism of muscle abnormalities in SLMAP3$^{-/-}$ embryos involves, at least partially, an impairment of nuclei positioning.

The fact that we could not identify differences in the number of nuclei per fibre in SLMAP3$^{-/-}$ embryos could be an indication that myoblast fusion was not as impaired as we observed in culture during differentiation of C2C12 myoblasts. Also, although the overall muscle is smaller and the inter-nuclei distance is reduced in SLMAP3$^{-/-}$ embryos, the muscle fibres are visibly formed (figure 6*a*). Additionally, at E16.5, the analysis of MHC expression in the limbs by western blot indicates no difference in SLMAP3$^{-/-}$ embryos compared to WT (figure 6*b*), despite the observed downregulation of skeletal muscle genes in these animals at E11.5. It could be that the muscle development in SLMAP3$^{-/-}$ embryos is delayed, but it reaches the formation of muscle fibres by E16.5 through endogenous compensatory mechanisms that are absent in tissue culture. It is also plausible that temporal expression of other SLMAP isoforms may compensate for SLMAP3 deficiency in the various fibre types [31,32].

Since SLMAP3 appears to be involved in the centrosomal MTOC switch to the NE in cultured myotubes, we investigated quadriceps muscles of SLMAP3$^{-/-}$ embryos to see if a similar MTOC switch was evident *in vivo*. Immunofluorescence staining indicated that pericentrin could be observed in the NE of MHC+ tissue, but this staining was weaker and much less defined in SLMAP3$^{-/-}$ muscles compared to WT (figure 6*c*). These data are similar to that seen in cultured myotubes derived from SLMAP3$^{-/-}$ C2C12 myoblasts (figure 4*b*). We also analysed the protein expression of AKAP6 and Kif5b in the limbs of E16.5 embryos lacking SLMAP3, and no differences were seen compared to the WT (figure 6*d*), which is consistent with our observations in C2C12 derived myotubes (figure 4*e*).

Collectively our data imply that loss of SLMAP3 in C2C12 myoblasts or *in vivo* negatively impacts muscle development at the level of NE-MTOC dynamics.

2.9. Differentiating SLMAP3$^{-/-}$ myoblasts have abnormal localization of LINC complex proteins

Given our data that the MTOC switch is critically dependent on SLMAP3 for myogenesis, we assessed if the localization of Nesprin-1 was also affected in differentiating MyoG+ myoblasts. Kinesin-1 was reported to be important for nuclei positioning in myoblasts, and it is recruited to the NE by Nesprin-1α [10,20,35–37,46,47]. Nesprin-1α is also responsible for the recruitment of AKAP6 [18,21,45]. Since SLMAP3 appears in complex with centrosomal proteins that are mislocalized in SLMAP$^{-/-}$ myoblasts, we examined any changes in anchorage of Nesprin-1 in the NE by comparing its mean intensity of staining between the NE band and distribution in the nucleoplasm. Surprisingly, the Nesprin-1 mean intensity in the NE was reduced in the SLMAP3$^{-/-}$ MyoG+ cells (figure 7*a*). If the lack of SLMAP3 was affecting solely the MTOC proteins and Kinesin-1, we would expect an intact Nesprin-1 staining, which does not seem to be the case.

Since Nesprin-1, a LINC complex member [48], was affected in the myoblasts lacking SLMAP3, we asked if lamins would also be changed in these cells. Lamins are intermediate filaments that decorate the inner side of the NE, and lamin A/C interacts with Nesprin-1α [48]. Lamins B1 and B2 have a constitutive expression in all cells and are encoded by two different genes, while lamin A/C are encoded by the single gene *lmna* and expressed only in differentiated cells [48]. For lamin A/C we analysed only MyoG+ cells since it has been demonstrated that myoblasts at this stage of differentiation already display higher lamin A/C recruitment from the nucleoplasm to the NE [49,50]. Indeed, the NE staining of lamin A/C was reduced in SLMAP3$^{-/-}$ MyoG+ cells when compared to the WT myoblasts (figure 7*b*). The NE recruitment of the constitutive lamin B1 was only slightly changed in SLMAP3$^{-/-}$ cells before differentiation (figure 7*c*). These results suggest that the lack of SLMAP3 also impacts the LINC complex and is important for the proper recruitment of Nesprin-1 and lamins to the NE in myoblasts.

2.10. SLMAP3 effects on developing muscle are independent of Hippo Signaling

SLMAP3 has been reported to be part of the STRIPAK complex [25,26], in an evolutionary conserved way [39,51], and proposed to negatively regulate the Hippo pathway (figure 8*a*), which consists of a cascade of kinases leading to the phosphorylation of the transcriptional coactivators YAP and TAZ, resulting in their cytoplasm sequestration and degradation. In the proposed mechanism, SLMAP3 recruits the serine/threonine sterile-20-like kinases MST1/2, to STRIPAK, where they are dephosphorylated and deactivated by PP2A phosphatase. The depletion of SLMAP3 could then result in higher activation of MST1/2, reducing the nuclear localization of YAP and TAZ and, consequently, decreasing the expression of genes associated with growth, proliferation and survival [27–30].

Due to the observed skeletal muscle abnormalities in SLMAP3 KO embryos, we analysed YAP phosphorylation in E16.5 limbs. No significant differences were detected between SLMAP3 KO and WT embryos (figure 8*b*). Further analysis of YAP and MST1/2 phosphorylation in C2C12 myoblasts does not indicate any changes in SLMAP3 KO myoblasts either, even with okadaic acid treatment to inhibit PP2A (figure 8*c,d*). Furthermore, the RNA-seq did not reveal any impact on Hippo-regulated genes due to SLMAP3 loss. Together, these results strongly suggest that the defective muscle development due to SLMAP3 loss is independent of any involvement of Hippo

signalling. Our data also indicated that STRN3, which is a key regulator of Hippo, was without effect on myotube formation or the NE-MTOC.

3. Discussion

We established that SLMAP3 is critical for the formation of muscle through mechanisms that involve the positioning of the nuclei and the switch of MTOC components from the centrosome to the NE during myogenesis. SLMAP3 is structurally designed to target the MTOC and NE; thus the impairment in MTOC dynamics due to SLMAP3 loss could be a result of defective attenuation of centrosomal activity, i.e. reduced microtubule nucleation from the centrosome and/or failure in the anchoring of the MTOC machinery to the NE. The newly identified interactors of SLMAP3 (AKAP9, PCNT, PCM1 and Kinesin-1 subunits) that are MTOC components further support the role of SLMAP3 in the positioning of centrosomal proteins. The impact of SLMAP3 loss on muscle-specific gene expression as well as nuclei mispositioning in developing myofibres point to a novel role at the NE in connecting cytoskeletal changes to nuclear function.

In microtubule nucleation assays, we observed microtubules growing from the Golgi of SLMAP3$^{-/-}$ myoblasts upon differentiation. It is tempting to assume that some level of centrosome attenuation was occurring to increase the MTOC activity in the Golgi instead of NE. In RPE1 cells, laser ablation of centrosome induces microtubule nucleation in the Golgi, suggesting that the excess of MTOC proteins go to this organelle [52]. However, we should consider that: firstly, the microtubule growth colocalizing with Golgi in SLMAP3$^{-/-}$ cells could correspond to centrosomes from the fused cells that failed to migrate to the NE. Clustering of centrosomes from fused cells is observed in osteoclasts [53]. Secondly, in the context of skeletal myogenesis, the microtubule growth from the Golgi could be independent of centrosome attenuation. Therefore, we suggest that SLMAP3 could be important for the attenuation of centrosome activity, as modelled in figure 9, where SLMAP3 interacts with centrosomal components via its N-terminal FHA domain and targets the NE through the C-terminal hydrophobic tail anchor. We know it is not important for microtubule nucleation because the centrosomal microtubule growth in SLMAP3$^{-/-}$ myoblasts was not impacted, and SLMAP3 is not associated with the Golgi [23,38,40], an organelle known to have microtubule nucleation activity [54–57].

Our data that the loss of SLMAP3 impacted the distribution of MTOC components at the NE during differentiation further imply a mechanism where SLMAP3 contributes to the anchorage of MTOC proteins at the NE (figure 9). In addition, the recruitment of Nesprin-1, which is not an MTOC protein and therefore independent of centrosomal attenuation, was also affected at the NE in differentiating SLMAP3$^{-/-}$ myoblasts (figure 9). We noted a reduction in lamin A/C at the NE with redistribution in the nucleoplasm in SLMAP3$^{-/-}$ myoblasts, which supports a role for SLMAP3 in organizing the nuclear cytoskeleton. In this regard, our data here also suggest interactions of SLMAP3 with nuclear lamins, indicating that SLMAP could potentially reside at the nuclear face of the NE to impact gene activity, although this remains to be tested.

The implication of defective recruitment of centrosomal proteins to the NE during skeletal myogenesis is nuclei mispositioning, a feature observed in patients with EDMD and CNM [11,12]. In EDMD, it is usually caused by mutations in genes encoding proteins from the LINC complex, such as emerin, SUN1, SUN2, lamin A/C and Nesprin-1 and Nesprin-2 [14,48,58], characterized

by progressive muscle weakness and wasting, early contractures and cardiac abnormalities [13,14]. In differentiating myoblasts, the NE up to the Golgi is organized as follows: in the LINC complex, Nesprin-1 and Nesprin-2 members localize in the outer nuclear membrane (ONM) [48], although their smaller isoforms can also localize in the inner nuclear membrane (INM) [59–61]. In the NE lumen, the KASH domain of Nesprin proteins interacts with the SUN domain proteins, which are anchored in the INM [46]. In the INM, both the SUN proteins and the smaller Nesprin isoforms interact with lamin A/C and emerin [48,62]. Additional proteins are recruited to the ONM by interaction with Nesprin-1α, a smaller isoform of Nesprin-1. These include the motor proteins from the dynein and kinesin-1 complexes [10,20,36,37,47] and the protein AKAP6 [18,21,45]. Another level of organization is the binding of the paralogues AKAP9 and pericentrin to AKAP6 [18,21]. The Golgi belt-like ring structure around the nucleus is then tethered by AKAP9 [18]. In this organization, microtubules could be nucleated from both NE and Golgi [17,18].

We found that SLMAP3 interacts with the outer layer proteins, such as Kinesin-1 and centrosomal proteins. However, because we observed abnormalities in the distribution of all these proteins in SLMAP3$^{-/-}$ myoblasts, SLMAP3 may also be important for the proper localization of the LINC complex. Our finding that SLMAP3 interacts with proteins of the nuclear cytoskeleton implies that SLMAP3 could integrate the MTOC-NE dynamics via its structural domains. The alternative hydrophobic C-terminal sequences in SLMAP3 would make it an ideal candidate to target both outer and INMs to orient the protein so as to serve functions across the NE thus integrating centrosomal activity with the nuclear lamina, although this needs to be tested.

Depletion or mutation of LINC complex members, AKAP6 and Kinesin-1, have been reported to lead to differentiation and myotube formation defects [47,49,63–68] (electronic supplementary material, table S3) much like that seen here with SLMAP3 loss, potentially indicative of a common pathological mechanism. Changes in emerin and lamin A/C can lead to changes in the tethering of heterochromatin in the NE and impact the expression of genes of the myogenic programme [61,69]. It is conceivable that loss of SLMAP3 leading to the redistribution of lamins at the NE may also impact chromatin dynamics and lead to the observed changes in muscle gene expression.

Although SLMAP3$^{-/-}$ myoblasts presented a reduced fusion index and decreased expression of MyoG and MHC, SLMAP3$^{-/-}$ embryos at E16.5 did not indicate any changes in MHC expression. E11.5 embryos showed a decrease in the expression of genes involved in muscle development, and the muscle from SLMAP3$^{-/-}$ E16.5 embryos was clearly abnormal, with reduced fibre size and inter-nuclei distance. Differentiation defects have been reported in culture for mutations in lamin A/C and emerin [49,63–67], while mice null for either of them are born without observable muscle defects [70,71]. Lamin A/C KO animals becomedystrophic a few weeks after birth [68], and the emerin KO mice have defective muscle regeneration [71]. Therefore, skeletal muscle differentiation problems in SLMAP3$^{-/-}$ animals could become even more evident in the context of muscle regeneration.

In our analysis of the microtubule cytoskeleton of differentiated SLMAP3$^{-/-}$ myoblasts, we noticed that parallel arrays of microtubules were present. However, with microtubule nucleation assay we could see that microtubules were growing from sites colocalizing with Golgi. The presence of parallel arrays of microtubules even when the NE-MTOC is impaired seems to be

a common feature, since it was observed in differentiated myoblasts with knockout or depletion of Nesprin-1α, Sun1, Sun2, Sun1/2, Kif5b and AKAP6 [10,20,21,36,72].

The fact that SLMAP3 as a STRIPAK component was found to be crucial in the NE-MTOC formation suggests that other members of the complex could also play a role in this process. However, the depletion of STRN3 had no impact on NE-MTOC or myogenesis. Whether other paralogues STRN or STRN4 could serve compensatory roles needs consideration, although the knockout of either STRN3 or STRN is enough to result in embryonic lethality.

Finally, despite the mechanistic descriptions of SLMAP3 as a negative regulator of the Hippo pathway [27–30], changes in this signalling cascade could not be detected in the limbs of SLMAP3$^{-/-}$ embryos or SLMAP3$^{-/-}$ myoblasts. In myoblasts, YAP was reported to be important in the early proliferative phase, but its cytoplasmic sequestration is essential for terminal differentiation [73]. In human cardiomyoblasts, the activation of MST and LATS kinases was sufficient to induce centrosome disassembly and relocation of PCM proteins to the NE [74]. If loss of SLMAP3 was inducing Hippo, then we would expect no defects in the terminal differentiation *in vivo* or in myoblasts. Therefore, the defects observed in SLMAP3 deficiency are most likely independent of Hippo and point to novel mechanisms involving the newly identified interactors of SLMAP3, including AKAP9, Kinesin-1 and centrosomal components. It is notable that STRN3 loss had no impact on the MTOC or myotube development implying that distinct STRIPAK components may serve unique roles in a cell-/tissue-specific manner as exemplified here by SLMAP3.

4. Conclusion

Here we identify SLMAP3 as an essential player in developing skeletal muscle by participating in positioning nuclei and the formation of MTOC at the NE to impact the differentiation programme. Our data define a novel role for SLMAP3 in the formation of non-centrosomal MTOCs and link to nuclear activity and tissue development. The ability of SLMAP3 to assemble with components of the MTOC and the nuclear membrane makes it an ideal player to serve such functions which appear to be independent from any involvement with Hippo signalling.

5. Methods and Materials

5.1. Transgenic Mice Generation

The generation of the flox-SLMAP mouse line was already described in detail [31]. The Cre transgenic mouse was a gift from Dr Nemer Mona, University of Ottawa. For the genotyping of both mouse lines and the breeding strategy, we followed the procedures already described [31]. The mice in this study were housed at the Animal Care and Veterinary Service (ACVS) Barrier Facility at the University of Ottawa and handled in compliance with the Canadian Council on Animal Care, Guide to the Care and Use of Experimental Animals, 2 vols. (Ottawa, Ont.: CCAC, 1980−1993) and Animals for Research Act, R.S.O. 1990, c.A. 22. The protocols for animal study were approved by the Animal Care Committee at the University of Ottawa.

5.2. Cell Culture and Treatment Conditions

MEFs were isolated from E14.5 embryos as described [75], and tails were used for genotyping. All WT MEFs used are from littermates of SLMAP3$^{-/-}$ embryos. The C2C12 myoblast

cell line was commercially provided by the American Type Culture Collection. Cells were kept in humidified atmosphere with 5% CO2 and at 37° C. For MEFs, we used a medium containing high glucose Dulbecco's Modified Eagle Medium (DMEM) (Wisent, cat. 319-005), 1× MEM (Gibco, cat. 11140050), 20 mM HEPES, 10% fetal bovine serum (FBS; Wisent, cat. 080-150), 1 × antibiotic-antimycotic (Gibco, cat. 15240062) and 0.1 mM β-mercaptoethanol, as described [76]. For C2C12 cells, we used a medium containing DMEM (Wisent, cat. 319-005), 10% FBS (Wisent, cat. 080-150) and 1× antibiotic-antimycotic (Gibco, cat. 15240062). The C2C12 differentiation medium was prepared with DMEM without sodium pyruvate (Wisent, cat. 319-015), 1× antibiotic-antimycotic (Gibco, cat. 15240062), 25 mM HEPES and 2% horse serum (Gibco, cat. 16050122). We considered 'differentiating myoblasts' all the cells incubated with differentiation medium. For okadaic acid (Cell Signaling, cat. 5934) condition, we used a final concentration of 1.5 μM for 1 h of treatment. For transfections, we used Lipofectamine 3000 (Invitrogen, cat. L3000001) following the protocol of the manufacturer. Microtubule nucleation assays were performed in cells as described elsewhere [77], with the final nocodazole concentration of 8.3 μM and incubation time of 2 h at 37° C. After nocodazole washout in cold medium, coverslips were kept in the saponin solution at 37°C for 45 s, followed by incubation with medium at 37°C for 50 s. Cells were subsequently fixed in freezer-cold methanol for 5 min.

5.3. SDS-PAGE and Western Blot

Protein lysates were extracted on ice from cells by cell scraping and by homogenization of snap-frozen tissue. The lysis buffer contained 20 mM Tris (pH 7.5), 150 mM NaCl, 1 mM EDTA, 1 mM EGTA and 1% Triton X-100. For each 10 ml of buffer, one tablet of Pierce Protease Inhibitor (Thermos Scientific, cat. A32955) and of Pierce Phosphatase Inhibitor (Thermo Scientific, cat. A32957) were used. Proteins were denatured with SDS buffer containing 10% glycerol, 2% SDS, 62.5 mM Tris-HCl (pH 6.8) and 10% β-mercaptoethanol and boiled for 5 min. The lysates were loaded on sodium dodecylsulfate polyacrylamide gel electrophoresis (SDS-PAGE) gel and posteriorly transferred to polyvinylidene fluoride membrane (Bio-Rad). For membrane wash, blocking and antibody solutions, we used Tris-buffered saline (TBS-T) buffer containing 1 M Tris, 290 mM NaCl and 0.1% Tween 20 (pH 7.4). Antibody solutions were prepared with 5% milk in TBS-T or with 5% BSA for primary antibodies targeting phosphorylated amino acid residues. Images were acquired on the Bio-Rad ChemiDoc system and analysed by densitometry on Image Lab Software (Bio-Rad). The list of the antibodies used for western blot (WB) is as follows:

Primary Antibodies				
Target	**Company**	**Catalog**	**Host**	**Dilution WB**
SLMAP	Novus Biologicals	NBP1-81397	Rabbit	1:500
SLMAP	Novus Biologicals	NBP1-81398	Rabbit	1:1000
STRN3/SG2NA (S68)	Novus Biologicals	NBP74572	Mouse	1:500
MST1 (KRS2)(H-8)	Santa Cruz	SC-515051	Mouse	1:200
MST2 (KRS1)(87.K)	Santa Cruz	SC-130405	Mouse	1:200

Phospho-MST1 (Thr183)/MST2 (Thr180) (E7U1D)	Cell Signaling	49332	Rabbit	1:500
YAP (1A12)	Cell Signaling	12395	Mouse	1:1000
Phospho-YAP (Ser127)(D9W2I)	Cell Signaling	13008	Rabbit	1:1000
MyoD (G-1)	Santa Cruz	SC-377460	Mouse	1:100
MyoG (F5D)	Santa Cruz	SC-12732	Mouse	1:100
MHC	Developmental Studies Hybridoma Bank	MF20	Mouse	1:50
Lamin B1	Abcam	ab16048	Rabbit	1:200
Vimentin (D21H3) XP	Cell Signaling Technology	5741	Rabbit	1:1000
Akap6	Millipore Sigma	HPA048741	Rabbit	1:100
Kif5B [EPR10276(B)]	Abcam	ab167429	Rabbit	1:100

Secondary Antibodies				
Target	**Company**	**Catalog**	**Host**	**Dilution WB**
Peroxidase AffiniPure Goat Anti-Rabbit IgG (H+L)	Jackson ImmunoResearch	111-035-144	Goat	1:10000
Peroxidase AffiniPure Goat Anti-Mouse IgG (H+L)	Jackson ImmunoResearch	115-035-146	Goat	1:10000

5.4. Real-Time Quantitative Polymerase Chain Reaction – RT-qPCR

Primers were designed using the Primer-Blast tool (NIH) and validated with standard curve and band size of PCR products from cDNA of C2C12 cells. RNAs were extracted from cells with RNeasy Mini Kit (cat. 74104) from Qiagen according to the protocol of the manufacturer. We synthesized cDNA from the RNAs with the iScript Reverse Transcription Supermix for RT-qPCR from Bio-Rad (cat. 1708840). RT-qPCR was performed with the FastStart Universal SYBR Green Master (Rox; Millipore Sigma, cat. 4913850001). Glyceraldehyde-3-phosphate dehydrogenase (GAPDH) was used as the housekeeping gene. The samples were read on a Bio-Rad CFX 96 thermal cycler, and the data were analysed on Bio-Rad CFX Maestro. The primers used are listed below:

Primers	**Forward (5`-3`)**	**Reverse (5`-3`)**
Myf5	CTATTACAGCCTGCCGGGAC	CTCGGATGGCTCTGTAGACG
Mrf4	CCCCACAGATCGTCGGAAAG	CAGAATCTCCACCTTGGGCA
MyoG	CAGCCCAGCGAGGGAATTTA	AGAAGCTCCTGAGTTTGCCC
MyoD	ATAGACTTGACAGGCCCCGA	GCAGGTCTGGTGAGTCGAAA
Pax3	TCGAGAGAACCCACTACCCA	CCCCCGGAATGAGATGGTTG
GAPDH	GGTTGTCTCCTGCGACTTCA	TGGTCCAGGGTTTCTTACTCC

5.5. RNA-Sequencing

Total RNA was isolated from E11.5 whole embryos by RNeasy Fibrous Tissue Mini Kit according to the manufacturer protocol (Qiagen). The samples were then submitted to the StemCore Laboratories Genomics Core Facility at the University of Ottawa for RNA sequencing as follows: total RNA (1 μg) was quantified using a Qubit (Thermo Scientific), and its integrity was assessed on an AATI Fragment Analyzer (Agilent Technologies). Library construction was performed using TruSeq RNA v2 Library Preparation Kit (Illumina). Following library quality assurance/quality control (QA/QC) (as above for input), the eight libraries were pooled on a NextSeq 500 75 cycle High Output Flow cell with 1% PhiX spike-in. RNA-seq post-processing and differential expression analysis were prepared by the Ottawa Bioinformatics Core Facility. Briefly, reads were assigned to the GRCm38_GENCODE.vM19 transcriptome model using Salmon [78], and the differential expression of transcripts was analysed by DESeq2 [79]. The data discussed from this study have been deposited in NCBI's Gene Expression Omnibus [80,81] and are accessible through GEO Series accession number GSE230748 (https://www.ncbi.nlm.nih.gov/geo/query/acc.cgi?acc=GSE230748). The data were validated by RT-qPCR, with the analysis of the expression of *myod1*, *myog*, *myf5*, *myf6* and *pax3*.

5.6. Immunoprecipitation-Mass Spectrometry - IP-MS

Immunoprecipitation of SLMAP3 was performed on 75 μg of E12.5 mouse brain WT lysates by anti-SLMAP (Novus, cat. NBP1-81397) with Pierce™ Protein A/G Magnetic Beads (Thermo Fisher, cat. 88802) based on the manufacturer protocol. Immunoprecipitation of anti-IgG (Protein Tech, cat. 30000-0-AP) was performed identically and simultaneously as a control to identify non-specific interactions. The resulting samples were submitted to the Montreal Clinical Research Institute for MS as follows: pulled-down lysates incubated with anti-SLMAP and anti-IgG were treated with acetone to precipitate and purify approximately 20 μg of pellet. Protein extracts were then re-solubilized in 6 M urea buffer and 100 mM ammonium bicarbonate, followed by reduction with reduction buffer (45 mM DTT and 100 mM ammonium bicarbonate). Finally, samples were alkylated in 100 mM iodoacetamide and 100 mM ammonium bicarbonate. After reducing the urea concentration to 2M, 20 ng μL^{-1} of trypsin (Promega) was added to each sample, and digestion was performed at 37° C overnight. Prior to liquid chromatography with tandem mass spectrometry (LC-MS/MS), protein digests were re-solubilized in 0.2% formic acid. Desalting/cleanup of the digests was performed using C18 ZipTip pipette tips (Millipore). Dried eluates were reconstituted in 2% acetronile/1% formic acid and loaded into a 75 μm i.d. × 150 mm Self-Pack C18 column installed in the Easy-nLC II system (Proxeon Biosystems). The buffers used for chromatography were 0.2% formic acid (buffer A) and 90% acetonitrile/0.2% formic acid (buffer B). The high-performance liquid chromatography (HPLC) system was coupled to Orbitrap Fusion mass spectrometer Xcalibur 4.0 and Tune 2.0 (Thermo Scientific) through a Nanospray Flex Ion Source. Nanospray and S-lens voltages were set to 1.3-1.8 kV and 60 V, respectively. The capillary temperature was set to 250° C. Full scan MS survey spectra (*m*/*z* 360-1560) in profile mode were acquired in the Orbitrap with a resolution of 120 000 with a target value at 3×10^5 and a maximum injection time of 50 ms. The 20 most intense peptide ions were fragmented in the higher-energy collisional dissociation (HCD) cell and analysed in the linear ion trap with a

target value at 2×10^4, a maximum injection time of 50 ms and a normalized collision energy at 29. Target ions selected for fragmentation were dynamically excluded for 25 s after two MS/MS events.

The protein database searches were launched using Proteome DiscovererTM software from Thermo Fisher Scientific (v.2.4) and were performed with Mascot 2.6.2 (Matrix Science) against the mouse UniProt protein database (version 23 September 2019). The mass tolerances for precursor and fragment ions were set to 10 ppm and 0.05 Dalton, respectively. Trypsin was used as the enzyme allowing for up to one missed cleavage. Cysteine carbamidomethylation was specified as a fixed modification and methionine oxidation as a variable modification. Scaffold 5.2.2 was used to validate MS/MS-based peptide and protein identifications. Protein identifications were accepted if they could be established at greater than 95.0% probability and contained at least one identified peptide by the Protein Prophet algorithm [82]. Proteins that contained similar peptides and could not be differentiated based on MS/MS analysis alone were grouped to satisfy the principles of parsimony. Proteins sharing significant peptide evidence were grouped into clusters. The mass spectrometry proteomics data have been deposited to the ProteomeXchange Consortium via the PRIDE [83] partner repository with the dataset identifier PXD041687 and 10.6019/PXD041687. The data were validated by IP, where the interactions of SLMAP3 with lamin B1 and STRN, both detected in IP-MS, were confirmed.

5.7. Immunofluorescence and Image Processing

All images were acquired at the Cell Biology and Image Acquisition Core Facility at the University of Ottawa. For the slides with H&E staining and cell plate phase contrast, a Thermo Fisher EVOS FL Auto 2 was used. For fluorescence, we used the widefield Zeiss AxioObserver Z1 microscope, with the exception of images for Lamin B1 staining for which we used the widefield Zeiss AxioObserver D1 microscope. The images acquired were exported from Zen Blue and analysed in Fiji for image cropping. Background subtraction and contrast enhancement were applied for brightfield images. For the quantification of perinuclear staining, multiple images of each biological sample were analysed on CellProfiler by pipelines that we created and validated. In the pipelines, objects were created using 4′ ,6-diamidino-2-phenylindole (DAPI) staining. Further masking with MyoG or MHC staining selected cells positive for these markers. Expansion and shrinkage of DAPI objects followed by subtraction of the smaller object was used to generate three concentric bands of 10 pixels (pixel size $0.102 \times 0.102\ \mu m^2$) each. The mean intensity of the staining was measured in these bands. For pericentrin, AKAP6 and Kif5b, the bands were the NE, PE and cytoplasm (Cyto) objects. For Golgin-97 intensity measurement, these bands were shifted five pixels towards the cytoplasm, creating the PE, cytoplasm 1 (Cyto1) and cytoplasm 2 (Cyto2) objects. For Nesprin-1, lamin A/C and lamin B1, the mean intensity was measured on the NE object and in the DAPI object subtracted the NE, which was called the nucleoplasm object. The size of the NE object for lamin A/C and lamin B1 was four pixels, whereas for Nesprin-1, it was 10 pixels. For quantification of microtubule growth from the NE, we measured the mean intensity of α-tubulin staining in the NE object. For the fusion index, we used CellProfiler. For that, MHC staining was used to mask the nuclei. Myotubes containing at least two nuclei were considered and divided by the total nuclei identified in the field and multiplied by 100. Images

with microtubule staining were acquired in Z-stack, and image deconvolution was applied using the Regularized Inverse Filter on Zen Blue. All other images were acquired in a single plane and followed image processing. The list of the antibodies used for immunofluorescence (IF) is as follows:

Primary Antibodies				
Target	**Company**	**Catalog**	**Host**	**Dilution IF**
SLMAP	Novus Biologicals	NBP1-81397	Rabbit	1:200
MyoG (F5D)	Santa Cruz	SC-12732	Mouse	1:100
MHC	Developmental Studies Hybridoma Bank	MF20	Mouse	1:50
GM130	BD Biosciences	610822	Mouse	1:200
Golgin 97	Proteintech	12640-1-AP	Rabbit	1:100
Calnexin	Novus Biologicals	NB100-1974	Rabbit	1:200
Lamin B1	Abcam	ab16048	Rabbit	1:200
Pericentrin	Covance/Biolegend	PRB-432C	Rabbit	1:100
Akap9	Novus Biologicals	NBP1-89167	Rabbit	1:150
α-tubulin (DM1A)	Millipore Sigma	T6199	Mouse	1:300
Akap6	Millipore Sigma	HPA048741	Rabbit	1:100
Kif5B [EPR10276(B)]	Abcam	ab167429	Rabbit	1:100
Nesprin-1	Wolfson Centre For Inherited Neuromuscular Disease	MANNES1A	Mouse	1:100
Lamin A/C	Wolfson Centre For Inherited Neuromuscular Disease	MANLAC3	Mouse	1:4

Secondary Antibodies				
Target	**Company**	**Catalog**	**Host**	**Dilution IF**
Anti-Mouse IgG (H+L) Cross-Adsorbed Secondary Antibody, Alexa Fluor 647	Invitrogen	A-21235	Goat	1:300
Anti-Rabbit IgG (H+L) Cross-Adsorbed Secondary Antibody, Alexa Fluor 555	Invitrogen	A-21428	Goat	1:300
Anti-Rabbit IgG H&L, Alexa Fluor 488	Abcam	ab150077	Goat	1:200

5.8. Histology

For H&E staining, tissues were fixed on formalin 10%. The embedding, paraffinization, sectioning and staining were performed by the Louise Pelletier Histology Core Facility of the University of Ottawa.

5.9. Plasmids, Cloning and Viruses

The SLMAP3 mouse sequence was cloned as follows: cDNA from a mouse heart was used for SLMAP3 PCR amplification with Phusion® High-Fidelity DNA Polymerase (BioLabs, cat. M0530) and using, respectively, the SLPN-forward and SLPN-reverse primers 5′ -GATGCCAGCTTCTAGAGGGAGGACG and 5′ -GGAATTCGATGCCGTCAGCCTTGGC. The SLPN-F contains an EcoRI restriction site before the start codon of SLMAP, and the SLP-R has an Xba I site after the stop codon. These two sites were used to clone SLMAP3 into the pcDNA3-CMV- (Invitrogen, cat. V79020) vector where we had previously cloned GFP between KpI and Eco RI restriction sites. The resulting GFP-SLMAP3, with the GFP in the N-terminus of SLMAP3, was sequenced by the DNA Sequencing Facility at the Ottawa Hospital, and the construct was validated by western blot and fluorescence analysis of transfected cells.

The GFP-SLMAP3 adenovirus was produced with the AdEasy Adenoviral Vector System from Agilent Technologies (cat. 240009), following the manufacturer protocol [84]. Briefly, the GFP-SLMAP3 from pCDNA3 was amplified with the primers GFP-shuttle 5′ -GCGTCTAGAATGGACAAA GGAGAAGAACTC and pcDNA3.1-R 5′ -CAACAGATGGCTGGCAACTAG and cloned into the pShuttle vector. The resulting plasmid was linearized with Pme I and transformed into BJ5183-AD cells, which were pre-transformed with the pAdEasy-1 vector. The resulting plasmid from the recombination of both vectors was digested with Pac I, followed by transfection in AD-293 packing cells. The virus production and infection were also performed according to the manufacturer`s guidelines [84].

The shRNAs for STRN3 were designed with the following target sequences: shRNA#1−CACTGGTAGTGCGGTAATTTA and shRNA#2−AGCAAGGCAGACAGCTATTAA. The SC control was designed with the target sequence AGGATAAGCGTC AACGAATAGGTGA. ShRNAs#1 and #2 target sequences were cloned into pLV[shRNA]-Neo-U6 vector, and the shRNA SC target sequence into pLV[shRNA]-Puro-U6 plasmid, all performed by VectorBuilder. The lentiviruses were packed in Lenti-X 293 T cells with the psPAX2 and pMD2.G plasmids following the Addgene protocol [85]. The transduction of C2C12 was performed following the Addgene protocol [86]. After 3 days, cells transduced with shRNA#1 and #2 lentiviruses were selected with G418 750 μ g ml^{-1} for 6 days. Cells transduced with shRNA SC lentivirus were selected with puromycin 2.5 μ g ml^{-1} for 3 days. The depletion of STRN3 and the shRNA control were validated by western blot.

5.10. Cell Line Generation

The polyclonal C2C12 lines with *slmap* genetic disruptions were generated, as described elsewhere [87], at the Genomic Editing and Molecular Biology Core Facility in the Faculty of Medicine at the University of Ottawa. The following guide RNAs targeting exon 3 were used for the generation of CRISPR/Cas9 knockout: 5′ -AGTCGGGCTTCCATACCATC and 5′ -ATACTCA CTCTGAACGAAGT. These guides were cloned into pLentiCRISPRv2 (Addgene plasmid 52961 [87]), and the transduced cells were selected with puromycin 2.5 μ g ml^{-1} for 3 days. The gene cleavage was confirmed with T7 endonuclease I (NEB) using the following primer pairs: 5′ -CGGCCAGGAGAGACTATCAC and 5′ -TCCAAGTCTCATGGCGTGTG. We isolated monoclonal colonies from the cell pools generated with both guide RNAs by limiting

diluting according to Addgene [88]. We confirmed the selection of knockout colonies by western blot and immunofluorescence. For non-targeting control (NTC), we used the pLentiCRISPRv2 carrying a guide RNA targeting GFP (Addgene plasmid 86153 [89]), and the transduced C2C12 cells were selected with puromycin. No statistically significant differences were identified between not transduced and NTC C2C12 WT myoblasts in terms of differentiation, myotube formation and MTOC switch to the NE after differentiation.

5.11. Statistical Analysis

All the statistical analyses were performed on GraphPad Prism. Data were represented by mean and standard error of mean. For analyses with one variable with two groups, we used *t*-test. For three or more groups, we used one-way ANOVA followed by Newman-Keuls post-test. Tests with multiple variables were performed with two-way ANOVA followed by Bonferroni post-test. Statistical significance is indicated as $*p < 0.05$, $**p < 0.01$, $***p < 0.001$ and n.s. for not significant. At least three biological samples were used for all statistical analyses in this study.

Ethics. The mice in this study were housed at the Animal Care and Veterinary Service (ACVS) Barrier Facility at the University of Ottawa and handled in compliance with the Canadian Council on Animal Care, Guide to the Care and Use of Experimental Animals, 2 vols. (Ottawa, Ont.: CCAC, 1980-1993) and the Animals for Research Act, R.S.O. 1990, c.A. 22. The protocols for animal study were approved by the Animal Care Committee at the University of Ottawa.

Data accessibility. The RNA-seq from this study have been deposited in NCBI's Gene Expression Omnibus and are accessible through GEO Series accession number GSE230748 (https://www.ncbi.nlm.nih.gov/geo/query/acc.cgi?acc=GSE230748). The IP-MS results have been deposited to the ProteomeXchange Consortium via the PRIDE partner repository with the dataset identifier PXD041687 and 10.6019/PXD041687. The raw images of all western blots of this study are available in electronic supplementary material, S2.

Electronic supplementary material is available online.

Declaration of AI use. We have not used AI-assisted technologies in creating this article.

Authors' contributions. A.P.D.: conceptualization, data curation, formal analysis, investigation, methodology, resources, validation, writing-original draft; T.R.: conceptualization, investigation, resources, writing-original draft; M.S.: investigation, methodology, resources; B.T.: conceptualization, funding acquisition, supervision, writing–review and editing. All authors gave final approval for publication and agreed to be held accountable for the work performed therein.

Conflict of interests. We declare we have no competing interests.

Funding. This project was funded with grant 220996-151999 from the Canadian Institute of Health Research (CIHR) to B.T.

Acknowledgements. We thank Dr Nemer Mona for the Cre transgenic mice. We are also grateful for the assistance of all the facilities involved in this study: StemCore Laboratories Genomics Core Facility (RRID: SCR_012601); Ottawa Bioinformatics Core Facility (RRID: SCR_022466); Cell Biology and Image Acquisition Core (RRID: SCR_021845); Louise Pelletier Histology Core Facility (RRID: SCR_021737); Flow Cytometry & Virometry (FCV) Core Facility at the

University of Ottawa; Genomic Editing and Molecular Biology Core Facility (RRID: SCR_022954); and the Montreal Clinical Research Institute (IRCM, Quebec, Canada).

Figure Titles and Legends

Figure 1. Genes downregulated in SLMAP3$^{-/-}$ mouse embryos enrich for muscle developmental processes. (*a*) Mice carrying floxed *slmap* gene [31] were bred with mice carrying cre under CMV promoter to nullify SLMAP3 expression. (*b*) Western blot with an anti-SLMAP antibody that detects all isoforms showing SLMAP expression in SLMAP3$^{-/-}$, SLMAP3$^{-/+}$ and SLMAP3$^{+/+}$ E11.5 embryos. (*c*) Phenotype of SLMAP3$^{-/-}$ P0 mice, with short limbs and tails. (*d*) SLMAP3$^{-/-}$ pups have significantly reduced body weight when compared to SLMAP3$^{+/-}$ or SLMAP3$^{+/+}$ animals. (*e*) The tissue-specific expression analysis (TSEA) shows a significant enrichment of muscle tissues of the downregulated genes in SLMAP3$^{-/-}$ embryos in all specificity index threshold (pSI) stringencies. (*f*) The downregulated genes in RNA-seq from SLMAP3$^{-/-}$ embryos enrich for muscle developmental processes. Three SLMAP3$^{-/-}$ and four wild-type (WT) embryos were sequenced. Gene ontology enrichment performed using g:Profiler.

Figure 2. SLMAP3 interacts with MTOC proteins. (*a*) SLMAP3 (80‑95 kDa) is the only isoform present in E12.5 mouse brains, as indicated by the western blot analysis and the smaller isoforms SLMAP1 (35 kDa) and SLMAP2 (45 kDa) are undetected. (*b*) Validation of IP‑MS, confirming the interaction of SLMAP3 with Lamin B1 and STRN. (*c*) Cellular component enrichment of SLMAP3 interactors, identified by IP‑MS, performed on g:Profiler. (*d*) SLMAP3 interactors enrich for cytoskeleton, supramolecular complex, supramolecular fibre, supramolecular polymer, microtubule cytoskeleton, centrosome and MTOC cellular component.

Figure 3. SLMAP3$^{-/-}$ myoblasts display differentiation and myotube formation defects. (*a*) RT-qPCR shows that KO1 and KO2 cells have altered the expression of MRFs. (*b*) The RNA-seq from E11.5 was validated by RT-qPCR, where we confirmed the reduced expression of myod1 and myog. (*c*) Comparison of the mean log2 fold change (log2FC) values from the transcripts of both KO C2C12 cells and E11.5 embryos obtained by RT-qPCR. The C2C12 cells and embryos null for SLMAP3 have significantly reduced myod and myog expression. (*d*) Differentiation assay was performed with low serum media, and protein lysates were collected on days 0, 2 and 4. The western blot shows that C2C12 myoblasts lacking SLMAP3 have reduced MHC and MyoG protein levels. (*e*) Myotube formation in SLMAP$^{-/-}$ C2C12 cells is impaired. On differentiation day 4, very few myotubes are observed, and by day 8, the fusion index is still significantly reduced for both KO1 and KO2 C2C12 cells. Scale bar, 125 μ m. (*f*) Two shRNAs were designed to reduce the expression of STRN3. The shRNA#2 had the highest depletion in expression and was used for further experiments. Depletion of STRN3 did not impart C2C12 differentiation (*g*) or myotube formation (*h*). For (*a*,*b*), the RT-qPCR was performed in three technical replicates for each of the three biological replicates. For (*e*), the quantification of the fusion index on day 8 of differentiation was performed in many fields of each of the three biological replicates. The average of each biological replicate is plotted. *$p < 0.05$; **$p < 0.01$; ***$p < 0.001$; n.s., not significant.

Figure 4. Differentiating SLMAP3$^{-/-}$ myoblasts present defective MTOC recruitment to the NE and reduced Golgi-belt like ring structure formation. The recruitment of Golgi (*a*) to PEs is reduced in SLMAP3$^{-/-}$ MyoG+ cells, as indicated by the mean intensities of its staining in PEs. In SLMAP3$^{-/-}$ MHC+, the recruitment of pericentrin (*b*), AKAP6 (*c*) and Kif5b (*d*) to the NE after 8 days of differentiation is also impaired. (*e*) In differentiated myoblasts, the protein expression of AKAP6 and Kif5b in SLMAP3 KO is not significantly different from the control WT cells. After 8 days of differentiation, the MHC expression is no longer significantly reduced in SLMAP3 KO cells, although the tendency of reduced expression is notable. (*f*) Depletion of STRN3 did not affect the recruitment of pericentrin to the NE in MHC+ C2C12 cells after 5 days of differentiation. Scale bar, 8 μm. For (*a–d*), multiple fields for each of the three biological replicates were analysed. The average of each biological replicate is plotted. For (*e*), three biological replicates for each genotype were analysed. $^{**}p < 0.01$; $^{***}p < 0.001$; n.s., not significant.

Figure 5. Differentiating SLMAP3$^{-/-}$ myoblasts display defective microtubule growth from the NE. (*a*) Microtubule cytoskeleton in undifferentiated C2C12 cells. No obvious abnormalities could be seen in SLMAP3$^{-/-}$ myoblasts. (*b*) In undifferentiated cells, microtubule nucleation assay shows a stronger microtubule growth from the centrosomes of SLMAP3$^{-/-}$ myoblasts (arrow), whereas microtubule nucleation in WT cells seems already partially switched to the NE (arrowhead). (*c*) Microtubule cytoskeleton in differentiated C2C12 cells. Parallel arrays of microtubules are present in both SLMAP3$^{-/-}$ and WT cells. (*d*) Microtubule nucleation assay in differentiated C2C12 cells shows that in WT cells, the microtubules mostly grow from the NE (arrowhead), whereas in SLMAP3$^{-/-}$ cells the growth is from sites in the cytoplasm (arrows). (*e*) Microtubule nucleation assay in differentiated C2C12 cells shows that the sites of microtubule growth in the cytoplasm in SLMAP3$^{-/-}$ cells correspond to fragments of the dispersed Golgi (sites of microtubule nucleation from the Golgi expanded from the merged images for clarity). (*f*) The quantification of the mean intensity of microtubules in the NE of MyoG+ myoblasts confirms the reduced microtubule growth from this site in SLMAP3$^{-/-}$ cells. Scale bar, 8 μm. For the quantification, multiple fields of each of the three biological replicates of each sample were analysed. The average of each biological replicate is plotted. $^{**}p < 0.01$; $^{***}p < 0.001$.

Figure 6. Skeletal Muscle of SLMAP3$^{-/-}$ embryos display defective recruitment of pericentrin to the NE and nuclear mispositioning. (*a*) H&E staining of E16.5 quadriceps indicates that SLMAP3$^{-/-}$ embryos have abnormal muscle fibres, with reduced length and reduced internuclear distance. Fifteen fibres analysed across the quadriceps of three animals of each genotype. The averages corresponding to each animal are plotted. (*b*) Western blot analysis of E16.5 limbs shows no difference in MHC expression in SLMAP3$^{-/-}$ embryos compared to WT. (*c*) Pericentrin and MHC staining in muscle quadriceps indicate that skeletal muscle fibres of SLMAP3$^{-/-}$ embryos have defective NE-MTOC. (*d*) The protein expression of AKAP6 and Kif5b in SLMAP3 KO limbs is not significantly different from the WT samples. Scale bars, (*a*,*e*) 200 μm and (*c*) 20 μm. $^{*}p < 0.05$; $^{***}p < 0.001$; n.s., not significant.

Figure 7. Differentiating SLMAP3$^{-/-}$ myoblasts have abnormal localization of LINC complex proteins. The LINC complex members Nesprin-1 (*a*) and Lamin A/C (*b*) have defective recruitment to the NE in SLMAP3$^{-/-}$ MyoG+ myoblasts, as indicated by the ratio between their mean intensity in NE and nucleoplasm. (*c*) Staining of Lamin B1 indicates the subtle difference between SLMAP3$^{-/-}$ and WT cells. Scale bar, 8 μ m. Multiple fields of each of the three biological replicates of each sample were analysed. The average of each biological replicate is plotted. *$p <$ 0.05; n.s., not significant.

Figure 8. SLMAP3$^{-/-}$ C2C12 cells and skeletal muscles do not present upregulated Hippo Signaling. (*a*) Diagram summarizing the proposed mechanism of SLMAP3 in repressing the Hippo pathway by recruiting MST1/2 kinases to STRIPAK, where they are deactivated [29,30]. Pa = activating phosphorylation; Pi = inhibitory phosphorylation. (*b*) Hippo signalling is not affected in the hind limbs of SLMAP3$^{-/-}$ E16.5 embryos since no changes in YAP phosphorylation were detected. (*c*) No significant changes in the Hippo pathway are observed in SLMAP3$^{-/-}$ C2C12 myoblasts, (*d*) even in the presence of the PP2A inhibitor okadaic acid.

Figure 9. Model for SLMAP action in myogenesis. SLMAP3 targets the NE and the centrosome to guide the MTOC switch from the centrosome to the NE during myogenesis. Its loss could either impact centrosome attenuation (reduction of centrosomal microtubule nucleation) and/or the distribution of centrosomal proteins to the NE. SLMAP3 binds to the centrosomal components (pericentrin, AKAP9 and kinesin-1 subunits) and its loss impairs the recruitment of these proteins and AKAP6 to the NE during skeletal myogenesis, reducing microtubule nucleation from this organelle. Consequently, this disrupts the formation of the Golgi belt-like ring structure since AKAP6 and AKAP9/pericentrin bridge Nesprin-1 and Golgi through GM130 [18,20,21]. Furthermore, loss of SLMAP3 disrupts the nucleoskeleton, affecting the recruitment of Nesprin-1 and potentially impacting lamins and gene expression.

Supplemental Information: Titles and Legends

Supplementary Figure S1. SLMAP3 is present in the centrosome and perinuclear membrane of skeletal myoblasts. a. The SLMAP3 protein contains a C-terminus TM domain that targets the protein to different organelles; CC domains along its structure that contribute to protein-protein interaction; and a N-terminus FHA domain that targets SLMAP3 to the centrosome. Structure from AlphaFold. **b.** Undifferentiated and differentiated C2C12 cells at day 3 transduced with adenovirus carrying GFP-SLMAP3 shows it localization in the centrosome (arrows) and nuclear envelope (arrowheads). Upon differentiation, GFP-SLMAP3 and pericentrin colocalizes in the NE, as indicated by the Pearson correlation coefficient. **c.** Transfected GFP-SLMAP3 has a poor colocalization with Golgi, but colocalizes with the ER, as indicated by the Pearson's and Mander's coefficients obtained in Fiji using the JaCoP plugin. GM130 and calnexin were used as Golgi and ER markers, respectively. For **b** and **c** scale bar is 8 µm.

Supplementary Figure S2. Generation of SLMAP3$^{-/-}$ C2C12 cell lines by CRISPR/Cas9. a. Two sgRNAs (sgRNA3/1 and sgRNA3/2) were used to target regions next to the start codon of SLMAP in the exon 3. A non-target control sgRNA was used to create the WT control. **b.** From

the polyclonal pool of cells generated monoclonal colonies with knockout of SLMAP3 were selected. Colony 90 from the sgRNA3/1 and 14 from sgRNA3/2 pools were selected for further experiments and were called KO1 and KO2, respectively. **c.** Immunofluorescence staining confirms the knockout of SLMAP3 in KO2 C2C12 cells. For **c** scale bar is 8 µm.

Supplementary Figure S4. Differentiating SLMAP3$^{-/-}$ myoblasts present defective MTOC recruitment to the NE. a. The recruitment of pericentrin (**a**), AKAP6 (**b**) and Kif5b (**c**) to perinuclear regions is reduced in SLMAP3$^{-/-}$ MyoG+ cells, as indicated by the mean intensities of their staining in perinuclear regions. For **a**, **b** and **c**, cells were differentiated with 2% horse serum for 5 days. Scale bar 8 µm. Multiple fields of three biological replicates of each sample were analyzed. The averages of each biological replicate are plotted.

Supplementary Figure S5. SLMAP3$^{-/-}$ MEFs do not have abnormalities in the centrosomal microtubule nucleation. a. Microtubule cytoskeleton stained with anti-α-tubulin, and Golgi stained with anti-Golgin-97 show no obvious abnormalities in SLMAP3$^{-/-}$ MEFs. **b.** Microtubule nucleation assay with Nocodazole treatment followed by drug washout does not show any defects in centrosomal microtubule nucleation in SLMAP3$^{-/-}$ MEFs, as indicated by microtubules stained with anti-α-tubulin, and centrosome stained with anti-pericentrin. **c.** Microtubule growth in SLMAP3$^{-/-}$ MEFs is mostly from the centrosome, and no obvious decentralization of microtubule nucleation to the Golgi is observed. Scale bar 8 µm.

Supplementary Table S1. RNA-sequencing of SLMAP3$^{-/-}$ and wild type E11.5 mouse embryos. Results from DEseq2 including reads in fragments per kilobase per million mapped fragments (FPKM), adjusted p-value (padj), and Log2FC of reads from knockout embryos compared to wild type with their respective standard error estimate (lfcSE). Results also available in the GEO genomics data repository with the accession number GSE230748.

Supplementary Table S2. Endogenous SLMAP IP-MS from E12.5 mouse brain lysates. Results from Scaffold 5.2.2 represented as exclusive unique spectrum count (number of different sequences of amino acid sequences associated only with the protein). Centrosomal proteins and Kinesin-1 light and heavy chains are highlighted in yellow. The results are also available via ProteomeXchange with the identifier PXD041687.

Supplementary Table S3. Defective Muscle Development Phenotypes. Phenotypes observed in muscle cells with depletion or mutation of Lamin A/C, emerin, SUN proteins, Nesprin-1, AKAP6, MTOC proteins and kinesin-1 in terms of differentiation, myotube formation and nuclear positioning. Not affected conditions are highlighted in green, and affected conditions are highlighted in red.

6. References

1. Starr DA. 2009 A nuclear-envelope bridge positions nuclei and moves chromosomes. *J. Cell. Sci*. **122**, 577–586. (doi:10.1242/jcs.037622)
2. Bone CR, Starr DA. 2016 Nuclear migration events throughout development. *J. Cell. Sci*. **129**, 1951–1961. (doi:10.1242/jcs.179788)
3. Chal J, Pourquie O. 2017 Making muscle: skeletal myogenesis *in vivo* and *in vitro*. *Development* **144**, 2104–2122. (doi:10.1242/dev.151035)
4. Ralston E. 1993 Changes in architecture of the golgi complex and other subcellular organelles during myogenesis. *J. Cell Biol*. **120**, 399–409. (doi:10.1083/jcb.120.2.399)
5. Lu Z, Joseph D, Bugnard E, Zaal KJM, Ralston E. 2001 Golgi complex reorganization during muscle differentiation: visualization in living cells and mechanism. *Mol. Biol. Cell* **12**, 795–808. (doi:10.1091/mbc.12.4.795)
6. Srsen V, Fant X, Heald R, Rabouille C, Merdes A. 2009 Centrosome proteins form an insoluble perinuclear matrix during muscle cell differentiation. *BMC Cell Biol*. **10**, 28. (doi:10.1186/1471-2121-10-28)
7. Tassin AM, Maro B, Bornens M. 1985 Fate of microtubule-organizing centers during myogenesis in vitro. *J. Cell Biol*. **100**, 35–46. (doi:10.1083/jcb.100.1.35)
8. Tassin AM, Paintrand M, Berger EG, Bornens M. 1985 The golgi apparatus remains associated with microtubule organizing centers during myogenesis. *J. Cell Biol*. **101**, 630–638. (doi:10.1083/jcb.101.2.630)
9. Bugnard E, Zaal KJM, Ralston E. 2005 Reorganization of microtubule nucleation during muscle differentiation. *Cell Motil. Cytoskeleton* **60**, 1–13. (doi:10.1002/cm.20042)
10. Espigat-Georger A, Dyachuk V, Chemin C, Emorine L, Merdes A. 2016 Nuclear alignment in myotubes requires centrosome proteins recruited by nesprin-1. *J. Cell. Sci*. **129**, 4227–4237. (doi:10.1242/jcs.191767)
11. Becker R, Leone M, Engel FB. 2020 Microtubule organization in striated muscle cells. *Cells* **9**, 1395. (doi:10.3390/cells9061395)
12. Starr DA. 2017 Muscle development: nucleating microtubules at the nuclear envelope. *Curr. Biol*. **27**, R1071–R1073. (doi:10.1016/j.cub.2017.08.030)
13. Bonne G, Leturcq F, Ben Yaou R. 1993 Emery-dreifuss muscular dystrophy. In *GeneReviews* (eds MP Adam, GM Mirzaa, RA Pagon, SE Wallace, LJ Bean, KW Gripp, A Amemiya).Seattle, WA: University of Washington.
14. Heller SA, Shih R, Kalra R, Kang PB. 2020 Emery-dreifuss muscular dystrophy. *Muscle Nerve* **61**, 436–448. (doi:10.1002/mus.26782)
15. Zaal KJM, Reid E, Mousavi K, Zhang T, Mehta A, Bugnard E. 2011 Who needs microtubules? Myogenic reorganization of MTOC, golgi complex and ER exit sites persists despite lack of normal microtubule tracks. *PLoS ONE* **6**, e29057. (doi:10.1371/journal.pone.0029057)
16. Oddoux S, Zaal KJ, Tate V, Kenea A, Nandkeolyar SA, Reid E, Liu W, Ralston E. 2013 Microtubules that form the stationary lattice of muscle fibers are dynamic and nucleated at Golgi elements. *J. Cell Biol*. **203**, 205–213. (doi:10.1083/jcb.201304063)
17. Ide K, Muko M, Hayashi K. 2021 The Golgi apparatus is the main microtubule-organizing center in differentiating skeletal muscle cells. *Histoch. Cell Biol*. **156**, 273–281. (doi:10.1007/s00418-021-01999-6)

18. Vergarajauregui S *et al*. 2020 AKAP6 orchestrates the nuclear envelope microtubule-organizing center by linking golgi and nucleus via AKAP9. *eLife* **9**, e61669. (doi:10.7554/eLife.61669)
19. Giacomello E, Ronchi P, Pepperkok R. 2019 GM130 and p115 play a key role in the organisation of the early secretory pathway during skeletal muscle differentiation. *J. Cell. Sci*. **132**, jcs222083. (doi:10.1242/jcs.222083)
20. Gimpel P *et al*. 2017 Nesprin-1α-dependent microtubule nucleation from the nuclear envelope via akap450 is necessary for nuclear positioning in muscle cells. *Curr. Biol.* **27**, 2999–3009. (doi:10.1016/j.cub.2017.08.031)
21. Becker R, Vergarajauregui S, Billing F, Sharkova M, Lippolis E, Mamchaoui K, Ferrazzi F, Engel FB. 2021 Myogenin controls via AKAP6 non-centrosomal microtubule-organizing center formation at the nuclear envelope. *eLife* **10**, e65672. (doi:10.7554/eLife.65672)
22. Guzzo RM, Sevinc S, Salih M, Tuana BS. 2004 A novel isoform of sarcolemmal membrane-associated protein (SLMAP) is A component of the microtubule organizing centre. *J. Cell. Sci*. **117**, 2271–2281. (doi:10.1242/jcs.01079)
23. Byers JT, Guzzo RM, Salih M, Tuana BS. 2009 Hydrophobic profiles of the tail anchors in SLMAP dictate subcellular targeting. *BMC Cell Biol*. **10**, 48. (doi:10.1186/1471-2121-10-48)
24. Guzzo RM, Salih M, Moore ED, Tuana BS. 2005 Molecular properties of cardiac tail-anchored membrane protein SLMAP are consistent with structural role in arrangement of excitation-contraction coupling apparatus. *Am. J. Physiol. Heart Circ. Physiol*. **288**, H1810–H1819. (doi:10.1152/ajpheart.01015.2004)
25. Glatter T, Wepf A, Aebersold R, Gstaiger M. 2009 An integrated workflow for charting the human interaction proteome: insights into the PP2A system. *Mol. Syst. Biol*. **5**, 237. (doi:10.1038/msb.2008.75)
26. Goudreault M *et al*. 2009 A PP2A phosphatase high density interaction network identifies a novel striatin-interacting phosphatase and kinase complex linked to the cerebral cavernous malformation 3 (CCM3) protein. *Mol. Cell Proteomics* **8**, 157–171. (doi:10.1074/mcp.M800266-MCP200)
27. Couzens AL *et al*. 2013 Protein interaction network of the mammalian hippo pathway reveals mechanisms of kinase-phosphatase interactions. *Sci. Signal*. **6**, rs15. (doi:10.1126/scisignal.2004712)
28. Hauri S, Wepf A, van Drogen A, Varjosalo M, Tapon N, Aebersold R, Gstaiger M. 2013 Interaction proteome of human hippo signaling: modular control of the co-activator YAP1. *Mol. Syst. Biol*. **9**, 713. (doi:10.1002/msb.201304750)
29. Zheng Y, Liu B, Wang L, Lei H, Pulgar Prieto KD, Pan D. 2017 Homeostatic control of hpo/MST kinase activity through autophosphorylation-dependent recruitment of the STRIPAK PP2A phosphatase complex. *Cell Rep*. **21**, 3612–3623. (doi:10.1016/j.celrep.2017.11.076)
30. Bae SJ, Ni L, Osinski A, Tomchick DR, Brautigam CA, Luo X. 2017 SAV1 promotes hippo kinase activation through antagonizing the PP2A phosphatase STRIPAK. *eLife* **6**, e30278. (doi:10.7554/eLife.30278)
31. Rehmani T, Mlynarova J, Byers J, Salih M, Tuana BS. 2021 Specific deletion of the FHA domain containing SLMAP3 isoform in postnatal myocardium has no impact on structure or function. *Cardiogenetics* **11**, 164–184. (doi:10.3390/cardiogenetics11040018)

32. Rehmani T, Dias AP, Kamal M, Salih M, Tuana BS. 2024 Deletion of sarcolemmal membrane-associated protein isoform 3 (SLMAP3) in cardiac progenitors delays embryonic growth of myocardium without affecting hippo pathway. *Int. J. Mol. Sci*. **25**, 2888. (doi:10.3390/ijms25052888)
33. Wielowieyski PA, Sevinc S, Guzzo R, Salih M, Wigle JT, Tuana BS. 2000 Alternative splicing, expression, and genomic structure of the 3′ region of the gene encoding the sarcolemmal-associated proteins (SLAPs) defines a novel class of coiled-coil tail-anchored membrane proteins. *J. Biol. Chem.* **275**, 38474–38481. (doi:10.1074/jbc.M007682200)
34. Wigle JT, Demchyshyn L, Pratt MAC, Staines WA, Salih M, Tuana BS. 1997 Molecular cloning, expression, and chromosomal assignment of sarcolemmal-associated proteins. *J. Biol. Chem.* **272**, 32384–32392. (doi:10.1074/jbc.272.51.32384)
35. Metzger T, Gache V, Xu M, Cadot B, Folker ES, Richardson BE, Gomes ER, Baylies MK. 2012 MAP and kinesin-dependent nuclear positioning is required for skeletal muscle function. *Nature* **484**, 120–124. (doi:10.1038/nature10914)
36. Wilson MH, Holzbaur ELF. 2012 Opposing microtubule motors drive robust nuclear dynamics in developing muscle cells. *J. Cell. Sci*. **125**, 4158–4169. (doi:10.1242/jcs.108688)
37. Wilson MH, Holzbaur ELF. 2015 Nesprins anchor kinesin-1 motors to the nucleus to drive nuclear distribution in muscle cells. *Development* **142**, 218–228. (doi:10.1242/dev.114769)
38. Guzzo RM, Wigle J, Salih M, Moore ED, Tuana BS. 2004 Regulated expression and temporal induction of the tail-anchored sarcolemmal-membrane-associated protein is critical for myoblast fusion. *Biochem. J*. **381**, 599–608. (doi:10.1042/BJ20031723)
39. Tang Y *et al*. 2019 Architecture, substructures, and dynamic assembly of STRIPAK complexes in hippo signaling. *Cell Discov*. **5**, 3. (doi:10.1038/s41421-018-0077-3)
40. Frost A *et al*. 2012 Functional repurposing revealed by comparing *S. pombe* and *S. cerevisiae* genetic interactions. *Cell* **149**, 1339–1352. (doi:10.1016/j.cell.2012.04.028)
41. The Dougherty Lab. Tissue specific expression analysis (TSEA). See http://doughertytools.wustl.edu/TSEAtool.html.
42. Wells A, Kopp N, Xu X, O'Brien DR, Yang W, Nehorai A, Adair-Kirk TL, Kopan R, Dougherty JD. 2015 The anatomical distribution of genetic associations. *Nucleic Acids Res.* **43**, 10804–10820. (doi:10.1093/nar/gkv1262)
43. Raudvere U, Kolberg L, Kuzmin I, Arak T, Adler P, Peterson H, Vilo J. 2019 G:profiler: a web server for functional enrichment analysis and conversions of gene lists (2019 update). *Nucleic Acids Res*. **47**, W191–W198. (doi:10.1093/nar/gkz369)
44. International Mouse Phenotype Consortium. Strn3. See https://www.mousephenotype.org/data/genes/MGI:2151064.
45. Pare GC, Easlick JL, Mislow JM, McNally EM, Kapiloff MS. 2005 Nesprin-1alpha contributes to the targeting of mAKAP to the cardiac myocyte nuclear envelope. *Exp. Cell Res*. **303**, 388–399. (doi:10.1016/j.yexcr.2004.10.009)
46. Wang Z *et al*. 2013 Kif5b controls the localization of myofibril components for their assembly and linkage to the myotendinous junctions. *Development* **140**, 617–626. (doi:10.1242/dev.085969)
47. Zhou C *et al*. 2017 Novel nesprin-1 mutations associated with dilated cardiomyopathy cause nuclear envelope disruption and defects in myogenesis. *Hum. Mol. Genet*. **26**, 2258–2276. (doi:10.1093/hmg/ddx116)

48. Mejat A, Misteli T. 2010 LINC complexes in health and disease. *Nucleus* **1**, 40–52. (doi:10.4161/nucl.1.1.10530)
49. Markiewicz E, Ledran M, Hutchison CJ. 2005 Remodelling of the nuclear lamina and nucleoskeleton is required for skeletal muscle differentiation in vitro. *J. Cell. Sci*. **118**, 409–420. (doi:10.1242/jcs.01630)
50. Muralikrishna Bh, Dhawan J, Rangaraj N, Parnaik VK. 2001 Distinct changes in intranuclear lamin A/C organization during myoblast differentiation. *J. Cell. Sci*. **114**, 4001–4011. (doi:10.1242/jcs.114.22.4001)
51. Kuck U, Radchenko D, Teichert I. 2019 STRIPAK, a highly conserved signaling complex, controls multiple eukaryotic cellular and developmental processes and is linked with human diseases. *Biol. Chem.* **400**, 1005–1022. (doi:10.1515/hsz-2019-0173)
52. Lin M, Xie SS, Chan KY. 2022 An updated view on the centrosome as a cell cycle regulator. *Cell Div*. **17**, 1. (doi:10.1186/s13008-022-00077-0)
53. Philip R, Fiorino C, Harrison RE. 2022 Terminally differentiated osteoclasts organize centrosomes into large clusters for microtubule nucleation and bone resorption. *Mol. Biol. Cell* **33**, ar68. (doi:10.1091/mbc.E22-03-0098)
54. Chabin-Brion K, Marceiller J, Perez F, Settegrana C, Drechou A, Durand G, Pous C. 2001 The golgi complex is a microtubule-organizing organelle. *Mol. Biol. Cell* **12**, 2047–2060. (doi: 10.1091/mbc.12.7.2047)
55. Efimov A *et al*. 2007 Asymmetric CLASP-dependent nucleation of noncentrosomal microtubules at the trans-golgi network. *Dev. Cell* **12**, 917–930. (doi:10.1016/j.devcel.2007.04.002)
56. Rivero S, Cardenas J, Bornens M, Rios RM. 2009 Microtubule nucleation at the cis-side of the golgi apparatus requires AKAP450 and GM130. *EMBO J.* **28**, 1016–1028. (doi:10.1038/emboj.2009.47)
57. Kodani A, Sutterlin C. 2009 A new function for an old organelle: microtubule nucleation at the Golgi apparatus. *EMBO J.* **28**, 995–996. (doi:10.1038/emboj.2009.85)
58. Storey EC, Holt I, Morris GE, Fuller HR. 2020 Muscle cell differentiation and development pathway defects in Emery-Dreifuss muscular dystrophy. *Neuromuscul. Disord.* **30**, 443–456. (doi:10.1016/j.nmd.2020.04.002)
59. Mislow JMK, Holaska JM, Kim MS, Lee KK, Segura-Totten M, Wilson KL, McNally EM. 2002 Nesprin-1α self-associates and binds directly to emerin and lamin A in vitro. *FEBS Lett.* **525**, 135–140. (doi:10.1016/s0014-5793(02)03105-8)
60. Mislow JMK, Kim MS, Davis DB, McNally EM. 2002 Myne-1, a spectrin repeat transmembrane protein of the myocyte inner nuclear membrane, interacts with lamin A/C. *J. Cell. Sci*. **115**, 61–70. (doi:10.1242/jcs.115.1.61)
61. Wheeler MA, Davies JD, Zhang Q, Emerson LJ, Hunt J, Shanahan CM, Ellis JA. 2007 Distinct functional domains in nesprin-1α and nesprin-2β bind directly to emerin and both interactions are disrupted in X-linked Emery-Dreifuss muscular dystrophy. *Exp. Cell Res.* **313**, 2845–2857. (doi:10.1016/j.yexcr.2007.03.025)
62. Haque F, Mazzeo D, Patel JT, Smallwood DT, Ellis JA, Shanahan CM, Shackleton S. 2010 Mammalian sun protein interaction networks at the inner nuclear membrane and their role in laminopathy disease processes. *J. Biol. Chem.* **285**, 3487–3498. (doi:10.1074/jbc.M109.071910)

63. Favreau C, Higuet D, Courvalin JC, Buendia B. 2004 Expression of a mutant lamin A that causes Emery-Dreifuss muscular dystrophy inhibits in vitro differentiation of C2C12 myoblasts. *Mol. Cell. Biol*. **24**, 1481–1492. (doi:10.1128/MCB.24.4.1481-1492.2004)
64. Frock RL, Kudlow BA, Evans AM, Jameson SA, Hauschka SD, Kennedy BK. 2006 Lamin A/C and emerin are critical for skeletal muscle satellite cell differentiation. *Genes Dev*. **20**, 486–500. (doi:10.1101/gad.1364906)
65. Bertrand AT, Brull A, Azibani F, Benarroch L, Chikhaoui K, Stewart CL, Medalia O, Ben Yaou R, Bonne G. 2020 Lamin A/C assembly defects in *LMNA*-congenital muscular dystrophy is responsible for the increased severity of the disease compared with Emery-Dreifuss muscular dystrophy. *Cells* **9**, 844. (doi:10.3390/cells9040844)
66. Kandert S, Wehnert M, Muller CR, Buendia B, Dabauvalle MC. 2009 Impaired nuclear functions lead to increased senescence and inefficient differentiation in human myoblasts with a dominant p.R545C mutation in the LMNA gene. *Eur. J. Cell Biol*. **88**, 593–608. (doi:10.1016/j.ejcb.2009.06.002)
67. Iyer A, Holaska JM. 2020 EDMD-causing emerin mutant myogenic progenitors exhibit impaired differentiation using similar mechanisms. *Cells* **9**, 1463. (doi:10.3390/cells9061463)
68. Lee SW, Won JY, Yang J, Lee J, Kim SY, Lee EJ, Kim HS. 2015 AKAP6 inhibition impairs myoblast differentiation and muscle regeneration: positive loop between AKAP6 and myogenin. *Sci. Rep*. **5**, 16523. (doi:10.1038/srep16523)
69. Solovei I *et al*. 2013 LBR and lamin A/C sequentially tether peripheral heterochromatin and inversely regulate differentiation. *Cell* **152**, 584–598. (doi:10.1016/j.cell.2013.01.009)
70. Sullivan T, Escalante-Alcalde D, Bhatt H, Anver M, Bhat N, Nagashima K, Stewart CL, Burke B. 1999 Loss of A-type lamin expression compromises nuclear envelope integrity leading to muscular dystrophy. *J. Cell Biol*. **147**, 913–920. (doi:10.1083/jcb.147.5.913)
71. Melcon G *et al*. 2006 Loss of emerin at the nuclear envelope disrupts the Rb1/E2F and MyoD pathways during muscle regeneration. *Hum. Mol. Genet*. **15**, 637–651. (doi:10.1093/hmg/ddi479)
72. Stroud MJ, Feng W, Zhang J, Veevers J, Fang X, Gerace L, Chen J. 2017 Nesprin 1α2 is essential for mouse postnatal viability and nuclear positioning in skeletal muscle. *J. Cell Biol*. **216**, 1915–1924. (doi:10.1083/jcb.201612128)
73. Wackerhage H, Del Re DP, Judson RN, Sudol M, Sadoshima J. 2014 The hippo signal transduction network in skeletal and cardiac muscle. *Sci. Signal*. **7**, re4. (doi:10.1126/scisignal.2005096)
74. Ng DCH, Richards DK, Mills RJ, Ho UY, Perks HL, Tucker CR, Voges HK, Pagan JK, Hudson JE. 2020 Centrosome reduction promotes terminal differentiation of human cardiomyocytes. *Stem Cell Rep.* **15**, 817–826. (doi:10.1016/j.stemcr.2020.08.007)
75. Qiu LQ, Lai WS, Stumpo DJ, Blackshear PJ. 2016 Mouse embryonic fibroblast cell culture and stimulation. *Bio Protoc*. **6**, e1859. (doi:10.21769/BioProtoc.1859)
76. Conner DA. 2000 Mouse embryo fibroblast (MEF) feeder cell preparation. *Curr. Protoc. Mol. Biol*. **51**, 23.2.1–23.2.7. (doi:10.1002/0471142727.mb2302s51)
77. Zhu X, Kaverina I. 2011 Quantification of asymmetric microtubule nucleation at subcellular structures. *Methods Mol. Biol.* **777**, 235–244. (doi:10.1007/978-1-61779-252-6_17)

78. Patro R, Duggal G, Love MI, Irizarry RA, Kingsford C. 2017 Salmon provides fast and bias-aware quantification of transcript expression. *Nat. Methods* **14**, 417–419. (doi:10.1038/nmeth.4197)
79. Love MI, Huber W, Anders S. 2014 Moderated estimation of fold change and dispersion for RNA-seq data with DESeq2. *Genome Biol*. **15**, 550. (doi:10.1186/s13059-014-0550-8)
80. Edgar R, Domrachev M, Lash AE. 2002 Gene expression omnibus: NCBI gene expression and hybridization array data repository. *Nucleic Acids Res*. **30**, 207–210. (doi:10.1093/nar/30.1.207)
81. Barrett T *et al*. 2013 NCBI GEO: archive for functional genomics data sets—update. *Nucleic Acids Res.* **41**, D991–5. (doi:10.1093/nar/gks1193)
82. Nesvizhskii AI, Keller A, Kolker E, Aebersold R. 2003 A statistical model for identifying proteins by tandem mass spectrometry. *Anal. Chem.* **75**, 4646–4658. (doi:10.1021/ac0341261)
83. Perez-Riverol Y *et al*. 2022 The Pride database resources in 2022: a hub for mass spectrometry-based proteomics evidences. *Nucleic Acids Res*. **50**, D543–D552. (doi:10.1093/nar/gkab1038)
84. Agilent Technologies. AdEasy Adenoviral Vector System. See https://www.agilent.com/cs/library/usermanuals/public/240009.pdf.
85. Addgene. Lentivirus production. See https://www.addgene.org/protocols/lentivirus-production/.
86. Addgene. Generating stable cell lines. See https://www.addgene.org/protocols/generating-stable-cell-lines/.
87. Sanjana NE, Shalem O, Zhang F. 2014 Improved vectors and genome-wide libraries for CRISPR screening. *Nat. Methods* **11**, 783–784. (doi:10.1038/nmeth.3047)
88. Addgene. Isolating a monoclonal cell population by limiting dilution. See https://www.addgene.org/protocols/limiting-dilution/ (accessed 2 July 2024).
89. Huang Y *et al*. 2021 Plexin-B2 facilitates glioblastoma infiltration by modulating cell biomechanics. *Commun. Biol*. **4**, 145. (doi:10.1038/s42003-021-01667-4)

Figures Main Text

Figure 1. Genes downregulated in SLMAP3$^{-/-}$ mouse embryos enrich for muscle developmental processes

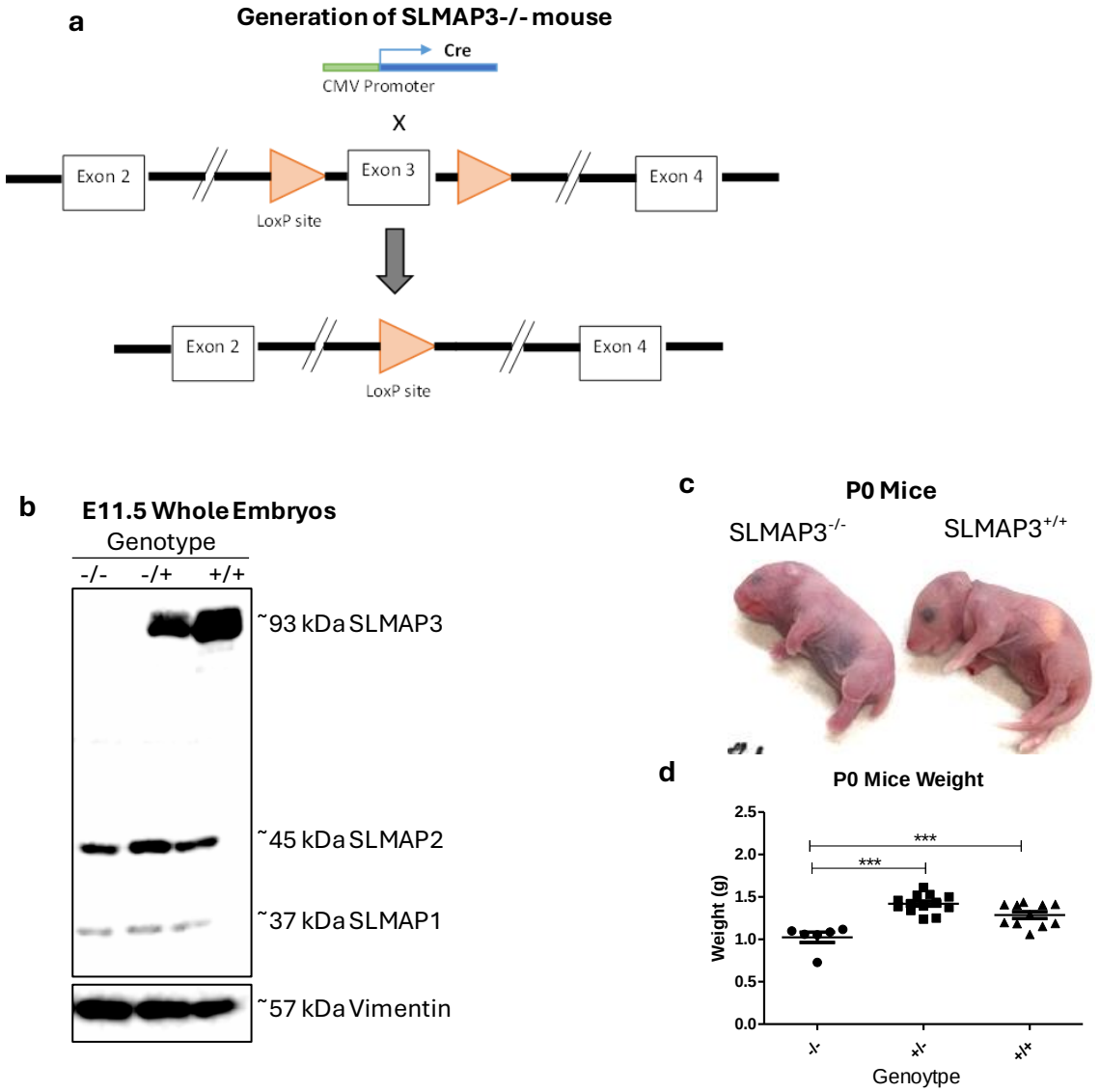

Figure 1. Genes downregulated in SLMAP3$^{-/-}$ mouse embryos enrich for muscle developmental processes

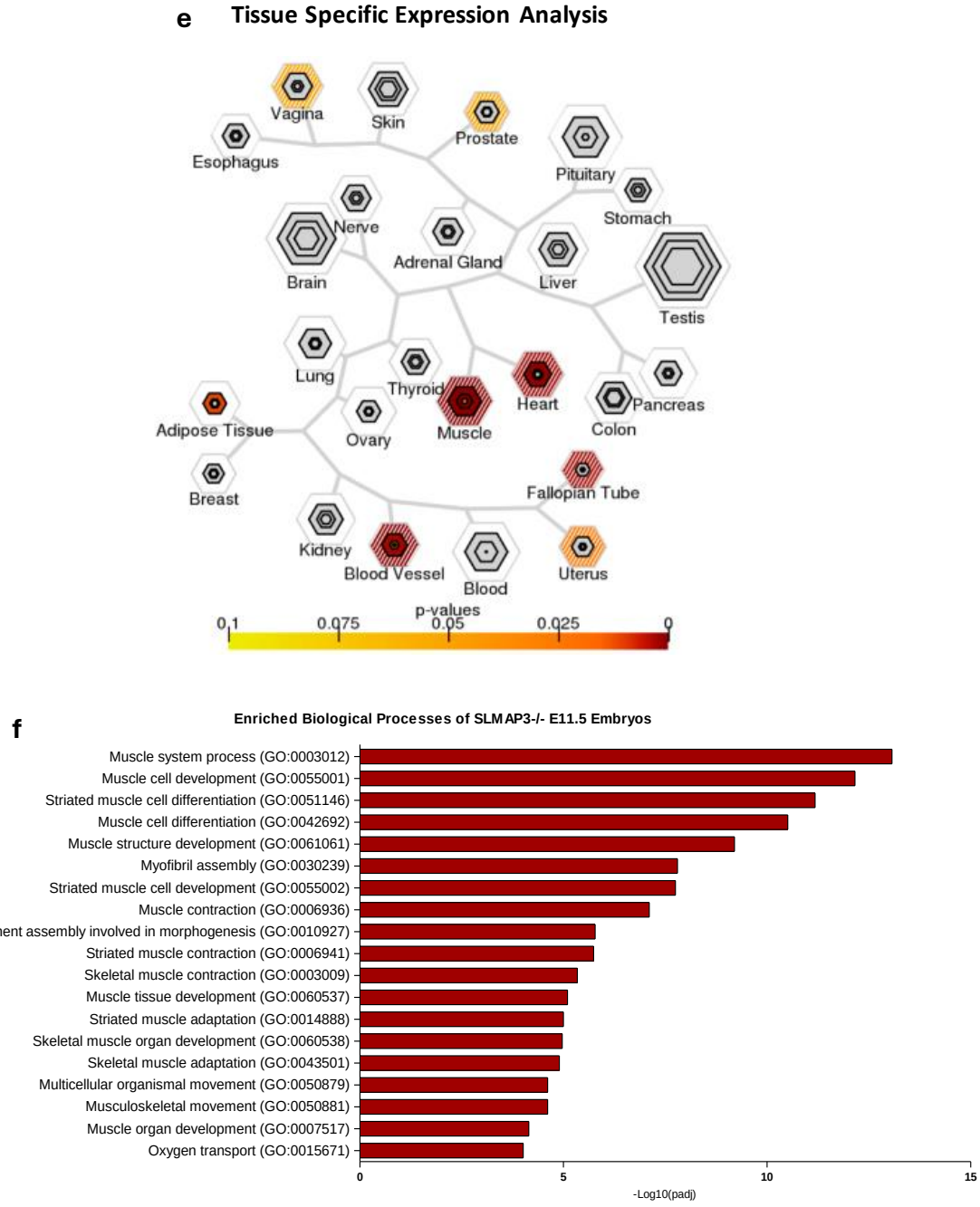

Figure 2. SLMAP3 interacts with MTOC proteins

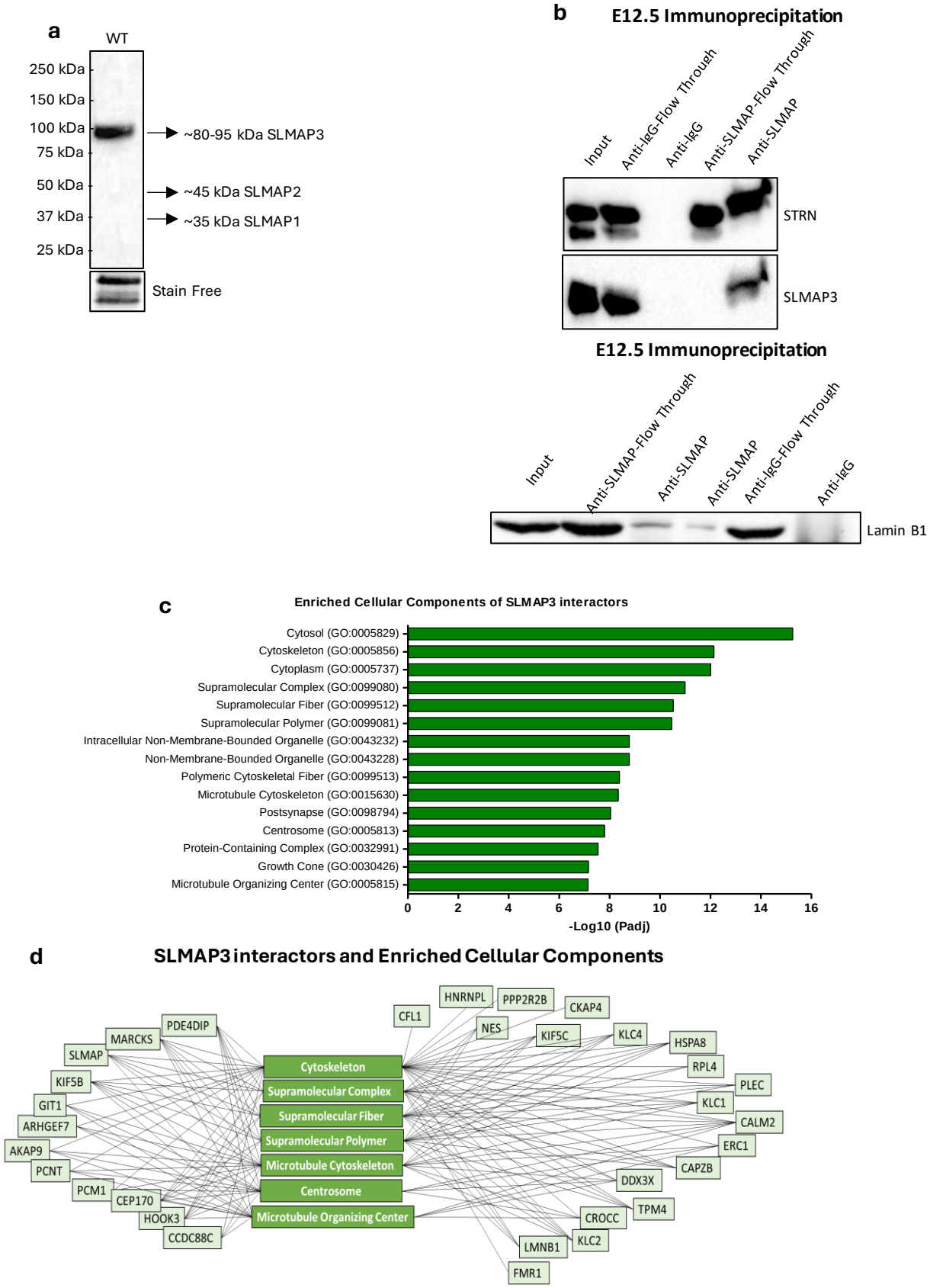

Figure 3. SLMAP3$^{-/-}$ myoblasts display differentiation and myotube formation defects

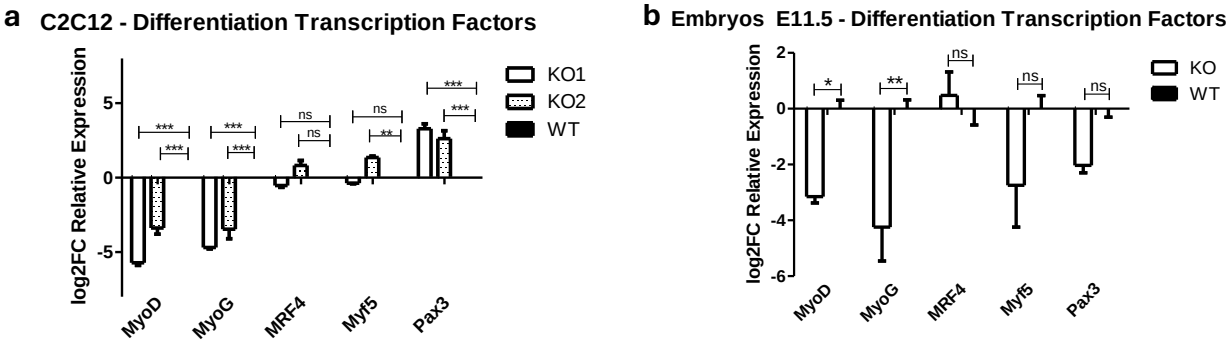

c

Mean Log2FC KO vs WT				
	C2C12 Cells		E11.5 Embryos	
Transcript	RT-qPCR	p-value	RT-qPCR	p-value
MyoD	-4.54628	p<0.001	-3.15111	p<0.05
MyoG	-4.07389	p<0.001	-4.24333	p<0.01
MRF4	0.145589	ns	0.47333	ns
Myf5	0.490847	ns	-2.74111	ns
Pax3	2.952549	p<0.001	-2.03111	ns

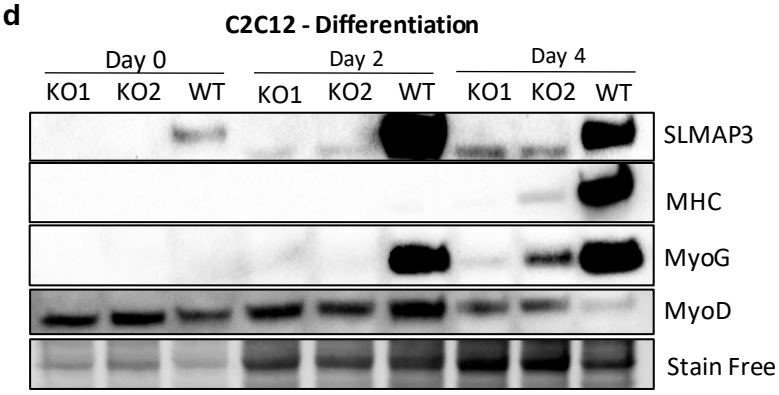

Figure 3. SLMAP3$^{-/-}$ myoblasts display differentiation and myotube formation defects

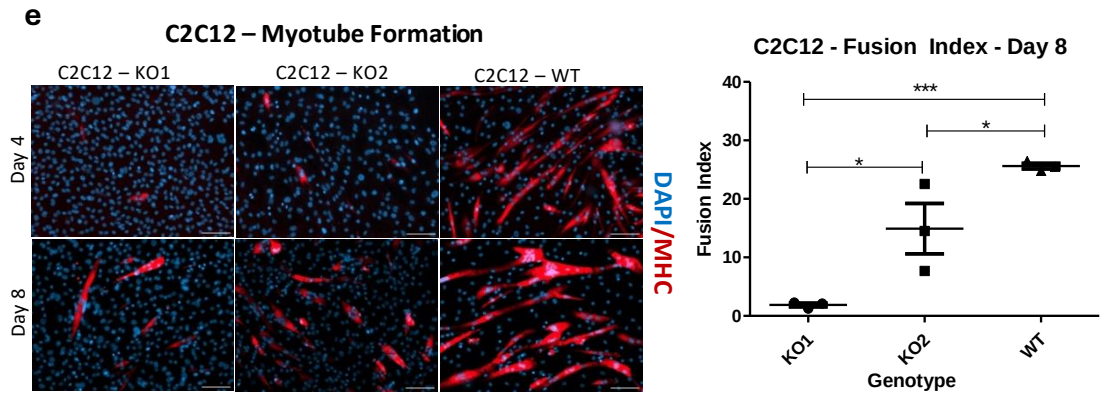

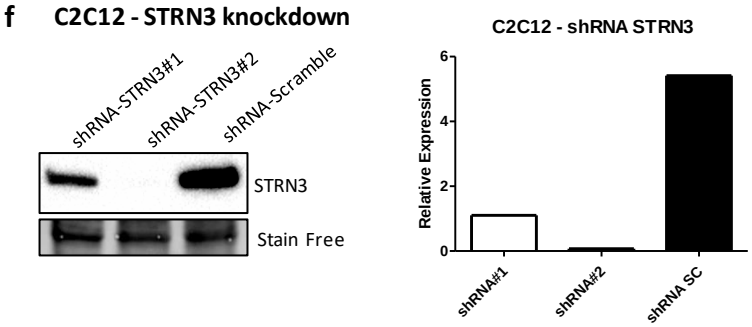

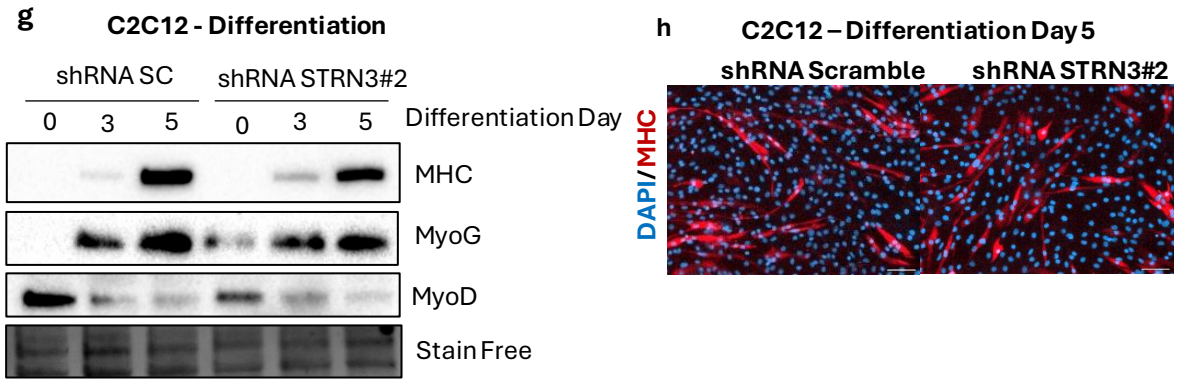

Figure 4. Differentiating SLMAP3$^{-/-}$ myoblasts present defective MTOC recruitment to the NE and reduced Golgi-belt like ring structure formation

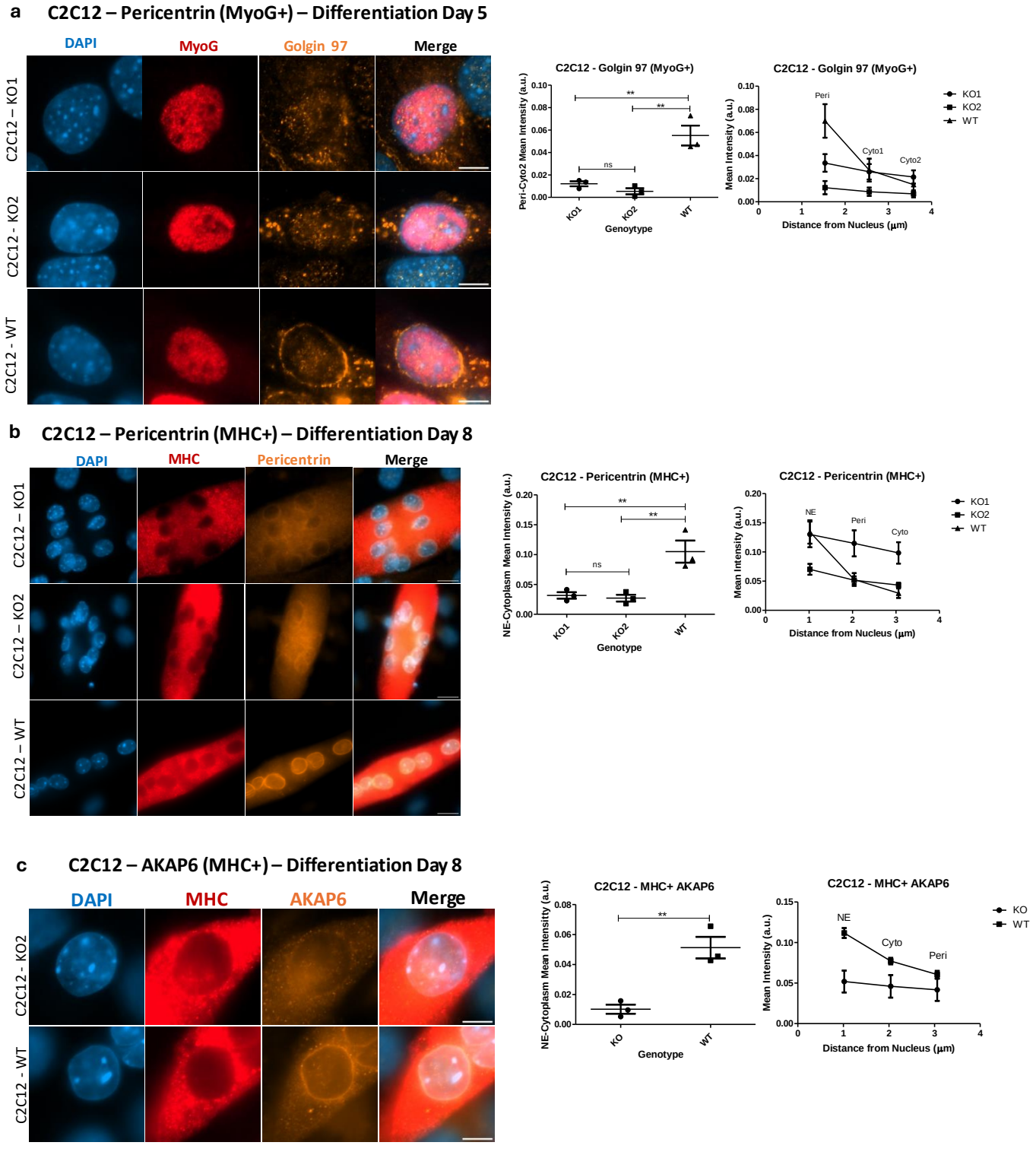

Figure 4. Differentiating SLMAP3$^{-/-}$ myoblasts present defective MTOC recruitment to the NE and reduced Golgi-belt like ring structure formation

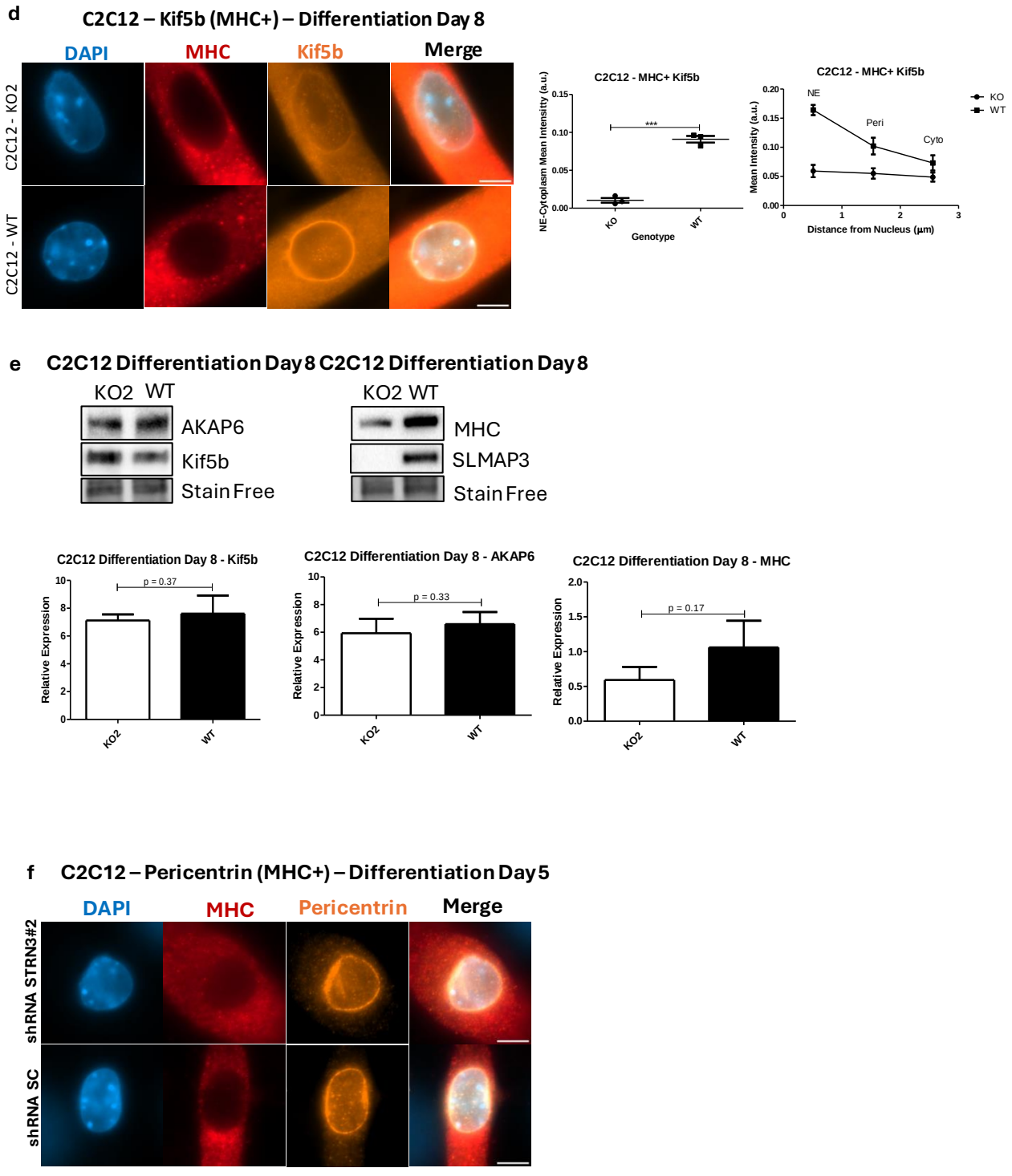

Figure 5. Differentiating SLMAP3$^{-/-}$ myoblasts display defective microtubule growth from the NE

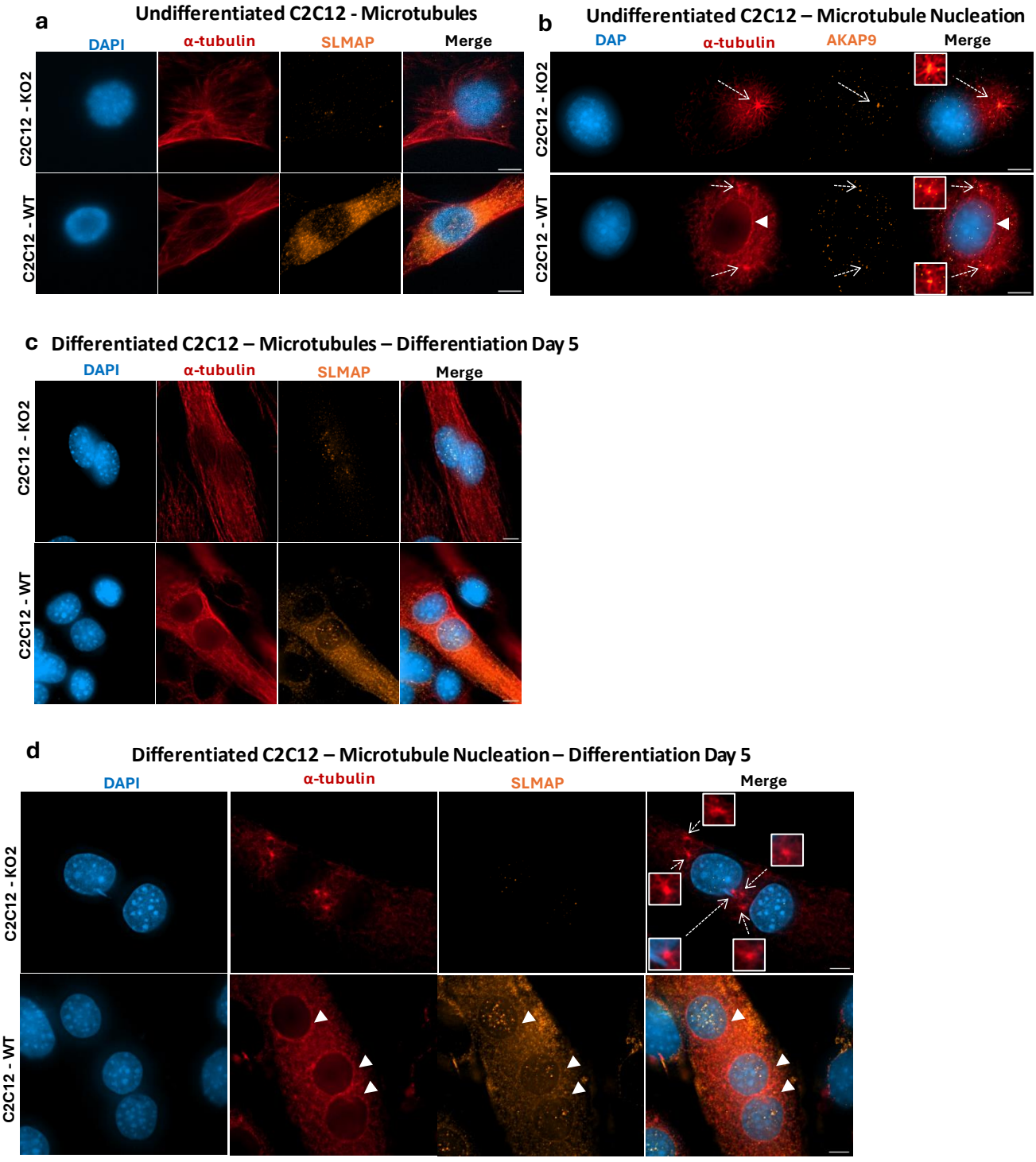

Figure 5. Differentiating SLMAP3$^{-/-}$ myoblasts display defective microtubule growth from the NE

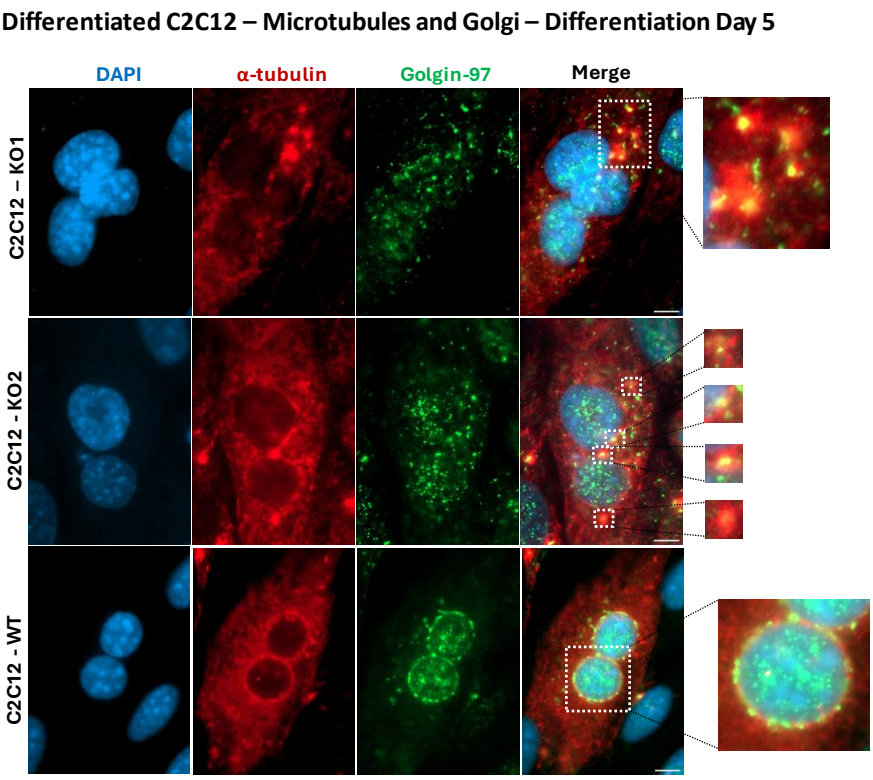

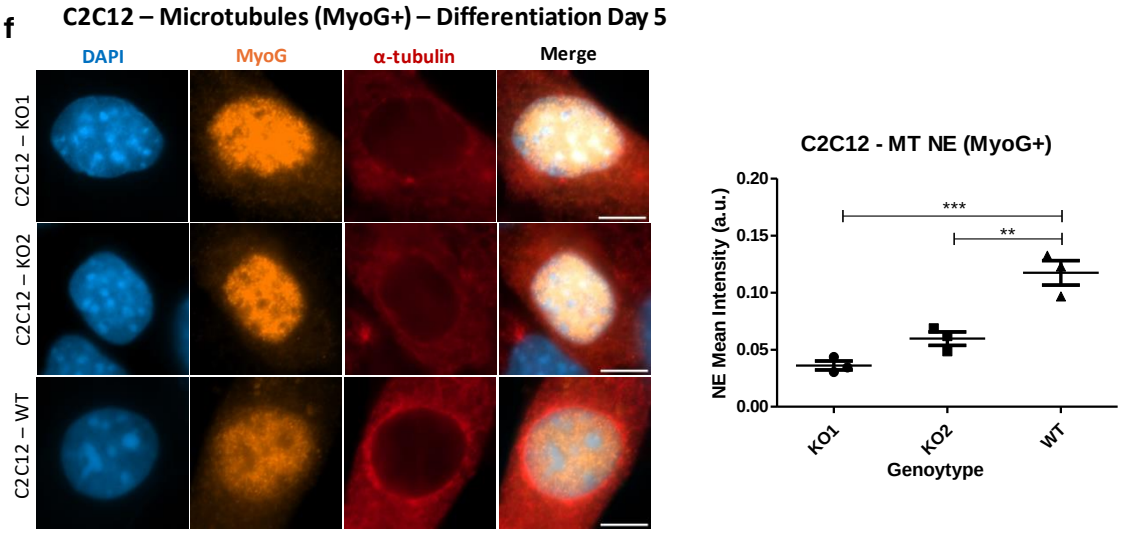

Figure 6. Skeletal Muscle of SLMAP3$^{-/-}$ embryos display defective recruitment of pericentrin to the NE and nuclear mispositioning

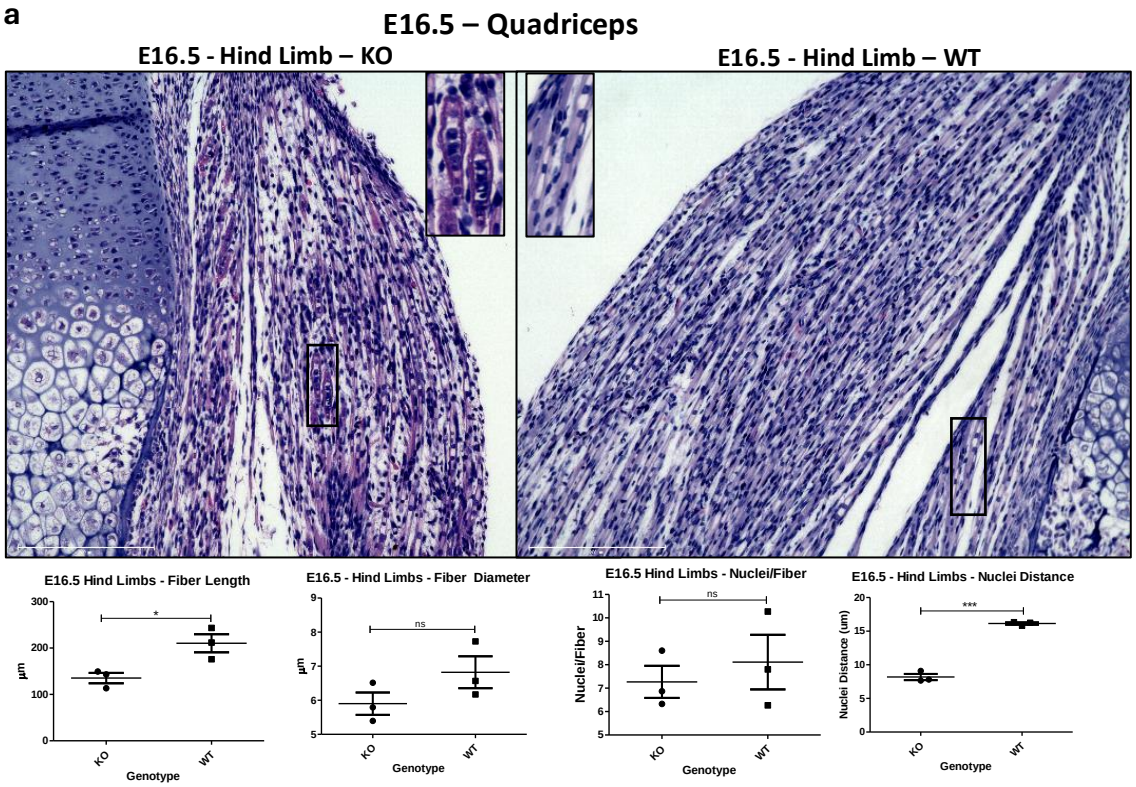

Figure 6. Skeletal Muscle of SLMAP3$^{-/-}$ embryos display defective recruitment of pericentrin to the NE and nuclear mispositioning

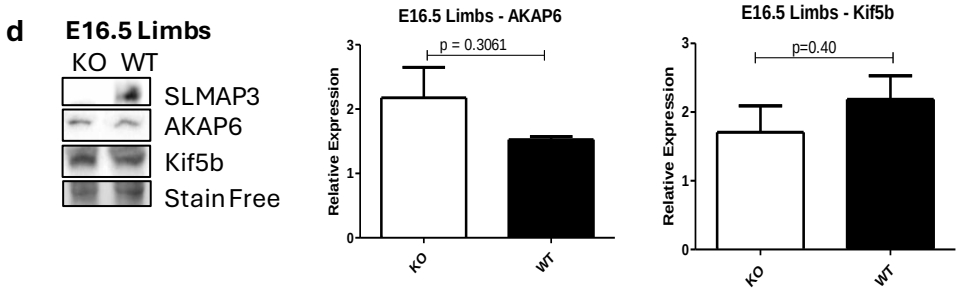

Figure 7. Differentiating SLMAP3$^{-/-}$ myoblasts have abnormal localization of LINC complex proteins

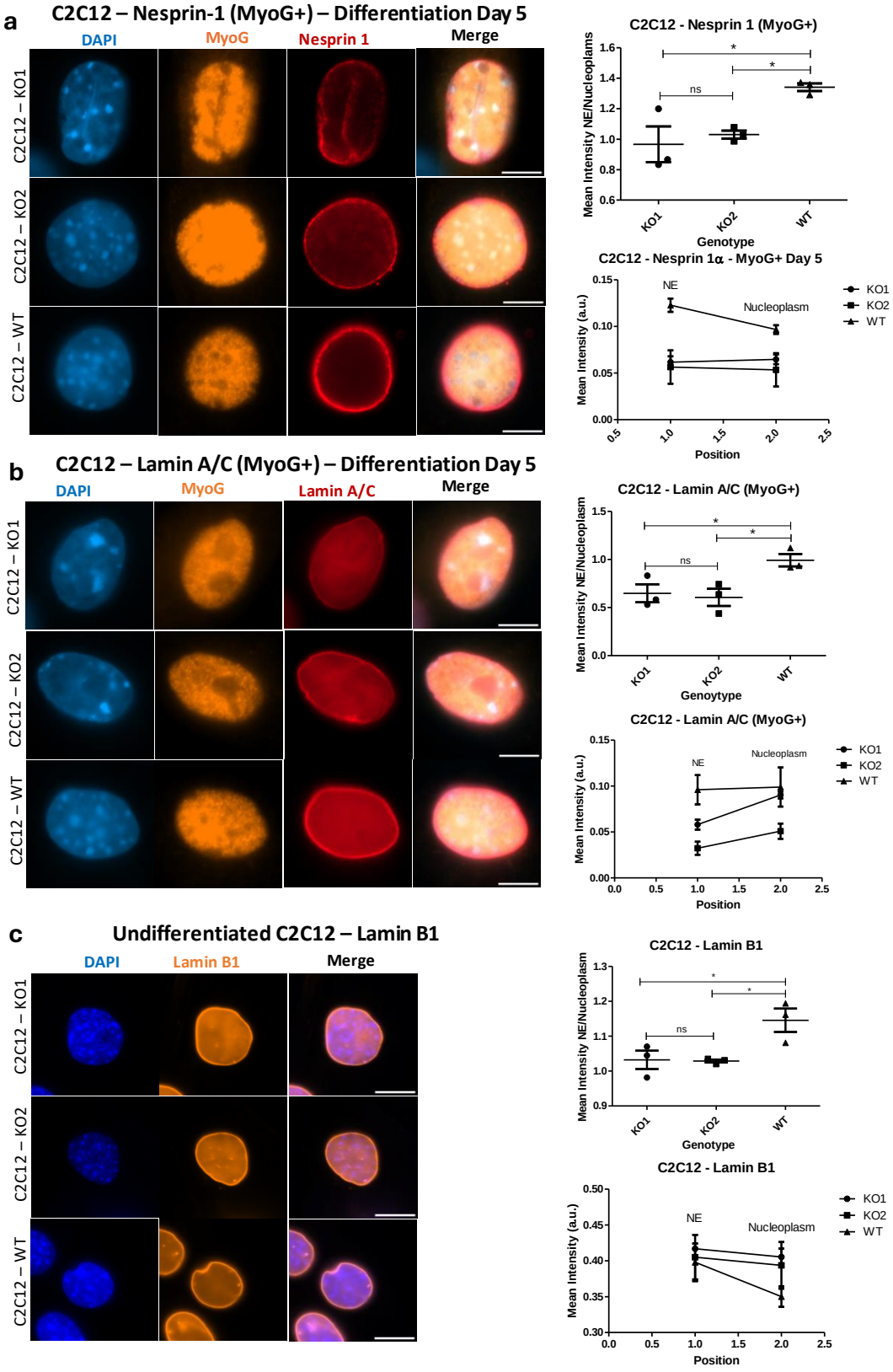

Figure 8. SLMAP3 effects on developing muscle are independent of Hippo Signaling

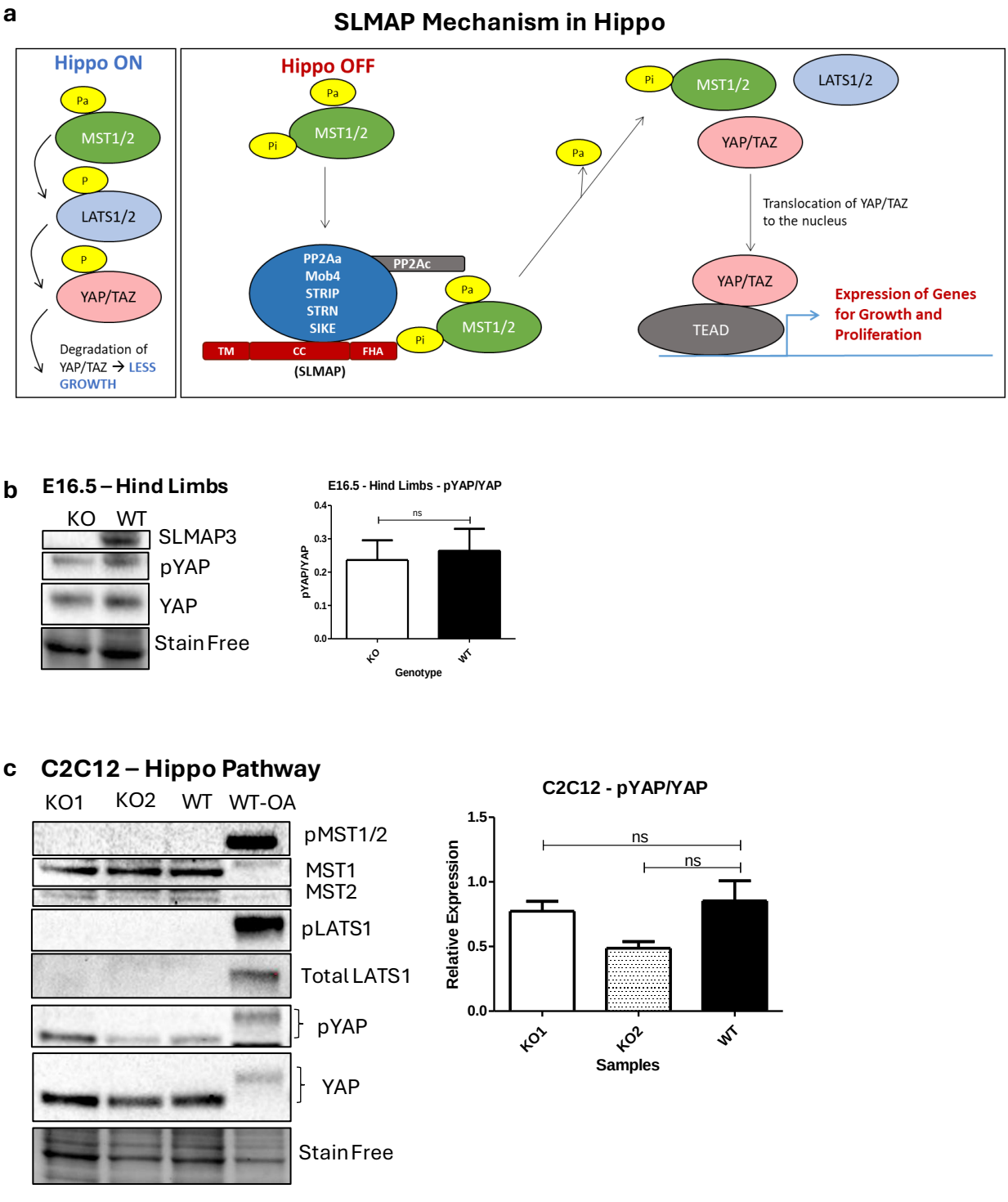

Figure 8. SLMAP3 effects on developing muscle are independent of Hippo Signaling

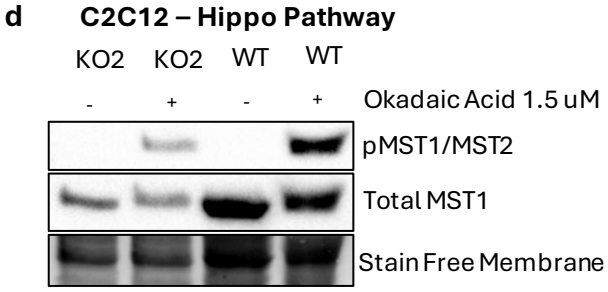

Figure 9. Model for SLMAP action in myogenesis

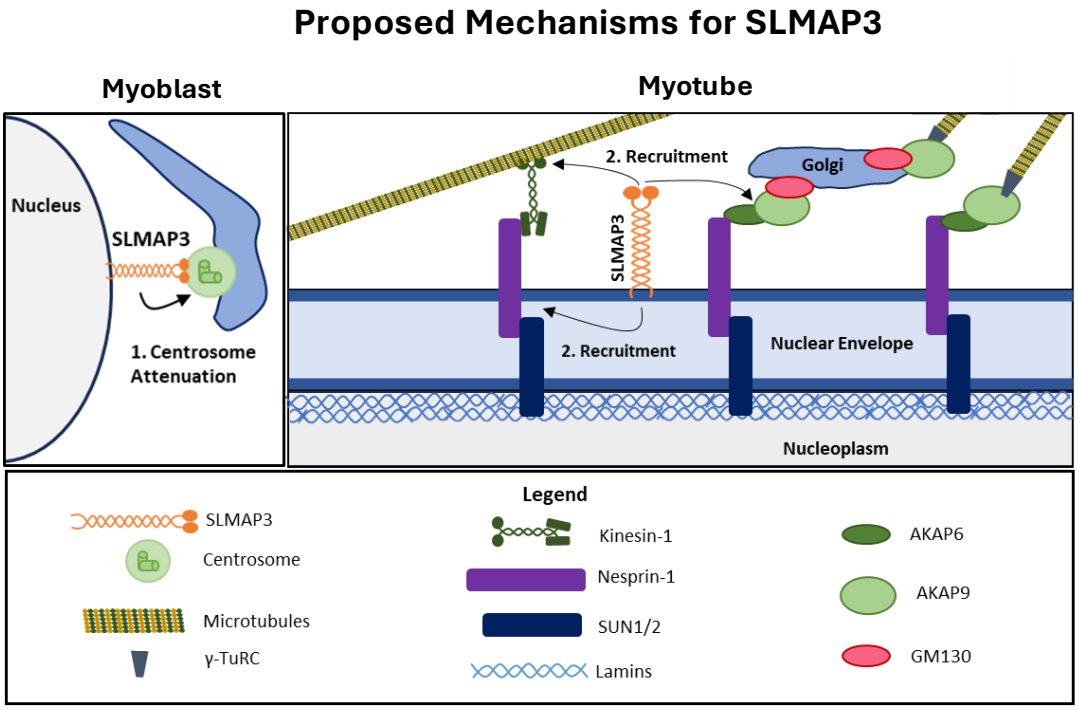

Supplemental Material 1

Supplementary Figure S1. SLMAP3 is present in the centrosome and perinuclear membrane of skeletal myoblasts

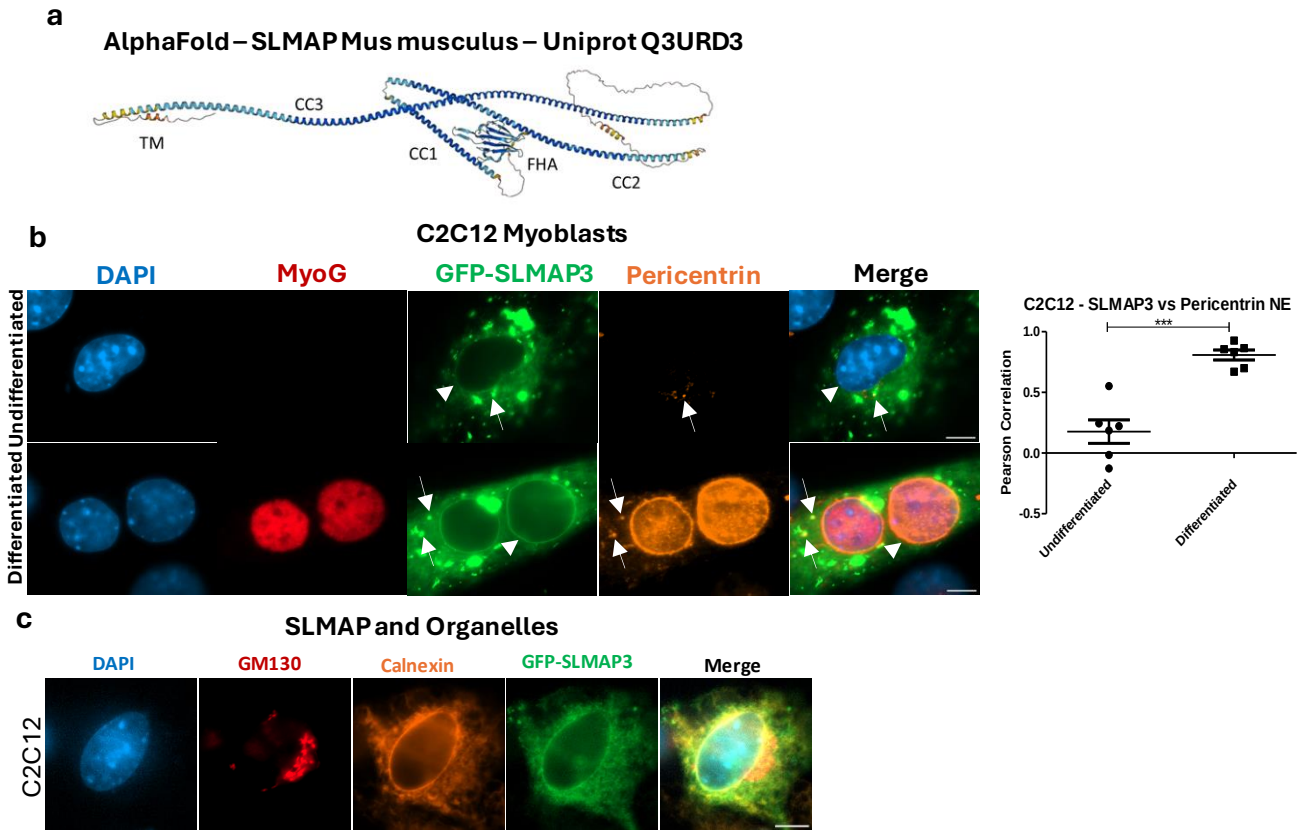

Colocalization Coefficients	
M1 (GFP-SLMAP3 overlapping with Golgi)	0.752
M2 (Golgi overlapping with GFP-SLMAP3)	0.990
Pearson's r	0.241

Colocalization Coefficients	
M1 (GFP-SLMAP3 overlapping with ER)	0.991
M2 (ER overlapping with GFP-SLMAP3)	0.963
Pearson's r	0.705

Supplementary Figure S2. Generation of SLMAP3$^{-/-}$ C2C12 cell lines by CRISPR/Cas9.

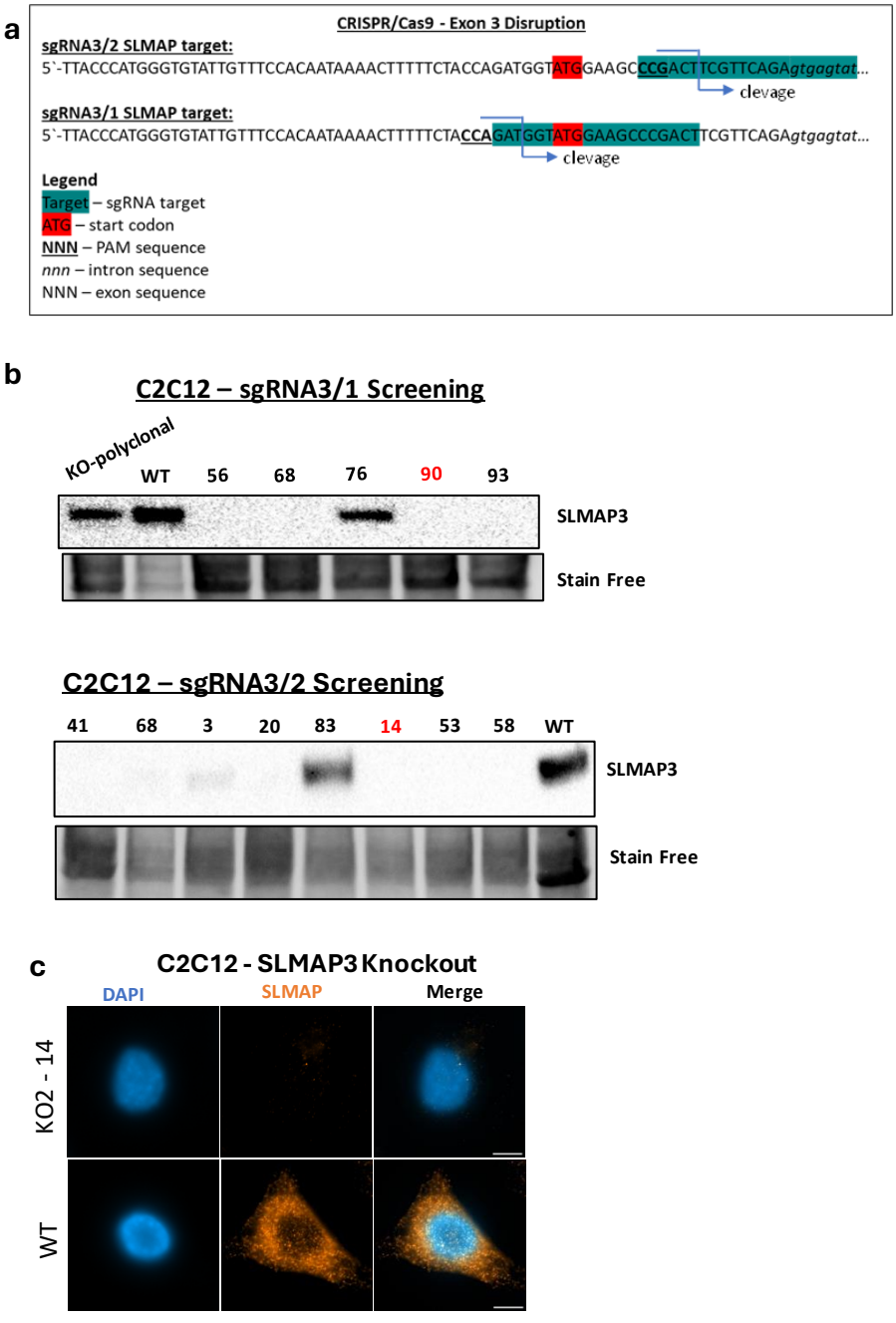

Supplementary Figure S3. Differentiating SLMAP3$^{-/-}$ myoblasts present defective MTOC recruitment to the NE

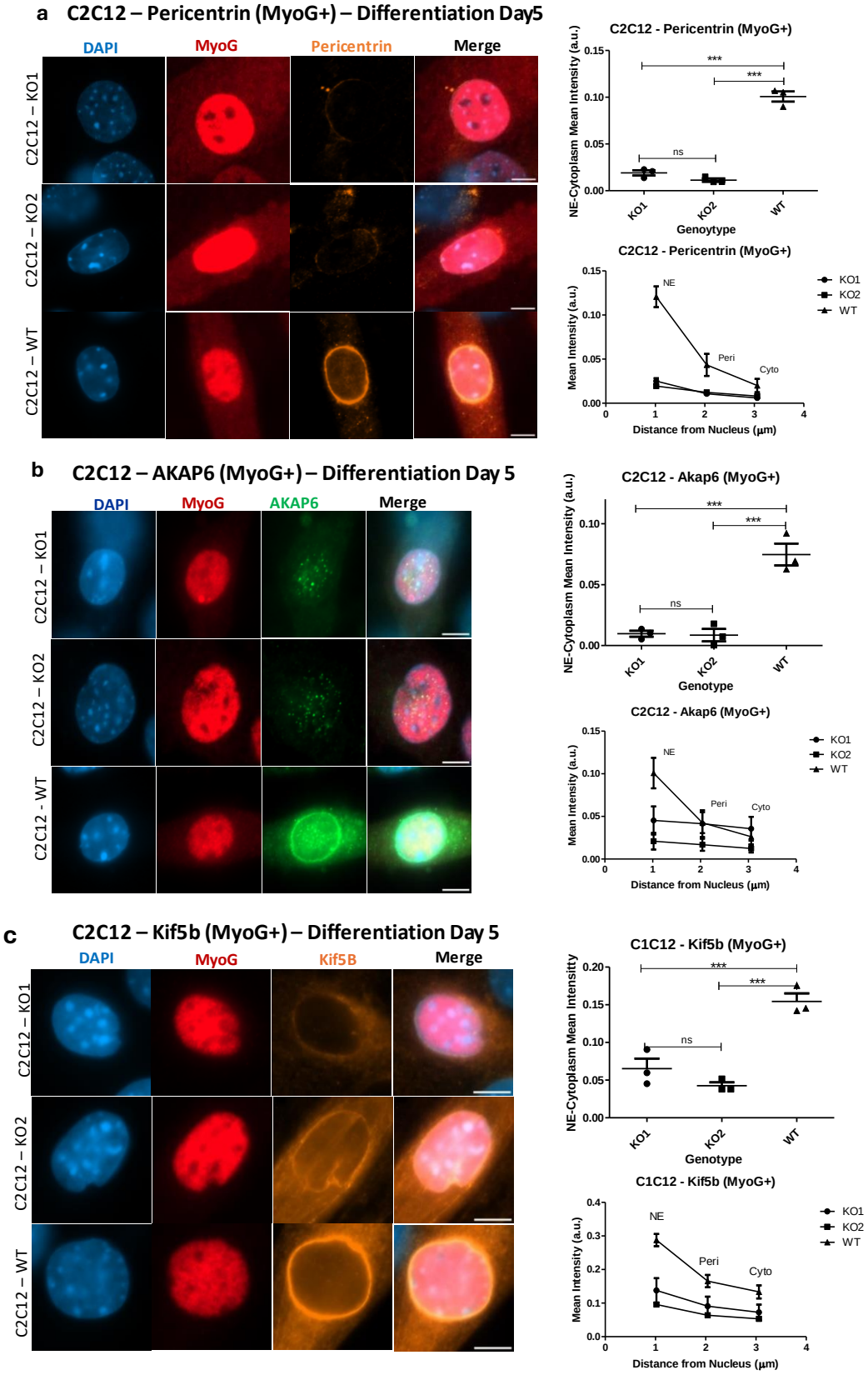

Supplementary Figure S3. Differentiating SLMAP3$^{-/-}$ myoblasts present defective MTOC recruitment to the NE

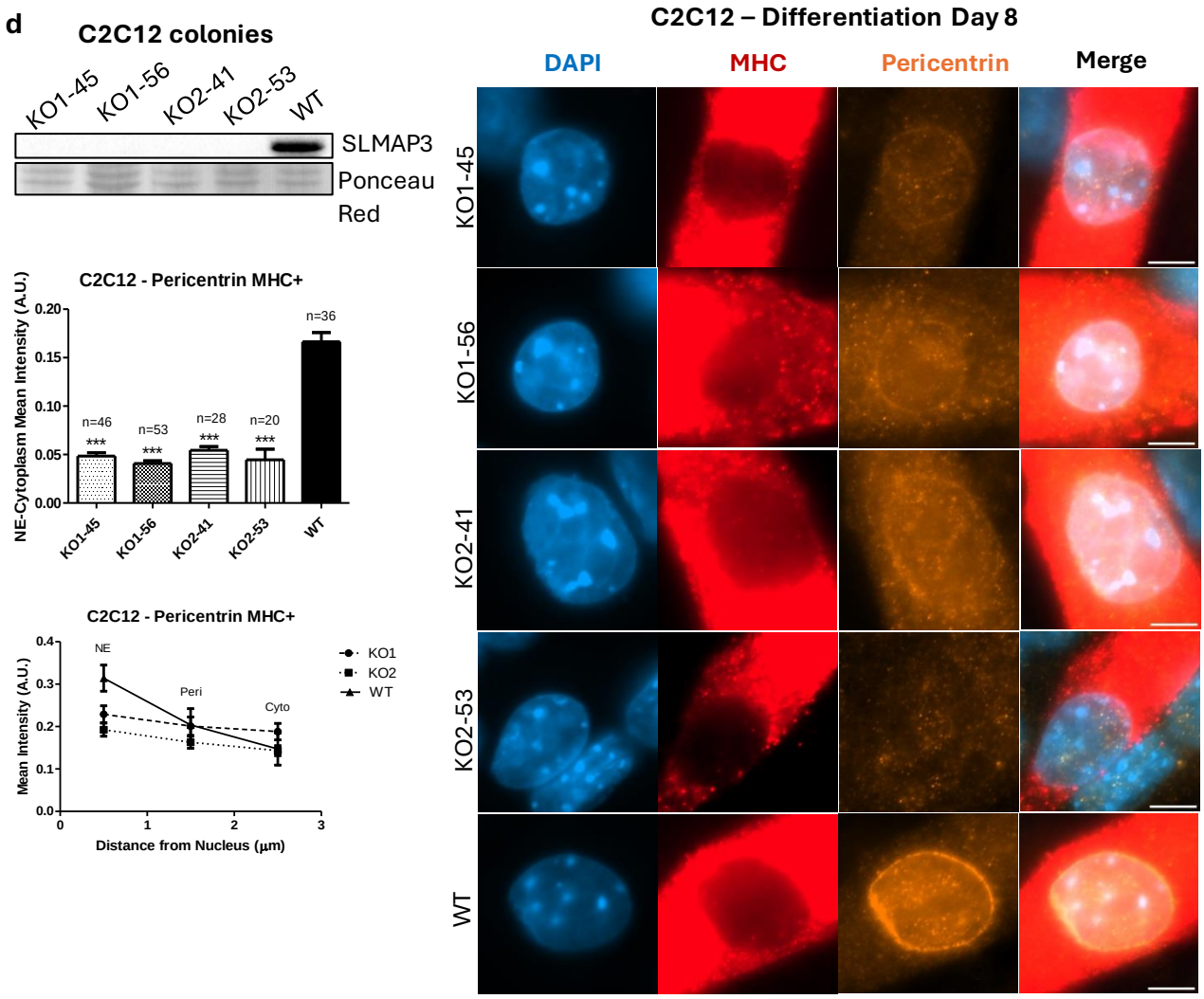

Supplementary Figure S4. SLMAP3$^{-/-}$ MEFs do not have abnormalities in the centrosomal microtubule nucleation

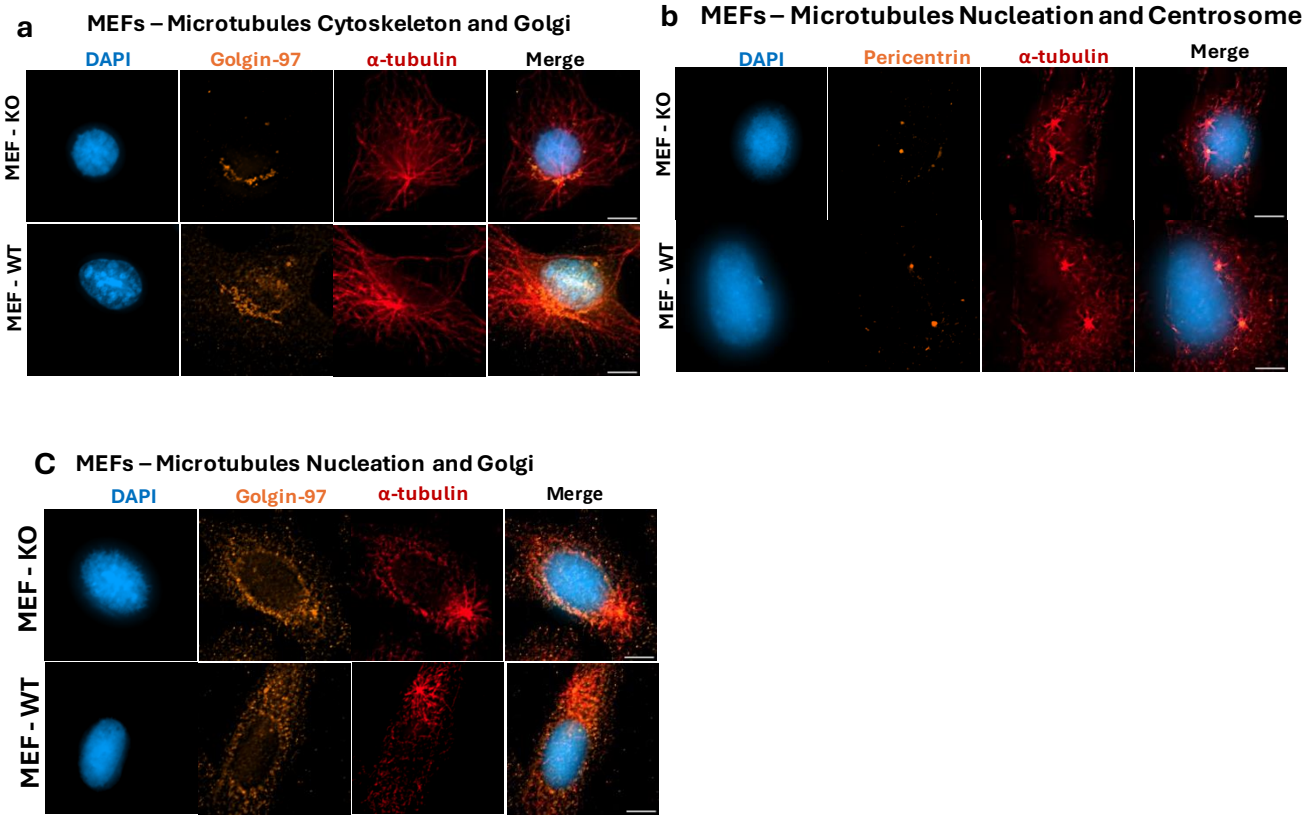

Supplementary Table 1. Defective Muscle Development Phenotypes

Supplementary Table 3

Defective Muscle Development Phenotypes			
Depletion or Mutant	**Differentiation**	**Myotube Formation**	**Nuclei Positioning**
Lamin A/C	Affected[S1-S5]	Affected[S1,S2,S5]	-
Emerin	Affected[S6]	-	-
SUN proteins	-	-	Affected[S7,S8]
Nesprin-1	Affected[S9]; Not affected[S10]	Affected[S9]	Affected[S11-S15]
AKAP6	Affected[S16]	Affected[S16]	Affected[S17]
MTOC proteins	-	-	Affected[S15]
Kinesin-1	Not Affected[S18,S19]; Affected[S9]	Not Affected[S18]; Affected[S9]	Affected[S15,S18-S21]

Supplemental References

S1. Favreau, C., Higuet, D., Courvalin, J.-C., and Buendia, B. (2004). Expression of a mutant lamin A that causes Emery-Dreifuss muscular dystrophy inhibits in vitro differentiation of C2C12 myoblasts. Molecular and Cellular Biology 24, 1481-1492. 10.1128/MCB.24.4.1481-1492.2004

S2. Frock, R. L., Kudlow, B. A., Evans, A. M., Jameson, S. A., Hauschka, S. D., and Kennedy, B. K. (2006). Lamin A/C and emerin are critical for skeletal muscle satellite cell differentiation. Genes & Development 20, 486-500. 10.1101/gad.1364906

S3. Markiewicz, E., Ledran, M., and Hutchison, C. J. (2005). Remodelling of the nuclear lamina and nucleoskeleton is required for skeletal muscle differentiation in vitro. Journal of Cell Science 118, 409-420. 10.1242/jcs.01630

S4. Bertrand, A. T., Brull, A., Azibani, F., Benarroch, L., Chikhaoui, K., Stewart, C. L., Medalia, O., Ben Yaou, R., and Bonne, G. (2020). Lamin A/C Assembly Defects in LMNA-Congenital Muscular Dystrophy Is Responsible for the Increased Severity of the Disease Compared with Emery-Dreifuss Muscular Dystrophy. Cells 9, 844. 10.3390/cells9040844

S5. Kandert, S., Wehnert, M., Müller, C. R., Buendia, B., and Dabauvalle, M. C. (2009). Impaired nuclear functions lead to increased senescence and inefficient differentiation in human myoblasts with a dominant p.R545C mutation in the LMNA gene. European Journal of Cell Biology 88, 593-608. 10.1016/j.ejcb.2009.06.002

S6. Iyer, A., and Holaska, J. M. (2020). EDMD-Causing Emerin Mutant Myogenic Progenitors Exhibit Impaired Differentiation Using Similar Mechanisms. Cells 9, 1463. 10.3390/cells9061463

S7. Lei, K., Zhang, X., Ding, X., Guo, X., Chen, M., Zhu, B., Xu, T., Zhuang, Y., Xu, R., and Han, M. (2009). SUN1 and SUN2 play critical but partially redundant roles in anchoring nuclei in skeletal muscle cells in mice. Proceedings of the National Academy of Sciences of the United States of America 106, 10207-10212. 10.1073/pnas.0812037106

S8. Meinke, P., Mattioli, E., Haque, F., Antoku, S., Columbaro, M., Straatman, K. R., Worman, H. J., Gundersen, G. G., Lattanzi, G., Wehnert, M., and Shackleton, S. (2014). Muscular dystrophy-associated SUN1 and SUN2 variants disrupt nuclear-cytoskeletal connections and myonuclear organization. PLoS Genetics 10, e1004605. 10.1371/journal.pgen.1004605

S9. Zhou, C., Li, C., Zhou, B., Sun, H., Koullourou, V., Holt, I., Puckelwartz, M. J., Warren, D. T., Hayward, R., Lin, Z., Zhang, L., Morris, G. E., McNally, E. M., Shackleton, S., Rao, L., Shanahan, C. M., and Zhang, Q. (2017). Novel nesprin-1 mutations associated with dilated cardiomyopathy cause nuclear envelope disruption and defects in myogenesis. Human Molecular Genetics 26, 2258-2276. 10.1093/hmg/ddx116

S10. Holt, I., Duong, N. T., Zhang, Q., Lam, L. T., Sewry, C. A., Mamchaoui, K., Shanahan, C. M., and Morris, G. E. (2016). Specific localization of nesprin-1-α2, the short isoform of nesprin-1 with a KASH domain, in developing, fetal and regenerating muscle, using a new monoclonal antibody. BMC Cell Biology 17, 26. 10.1186/s12860-016-0105-9

S11. Zhang, X., Xu, R., Zhu, B., Yang, X., Ding, X., Duan, S., Xu, T., Zhuang, Y., and Han, M. (2007). Syne-1 and Syne-2 play crucial roles in myonuclear anchorage and motor neuron innervation. Development 134, 901-908. 10.1242/dev.02783

S12. Puckelwartz, M. J., Kessler, E., Zhang, Y., Hodzic, D., Randles, K. N., Morris, G., Earley, J. U., Hadhazy, M., Holaska, J. M., Mewborn, S. K., Pytel, P., and McNally, E. M. (2009). Disruption of nesprin-1 produces an Emery Dreifuss muscular dystrophy-like phenotype in mice. Human Molecular Genetics 18, 607-620. 10.1093/hmg/ddn386

S13. Zhang, J., Felder, A., Liu, Y., Guo, L. T., Lange, S., Dalton, N. D., Gu, Y., Peterson, K. L., Mizisin, A. P., Shelton, G. D., Lieber, R. L., and Chen, J. (2010). Nesprin 1 is critical for nuclear positioning and anchorage. Human Molecular Genetics 19, 329-341. 10.1093/hmg/ddp499

S14. Stroud, M. J., Feng, W., Zhang, J., Veevers, J., Fang, X., Gerace, L., and Chen, J. (2017). Nesprin 1α2 is essential for mouse postnatal viability and nuclear positioning in skeletal muscle. Journal of Cell Biology 216, 1915-1924. 10.1083/jcb.201612128

S15. Gimpel, P., Lee, Y. L., Sobota, R. M., Calvi, A., Koullourou, V., Patel, R., Mamchaoui, K., Nédélec, F., Shackleton, S., Schmoranzer, J., Burke, B., Cadot, B., and Gomes, E. R. (2017). Nesprin-1α-dependent microtubule nucleation from the nuclear envelope via Akap450 is necessary for nuclear positioning in muscle cells. Current Biology 27, 2999-3009.e9. 10.1016/j.cub.2017.08.031

S16. Lee, S. W., Won, J. Y., Yang, J., Lee, J., Kim, S. Y., Lee, E. J., and Kim, H. S. (2015). AKAP6 inhibition impairs myoblast differentiation and muscle regeneration: Positive loop between AKAP6 and myogenin. Scientific Reports 5, 16523. 10.1038/srep16523

S17. Becker, R., Vergarajauregui, S., Billing, F., Sharkova, M., Lippolis, E., Mamchaoui, K., Ferrazzi, F., and Engel, F. B. (2021). Myogenin controls via AKAP6 non-centrosomal

microtubule-organizing center formation at the nuclear envelope. eLife 10, e65672. 10.7554/eLife.65672

S18. Metzger, T., Gache, V., Xu, M., Cadot, B., Folker, E. S., Richardson, B. E., Gomes, E. R., and Baylies, M. K. (2012). MAP and kinesin-dependent nuclear positioning is required for skeletal muscle function. Nature 484, 120-124. 10.1038/nature10914

S19. Wang, Z., Cui, J., Wong, W. M., Li, X., Xue, W., Lin, R., Wang, J., Wang, P., Tanner, J. A., Cheah, K. S. E., Wu, W., and Huang, J. D. (2013). Kif5b controls the localization of myofibril components for their assembly and linkage to the myotendinous junctions. Development 140, 617-626. 10.1242/dev.085969

S20. Wilson, M. H., and Holzbaur, E. L. F. (2012). Opposing microtubule motors drive robust nuclear dynamics in developing muscle cells. Journal of Cell Science 125, 4158-69. 10.1242/jcs.108688

S21. Wilson, M. H., and Holzbaur, E. L. F. (2015). Nesprins anchor kinesin-1 motors to the nucleus to drive nuclear distribution in muscle cells. Development 142, 218-28. 10.1242/dev.114769

Chapter Four - SLMAP3 is crucial for organogenesis through mechanisms involving primary cilia formation

Manuscript Acceptance and Copyright

From: openbiology@royalsociety.org
To: btuana@uottawa.ca
CC:
Subject: Open Biology - Decision on Manuscript RSOB-240206.R1
Body: 05-Sep-2024

Dear Professor Tuana,

We are pleased to inform you that your manuscript entitled "SLMAP3 is crucial for organogenesis through mechanisms involving primary cilia formation" has been accepted by the Editor for publication in Open Biology.

You can expect to receive a proof of your article from our Production office in due course, please check your spam filter if you do not receive it within the next 10 working days. Please let us know if you are likely to be away from e-mail contact during this time.

Article processing charge
Please note that the article processing charge is immediately payable. A separate email will be sent out shortly to confirm the charge due. The preferred payment method is by credit card; however, other payment options are available.

Thank you for your fine contribution. On behalf of the Editors of Open Biology, we look forward to your continued contributions to the journal.

Sincerely,

The Open Biology Team
mailto: openbiology@royalsociety.org

Date Sent: 05-Sep-2024

OPEN BIOLOGY

royalsocietypublishing.org/journal/rsob

Research

Cite this article: Dias AP, Rehmani T, Applin BD, Salih M, Tuana B. 2024 SLMAP3 is crucial for organogenesis through mechanisms involving primary cilia formation. *Open Biol.* **14**: rsob240206.
https://doi.org/10.1098/rsob.240206

Received: 18 July 2024
Accepted: 5 September 2024

SLMAP3 is crucial for organogenesis through mechanisms involving primary cilia formation

Ana Paula Dias, Taha Rehmani, Billi Dawn Applin, Maysoon Salih and Balwant Tuana

Department of Cellular and Molecular Medicine, University of Ottawa, Ottawa K1H 8M5, Canada

THE ROYAL SOCIETY PUBLISHING

SLMAP3 is crucial for organogenesis through mechanisms involving primary cilia formation

Ana Paula Dias[1], Taha Rehmani[1], Billi Dawn Applin[1], Maysoon Salih[1], Balwant Tuana[1*]
[1]Deparment of Cellular and Molecular Medicine, University of Ottawa, Ottawa, K1H 8M5, Canada

*Correspondence: btuana@uottawa.ca

Abstract

SLMAP3 is a constituent of the centrosome and is known to assemble with the striatin-interacting phosphatase and kinase (STRIPAK) complex, where it has been reported to repress Hippo signalling. The global knockout of SLMAP3 in mice results in embryonic/perinatal lethality and stunted growth without changes in the phosphorylation status of YAP. Diverse phenotypes present in the SLMAP3$^{-/-}$ embryos include reduced body axis, small and abnormal organs resembling defects in Planar Cell Polarity (PCP) signalling, while also displaying the notable polycystic kidneys, a known manifestation of ciliopathies. Analysis of cell polarity in primary mouse embryonic fibroblasts (MEFs) including cell migration, orientation and mitotic spindle angle did not reveal any changes due to SLMAP3 loss in these cells, although the expression of DVL3 was significantly reduced. Furthermore, MEFs lacking FGFR1OP2 or STRN3, two other STRIPAK members, did not reveal any significant changes in any of these parameters either. Significant changes in the number of ciliated cells and primary cilium length in SLMAP3 and FGFR1OP2 deficient MEFs were evident, while a reduced primary cilium length was notable in chondrocytes of SLMAP3 deficient embryos. Our findings suggest that SLMAP3 is essential for mouse embryogenesis through novel mechanisms involving the primary cilium/PCP and protein stability independent of Hippo signalling.

Keywords: SLMAP3, STRIPAK, FGFR1OP2, PCP, primary cilia, Hippo Pathway

1. Introduction

Congenital disorders are pathological conditions that stem from functional or structural defects, causing an estimated death of 295 000 infants worldwide every year and are one of the leading causes of death of people under 5 years old [1]. With 50% of these disorders without a specific cause [1], studies investigating birth defects can contribute to prevention strategies, treatment and early diagnosis.

Here, we investigated the impact of SLMAP3 deficiency on mouse embryonic development. The slmap gene encodes multiple protein isoforms that are expressed in tissue-specific manner generated through alternative splicing [2-4]. SLMAP proteins have in common coiled-coil domains, which favour protein-protein interactions, and C-terminal transmembrane domains that can target the protein to subcellular organelles, including endoplasmic reticulum, sarcolemma, mitochondria and nuclear envelope [2-6]. SLMAP3, which is ubiquitously expressed, encompasses the largest isoform that additionally has a N-terminal forkhead-associated (FHA) domain [4], known to bind to phosphothreonine residues [7,8] and to target SLMAP to the centrosome [4,9]. We reported that the deficiency of SLMAP3 in skeletal myoblasts impairs the microtubule organizing centre formation (MTOC) in the nuclear envelope leading to defective

myogenesis [6]. SLMAP has also been associated with Brugada syndrome, a fatal cardiomyopathy due to defective ion channel trafficking [10].

SLMAP3 and its paralog TRAF3IP3 are constituents of the striatin-interacting phosphatase and kinase (STRIPAK) complex [11,12], composed of the phosphatase PP2A, kinases from the germinal centre kinases families II, III and IV, the adaptors paralogs STRIP1 and STRIP2, Mob4, the paralogs STRN, STRN3 and STRN4, CCM3, the paralogs CTTNBP2 and CTTNBP2NL and the paralogs SIKE1 and FGFR1OP2 [11–17]. STRIPAK is evolutionarily conserved, being described in fungi [18], in invertebrates such as *Drosophila melanogaster* [19–22], *Caenorhabditis elegans* [23] and planarians [24], and in vertebrates [11,12]. The high conservation of SLMAP3 in the context of STRIPAK suggests that it might share essential roles in eukaryotes. The importance of STRIPAK in mammals is further evidenced by the deficiency of many of its components resulting in mouse embryonic lethality, as observed in the case of PP2A-C [25,26], PP2A-A [27,28], MAP4K4 [29], STRN [30], STRN3 [31,32], STRIP1 [33], Mob4 [34], CCM3 [35,36] and FGFR1OP2 [37]. The crystal structure of STRIPAK revealed that STRN3 proteins function as a scaffold, and STRIP1 and Mob4 help stabilize the complex [38]. SIKE1 interacts with STRN3 at an outer layer by which it recruits SLMAP3 to the complex [38,39]. FGFR1OP2 as a paralog of SIKE1 could recruit SLMAP3 in a similar fashion although little is known about its role. FGFR1OP2 was described to enhance wound healing [40–42] and found fused with FGFR1 receptor in myelomas [43–45].

In the context of STRIPAK, SLMAP3 was shown to be a negative regulator of Hippo signalling by recruiting the germinal centre kinases II MST1/2 to the complex via its FHA domain, where these kinases are dephosphorylated and inactivated by the PP2A [13,14,20,46]. This ultimately reduces the phosphorylation of the transcriptional co-activators YAP/TAZ, allowing their translocation from the cytoplasm to the nucleus, where they induce the expression of genes for cellular proliferation and growth [47,48]. The isoforms SLMAP1/2 (Uniprot B7Z863 and B7Z964, respectively) do not participate in this signalling because they lack the FHA required for the interaction with MST1/2. Because the Hippo pathway studies were conducted in cultured cells, we investigated the impact of the global ablation of SLMAP3 *in vivo*. We used the cre-lox to engineer the global knockout of *slmap* in mice, which presented embryonic/perinatal lethality [6]. Here, we delved into detailed analysis of the phenotypes and potential mechanisms of SLMAP3 action including Hippo signalling. The phenotypes observed with SLMAP3 loss include overall stunted growth with underdeveloped lungs, fused skeleton, disorganized chondrocytes in the growth plate, short intestines, polycystic kidneys and short tails, deficits that are consistent with those reported for aberrant planar cell polarity (PCP) [49–63].

PCP is crucial for cell polarity by guiding the asymmetric distribution of proteins such as DVLs to govern the morphogenic process of convergent extension and organogenesis [64–68]. The primary cilium, a non-motile microtubule-based projection, which is present in virtually all cells of the body and is crucial for detecting environmental cues to dictate cell behaviour [69,70], has also been linked to PCP [71–81]. PCP has been described to influence the polarization of migratory cells [82–86] and the orientation of mitotic spindle [87–91], and the latter also regulated by the centrosomal protein pericentrin [92] and ciliary protein IFT20 [93]. We report that loss of SLMAP3 reduces the expression of the PCP protein DVL3 and impacts the primary cilium without

any effect on Hippo signalling. Given that SLMAP3 is a centrosomal component, our results point towards an entirely new mode of action for this protein through mechanisms involving primary cilium and PCP components.

2. Results

2.1. SLMAP3$^{-/-}$ mice display embryonic/perinatal lethality with defective tissue architecture

Previously, we have generated global SLMAP3$^{-/-}$ mice using the Cre-Lox system [6]. The lack of SLMAP3 results in embryonic/perinatal lethality with 100% penetrance, and smaller embryos with small limbs and tails, abnormal face morphology and some embryos exhibit severe case of open neural tube known as craniorachischisis (figure 1*a*). The thymus of these animals are formed, with a notable reduced cell density (figure 1*b*). Furthermore, using our previous RNA-seq from E11.5 embryos [6] for gene ontology enrichment analysis with G:Profiler [94], we found that significantly altered genes with Log2 Fold Change > 0.75 in SLMAP3$^{-/-}$ embryos enrich for T-cell differentiation/activation (figure 1*c*), supporting the finding of abnormal thymus. Although smaller, the liver architecture of mice lacking SLMAP3 does not seem to be affected (figure 1*d*). The intestines have reduced length (figure 1*e*), but the different regions of small and large intestines are properly specified (figure 1*f*). The lungs are underdeveloped, displaying thick alveolar epithelium with deficit in the formation of alveolar sacs, although terminal bronchioles and alveolar ducts are observable (figure 1*g*). The pulmonary defects may explain the respiratory distress and cyanosis observed in SLMAP3$^{-/-}$ animals that are born alive but die soon after birth (electronic supplementary material, video S1). The changes in the lung development cannot be attributed to defective branching morphogenesis, as lung explants of embryos lacking SLMAP3 presented branch formation comparable to the controls after 72 h in culture (figure 1*h*).

Additional noticeable phenotype observed in SLMAP3$^{-/-}$ is the skeleton defects, with fused bones and cartilages (figure 2*a*). Examination of the humerus growth plate revealed defective organization of chondrocytes into columns (figure 2*b*), with defective orientation angle of the cells (figure 2*c*), which could explain the observed fused bones and cartilages. The proliferation of chondrocytes in the proliferative zone of the growth plate, assessed by Ki67 immunofluorescence staining, was found to be significantly reduced (figure 2*d*). Disoriented chondrocytes together with reduced proliferation could explain the defective limbs present in SLMAP3$^{-/-}$ embryos.

The kidneys of SLMAP3$^{-/-}$ mice are notably underdeveloped and present cysts (figure 2*e*). This type of polycystic kidney resembles those observed in the autosomal recessive disorder nephronophthisis, a typical infantile and bilateral disease where instead of massively large kidneys with cysts observed even in the surface of the organ, the kidneys can exhibit reduced size with cysts commonly located in the corticomedullary junction [95]. To investigate whether the cysts were formed due to uncontrolled proliferation, as it is seen in autosomal dominant polycystic kidney disease with mutations PKD1 and PKD2 genes [96], we assessed Ki67 staining in the epithelial cells of proximal and distal tubules and found no significant changes (figure 2*f*). Therefore, the cysts formation observed in SLMAP3$^{-/-}$ is not attributable to increased cellular proliferation.

2.2. SLMAP3 functions independently of Hippo signaling during mouse embryogenesis

Given the stunted development and widespread organ deficits of SLMAP3$^{-/-}$ embryos and the association of SLMAP with Hippo signalling and cell proliferation, we interrogated any impact on the phosphorylation status of YAP. Western blot analysis of multiple organs, including brain and lungs, indicated that there was no change in status of phosphorylated YAP due to SLMAP3 loss (figure 3*a*). This is in accordance with no changes in YAP phosphorylation in whole embryos, limbs and hearts lacking SLMAP3 [6,97–99]. Furthermore, we isolated mouse embryonic fibroblast (MEFs) from E14.5 SLMAP3 null embryos, which also indicated no significant changes in phosphorylation of YAP at serine 397 compared with WT cells (figure 3*b*). The immunofluorescence staining of YAP indicated similar nuclear localization in both WT and SLMAP$^{-/-}$ MEFs without any significant differences (figure 3*c*). We also analysed the phosphorylation of YAP at low cell densities (figure 3*d*) and compared the distribution of YAP in the nuclear and cytoplasmic fractions (figure 3*e*), but found no differences between SLMAP-/- MEFs and WT. Treatment of cells with either XMU-MP-1, an inhibitor of MST1/2 kinases [100], or okadaic acid, a PP2A inhibitor [101,102], did not reveal any changes in the phosphorylation status of YAP and MST1/2 between SLMAP3$^{-/-}$ and WT MEFs (figure 3*f*). MST1/2 were particularly active only in the presence of okadaic acid in both cell types (figure 3*f*), indicating that in culture conditions, these kinases are normally kept inactive by mechanisms independent of SLMAP3. Furthermore, RNA-sequencing analysis of the two MEF genotypes (electronic supplementary material, table S1) indicated no differences in the expression of the YAP target genes Birc5, CCN1, CCN2 and Myc [103], similar to what is observed in our previous RNA-seq from whole SLMAP3$^{-/-}$ [6] (figure 3g).

We further examined protein lysates of proliferating MEFs by Reverse Phase Protein Array (RPPA) Assay [104], in a panel consisting of 407 antibodies. The resulting relative protein expression is available in electronic supplementary material, table S2, and the unsupervised clustering and heat maps of these expressions are found in the electronic supplementary material S2. These antibodies targeted proteins from a large variety of biological processes, including Hippo pathway, canonical Wnt signalling, glycolysis, autophagy, embryonic development, mTOR, DNA damage, cell survival, proliferation, apoptosis and others. Despite the broad panel of antibodies, no obvious changes in protein levels/phosphorylation could be identified in SLMAP3$^{-/-}$ MEFs. RNA-seq analysis of proliferating MEFs (electronic supplementary material, table S1) indicated that only 11 genes were expressed differently (electronic supplementary material, figure S1A), most notably Arhgap36 and CDKN1A with Log2 fold change of −2.34 and −0.60, respectively. The data were validated by RT-qPCR, confirming the downregulation of Arhgap36 (electronic supplementary material, figure S1B) and CDKN1A (electronic supplementary material, figure S1C).Together, these results suggest that gene expression in proliferating MEFs were not broadly impacted by the lack of SLMAP3, despite the severity of the phenotypes observed in SLMAP3$^{-/-}$ embryos.

Cell cycle dynamics of SLMAP3$^{-/-}$ MEFs with propidium iodide (PI) staining indicated no significant changes (figure 4*a*). Cellular senescence was not observed either, and with H2O2 treatment, the senescence in SLMAP3$^{-/-}$ MEFs was comparable to that in WT cells (figure 4*b*). Annexin V and PI staining analysis did not indicate changes in cell death, even after the induction

of cellular stress with H2O2 (figure 4*c*). In comparison, we noted that myoblasts lacking SLMAP3 (electronic supplementary material, figure S2A) that we previously generated by CRISPR/Cas9 [6], resulted in accumulation of cells in G1 phase (figure 4*d*), followed by increased cellular senescence (figure 4*e*) without any changes in cell death (figure 4*f*). The increased cellular senescence in SLMAP3$^{-/-}$ C2C12 myoblasts is in accordance with what we observed in H9C2 cardiomyoblasts with depletion of all SLMAP isoforms, which also exhibited reduced proliferation and increased senescence [98]. These findings suggest that SLMAP3 can influence cell cycle dynamics in a cell-specific manner and works through mechanisms that are independent of Hippo signalling.

2.3. Loss of SLMAP3 impacts cell shape independent of changes in cortical F-actin or focal adhesions

SLMAP3$^{-/-}$ MEFs presented subtle change in cell morphology observable in phase contrast microscope, with rounder and smaller appearance. To examine this further, we stained cells for F-actin with phalloidin and measured their dimensions with the parameters area, eccentricity, major axis length, minor axis length and perimeter and some of them were significantly different in SLMAP3$^{-/-}$ MEFs versus WT (figure 5*a*). Since SLMAP3 localizes at the nuclear envelope [4–6], we also assessed any changes in nuclear dimension, but none of the parameters reached statistical significance in SLMAP3$^{-/-}$ MEFs (figure 5*b*).

Cytoskeleton regulation has been associated with multiple STRIPAK members [33,105–112]. One of the mechanisms involves the regulation of ERM proteins, known to control F-actin in the cell cortex. The kinases MST3/4 and MAP4K4 were demonstrated to induce the phosphorylation and activation of ERM proteins [106,110,112,113], whereas STRN3 and STRIP1 negatively regulate MST3/4 in this process [106]. Given the association of SLMAP3 with STRIPAK and the changes in morphology of SLMAP3 deficient MEFs, we measured the F-actin staining in the cell cortex, but no statistical differences were found compared to WT cells (figure 5*c*).

The second mechanism proposed for the STRIPAK members to affect cell morphology by focal adhesion (FA) regulation [33,109,111,112]. MAP4K4 was shown to be involved with FA disassembly [111,112]; STRIP1 deficient MEFs exhibited reduced number of FA with increase in their clustering [33]; and depletion of CCM3 in cancer-associated fibroblasts increased the size and number of FA per cell [109]. To assess if FA was affected in SLMAP3$^{-/-}$, we stained cells for paxillin. We also included in this analysis STRN3 deficient MEFs generated with shRNA (electronic supplementary material, figure S2B). Although both SLMAP3$^{-/-}$ and STRN3 depleted MEFs had significantly reduced area, we could not find statistical difference between focal adhesion density in the cells, or changes in the focal adhesion dimension, such as area, major axis length, minor axis length and perimeter (figure 5*d*). These results suggest that SLMAP3 acts differently from other STRIPAK members in regulating cell morphology through mechanisms independent of increased F-actin in the cell cortex or alterations in focal adhesions.

2.4. Impact of SLMAP3 on migration and orientation of MEFs

Polarized cell migration is known to be affected by PCP [82–86], and we examined if the loss of SLMAP3 in MEFs would lead to any polarity defects. Immortalized SLMAP3$^{-/-}$ MEFs which also lack SLMAP2 were first starved for 24 h, followed by scratch and migration for 6 h with or without the PCP ligand Wnt5a [57]. Cells of only the first or second layers in the migration edge were considered, and the angles were measured in individual cells in reference to their centrosome and Golgi localization, found in the front of the nucleus towards the migration edge [114]. We also generated and examined FGFR1OP2 and STRN3 depleted MEFs for comparison because of the lethality caused in mice with the knockout of either of these STRIPAK components [31,37] is similar to that observed in SLMAP3$^{-/-}$ embryos. Although we found a shRNA that could deplete STRN3 expression (electronic supplementary material, figure S2B), the four shRNAs designed to target FGFR1OP2 could not reduce its expression (electronic supplementary material, figure S2C). Then, we designed two sgRNAs for CRISPR/Cas9 mediated knockout (electronic supplementary material, figure S2D,E), and we obtained a FGFR1OP2 knockout colony with sgRNA723# (colony 12) (electronic supplementary material, figure S2E), which was used for the experiments. The analysis with these generated cells indicated no changes in the angle of orientation, with the angles varying between 0° and 60° in all genotype types (figure 6*a*), even after treatment of the cells with Wnt5a (figure 6*b*).

We assessed the mitotic spindle orientation because it is known to be regulated by PCP as well [87–91]. Changes in this angle may also lead to the formation of the polycystic kidney, where disoriented division of the epithelial cells from the nephron tubules results in the enlargement of the diameter of these structures and reduced lengthening [115–117]. The mitotic spindle is also affected in MEFs lacking pericentrin [92], centrosomal protein that we identified as an interactor of SLMAP3 [6]. Mitotic spindle orientation was assessed by staining for γ-tubulin as a centrosome marker and acquisition of images in Z-stack. SLMAP3, FGFR1OP2 and STRN3 depleted MEFs were examined and the coordinates of the centrosomes were used for the arctan function to obtain the angle of the mitotic spindle, as described [92]. Although we observed a subtle reduction in the mitotic spindle angles in SLMAP3 KO MEFs, the angles in FGFR1OP2 KO MEFs, cells with drastically reduced SLMAP3 expression, was similar to that in control cells, so we attributed the changes to experimental variability (figure 6*c*).

We further investigated the PCP pathway and noted a significant reduction in the expression of DVL3 protein in the affected tissues, including lungs (figure 7*a*), brain (figure 7*b*) and skeleton (figure 7*c*). Surprisingly, DVL3 expression was not reduced in SLMAP3$^{-/-}$ MEFs (electronic supplementary material, figure S3A), nor was its activation affected upon Wnt5a treatment (electronic supplementary material, figure S3B). Expression of the PCP-associated proteins including MUSK1, RhoA (electronic supplementary material, figure S3C) and ROR2 (electronic supplementary material, figure S3DE) was not impacted. Phosphorylation and activation of ROCK2 and JNK1/2 were not affected in SLMAP3$^{-/-}$ MEFs either, even after Wnt5a treatment (electronic supplementary material, figure S3F). The migration of MEFs after 16 h, with or without Wnt5a treatment, did not indicate any changes (figure 7*d*).

As no changes in DVL3 protein levels were seen in MEFs despite changes observed in SLMAP3$^{-/-}$ embryos, we analysed DVL3 expression after the immortalization of MEFs. Primary

MEFs from E14.5 embryos were found to still express the approx. 45 KDa SLMAP2 isoform, which is lost upon their immortalization (figure 7*e*). We hypothesized that SLMAP2 may be compensating in primary SLMAP3-/− MEFs to maintain DVL3 protein levels. Analysis after immortalization of primary SLMAP3-/− MEFs indicates a dramatic decrease in DVL3 protein levels (figure 7*f*), with no changes in transcripts (figure 7*g*). However, even with reduced DVL3 expression, its activation was not altered (figure 7*f*), nor was its response to Wnt5a (figure 7h). ROCK2 activation and protein levels did not change either (figure 7h,i).

DVL3 protein can be degraded by both lysosomal and proteasomal mechanisms [118-120], and we examined if SLMAP was responsible for its stability by regulating these pathways. MEFs were treated with MG132, a proteasome inhibitor [121], or NH4Cl, a lysosomal degradation pathway inhibitor [122,123]. NH4Cl treatment was found to restore DVL3 protein levels in SLMAP3 deficient MEFs to that seen in WT cells after 48 h (figure 7*j*) while MG132 was without any effect on DVL3 after 24 h (electronic supplementary material, figure S3G). These results demonstrate that SLMAP is important for regulating DVL3 protein levels specifically by preventing its degradation by the lysosome. Thus, MEFs lacking SLMAP3 do not have orientation deficits in our experimental conditions, despite the reduced expression of DVL3, which was also notable in SLMAP3-/− embryos and may contribute to the phenotypes observed.

2.5. The knockout of SLMAP3 or FGFR1OP2/Wit3.0 results in defective primary cilia formation

Given the associations of SLMAP3 with the centrosome [4,6,9], it is plausible that the lack of SLMAP3 could cause disturbances in this structure and result in the phenotypes observed in SLMAP3-/− mice. However, the orientation assays indicated that during migration and cell division, the centrosomes are properly localized (figure 6*a, b* and *c*). Depletion of SLMAP3 in HeLa was reported to increase the number of centrosomes per cell [9]; however, no changes in centrosome numbers were found in MEFs depleted of SLMAP3 (figure 8*a*). Considering the association between centrosome and Golgi, we also assessed this organelle. Studies showed that depletion of CCM3, STK24 and MST4 induces the dispersal of Golgi apparatus [113,124], suggesting a role of STRIPAK in this organelle. However, we did not detect any changes in the Golgi in SLMAP3-/− MEFs (figure 8*a*). In microtubule nucleation assays, we found that SLMAP3 was not important for the microtubule nucleation activity either [6].

The mother centriole from the centrosome gives rise to the primary cilium, and mutations in associated proteins result in birth anomalies with systemic manifestation [69,125]. Disturbances in primary cilium could potentially explain the phenotypes observed in SLMAP3-/− embryos. To analyse this structure in MEFs lacking SLMAP3, we first examined if they could undergo cell cycle arrest after 24 h of starvation to allow primary cilium growth. Both MEFs and C2C12 lacking SLMAP3 have reduced expression of the cyclin/CDK inhibitor CDKN1A (electronic supplementary material, figure S1C) and that could impair cell cycle arrest. However, SLMAP3-/− MEF arrested in G1 phase as seen for WT cells (figure 8*b*). Next, we aimed to analyse primary cilium not only in SLMAP3-/− but also in FGFR1OP2 and STRN3 depleted cells, given their partnership with SLMAP3 in the STRIPAK. After 24 h of starvation, we found that SLMAP3 or FGFR1OP2 knockout MEFs had reduced number of ciliated cells and cilium length, but not

STRN3 deficient cells (figure 8*c*). The reduced cilium length was also observed in SLMAP3$^{-/-}$ chondrocytes of humerus growth plate (figure 8*d*). These results suggest that both SLMAP3 and FGFR1OP2 are important in the formation of primary cilium, which may account for the similar phenotypes observed in mice with their respective knockout of either of them.

2.6. SLMAP3 is important for the protein stability of the STRIPAK members SIKE1 and FGFR1OP2

To gain insight into how the knockout of SLMAP3 could affect the STRIPAK complex, we analysed the protein expression of multiple STRIPAK members. No significant changes in expression of STRIP1, STRN and the catalytic subunit of PP2A were detected (figure 9*a*). However, we were particularly interested in the expression of SIKE1 and FGFR1OP2. SIKE1 was shown to recruit SLMAP3 to the STRIPAK by interacting with STRN3, and depletion of SIKE1 or SLMAP3 reduced the expression of each other in HGC-27 cells [39]. Decreased SIKE1 expression was notable in SLMAP3$^{-/-}$ MEFs (figure 9*b*), whole embryos (figure 9*c*) and in different tissues (figure 9*d*). Although cells lacking SLMAP3 have reduced expression of SIKE1, the biological significance of this remains to be further addressed, since the knockout of SIKE1 in mouse does not result in any obvious phenotype [126]. Nevertheless, the knockout of FGFR1OP2 results in an astonishing resemblance to the phenotype of SLMAP3$^{-/-}$ embryos, with lethality of 100% penetrance, shorter body size, reduced limbs and tails and abnormal face morphology [37]. Similarly to SIKE1, FGFR1OP2 expression was reduced in SLMAP3$^{-/-}$ MEFs at protein level (figure 9*e*), with no changes in transcripts (figure 9*f*).

To examine if SLMAP3 affects SIKE1 stability through proteasomal mechanisms, we incubated cells with the proteasome inhibitor MG132 [121], and after 24 h of treatment, SIKE1 expression in SLMAP3$^{-/-}$ MEFs was restored to levels seen in WT cells (figure 9g). These data imply that SLMAP3 protects SIKE1 from proteasome degradation. Next, we sought to examine the importance of FGFR1OP2 for SLMAP3 expression and observed that the expression of not only SLMAP3 but also SIKE1 protein was reduced in FGFR1OP2 KO MEFs (figure 9*h*), without changes in their transcripts (figure 9*i*). Treatment of these cells with MG132 lead to preservation SIKE1 while SLMAP3 protein was still absent even after 24 h of treatment (figure 9*j*). We also subjected these cells to NH4Cl, a known inhibitor of lysosomal degradation [122,123], and the level of SLMAP3 remained undetectable (figure 9*k*). This suggests that FGFR1OP2 regulates SLMAP3 protein levels by mechanisms other than the proteasome and lysosomal degradation.

3. Discussion

We report that loss of SLMAP3 is embryonic lethal in mice and stunts the development of multiple organs. Our data reveal that SLMAP3 may operate at multiple levels to guide development in a cell-/tissue-specific manner. The data indicate that SLMAP3 influences cell shape, growth and orientation and operates through mechanisms involving the centrosome, cilia formation, protein stability of DVL3 and key STRIPAK components including SIKE and FGFR10P2. The discovery that SLMAP3 can selectively impact cilia formation in the growth plate *in vivo* and primary MEFs in culture define a unique mode of SLMAP action in this process.

Given the reports of the association of SLMAP3 with Hippo pathway, our first hypothesis was that the lack of SLMAP3 increased Hippo activity, resulting in smaller embryos. However,

this is very unlikely to be the case since no changes in YAP phosphorylation or translocation were noted in SLMAP3 deficient cells. Furthermore, knockout of YAP in mouse results in embryonic lethality prior to organogenesis due to defects in placenta and in yolk sac vasculogenesis [127], while the knockout of both YAP and TAZ causes even a more severe phenotype, with lethality before embryonic implantation [128]. Previously, it was shown that depletion of SLMAP3 increases YAP phosphorylation and causes total exclusion from the nucleus in cell culture [46]; however, we never observed this in any tissues and cells analysed [6,97–99]. The knockout of SLMAP3 causing the complete absence of YAP in the nucleus should result in a phenotype at least similar to the complete ablation of YAP [127], which is not the case as SLMAP3–/− animals can develop enough to be born and without observable placenta abnormalities. This highlights the importance of validation of cell culture findings with *in vivo* systems.

Detailed analysis of multiple organs of SLMAP3–/− embryos implied that the PCP pathway could be responsible for the phenotypes observed. Similar defects with knockout of multiple PCP members are noted in lungs [52,53,61], skeleton [50,52,56], guts [59,60] and kidneys [49,55,61], as is the craniorachischisis [62,63] present in some of these embryos [99]. Furthermore, orientation defects were observed in the growth plate of SLMAP3-/- embryos, a region known to be impacted by the PCP ligand Wnt5a [129]. In the case of kidney, nephronophthisis is a common manifestation of ciliopathies, and it is normally caused by mutations in NPHP genes, which encode for proteins from the transition zone of the cilia [125]. Knockout of VANLG2 and inversin/NPHP2 causes a similar type of polycystic kidney [49,55,61], highlighting the connections between PCP and cilia with a potential novel connection to SLMAP3.

Other investigations have also emphasized the relationship between cilia and Wnt signalling [77]. The depletion of ciliary proteins such as NPHP4, BBS4, BBS6, KIF3A, IFT88 and OFD1 was shown to positively influence the Wnt canonical pathway [74,75,78] while the overexpression of inversin/NHPH2 antagonized this effect [73]. Additionally, RPGRIP1L/NPHP8, BBS4, BBS6 and IFT88 were demonstrated to be required for the proper orientation and organization of stereociliary bundle of the cells from the organ of Corti [76,79,80]. Furthermore, Vangl2 was shown to genetically interact with BBS1 and BBS6 in mice and to localize in the cilium base of IMCD3 kidney cells [80]. Likewise, PCP proteins are required in determining ciliary patch orientation in ependymal cells, positioning the primary cilium in radial glial progenitor cells and organizing cell–cell polarity in both cell types [81]. Moreover, in *Xenopus laevis* mucociliary epithelium, DVL proteins regulate the docking of the basal body to the cell surface through a mechanism involving RhoA GTPase and contribute to the planar polarization of the basal body and directional cilia beating [130]. These studies support a role for PCP components and Wnt signalling pathways in primary cilium.

SLMAP3 is a centrosomal component [4] and serves a critical role in muscle development by guiding the formation of the MTOC in the nuclear envelope of differentiating myoblasts [6]. Given that depletion of SLMAP3 reduced the number of ciliated cells and cilium length and the similarities between SLMAP3–/− embryos to that reported for models with PCP defects, it is plausible to think that the absence of SLMAP3 could disturb basal body functions. This contention is further supported by our finding that loss of SLMAP3 reduced DVL3 protein levels, which is similar to what is observed in aberrant expression of the ciliary proteins NPHP2 and NHPH4 that leads to enhanced degradation of DVL1, DVL2 and DVL3 [73,74], while suppression of BBS4 results in higher levels of DVL1 [75]. Conversely, a separate study found that depleting NPHP8 (Rpgrip1l), which reduces ciliated cell count and cilium length, is necessary for maintaining the stability and proper localization of DVL2 and DVL3 in the base of primary cilia in MDCK cells

[76]. In MEFs, the knockout of NPHP2 increases DVL1 expression but depletes protein levels of DVL2/3 [84]. These studies exemplify the close relationship between DVL protein levels and the primary cilium and now point to SLMAP3 as a potential link between both.

Further credence to the role of SLMAP3 in cilia comes from interactome studies that detected not only SLMAP but also several STRIPAK members including STRN/3/4, STK26, STRK24, Mob4, MAP4K4 and STRIP1/2 in centrosome–cilium interface and centriolar satellites [131–133]. The SLMAP paralogs TRAF3IP3/T3JAM and CCDC136/NAG6 were also identified in these interactomes [132,133], and depletion of TRAF3IP3 was shown to reduce the number of ciliated lymphocytes [133]. Although FGFR1OP2 depleted MEFs had reduced number of ciliated cells and cilium length, similarly to SLMAP3–/− cells, no changes were noted in STRN3-deficient MEFs. This suggest distinct roles for STRIPAK members in biology of cilia with SLMAP being prominent.

Considering the phenotypes observed in SLMAP3–/− embryos, defective orientation is expected. Additionally, STRIPAK members STK25 and CCM3 were demonstrated to be required to polarized cell migration [113,124,134]. Depletion of FGFR1OP2 in rat fibroblasts impacted cell migration [42], and given its association with SLMAP3, the latter could have contributed to disorientation of cells to decrease migration. However, SLMAP3–/− MEFs exhibited oriented migration and mitotic spindle angles comparable to the WT, implying that PCP defects observed in animals are not always reproducible as disorientation in cell culture. It is conceivable that SLMAP3 deficiency impacts cellular polarization in a cell-specific manner or that three-dimensional model systems might be required to reproduce the PCP defects observed *in vivo*.

Given the comparable phenotypes of SLMAP3 and FGFR1OP2 knockout mice and their association in the STRIPAK, one can envisage that they work together, with FGFR1OP2 being one of the most important adaptors for SLMAP3. Indeed, we found that SLMAP3 influences protein levels of both SIKE1 and FGFR1OP2, and in the case of SIKE1, SLMAP3 protects it from proteasomal degradation. Unfortunately, the mechanism of how FGFR1OP2 affects SLMAP3 protein levels remains elusive, but future investigations of degradation pathways with alternative compounds and tools [135] should clarify this. The finding that SLMAP3 protects SIKE1 from degradation is also intriguing. SIKE1 was reported to have protective roles in induced cardiac hypertrophy by repressing TBK1-AKT-mTOR cascade [136]. The specific knockout of SLMAP3 in cardiac progenitors resulted in smaller embryonic hearts but did not show significant changes in mTOR pathway activation [98]. Assessments of SLMAP3 cardiac protective roles with the induction of pathological hypertrophic program might reveal novel roles of this protein in cardiac physiology.

A key feature of SLMAP3–/− MEFs was changes in cell morphology, with reduction in cell size and a shift towards a more rounded shape. However, no alteration in F-actin in the cell cortex and focal adhesions, which are regulated by STRIPAK [33,106,108–112], was detected. No changes in the activation of ROCK2 and JNK1/2, effector kinases of PCP known to regulate actin cytoskeleton [137,138], was observed. A more detailed investigation of F-actin cytoskeleton, including stress fibre measurements, analysis of the activation of the small GTPases RhoA, Rac or Cdc42, quantification of F- and G-actin and measurements of lamellipodia, might shed light into the mechanisms through which SLMAP3 orchestrates these cellular changes.

It is notable that SLMAP3 affects proliferation in a cell-specific manner since SLMAP3–/− MEFs do not present aberrations in cell cycle dynamics, changes in proliferation and cellular senescence, which were evident in C2C12 cells devoid of SLMAP3, similar to that observed in H9C2 cardiomyoblasts [98]. Further studies examining the impact of SLMAP on the cell cycle

dynamics in different cell types will reveal which tissues it can impact. It will also clarify whether the reduced proliferation of chondrocytes in the growth plate of SLMAP3–/− embryos is an autonomous or non-autonomous phenomenon, taking into account the widespread organ abnormalities.

Although RNA-seq analysis of E11.5 SLMAP3–/− embryos indicated downregulation in genes associated with muscle development processes [6], interrogation by RPPA and RNAseq in SLMAP3-depleted MEFs did not reveal widespread changes. However, SLMAP3 loss did lead to a notable decrease in Arhgap36 transcripts in MEFs. Arhgap36 belongs to the Rho GTPase family and is involved in Gli transcription factors activation in the primary cilia [139]. How SLMAP3 may regulate this process needs consideration given the impact on cilia and is in line with our studies in muscle where it is crucial for guiding the MTOC and regulating gene expression in myogenesis [6].

Finally, the ubiquitous expression of SLMAP3 and the prevalent organ deficits observed in its absence implies that it is a crucial player in development. The data are revealing that SLMAP3 may serve diverse roles in a cell-specific manner that influence cell shape, growth and behaviour through mechanisms that involve the MTOC, cilia, PCP components and STRIPAK members. A model depicting the action of SLMAP3 is proposed (figure 10). As a member of STRIPAK, SLMAP3 could impact actin cytoskeleton, while its membrane association could help with docking of basal body at the plasma membrane by interactions with centrosome and centriolar satellite proteins, allowing the development of primary cilia. The ability of SLMAP to protect DVL3 against degradation would maintain PCP signalling, while its action at the nuclear envelope could account for gene regulation of Arhgap36. Given that SLMAP has no impact on YAP activity, the model here represents a logical segue into investigations on new mode of SLMAP3 action and its critical importance in organogenesis.

4. Conclusion

SLMAP3 is critical for development as its loss in mice results in widespread deficits in organogenesis with phenotypes reminiscent of defective PCP. Our data suggest that SLMAP3 modulates PCP at the level of primary cilium, a function that might be shared with its partner FGFR1OP2, with mechanisms involving protein stability of DVL3 and STRIPAK independent of Hippo signalling.

5. Methods and Materials

5.1. Transgenic Mice Generation

In this study, we used mice generated with the CMV driven Cre for the recombination of floxed SLMAP at exon 3 (reference transcript ENSMUST00000139075.8), as described elsewhere [6,97]. The Cre transgenic mouse was a gift from Dr. Nemer Mona, University of Ottawa. Genotyping was performed following the procedures previously detailed [97]. The mice involved in this research were kept at the Animal Care and Veterinary Service Barrier Facility at the University of Ottawa and were handled according to the guidelines set forth by the Canadian Council on Animal Care, as outlined in the Guide to the Care and Use of Experimental Animals (2 vols., Ottawa, Ont.: CCAC, 1980−1993), and the Animals for Research Act, R.S.O. 1990, c.A. 22. All animal study procedures were approved by the Animal Care Committee at the University of Ottawa.

5.2. Cell Line Generation and Culture Conditions

MEFs were isolated from E14.5 embryos as described [140]. For immortalization, MEFs were transfected with the plasmid SV40 1: pBSSVD2005 (a gift from David Ron, RRID: Addgene_21826) [141], following the protocol of the supplier. The immortalization consisted of at least five rounds of 1/10 splits of the transfected cells or until cellular senescence was no longer observed. Immortalized cells grew in culture for months without ever losing proliferation potential.

To generate MEF lines with depleted STRN3, we utilized shRNAs. As a control for the shRNAs, we employed a scramble sequence used before [97]. The shRNAs designed to target FGFR1OP2 failed to decrease its expression by more than 50%, and because of that we turned to CRISPR/Cas9. The sgRNAs for FGFR1OP2 are listed in the table below, and the Cas9 cleavage was confirmed with T7 endonuclease-based EnGen® Mutation Detection Kit (New England Biolabs, cat# E3321S). For FGFR1OP2-sgRNA#2, we used the following pair of primers: 5′ -GATGGCCTGCTCTAGACACT and 5′ -TGGCGGTGAAGGATGTCTTA; for FGFR1OP2-sgRNA#723, we used the primers: 5′ -TGAAAGTTGCCTGTAGTGGCT and 5′ -AAACAAACATACAAGTGAGGCTAC. All these constructs were cloned into a lentivirus plasmid by Vectorbuilder. As a non-target control for CRISPR/Cas9, pLentiCRISPRv2 carrying a guide RNA targeting EGFP (a gift from Roland Friedel; RRID: Addgene_86153) (Addgene plasmid #86153) [142,143] was used, similarly to before [6]. The C2C12 myoblast cells utilized in this study, originally sourced from the American Type Culture Collection (ATCC), were previously engineered to possess a knockout of SLMAP3 via CRISPR/Cas9 technology, employing the pLentiCRISPRv2 vector (gift from Feng Zhang; RRID: Addgene_52961) [6,144,145]. All these constructs and target sequences are listed below.

Target	Construct Type	Name	Target Sequence 5`- 3`
Scramble	pLV -shRNA [146]	shRNA-SC	AGGATAAGCGTCAACGAATAGGTGA
STRN3	pLV -shRNA [147]	STRN3-shRNA#1	CACTGGTAGTGCGGTAATTTA
STRN3	pLV -shRNA [148]	STRN3-shRNA#2	AGCAAGGCAGACAGCTATTAA
FGFR1OP2	pLV -shRNA [149]	FGFR1OP2-shRNA#2	GAAAGATGACCCAGGTATAAT
FGFR1OP2	pLV -shRNA [150]	FGFR1OP2-shRNA_all	AGTCTGCCCTGGAACTGATAA
FGFR1OP2	pLV -shRNA [151]	FGFR1OP2-shRNA#1	GTCTATTGTGAAACGTTATTT
FGFR1OP2	pLV -shRNA [152]	FGFR1OP2-shRNA_custom#2	GTCTTACCTTCCTGTTCAG
FGFR1OP2	pLV-CRISPR-Cas9 [153]	FGFR1OP2-sgRNA#723	GCGAGTGGAAGCGATGAAGC
FGFR1OP2	pLV-CRISPR-Cas9 [154]	FGFR1OP2-sgRNA#2	TTCCTCCTGATACTAACGAA
SLMAP3	pLV-CRISPR-Cas9 [6]	SLMAP3-sgRNA#1	AGTCGGGCTTCCATACCATC
SLMAP3	pLV-CRISPR-Cas9 [6]	SLMAP3-sgRNA#2	ATACTCACTCTGAACGAAGT
EGFP	pLV-CRISPR-Cas9 [142]	sgRNA-NTC	GGGCGAGGAGCTGTTCACCG

We packed lentiviruses with Lenti-X 293 T cells, obtained from ATCC, using the psPAX2 and pMD2.G plasmids following Addgene protocol [155]. The lentivirus harvests were concentrated with Lenti-X-Concentrator (Clontech, cat# PT4421-2) and subsequently tittered with

PCR Lentivirus Titer Kit (abm #LV900). Multiplicity of 20 was applied for transduction in MEFs, following the Addgene protocol [156]. MEFs transduced with shRNA-SC or sgRNA-NTC were subjected to puromycin selection at a concentration of 3 μg mL^{-1} for 3 days; cells transduced with STRN3-shRNA#1, STRN3-shRNA#2, FGFR1OP2-shRNA#2, FGFR1OP2-shRNA_all, FGFR1OP2-shRNA#1 and FGFR1OP2-shRNA_custom#2 underwent selection with G418 at 750 μg mL^{-1} for 6 days; and MEFs transduced with FGFR1OP2-sgRNA#723 and FGFR1OP2-sgRNA#2 were selected with blasticin at 1.5 μg mL^{-1} for 3 days. Depletion of STRN3 was confirmed by western blot. Expression of FGFR1OP2 was quantified in single-cell colonies generated by limiting dilution of the polyclonal cells transduced with sgRNA, according to Addgene protocol [157]. RT-qPCR was used for this quantification due to the technical challenges associated with FGFR1OP antibodies.

Cells were kept in humidified atmosphere with 5% CO2 and at 37° C. For MEFs, we used a medium containing high glucose DMEM (Wisent, cat# 319-005), 1 × MEM (Gibco, cat# 11140050), 20 mM HEPES, 10% fetal bovine serum (FBS) (Wisent, cat# 080-150), 1 × antibiotic-antimycotic (Gibco, cat# 15240062) and 0.1 mM β-mercaptoethanol, as described [158]. For C2C12 and Lenti-X cells, we used a medium containing DMEM (Wisent, cat# 319-005), 10% FBS (Wisent, cat# 080-150) and 1 ×antibiotic-antimycotic (Gibco, cat# 15240062). Starvation medium consisted of DMEM (Wisent, cat# 319-005), 0.1% FBS (Wisent, cat# 080-150) and 1 × antibiotic-antimycotic (Gibco, cat# 15240062).

Regarding cell treatments, okadaic acid (Cell Signaling, cat# 5934) was used at 0.4 μM for 1 h and XMU-MP-1 (Selleckchem, cat# S8334) at 15 μM for 1 h. For PCP induction, MEFs were treated with 400 ng ml^{-1} of Wnt5a (R&D Systems, cat# 645-WN) for 2 h, or 16 h for migration assay and 6 h for the quantification of orientation of the migratory cells (scratch assay). Due to the availability of Wnt5a, for scratch assay, only one biological sample of each SLMAP3 KO, FGFR1OP2 KO and STRN3 KD and their controls was treated. For protein degradation studies, MEFs were treated with MG132 (Sigma, cat# 474790) at 1 μM for 8 and 24 h, and with NH4Cl at 40 mM for 24 and 48 h.

5.3. Lung Explants

Lungs were isolated from E12.5 embryos for the explant growth. Dissection was done on cold PBS following the procedures described [159,160]. Dissected lungs were placed on autoclaved Whatman® Nuclepore™ Track-Etched Membranes (Millipore Sigma, cat# WHA10417506), which was floating on a medium consisting of DMEM/F-12 containing l-glutamine, penicillin and streptomycin. The explants were kept in humidified atmosphere with 5% CO2 and at 37° C for up to 3 days. Images were acquired after isolation and every 24 h with the ThermoFisher EVOS FL Auto 2 system.

5.4. Histology

Tissues designated for histological analysis were fixed with 10% formalin. Subsequent procedures including embedding, paraffinization, sectioning and H&E staining were conducted by the Louise Pelletier Histology Core Facility at the University of Ottawa. For immunofluorescence

studies, tissue deparaffinization, rehydration and antigen retrieval with citrate buffer pH 6.0 were performed according to an established protocol [161].

5.5. Alcian Blue and Alizarin Red

For general skeleton visualization, P0 mice were subjected to alizarin red and alcian blue staining of bones and cartilages, respectively, following an established protocol [162]. In brief, after euthanasia, the specimens were submerged for 30 s in 65° C to facilitate the removal of skin and organs. Subsequently, the samples were kept submerged overnight in each of the following solutions: 95% ethanol, acetone and then Alcian blue. The excess of staining was removed with washes with 70% ethanol, followed by another overnight incubation with 95% ethanol. In the following day, the samples were kept in 1% KOH for 1 h, followed by incubation with Alizarin red overnight. The excess and staining were eliminated with 50% glycerol : 50% (1%) KOH solution. For long-term storage, the specimens were kept in 100% glycerol. All the incubations were conducted at room temperature.

5.6. SDS-PAGE and Western Blot

Protein lysates from cells were extracted on ice by cell scraping and by homogenization of snap-frozen tissue. The lysis buffer consisted of 20 mM Tris pH 7.5, 150 mM NaCl, 1 mM EDTA, 1 mM EGTA and 1% Triton X-100. To each 10 ml of buffer, one tablet of Pierce Protease Inhibitor (Thermos Scientific, cat# A32955) and of Pierce Phosphatase Inhibitor (Thermo Scientific, cat# A32957) was added. For nuclear and cytoplasmic fractionation, we used a similar protocol described elsewhere [163]. In brief, cells were washed twice with cold PBS, followed by scrapping on ice with PBS containing 1 mM DTT and the Peirce Protease Inhibitor. The harvest was centrifuged at 1000*g* for 15 min at 4° C, followed by pellet resuspension with buffer A, consisting of 10 mM HEPES, 10 mM KCl, 1.5 mM MgCl2, 0.5 mM DTT and the Peirce Protease Inhibitor. After 15 min of incubation on ice, samples were handheld homogenized, and the cell lysis was verified with trypan blue staining of the nucleus every 20 strokes. The lysates were then centrifuged at 1000*g* for 5 min at 4° C, and the resulting supernatant was stored as cytoplasmic fraction. Using buffer A, the pellet was washed twice with centrifugation (1000*g* for 5 min at 4° C). After the final wash, the pellet was resuspended with the buffer A and homogenized with 20 strokes of a syringe attached to a 27 G needle, producing the final nuclear fraction. The denaturation of all protein lysates was achieved using SDS buffer containing 10% glycerol, 2% SDS, 62.5 mM Tris.HCl pH 6.8 and 10% β-mercaptoethanol and boiled for 5 min. Lysates were loaded on SDS-PAGE gel and posteriorly transferred to polyvinylidene fluoride membrane (Bio-Rad). Tris-buffered saline (TBS-T; 1 M Tris, 290 mM NaCl, 0.1% Tween 20 pH 7.4) was employed for membrane wash, blocking and antibody solutions. Antibody solutions were prepared with 5% milk in TBS-T or 5% BSA for primary antibodies targeting phosphorylated amino acid residues. Imaging was performed using the Bio-Rad ChemiDoc system, and densitometry analysis was conducted using Image Lab Software (Bio-Rad). Below is the list of antibodies utilized for western blot analysis.

Primary Antibodies				
Target	**Company**	**Catalog**	**Host**	**Dilution WB**
SLMAP	Novus Biologicals	NBP1-81397	Rabbit	1:500
SLMAP	Novus Biologicals	NBP1-81398	Rabbit	1:1000
STRN3/SG2NA (S68)	Novus Biologicals	NBP74572	Mouse	1:500
MST1 (KRS2)(H-8)	Santa Cruz	SC-515051	Mouse	1:200
MST2 (KRS1)(87.K)	Santa Cruz	SC-130405	Mouse	1:200
Phospho-MST1 (Thr183)/MST2 (Thr180) (E7U1D)	Cell Signaling	49332	Rabbit	1:500
YAP (1A12)	Cell Signaling	12395	Mouse	1:1000
Phospho-YAP (Ser127) (D9W2I)	Cell Signaling	13008	Rabbit	1:1000
Phospho-YAP(S397) (D1E7Y)	Cell Signaling	13619	Rabbit	1:1000
β-actin (AC-15)	Abcam	ab6276	Mouse	1:2000
α-tubulin	Abcam	ab176560	Rabbit	1:5000
GAPDH (GA1R)	Invitrogen	MA5-15738	Mouse	1:5000
Lamin B1	Abcam	ab16048	Rabbit	1:200
Vimentin (D21H3) XP	Cell Signaling	5741	Rabbit	1:1000
Strn	BD Biosciences	610838	Mouse	1:1000
STRIP1/FAM40A	Bethyl Laboratories	A304-644A	Rabbit	1:2500
PP2A-Cα/β (1D6)	Santa Cruz	SC-80665	Mouse	1:200
SIKE1	Abcam	Ab121860	Rabbit	1:200
FGFR1OP2	Novus Biologicals	NBP1-84148	Rabbit	1:1000
DVL3	Cell Signaling	3218	Rabbit	1:500
β-catenin (E247)	Abcam	ab32572	Rabbit	1:8000
Vangl1 (D1J7X)	Cell Signaling	14783	Rabbit	1:1000
MUSK1	Invitrogen	PA1-1741	Rabbit	1:500
RhoA (26C4)	Santa Cruz	sc-418	Mouse	1:1000
ROR2 (D3B6F)	Cell Signaling	88639	Rabbit	1:1000
Cofilin (D3F9) XP	Cell Signaling	5175	Rabbit	1:1000
Phospho-ROCK2 (S1366)	GeneTex	GTX122651	Rabbit	1:750
ROCK2 (D-11)	Santa Cruz	SC-398519	Mouse	1:200
Phospho-SAPK/JNK (Thr183/Tyr185) (81E11)	Cell Signaling	4668	Rabbit	1:2000
JNK (D-2)	Santa Cruz	SC-7345	Mouse	1:200
Vinculin (EPR8185)	Abcam	Ab129002	Rabbit	1:5000

Secondary Antibodies				
Target	**Company**	**Catalog**	**Host**	**Dilution WB**
Peroxidase AffiniPure Goat Anti-Rabbit IgG (H+L)	Jackson ImmunoResearch	111-035-144	Goat	1:10000
Peroxidase AffiniPure Goat Anti-Mouse IgG (H+L)	Jackson ImmunoResearch	115-035-146	Goat	1:10000

5.7. Reverse Phase Protein Array (RPPA)

For the preparation of protein lysates for RPPA, primary MEFs isolated from E14.5 embryos were subjected to protein extraction with a buffer consisting of 1% Triton-X100, 50 mM HEPES pH 7.4, 150 mM NaCl, 1.5 mM MgCl2, 1 mM EGTA, 100 mM NaF, 10 mM Na4P2O7, 1 mM Na3VO4, 10% glycerol and one tablet of Pierce Protease Inhibitor (Thermos Scientific, cat# A32955) and of Pierce Phosphatase Inhibitor (Thermo Scientific, cat# A32957) to each 10 ml of the buffer. The extraction was carried out following the Functional Proteomics RPPA Core Facility procedures [104]. Proteins were denatured with one part of the 4 $\times$ SDS buffer containing 40% glycerol, 8% SDS, 0.25 M Tris-HCl pH 6.8 and 1/10 (volume/volume) β-mercaptoethanol and using three parts of the lysates. Samples were kept in -80° C until submission to the Functional Proteomics RPPA Core Facility.

At the facility, the lysates were diluted in five twofold serial dilutions in lysis buffer. Serially diluted lysates were arrayed on nitrocellulose-coated slides (Grace Bio-Labs) by the Quanterix (Aushon) 2470 Arrayer (Quanterix Corporation). A total of 5808 spots were arrayed on each slide including spots corresponding to serially diluted (a) standard lysates, and (b) positive and negative controls prepared from mixed cell lysates or dilution buffer, respectively. Each slide was probed with a validated primary antibody plus a biotin-conjugated secondary antibody. Antibody validation for RPPA is described in the RPPA Core website [104]. Signal detection was amplified using an Agilent GenPoint staining platform (Agilent Technologies) and visualized by DAB colourimetric reaction. The slides were scanned (Huron TissueScope, Huron Digital Pathology) and quantified using customized software (Array-Pro Analyzer, Media Cybernetics) to generate spot intensity.

Relative protein level for each sample was determined by RPPA SPACE, developed by MD Anderson Department of Bioinformatics and Computational Biology [164,165], by which each dilution curve was fitted with a logistic model. RPPA SPACE fits a single curve using all the samples (i.e. dilution series) on a slide with the signal intensity as the response variable and the dilution steps as the independent variable. The fitted curve is plotted with the signal intensities, both observed and fitted, on the *y*-axis and the log2 concentration of proteins on the *x*-axis for diagnostic purposes. The protein concentrations of each set of slides were then normalized for protein loading. Correction factor was calculated by (a) median-centring across samples of all antibody experiments and (b) median-centring across antibodies for each sample. Results were then normalized across RPPA sets by replicates-based normalization as described [166]. Details of the RPPA platform as performed by the RPPA Core are described in Siwak *et al*. [167].

5.8. Real-Time Quantitative Polymerase Chain Reaction – RT-qPCR

The Primer-Blast tool (NIH) was used to design primers targeting all transcript isoforms of the gene of interest. Primers were validated by PCR product band size. RNeasy Mini Kit (Qiagen, cat# 74104) was employed for RNA extraction. For cDNA synthesis, we used iScript Reverse Transcription Supermix (Bio-Rad, cat#1708840). RT-qPCR was performed with the FastStart Universal SYBR Green Master (Rox) (Millipore Sigma, cat# 4913850001). GAPDH was used as the housekeeping gene. The samples were read on BioRad CFX 96 thermal cycler and data analysed on Bio-Rad CFX Maestro. The primers used are listed below.

Primers	Forward (5`-3`)	Reverse (5`-3`)
Arhgap36	AGAGACTGCTTACCACGAACTC	AAGCTCGTTCACCAGTACCTC
Cdkn1a	CCCGAGAACGGTGGAACTTT	AGAGTGCAAGACAGCGACAA
DVL3	AGTCAGCACAGTGAAGGCAGTCG	ATCAGCATCGGGGGACCATAGAGAG
SIKE1	GCTGTTCAGGTGGACGATAAC	AGCCACAGAGCTTTCTTTTCC
FGFR1OP2	CAAGCGAGTGGAAGCGATGA	GGGATGTCCGCAGTTCTTTG
SLMAP	AGATGTCATCCATGCTCCATTACC	GTATCTGAAGCCTCTTGGGTGATG
GAPDH	GGTTGTCTCCTGCGACTTCA	TGGTCCAGGGTTTCTTACTCC

5.9. RNA-Sequencing

Total RNA was isolated from four SLMAP3$^{-/-}$ and four wild-type E14.5 immortalized MEFs using the RNeasy Mini Kit (Qiagen, cat# 74104). Subsequently, the samples were submitted to the StemCore Laboratories Genomics Core Facility at University of Ottawa for library generation and RNA-sequencing as follows: total RNA was quantified using a Qubit (ThermoScientific) and its integrity was assessed on the 5200 Fragment Analyzer (Agilent Technologies). The libraries were constructed using Illumina Stranded mRNA Library Prep (Illumina). Following library QA/QC, the eight libraries were pooled on a NextSeq 2000, with the run module P2 100 cycles and approximately 400 M per run. RNA-seq post-processing and differential expression analysis were prepared by the Ottawa Bioinformatics Core Facility. Briefly, the reads were assigned to the GRCm38_GENCODE M25 transcriptome model using Salmon [168], and the differential expression of transcripts was analysed by DESeq2 [169]. The sequencing results have been deposited in NCBI Gene Expression Omnibus [170,171] and are accessible through GEO Series accession number GSE266611 (https://www.ncbi.nlm.nih.gov/geo/query/acc.cgi?acc=GSE266611). The data were validated by RT-qPCR, with the analysis of the expression of *arhgap36* and *cdkn1a*.

5.10. Image Acquisition and Processing

Images were acquired at the Cell Biology and Image Acquisition Core Facility at the University of Ottawa. For the slides with H&E staining and cell plates, we used the ThermoFisher EVOS FL Auto 2 for image acquisition. For the cell migration, MEFs were incubated in the Incucyte ZOOM System (Sartorius) for 16 h, and images were analysed with the Scratch Wound Analysis Software Module for the measurements of wound width during the migration period. For the immunofluorescence experiments, we used the widefield microscopes as follows: images

capturing cell migration orientation and mitotic spindle angles were acquired using the Zeiss AxioImager M2; the slides with anti-YAP/TAZ staining were analysed using Zeiss AxioObserver D1; the remaining immunofluorescent experiments were examined with Zeiss AxioObserver Z1. Slides for immunofluorescence were mounted using VECTASHIELD® PLUS Antifade with DAPI (Vector Laboratories, cat# H-2000).

For quantification of YAP staining intensity in the nucleus, we used CellProlifer. First, we used the DAPI staining to segment the image and create the 'nucleus' object. The mean intensity of anti-YAP staining was measured inside these objects. We plotted the average of multiple fields of three biological replicates.

Chondrocyte orientation was quantified by determining the angle between the major axis of each chondrocyte and the growth plate axis, which we considered to be parallel to the different zones of the growth plate. Measurements were manually done with Fiji. For proliferation analysis in the proliferative zone of the growth plate, we counted the total number of cells in the field and compared it to the number of Ki67+ cells. In the kidney, we quantified the number of Ki67+ cells only in the epithelium of the proximal/distal tubules. These measurements were conducted across three biological replicates of SLMAP3$^{-/-}$ and controls (wild type or SLMAP3−/+ that do not exhibit any phenotype).

The quantification of F-actin in the cell cortex was done using cell objects generated with the segmentation of phalloidin staining. These objects were shrunk in 8 pixels (2.58 μm), and the band generated between the cells and the shrunk objects was considered cell cortex where phalloidin intensity was measured. For FA analysis, we used paxillin staining by applying the tool 'enhance speckles' on CellProfiler. Subsequently to image segmentation, we considered the parameters area, major axis length, minor axis length and perimeter for FAs. We excluded objects with either a major or minor axis smaller than 2.45 pixels (0.25 μm) because they fell outside the dimensions considered for FA [172]. For focal adhesion density, we considered the number of FA per area of cells.

In the migratory orientation assay, seeded cells were scratched and allowed to migrate for 6 h with or without Wnt5a. The angle of the cells was measured on Fiji between the overall migration axis (perpendicular to the scratch) and the individual cell migration axis (axis determined by the position of the Golgi and centrosome in front of the nucleus). For the quantification of mitotic spindle angle, MEFs were seeded at cell density of 8000 cell cm^{-2} and subjected to double thymidine treatment for cell cycle synchronization to increase the number of mitotic cells at the time of cell fixation. The treatment protocol consisted of 16 h with 10 mM thymidine, followed by 7 h of release. This was followed by another 16 h with 10 mM thymidine and subsequent 6 h of release, followed by immediate cell fixation and immunofluorescence. Images were acquired from the prepared slides by Z-stack, and the *x*, *y* and *z* coordinates of both centrosomes (**x1, y1, z1 and x2, y2, z2**) were acquired using the View5D from Fiji. The coordinates were applied in the arctan function, as previously described [92], that gives the mitotic spindle angle in radians using the equation below. The angles were converted to degrees and plotted. Imaris was used to validate this angle measurement method.

$$\theta\ (rad) = arctan\left(\frac{z2 - z1}{\sqrt{(x2 - x1)^2 + (y2 - y1)^2}}\right)$$

For all F-actin staining, we utilized Phalloidin-AF488 (Biotium, cat# 00042). The list of the antibodies used for immunofluorescence follows below.

Primary Antibodies				
Target	**Company**	**Catalog**	**Host**	**Dilution IF**
YAP/TAZ (D24E4)	Cell Signaling	8418	Rabbit	1:100
Ki67	Abcam	ab15580	Rabbit	1:200
Paxillin	Abcam	ab32084	Rabbit	1:100
Arl13b	Proteintech	17711-1-AP	Rabbit	1:300
Golgin 97	Proteintech	12640-1-AP	Rabbit	1:100
α-tubulin (DM1A)	Millipore Sigma	T6199	Mouse	1:300

Secondary Antibodies				
Target	**Company**	**Catalog**	**Host**	**Dilution IF**
Anti-Mouse IgG (H+L) Cross-Adsorbed Secondary Antibody, Alexa Fluor 647	Invitrogen	A-21235	Goat	1:300
Anti-Rabbit IgG (H+L) Cross-Adsorbed Secondary Antibody, Alexa Fluor 555	Invitrogen	A-21428	Goat	1:300
Anti-Rabbit IgG H&L, Alexa Fluor 488	Abcam	ab150077	Goat	1:200

5.11. Flow Cytometry

The flow cytometry readings were obtained at the Flow Cytometry & Virometry Core Facility at the University of Ottawa with the BD FACS Celesta system and processed on FlowJo software. For all analyses, doublet discrimination was done using the width and area for the forward scatter. Events gated from the plot with areas for forward and side scatter were used for quantification. Cell cycle analysis was conducted with DNA staining with PI according to the protocol by Moores Cancer Center, UC San Diego [173] and with the following details. After one wash with cold PBS, cells were resuspended with dropwise addition of 4 ml of 70% ethanol with concomitant gentle vortexing. Cells were maintained at 4° C for 24 h before further processing. PI staining was done by incubating cells at room temperature for 30 min and protected from light. Plots were obtained with the histogram of the linear PI intensity, and the cell cycle tool from FlowJo was used to gate the resulting plot in G1, S or G2/M phase. For apoptosis analysis, we used the Invitrogen kit (cat# V13242) containing PI and Annexin V conjugated to FITC following the protocol of the manufacturer. For positive death controls, cells were incubated with 1.6 mM H2O2 for 1 h. The events were plotted in log of FITC $\times$ PI intensity and gated in four quadrants according to the positive death controls. For SA-β-Gal assay with Cell Event Green Probe kit (Invitrogen, cat# C10850), we followed the protocol provided by the manufacturer. For positive control, we induced cellular senescence following the protocol previously described [174], treating cells with 600 μM of H2O2 for 2 h, and repeating the treatment in the following day. The induction of senescence was monitored by analysing changes in cell morphology in phase contrast microscope. The results were plotted as histograms of the log FITC intensity.

5.12. Statistical Analysis

GraphPad Prism was used for all the statistical analyses. Data are represented by mean and standard error of mean. For single variable analyses comparing two groups, we employed *t*-tests. For analyses with three or more groups, we used one-way ANOVA followed by Newman-Keuls post-test. Analyses involving multiple variables were conducted using two-way ANOVA followed by Bonferroni post-test. Significance levels were denoted as * for $p < 0.05$, ** for $p < 0.01$, *** for $p < 0.001$, and ns for non-significant results.

Ethics. The mice involved in this research were kept at the Animal Care and Veterinary Service (ACVS) Barrier Facility at the University of Ottawa and were handled according to the guidelines set forth by the Canadian Council on Animal Care, as outlined in the Guide to the Care and Use of Experimental Animals (2 vols., Ottawa, Ont.: CCAC, 1980–1993), and the Animals for Research Act, R.S.O. 1990, c.A. 22. All animal study procedures were approved by the Animal Care Committee at the University of Ottawa.

Data accessibility. The RNA-seq results of MEFs from this study have been deposited in NCBI's Gene Expression Omnibus and are accessible through GEO Series accession number GSE266611 [175]. The RNA-seq data of E11.5 embryos from our previous study (6) were deposited in NCBI's Gene Expression Omnibus and are accessible through GEO Series accession number GSE230748 (https://www.ncbi.nlm.nih.gov/geo/query/acc.cgi?acc=GSE230748). Supplementary Figures are provided in the Supplementary Material 1. The results obtained with RPPA are available as Supplementary Table 2, and the clustering and heat map of the relative protein expression are present in the Supplementary Material 2. The uncropped images of all western blots of this study are available in the Supplementary Material 3.

Supplementary material is available online.

Declaration of AI use. We have not used AI-assisted technologies in creating this article.

Authors' contributions. A.P.D.: conceptualization, formal analysis, investigation, methodology, resources, validation, visualization and writing-original draft; T.R.: conceptualization, investigation and resources; B.D.A.: investigation; M.S.: investigation, methodology and resources; B.T.: conceptualization, funding acquisition, project administration and writing-review and editing. All authors gave final approval for publication and agreed to be held accountable for the work performed therein.

Conflict of interest declaration. We declare we have no competing interests.

Funding. This project was funded with grant 220996-151999 from the Canadian Institute of Health Research (CIHR) to B.T.

Acknowledgements. We thank Dr. Nemer Mona for the Cre transgenic mice. We also thank the assistance of all the facilities involved in this study: StemCore Laboratories Genomics Core Facility (RRID: SCR_012601); Ottawa Bioinformatics Core Facility (RRID: SCR_022466); Cell Biology and Image Acquisition Core (RRID: SCR_021845); Louise Pelletier Histology Core Facility (RRID: SCR_021737); Flow Cytometry & Virometry (FCV) Core Facility at the University of Ottawa; Genomic Editing and Molecular Biology Core Facility (RRID: SCR_022954); the RPPA Core supported in part by The University of Texas MD Cancer Center, P30CA016672 and R50CA221675; and the Animal Care and Veterinary Service Facility at University of Ottawa.

Figure Titles and Legends

Figure 1. SLMAP3-/- mice display embryonic/perinatal lethality, with abnormalities in multiple organs. (*a*) Knockout of SLMAP3 leads to embryonic/perinatal lethality, with animals presenting smaller limbs and tails, reduced body size and cases of craniorachischisis. (*b*) Thymus of animals lacking SLMAP3 shows reduced cell density, (*c*) which is consistent with the enrichment of biological processes associated with T-cell differentiation/activation. For the gene ontology enrichment analysis, we used the G:Profiler tool [94] with genes with significantly altered expression and Log2 Fold Change > 0.75 comparing SLMAP3$^{-/-}$ and WT, from data obtained in our previous RNA-seq with E11.5 embryos [6]. N=3 for KO and n=4 for WT. (*d*) The histology of the liver does not indicate major structural defects, although the organs are smaller in SLMAP3$^{-/-}$ embryos. Scale bar = 100 μ m. (*e*) Intestines of SLMAP3$^{-/-}$ mice are shorter (scale bar = 5 mm), but (*f*) the regions of small and large intestines are properly specified. Scale bar = 200 μ m. (*g*) Lungs of animals lacking SLMAP3 are underdeveloped with the absence of air sacs. Scale bar = 200 μ m. (*h*) E12.5 lung explant of SLMAP3$^{-/-}$ mouse displays branching morphogenesis comparable to control. Scale bar = 650 μ m.

Figure 2. Loss of SLMAP3 results in organ structural defects. (*a*) Alcian blue (cartilage) and alizarin red (bones) staining of SLMAP3$^{-/-}$ mice reveals skeletal defects, with fused bones and cartilages of the ribs. (*b*) H&E staining of the humerus growth showing that chondrocytes lacking SLMAP3 have defective organization into columns and are disoriented, as indicated in the histograms. The number of cells considered for the histograms is indicated in the image and cells are from three different biological replicates. Scale bar = 100 μ m. (*c*) The angle averages of the three biological replicates are plotted (n = 3). (*d*) The proliferative zone of the growth plate in SLMAP3$^{-/-}$ mice has reduced Ki67+staining, suggesting reduced proliferation. Scale bar = 20 μ m (n = 3). (*e*) The kidneys of SLMAP3$^{-/-}$ mice are underdeveloped and polycystic. Scale bar = 100 μ m. (*f*) Quantification of ki67+cells in the epithelium of proximal/distal tubules do not indicate increased proliferation in the cysts of SLMAP3$^{-/-}$ mice (n = 3). Scale bar = 20 μ m. **p < 0.01.

Figure 3. SLMAP3 functions independently of Hippo signaling during mouse embryogenesis. (*a*) Loss of SLMAP3 does not affect the phosphorylation status of YAP in brain, lungs and (*b*) MEFs (n = 3). (*c*) Immunofluorescence for YAP/TAZ reveals their preferably nuclear localization in both SLMAP3$^{-/-}$ and WT cells. Scale bar = 100 μ m (n = 3) (*d*) Phosphorylation of YAP in SLMAP3$^{-/-}$ MEFs in low and high cell density is similar to what is observed in WT cells (n = 3). (*e*) Analysis of YAP in both nuclear and cytoplasmic fraction does not indicate any enrichment of the protein in the cytoplasm of SLMAP3$^{-/-}$ MEFs (n = 3). (*f*) Phosphorylation of MST1/2 is only observed when MEFs are treated with okadaic acid, indicating that these kinases are kept inactive independently of SLMAP3 presence. (*g*) RNA-sequencing of both embryos [6] and MEFs lacking SLMAP3 do not show changes in the expression of YAP target genes. For RNA-seq from embryos, for SLMAP3$^{-/-}$ (n = 3), and for WT (n = 4); for RNA-seq in MEFs (n = 4) for both SLMAP3$^{-/-}$ and WT cells. Ns, not significant.

Figure 4. The knockout of SLMAP3 affects cell cycle in a cell specific manner. (*a*) Cell cycle analysis by DNA staining with propidium iodide shows that knockout of SLMAP3 in MEFs does not cause any cell cycle arrest ($n = 6$), or (*b*) cellular senescence ($n = 6$), evaluated by SA- β -gal assay. (*c*) PI and Annexin V staining shows that the lack of SLMAP3 does not cause cell death in MEFs ($n = 5$). (*d*) Cell cycle analysis by DNA staining with propidium iodide indicates that both C2C12 KO cells have G1 cell cycle arrest ($n = 3$). (*e*) The phase contrast images of SLMAP3$^{-/-}$ C2C12 cells show signs of cellular senescence: large, flat and vacuolated cells. Scale bar = 100 μ m. This is consistent with their significantly higher β -galactosidase activity. For SLMA3 KO, $n = 5$, and for WT, $n = 3$. (*f*) PI and Annexin V staining do not suggest cellular death of both SLMAP3 $^{-/-}$ C2C12 myoblasts ($n = 3$). The positive controls for (*b*) and (e) consisted of WT cells treated with 600 μ M of H2O2 to induce cellular senescence. For (*c*) and (*f*), the positive controls were treated with 1.6 mM H2O2 to induce cellular death, and the quadrants are Q1: necrosis; Q2: late apoptosis; Q3: early apoptosis; Q4: survival. For (*e*), the statistical analysis was performed by grouping the three biological samples of KO1 with two biological samples of KO2 and comparing to a group of WT with three biological replicates. ***$p < 0.001$; ns, not significant.

Figure 5. Loss of SLMAP3 impacts cell shape independent of changes in F-actin or focal adhesions. (*a*) MEFs lacking SLMAP3 display changes in cell shape parameters, while (*b*) no changes are observed in the nucleus. (*c*) Quantification of F-actin staining in the cell cortex does not suggest any changes in SLMAP3$^{-/-}$ MEFs. (*d*) Depletion of SLMAP3, STRN3 or both have very little impact in focal adhesion of MEFs, as increase in number or size of focal adhesion in these cells were not observed. Images scale bar = 8 μ m. Averages from multiple fields of each of three biological replicates plotted. **$p < 0.01$, ***$p < 0.001$.

Figure 6. SLMAP3$^{-/-}$ MEFs do not present orientation defects. (*a*) Cell orientation of migratory cells in a scratch assay was measured for MEFs with depletion of either SLMAP3, FGFR1OP2 or STRN3, but the average migration angles were similar to their corresponding controls, (*b*) even when cells were treated with Wnt5a. (*c*) Quantification of mitotic spindle angle does not suggest orientation defects on MEFs with depletion of either SLMAP3, FGFR1OP2 or STRN3, with average angles without statistical significance. For all analyses, the number of cells considered for the histogram (across three biological replicates) is indicated in the images. For each histogram, we plotted the averages of each of the three biological replicates (angle averages plots), therefore $n = 3$. Exception is (*b*), in which we plotted all cells together in the angle average plot. Ns, not significant.

Figure 7. SLMAP3$^{-/-}$ MEFs do not present defects in PCP or migration. (*a*) E20.5 lungs, (*b*) E19.5 brains and (***c***) E18.5 skeleton lacking SLMAP3 display reduced expression of DVL3. (*d*) Primary MEFs do not display migration defects. After 16 h, the migration of SLMAP3$^{-/-}$ MEFs was comparable to the WT cells ($n = 9$). (*e*) Differently from primary MEFs, immortalized cells have almost no expression of SLMAP2. (*f*) DVL3 expression is reduced in immortalized cells, although its activation is not different from what is seen in WT MEFs ($n = 3$). (*g*) DVL3 transcripts are not reduced in cells lacking SLMAP3, as indicated by our RT-qPCR analysis ($n = 3$). (*h*) DVL3

in immortalized SLMAP3$^{-/-}$ MEFs is still responsive to Wnt5a. (*i*) Immortalized MEFs do not have changes in ROCK2 activation status. $n = 3$. (*j*) With NH4Cl treatment the DVL3 protein levels in SLMAP3$^{-/-}$ MEFs is comparable to WT cells. $*p < 0.05$.

Figure 8. The knockout of SLMAP3 or FGFR1OP2/Wit3.0 results in defective primary cilia formation. (*a*) Loss of SLMAP3 in MEFs does not cause centrosome or Golgi abnormalities. Averages of multiple fields of each of three biological replicates plotted, therefore $n = 3$. (*b*) Starvation of both SLMAP3$^{-/-}$ and WT MEFs for 24 h with medium containing 0.1% FBS (*s*) enriched cells in G1 phase when compared with cells treated with 10% FBS medium (*n*). $n = 3$. Statistical significance is shown for %G1. (*c*) Knockout of either SLMAP3 or FGFR1OP2 reduced the number of ciliated cells and cilium length, which was not observed in MEFs with depleted STRN3. Arrows indicate ciliated cells. Averages of multiple fields of each of three biological replicates plotted, therefore $n = 3$. (*d*) Reduced cilium length was also observed in chondrocytes from SLMAP3$^{-/-}$ growth plates. Averages of multiple fields of each of three biological replicates plotted, therefore $n = 3$. For (*a*), (*c*) and (*d*), single-cell images, scale bar is 8 μ m; for images with multiple cells, scale bar is 20 μ m. $**p < 0.01$, $***p < 0.001$.

Figure 9. SLMAP3 is important for the protein stability of the STRIPAK members SIKE1 and FGFR1OP2. (*a*) Loss of SLMAP3 does not affect the protein levels of STRIP1, Strn and the catalytic subunit of PP2A (PP2A-C) ($n = 3$). (*b*) Knockout of SLMAP3 leads to reduced protein levels of SIKE1 in MEF ($n = 3$), (*c*) whole embryos ($n = 3$) and (*d*) in multiple tissue. (*e*) The protein levels of FGFR1OP2 is also reduced in SLMAP3-/- MEFs ($n = 3$). (*f*) Transcripts of SIKE1 and FGFR1OP2, assessed by RT-qPCR, are not significantly altered in cells deficient of SLMAP ($n = 3$). (*g*) Treatment of SLMAP3-/- MEFs with MG132 was enough to increase SIKE1 expression after 24 h. (*h*) The knockout of FGFR1OP2 reduced protein levels of both SLMAP3 and SIKE1, but (***i***) did not change their transcripts, which was assessed by RT-qPCR ($n = 3$). (*j*) Treatment of MEFs deficient in FGFROP2 with MG132 increased the protein levels of SIKE1 but not SLMAP3. (*k*) The protein levels of SLMAP3 did not increase even with NH4Cl treatment. $*p < 0.05$, $**p < 0.01$, $***p < 0.001$.

Figure 10. Proposed mechanisms of SLMAP3 for embryonic development and organogenesis. SLMAP3 is a tail-anchored membrane that targets the centrosome and impact embryonic development and organogenesis by (1) protecting DVL3 from lysosomal degradation, allowing a proper PCP signalling; (2) remodelling the actin cytoskeleton, a function that is shared with STRIPAK complex of which SLMAP3 is a component; (3) regulating primary cilia formation through basal body and cell membrane by interactions with centrosomal (AKAP9, pericentrin, myomegalin) and centriolar satellite (PCM1 and HOOK3) proteins, which were detected in our previous proteomics study (6). Furthermore, SLMAP3 actions in the nuclear envelope could account for the gene expression of Arhgap36. FHA, forkhead-associated domain; TM, transmembrane domain; PCP, planar cell polarity; PCM, pericentriolar material.

Supplementary Material 1 Tiles and Legends

Figure S1. Gene Expression in SLMAP3$^{-/-}$ MEFs. A) Genes with expression significantly changing in immortalized SLMAP3$^{-/-}$ MEFs found by RNA-seq. N=4 for SLMAP3 KO and WT MEFs. B) Validation of the RNA-seq by RT-qPCR analysis of Arhgap36 and C) cdkn1a. N=3. The expression of cdKn1a was also reduced in C2C12 cells lacking SLMAP3. ** $p< 0.01$, *** $p<0.001$.

Figure S2. Depletion of the Expression of STRN3 and FGFR1OP2. . A) Western Blot showing the knockout of SLMAP3 in C2C12 cells by two sgRNAs (KO1 and KO2) via CRISPR/Cas9 from our previous study (6). B) For the depletion of STRN3 in MEFs, we tested two shRNA called STRN3-shRNA#1 and STRN3-shRNA#2, with the latter ablating STRN3 expression. C) Testing of FGFR1OP2 depletion by four different shRNAs. None of them reduced the expression of FGFR1OP2 in more than 50%. N=3. D) FGFR1OP2 expression in single cell colonies subjected to CRISPR/Cas9 with FGFR1OP2-sgRNA2 and E) FGFR1OP2-sgRNA#723. N=3. Only colony 12 from MEFs treated with sgRNA#723 was selected for further experiments.

Figure S3. SLMAP3$^{-/-}$ Primary MEFs do not present defects in PCP. A) Primary MEFs do not have significantly reduced DVL3 expression or phosphorylation (n=3) or B) activation upon Wnt5a treatment, analyzed by the mobility shift of DVL3. C) Primary MEFs deficient in SLMAP3 do not have altered the protein levels of the PCP members MUSK1, RhoA and D) ROR2. N=3. E) No changes in ROR2 are observed in whole embryos either. N=3. F) Primary MEFs do not have changes in the phosphorylation of PCP kinases ROCK2 and JNK1/2. N=3. G) MG132 treatment is not enough to increase DVL3 in SLMAP3$^{-/-}$ MEFs. Ns – not significant.

Supplementary Material 2. Unsupervised clustering and heat map obtained with the relative protein levels obtained from our RPPA screening. N=3 for SLMAP3 KO and WT MEFs.

Supplementary Material 3. Raw images of the Western Blot from the main figures and Supplementary Material 1.

Movie S1. Animals deficient in SLMAP3 have respiratory distress. Newborn SLMAP3-/- mouse (right) display cyanosis and respiratory distress, likely due to lungs abnormalities. The control mouse (left) breathes normally.

Supplementary Table 1. RNA-seq results from MEFs (GSE266611). The table shows the Log2 Fold Change of gene expression in SLMAP3 knockout samples compared to the wild type controls. Four SLMAP3 KO and four WT different MEFs were sequenced.

Supplementary Table 2. Relative protein level results from RPPA, which was obtained with three SLMAP3$^{-/-}$ and three WT MEFs.

6. References

1. World Health Organization. *Congenital disorders [Internet]*. See https://www.who.int/news-room/fact-sheets/detail/birth-defects (accessed 14 July 2024).

2. Wigle JT, Demchyshyn L, Pratt MAC, Staines WA, Salih M, Tuana BS. 1997 Molecular cloning, expression, and chromosomal assignment of sarcolemmal-associated proteins. *J. Biol. Chem.* **272**, 32384–32392. (doi:10.1074/jbc.272.51.32384)

3. Wielowieyski PA, Sevinc S, Guzzo R, Salih M, Wigle JT, Tuana BS. 2000 Alternative splicing, expression, and genomic structure of the 3' region of the gene encoding the sarcolemmal-associated proteins (SLAPs) defines a novel class of coiled-coil tail-anchored membrane proteins. *J. Biol. Chem.* **275**, 38474–38481. (doi:10.1074/jbc.M007682200)

4. Guzzo RM, Sevinc S, Salih M, Tuana BS. 2004 A novel isoform of sarcolemmal membrane-associated protein (SLMAP) is a component of the microtubule organizing centre. *J. Cell. Sci*. **117**, 2271–2281. (doi:10.1242/jcs.01079)

5. Byers JT, Guzzo RM, Salih M, Tuana BS. 2009 Hydrophobic profiles of the tail anchors in SLMAP dictate subcellular targeting. *BMC Cell Biol*. **10**, 48. (doi:10.1186/1471-2121-10-48)

6. Dias AP, Rehmani T, Salih M, Tuana B. 2024 Tail anchored membrane protein SLMAP3 is essential for targeting centrosomal proteins to the nuclear envelope in skeletal myogenesis. *Open Biol*. **14**, 240094. (doi: 10.1098/rsob.240094)

7. Durocher D, Taylor IA, Sarbassova D, Haire LF, Westcott SL, Jackson SP, Smerdon SJ, Yaffe MB. 2000 The molecular basis of FHA domain:phosphopeptide binding specificity and implications for phospho-dependent signaling mechanisms. *Mol. Cell*. **6**, 1169–1182. (doi:10.1016/s1097-2765(00)00114-3)

8. Durocher D, Jackson SP. 2002 The FHA domain. *FEBS Lett*. **513**, 58–66. (doi:10.1016/s0014-5793(01)03294-x)

9. Frost A *et al*. 2012 Functional repurposing revealed by comparing S. pombe and S. cerevisiae genetic interactions. *Cell* **149**, 1339–1352. (doi:10.1016/j.cell.2012.04.028)

10. Ishikawa T *et al*. 2012 A novel disease gene for brugada syndrome. *Circ. Arrhythm. Electrophysiol.* **5**, 1098–1107. (doi:10.1161/CIRCEP.111.969972)

11. Glatter T, Wepf A, Aebersold R, Gstaiger M. 2009 An integrated workflow for charting the human interaction proteome: insights into the PP2A system. *Mol. Syst. Biol*. **5**, 237. (doi: 10.1038/msb.2008.75)

12. Goudreault M *et al*. 2009 A PP2A phosphatase high density interaction network identifies a novel striatin-interacting phosphatase and kinase complex linked to the cerebral cavernous malformation 3 (CCM3) protein. *Mol. Cell. Proteomics.* **8**, 157–171. (doi:10.1074/mcp.M800266-MCP200)

13. Couzens AL *et al*. 2013 Protein interaction network of the mammalian hippo pathway reveals mechanisms of kinase-phosphatase interactions. *Sci. Signal.* **6**. (doi:10.1126/scisignal.2004712)

14. Hauri S, Wepf A, van Drogen A, Varjosalo M, Tapon N, Aebersold R, Gstaiger M. 2013 Interaction proteome of human hippo signaling: modular control of the co-activator YAP1. *Mol. Syst. Biol*. **9**, 713. (doi:10.1002/msb.201304750)

15. Herzog F *et al*. 2012 Structural probing of a protein phosphatase 2A network by chemical cross-linking and mass spectrometry. *Science* **337**, 1348–1352. (doi:10.1126/science.1221483)

16. Hyodo T, Ito S, Hasegawa H, Asano E, Maeda M, Urano T, Takahashi M, Hamaguchi M, Senga T. 2012 Misshapen-like kinase 1 (MINK1) is a novel component of striatin-interacting

phosphatase and kinase (STRIPAK) and is required for the completion of cytokinesis. *J. Biol. Chem.* **287**, 25019–25029. (doi:10.1074/jbc.M112.372342)
17. Seo G, Han H, Vargas RE, Yang B, Li X, Wang W. 2020 MAP4K interactome reveals STRN4 as a key STRIPAK complex component in hippo pathway regulation. *Cell Rep.* **32**, 107860. (doi:10.1016/j.celrep.2020.107860)
18. Kuck U, Radchenko D, Teichert I. 2019 STRIPAK, a highly conserved signaling complex, controls multiple eukaryotic cellular and developmental processes and is linked with human diseases. *Biol. Chem.* **400**, 1005–1022. (doi:10.1515/hsz-2019-0173)
19. Ribeiro PS, Josue F, Wepf A, Wehr MC, Rinner O, Kelly G, Tapon N, Gstaiger M. 2010 Combined functional genomic and proteomic approaches identify a PP2A complex as a negative regulator of hippo signaling. *Mol. Cell* **39**, 521–534. (doi:10.1016/j.molcel.2010.08.002)
20. Zheng Y, Liu B, Wang L, Lei H, Pulgar Prieto KD, Pan D. 2017 Homeostatic control of hpo/MST kinase activity through autophosphorylation-dependent recruitment of the STRIPAK PP2A phosphatase complex. *Cell Rep.* **21**, 3612–3623. (doi:10.1016/j.celrep.2017.11.076)
21. Neal SJ, Zhou Q, Pignoni F. 2020 STRIPAK-PP2A regulates hippo-yorkie signaling to suppress retinal fate in the *D*rosophila eye disc peripodial epithelium. *J. Cell. Sci.* **133**. (doi:10.1242/jcs.237834)
22. Kaya-Copur A *et al*. 2021 The hippo pathway controls myofibril assembly and muscle fiber growth by regulating sarcomeric gene expression. *eLife* **10**, 1–34. (doi:10.7554/eLife.63726)
23. Lant B *et al*. 2015 CCM-3/STRIPAK promotes seamless tube extension through endocytic recycling. *Nat. Commun.* **6**, 6449. (doi:10.1038/ncomms7449)
24. Schad EG, Petersen CP. 2020 STRIPAK limits stem cell differentiation of a WNT signaling center to control planarian axis scaling. *Curr. Biol.* **30**, 254–263.(doi:10.1016/j.cub.2019.11.068)
25. Gotz J, Probst A, Ehler E, Hemmings B, Kues W. 1998 Delayed embryonic lethality in mice lacking protein phosphatase 2A catalytic subunit C α. *Proc. Natl Acad. Sci.* **95**, 12370–12375.
26. Gu P, Qi X, Zhou Y, Wang Y, Gao X. 2012 Generation of Ppp2Ca and Ppp2Cb conditional null alleles in mouse. *Genesis* **50**, 429–436. (doi:10.1002/dvg.20815)
27. Ruediger R, Ruiz J, Walter G. 2011 Human cancer-associated mutations in the A α subunit of protein phosphatase 2A increase lung cancer incidence in A α knock-in and knockout mice. *Mol. Cell. Biol.* **31**, 3832–3844. (doi:10.1128/MCB.05744-11)
28. Lange L, Marks M, Liu J, Wittler L, Bauer H, Piehl S *et al*. Patterning and gastrulation defects caused by the *tw*18 lethal are due to loss of Ppp2r1a. *Biol. Open* **6**, 752–764.
29. Xue Y, Wang X, Li Z, Gotoh N, Chapman D, Skolnik EY. 2001 Mesodermal patterning defect in mice lacking the ste20 NCK interacting kinase (NIK). *Development* **128**, 1559–1572. (doi:10.1242/dev.128.9.1559)
30. Garza AE *et al*. 2015 Variants in striatin gene are associated with salt-sensitive blood pressure in mice and humans. *Hypertension* **65**, 211–217. (doi:10.1161/HYPERTENSIONAHA.114.04233)
31. The International Mouse Phenotype Consortium. Strn3. See https://www.mousephenotype.org/data/genes/MGI:2151064 (accessed 2 July 2024).
32. Dickinson ME *et al*. 2016 High-throughput discovery of novel developmental phenotypes. *Nature* **537**, 508–514. (doi:10.1038/nature19356)

33. Bazzi H, Soroka E, Alcorn HL, Anderson KV. 2017 STRIP1, a core component of STRIPAK complexes, is essential for normal mesoderm migration in the mouse embryo. *Proc. Natl Acad. Sci. USA* **114**, E10928–E10936. (doi:10.1073/pnas.1713535114)
34. International Mouse Phenotype Consortium. *Mob4*. See https://www.mousephenotype.org/data/genes/MGI:104899 (accessed 15 July 2024).
35. He Y, Zhang H, Yu L, Gunel M, Boggon TJ, Chen H, Min W. 2010 Stabilization of VEGFR2 signaling by cerebral cavernous malformation 3 is critical for vascular development. *Sci. Signal.* **3**. (doi:10.1126/scisignal.2000722)
36. Chan AC *et al*. 2011 Mutations in 2 distinct genetic pathways result in cerebral cavernous malformations in mice. *J. Clin. Invest*. **121**, 1871–1881. (doi:10.1172/JCI44393)
37. International Mouse Phenotype Consortium. *Fgfr1op2*. See https://www.mousephenotype.org/data/genes/MGI:1914779 (accessed 15 July 2024).
38. Jeong BC, Bae SJ, Ni L, Zhang X, Bai XC, Luo X. 2021 CRYO-EM structure of the hippo signaling integrator human STRIPAK. *Nat. Struct. Mol. Biol*. **28**, 290–299. (doi:10.1038/s41594-021-00564-y)
39. Tang Y *et al*. 2019 Architecture, substructures, and dynamic assembly of STRIPAK complexes in hippo signaling. *Cell Discov*. **5**, 3. (doi:10.1038/s41421-018-0077-3)
40. Sukotjo C, Abanmy A, Ogawa T, Nishimura I. 2002 Molecular Cloning of Wound Inducible Transcript (wit 3.0) Differentially Expressed in Edentulous Oral Mucosa Undergoing Tooth Extraction Wound-healing. *J Dent Res*. **81**, 229-235. (doi: 10.1177/154405910208100402)
41. Sukotjo C, Lin A, Song K, Ogawa T, Wu B, Nishimura I. 2003 Oral fibroblast expression of wound-inducible transcript 3.0 (wit3.0) accelerates the collagen gel contraction in vitro. *J. Biol. Chem.* **278**, 51527–51534. (doi:10.1074/jbc.M309616200)
42. Lin A, Hokugo A, Choi J, Nishimura I. 2010 Small cytoskeleton-associated molecule, fibroblast growth factor receptor 1 oncogene partner 2/wound inducible transcript-3.0 (FGFR1OP2/wit3.0), facilitates fibroblast-driven wound closure. *Am. J. Pathol*. **176**, 108–121. (doi:10.2353/ajpath.2010.090256)
43. Grand EK, Grand FH, Chase AJ, Ross FM, Corcoran MM, Oscier DG, Cross NCP. 2004 Identification of a novel gene, FGFR1OP2, fused to FGFR1 in 8p11 myeloproliferative syndrome. *Genes. Chromosomes Cancer* **40**, 78–83. (doi:10.1002/gcc.20023)
44. Onozawa M *et al*. 2011 The 8p11 myeloproliferative syndrome owing to rare FGFR1OP2-FGFR1 fusion. *Eur. J. Haematol*. **86**, 347–349. (doi:10.1111/j.1600-0609.2010.01568.x)
45. Qin H, Wu Q, Cowell JK, Ren M. 2016 FGFR1OP2-FGFR1 induced myeloid leukemia and T-cell lymphoma in a mouse model. *Haematologica* **101**, e91–4. (doi:10.3324/haematol.2015.137695)
46. Bae SJ, Ni L, Osinski A, Tomchick DR, Brautigam CA, Luo X. 2017 SAV1 promotes hippo kinase activation through antagonizing the PP2A phosphatase STRIPAK. *eLife* **6**, e30278. (doi: 10.7554/eLife.30278)
47. Pan D. 2010 The hippo signaling pathway in development and cancer. *Dev. Cell* **19**, 491–505. (doi:10.1016/j.devcel.2010.09.011)
48. Ma S, Meng Z, Chen R, Guan KL. 2019 The hippo pathway: biology and pathophysiology. *Annu. Rev. Biochem.* **88**, 577–604. (doi:10.1146/annurev-biochem-013118-111829)
49. Mochizuki T *et al*. 1998 Cloning of inv, a gene that controls left/right asymmetry and kidney development. *Nature* **395**, 177–181. (doi:10.1038/26006)

50. Yamaguchi TP, Bradley A, McMahon AP, Jones S. 1999 A Wnt5a pathway underlies outgrowth of multiple structures in the vertebrate embryo. *Development* **126**, 1211-1223. (doi: 10.1242/dev.126.6.1211)
51. Takeuchi S *et al*. 2000 Mouse Ror2 receptor tyrosine kinase is required for the heart development and limb formation. *Genes Cells* **5**, 71-78. (doi:10.1046/j.1365-2443.2000.00300.x)
52. Nomi M *et al*. 2001 Loss of mRor1 enhances the heart and skeletal abnormalities in mRor2-deficient mice: redundant and pleiotropic functions of mRor1 and mRor2 receptor tyrosine kinases. *Mol. Cell. Biol*. **21**, 8329-8335. (doi:10.1128/MCB.21.24.8329-8335.2001)
53. Li C, Xiao J, Hormi K, Borok Z, Minoo P. 2002 Wnt5a participates in distal lung morphogenesis. *Dev. Biol*. **248**, 68-81. (doi:10.1006/dbio.2002.0729)
54. Oishi I *et al*. 2003 The receptor tyrosine kinase Ror2 is involved in non-canonical Wnt5a/JNK signalling pathway. *Genes Cells* **8**, 645-654. (doi:10.1046/j.1365-2443.2003.00662.x)
55. Phillips CL *et al*. 2004 Renal cysts of inv/inv mice resemble early infantile nephronophthisis. *J. Am. Soc. Nephrol*. **15**, 1744-1755. (doi:10.1097/01.asn.0000131520.07008.b3)
56. Schwabe GC, Trepczik B, Suring K, Brieske N, Tucker AS, Sharpe PT, Minami Y, Mundlos S. 2004 Ror2 knockout mouse as a model for the developmental pathology of autosomal recessive robinow syndrome. *Dev. Dyn*. **229**, 400-410. (doi:10.1002/dvdy.10466)
57. Qian D, Jones C, Rzadzinska A, Mark S, Zhang X, Steel KP, Dai X, Chen P. 2007 Wnt5a functions in planar cell polarity regulation in mice. *Dev. Biol*. **306**, 121-133. (doi:10.1016/j.ydbio.2007.03.011)
58. Etheridge SL *et al*. 2008 Murine dishevelled 3 functions in redundant pathways with dishevelled 1 and 2 in normal cardiac outflow tract, cochlea, and neural tube development. *PLoS Genet*. **4**, e1000259. (doi:10.1371/journal.pgen.1000259)
59. Cervantes S, Yamaguchi TP, Hebrok M. 2009 Wnt5a is essential for intestinal elongation in mice. *Dev. Biol*.**326**, 285-294. (doi:10.1016/j.ydbio.2008.11.020)
60. Yamada M, Udagawa J, Matsumoto A, Hashimoto R, Hatta T, Nishita M, Minami Y, Otani H. 2010 Ror2 is required for midgut elongation during mouse development. *Dev. Dyn*. **239**, 941-953. (doi:10.1002/dvdy.22212)
61. Yates LL, Schnatwinkel C, Murdoch JN, Bogani D, Formstone CJ, Townsend S, Greenfield A, Niswander LA, Dean CH. 2010 The PCP genes Celsr1 and Vangl2 are required for normal lung branching morphogenesis. *Hum. Mol. Genet*. **19**, 2251-2267. (doi:10.1093/hmg/ddq104)
62. Robinson A, Escuin S, Doudney K, Vekemans M, Stevenson RE, Greene NDE, Copp AJ, Stanier P. 2012 Mutations in the planar cell polarity genes CELSR1 and SCRIB are associated with the severe neural tube defect craniorachischisis. *Hum. Mutat*. **33**, 440-447. (doi:10.1002/humu.21662)
63. Murdoch JN, Damrau C, Paudyal A, Bogani D, Wells S, Greene NDE, Stanier P, Copp AJ. 2014 Genetic interactions between planar cell polarity genes cause diverse neural tube defects in mice. *Dis. Model. Mech*. **7**, 1153-1163. (doi:10.1242/dmm.016758)
64. Devenport D. 2014 The cell biology of planar cell polarity. *J. Cell Biol*. **207**, 171-179. (doi:10.1083/jcb.201408039)
65. Butler MT, Wallingford JB. 2017 Planar cell polarity in development and disease. *Nat. Rev. Mol. Cell Biol*. **18**, 375-388. (doi:10.1038/nrm.2017.11)
66. Adler PN. 2012 The frizzled/stan pathway and planar cell polarity in the drosophila wing. *Curr. Top. Dev. Biol*. **101**, 1-31. (doi:10.1016/B978-0-12-394592-1.00001-6)

67. Humphries AC, Mlodzik M. 2018 From instruction to output: wnt/PCP signaling in development and cancer. *Curr. Opin. Cell Biol.* **51**, 110–116. (doi:10.1016/j.ceb.2017.12.005)
68. Harrison C, Shao H, Strutt H, Strutt D. 2020 Molecular mechanisms mediating asymmetric subcellular localisation of the core planar polarity pathway proteins. *Biochem. Soc. Trans.* **48**, 1297–1308. (doi:10.1042/BST20190404)
69. Mill P, Christensen ST, Pedersen LB. 2023 Primary cilia as dynamic and diverse signalling hubs in development and disease. *Nat. Rev. Genet.* **24**, 421–441. (doi:10.1038/s41576-023-00587-9)
70. Irigoin F, Badano JL. 2011 Keeping the balance between proliferation and differentiation: the primary cilium. *Curr. Genomics* **12**, 285–297. (doi:10.2174/138920211795860134)
71. Adler PN, Wallingford JB. 2017 From planar cell polarity to ciliogenesis and back: the curious tale of the PPE and CPLANE proteins. *Trends Cell Biol.* **27**, 379–390. (doi:10.1016/j.tcb.2016.12.001)
72. Vuong LT, Mlodzik M. 2023 The complex relationship of Wnt-signaling pathways and cilia. *Curr. Top. Dev. Biol.* **155**, 95–125. (doi:10.1016/bs.ctdb.2023.09.002)
73. Simons M *et al*. 2005 Inversin, the gene product mutated in nephronophthisis type II, functions as a molecular switch between Wnt signaling pathways. *Nat. Genet.* **37**, 537–543. (doi:10.1038/ng1552)
74. Burckle C, Gaude HM, Vesque C, Silbermann F, Salomon R, Jeanpierre C, Antignac C, Saunier S, Schneider-Maunoury S. 2011 Control of the Wnt pathways by nephrocystin-4 is required for morphogenesis of the zebrafish pronephros. *Hum. Mol. Genet.* **20**, 2611–2627. (doi:10.1093/hmg/ddr164)
75. Gerdes JM *et al*. 2007 Disruption of the basal body compromises proteasomal function and perturbs intracellular Wnt response. *Nat. Genet.* **39**, 1350–1360. (doi:10.1038/ng.2007.12)
76. Mahuzier A *et al*. 2012 Dishevelled stabilization by the ciliopathy protein Rpgrip1l is essential for planar cell polarity. *J. Cell Biol.* **198**, 927–940. (doi:10.1083/jcb.201111009)
77. Wallingford JB, Mitchell B. 2011 Strange as it may seem: the many links between Wnt signaling, planar cell polarity, and cilia: figure 1. *Genes Dev.* **25**, 201–213. (doi:10.1101/gad.2008011)
78. Corbit KC, Shyer AE, Dowdle WE, Gaulden J, Singla V, Chen MH, Chuang PT, Reiter JF. 2008 Kif3a constrains β-catenin-dependent wnt signalling through dual ciliary and non-ciliary mechanisms. *Nat. Cell Biol.* **10**, 70–76. (doi:10.1038/ncb1670)
79. Jones C, Roper VC, Foucher I, Qian D, Banizs B, Petit C, Yoder BK, Chen P. 2008 Ciliary proteins link basal body polarization to planar cell polarity regulation. *Nat. Genet.* **40**, 69–77. (doi:10.1038/ng.2007.54)
80. Ross AJ *et al*. 2005 Disruption of bardet-biedl syndrome ciliary proteins perturbs planar cell polarity in vertebrates. *Nat. Genet.* **37**, 1135–1140. (doi:10.1038/ng1644)
81. Boutin C *et al*. 2014 A dual role for planar cell polarity genes in ciliated cells. *Proc. Natl Acad. Sci. USA* **111**. (doi:10.1073/pnas.1404988111)
82. Nomachi A, Nishita M, Inaba D, Enomoto M, Hamasaki M, Minami Y. 2008 Receptor tyrosine kinase Ror2 mediates Wnt5a-induced polarized cell migration by activating c-jun N-terminal kinase via actin-binding protein filamin A. *J. Biol. Chem.* **283**, 27973–27981. (doi:10.1074/jbc.M802325200)

83. Cui C *et al*. 2013 Wdpcp, a PCP protein required for ciliogenesis, regulates directional cell migration and cell polarity by direct modulation of the actin cytoskeleton. *PLoS Biol*. **11**, e1001720. (doi:10.1371/journal.pbio.1001720)
84. Veland IR *et al*. 2013 Inversin/nephrocystin-2 is required for fibroblast polarity and directional cell migration. *PLoS One* **8**, e60193. (doi:10.1371/journal.pone.0060193)
85. Zilber Y, Babayeva S, Seo JH, Liu JJ, Mootin S, Torban E. 2013 The PCP effector fuzzy controls cilial assembly and signaling by recruiting Rab8 and dishevelled to the primary cilium. *Mol. Biol. Cell* **24**, 555–565. (doi:10.1091/mbc.E12-06-0437)
86. Gibbs BC *et al*. 2016 Prickle1 mutation causes planar cell polarity and directional cell migration defects associated with cardiac outflow tract anomalies and other structural birth defects. *Biol. Open* **5**, 323–335. (doi:10.1242/bio.015750)
87. Fischer E, Legue E, Doyen A, Nato F, Nicolas JF, Torres V, Yaniv M, Pontoglio M. 2006 Defective planar cell polarity in polycystic kidney disease. *Nat. Genet*. **38**, 21–23. (doi:10.1038/ng1701)
88. Saburi S *et al*. 2008 Loss of Fat4 disrupts PCP signaling and oriented cell division and leads to cystic kidney disease. *Nat. Genet*. **40**, 1010–1015. (doi:10.1038/ng.179)
89. Tao H, Suzuki M, Kiyonari H, Abe T, Sasaoka T, Ueno N. 2009 mouse Prickle*1* , the homolog of a PCP gene, is essential for epiblast apical-basal polarity . *Proc. Natl Acad. Sci. USA* **106**, 14426–14431. (doi:10.1073/pnas.0901332106)
90. Gros J, Hu JKH, Vinegoni C, Feruglio PF, Weissleder R, Tabin CJ. 2010 WNT5A/JNK and FGF/MAPK pathways regulate the cellular events shaping the vertebrate limb bud. *Curr. Biol*. **20**, 1993–2002. (doi:10.1016/j.cub.2010.09.063)
91. Suizu F *et al*. 2016 Phosphorylation-dependent akt-inversin interaction at the basal body of primary cilia. *EMBO J*. **35**, 1346–1363. (doi:10.15252/embj.201593003)
92. Chen CT *et al*. 2014 A unique set of centrosome proteins requires pericentrin for spindle-pole localization and spindle orientation. *Curr. Biol*. **24**, 2327–2334. (doi:10.1016/j.cub.2014.08.029)
93. Jonassen JA, San Agustin J, Follit JA, Pazour GJ. 2008 Deletion of IFT20 in the mouse kidney causes misorientation of the mitotic spindle and cystic kidney disease. *J. Cell Biol*. **183**, 377–384. (doi:10.1083/jcb.200808137)
94. Raudvere U, Kolberg L, Kuzmin I, Arak T, Adler P, Peterson H, Vilo J. 2019 G:profiler: a web server for functional enrichment analysis and conversions of gene lists. *Nucleic Acids Res.* **47**, W191–W198. (doi:10.1093/nar/gkz369)
95. Wolf MTF, Hildebrandt F. 2011 Nephronophthisis. *Pediatr. Nephrol.* **26**, 181–194. (doi: 10.1007/s00467-010-1585-z)
96. Lee K, Gusella GL, He JC. 2021 Epithelial proliferation and cell cycle dysregulation in kidney injury and disease. *Kidney Int.* **100**, 67–78. (doi:10.1016/j.kint.2021.03.024)
97. Rehmani T, Mlynarova J, Byers J, Salih M, Tuana BS. 2021 Specific deletion of the FHA domain containing SLMAP3 isoform in postnatal myocardium has no impact on structure or function. *Cardiogenetics* **11**, 164–184.
98. Rehmani T, Dias AP, Kamal M, Salih M, Tuana BS. 2024 Deletion of sarcolemmal membrane-associated protein isoform 3 (SLMAP3) in cardiac progenitors delays embryonic growth of myocardium without affecting hippo pathway. *Int. J. Mol. Sci*. **25**, 2888. (doi:10.3390/ijms25052888)

99. Rehmani T, Dias AP, Salih M, Tuana B. 2024 SLMAP3 is essential for neurulation through mechanisms involving cytoskeletal elements, ABP, and PCP. *Life Sci. Allian.* **7**, e202302545. (doi: 10.26508/lsa.202302545)
100. Fan F *et al*. 2016 Pharmacological targeting of kinases MST1 and MST2 augments tissue repair and regeneration. *Sci. Transl. Med.* **8**, 352ra108. (doi:10.1126/scitranslmed.aaf2304)
101. Hescheler J, Mieskes G, Ruegg JC, Takai A, Trautwein W. 1988 Effects of a protein phosphatase inhibitor, okadaic acid, on membrane currents of isolated guinea-pig cardiac myocytes. *Pflugers Arch*. **412**, 248–252. (doi:10.1007/BF00582504)
102. Bialojan C, Takai A. 1988 Inhibitory effect of a marine-sponge toxin, okadaic acid, on protein phosphatases. specificity and kinetics. *Biochem. J*. **256**, 283–290. (doi:10.1042/bj2560283)
103. Hong W, Guan KL. 2012 The YAP and TAZ transcription co-activators: key downstream effectors of the mammalian hippo pathway. *Semin. Cell Dev. Biol*. **23**, 785–793. (doi:10.1016/j.semcdb.2012.05.004)
104. MD Anderson Cancer Center. 2024 *RPPA.* See https://www.mdanderson.org/research/research-resources/core-facilities/functional-proteomics-rppa-core.html.
105. Bai SW *et al*. 2011 Identification and characterization of a set of conserved and new regulators of cytoskeletal organization, cell morphology and migration. *BMC Biol*. **9**, 54. (doi:10.1186/1741-7007-9-54)
106. Madsen CD, Hooper S, Tozluoglu M, Bruckbauer A, Fletcher G, Erler JT, Bates PA, Thompson B, Sahai E. 2015 STRIPAK components determine mode of cancer cell migration and metastasis. *Nat. Cell Biol*. **17**, 68–80. (doi:10.1038/ncb3083)
107. Chen Z, Zhang Y, Zhao X. 2019 FAM40A alters the cytoskeleton of podocytes in familial focal and segmental glomerulosclerosis by regulating F-actin and nephrin. *Arch. Med. Sci*.**15**, 165–173. (doi:10.5114/aoms.2018.73138)
108. Fidalgo M, Guerrero A, Fraile M, Iglesias C, Pombo CM, Zalvide J. 2012 Adaptor protein cerebral cavernous malformation 3 (CCM3) mediates phosphorylation of the cytoskeletal proteins ezrin/radixin/moesin by mammalian ste20-4 to protect cells from oxidative stress. *J. Biol. Chem.* **287**, 11556–11565. (doi:10.1074/jbc.M111.320259)
109. Wang S *et al*. 2021 CCM3 is a gatekeeper in focal adhesions regulating mechanotransduction and YAP/TAZ signalling. *Nat. Cell Biol*. **23**, 758–770. (doi:10.1038/s41556-021-00702-0)
110. Baumgartner M, Sillman AL, Blackwood EM, Srivastava J, Madson N, Schilling JW, Wright JH, Barber DL. 2006 The nck-interacting kinase phosphorylates ERM proteins for formation of lamellipodium by growth factors. *Proc. Natl Acad. Sci. USA* **103**, 13391–13396. (doi:10.1073/pnas.0605950103)
111. Yue J, Xie M, Gou X, Lee P, Schneider MD, Wu X. 2014 Microtubules regulate focal adhesion dynamics through MAP4K4. *Dev. Cell* **31**, 572–585. (doi:10.1016/j.devcel.2014.10.025)
112. Vitorino P *et al*. 2015 MAP4K4 regulates integrin-FERM binding to control endothelial cell motility. *Nature New Biol*. **519**, 425–430. (doi:10.1038/nature14323)
113. Fidalgo M, Fraile M, Pires A, Force T, Pombo C, Zalvide J. 2010 CCM3/PDCD10 stabilizes GCKIII proteins to promote golgi assembly and cell orientation. *J. Cell. Sci*. **123**, 1274–1284. (doi:10.1242/jcs.061341)
114. Yadav S, Linstedt AD. 2011 Golgi positioning. *Cold Spring Harb. Perspect. Biol*. **3**, a005322–a005322. (doi:10.1101/cshperspect.a005322)

115. Simons M, Mlodzik M. 2008 Planar cell polarity signaling: from fly development to human disease. *Annu. Rev. Genet*. **42**, 517–540. (doi:10.1146/annurev.genet.42.110807.091432)
116. Simons M, Walz G. 2006 Polycystic kidney disease: cell division without a c(l)ue? *Kidney Int*. **70**, 854–864. (doi:10.1038/sj.ki.5001534)
117. Torban E, Sokol SY. 2021 Planar cell polarity pathway in kidney development, function and disease. *Nat. Rev. Nephrol*. **17**, 369–385. (doi:10.1038/s41581-021-00395-6)
118. Gao C *et al*. 2010 Autophagy negatively regulates wnt signalling by promoting dishevelled degradation. *Nat. Cell Biol*. **12**, 781–790. (doi:10.1038/ncb2082)
119. Chan DW, Chan CY, Yam JWP, Ching YP, Ng IOL. 2006 Prickle-1 negatively regulates Wnt/β-catenin pathway by promoting dishevelled ubiquitination/degradation in liver cancer. *Gastroenterology* **131**, 1218–1227. (doi:10.1053/j.gastro.2006.07.020)
120. Kwan HT, Chan DW, Cai PCH, Mak CSL, Yung MMH, Leung THY, Wong OGW, Cheung ANY, Ngan HYS. 2013 AMPK activators suppress cervical cancer cell growth through inhibition of DVL3 mediated wnt/β-catenin signaling activity. *PLoS One* **8**, e53597. (doi:10.1371/journal.pone.0053597)
121. Myung J, Kim KB, Crews CM. 2001 The ubiquitin-proteasome pathway and proteasome inhibitors. *Med. Res. Rev*. **21**, 245–273. (doi:10.1002/med.1009)
122. Seglen PO, Reith A. 1976 Ammonia inhibition of protein degradation in isolated rat hepatocytes. *Exp. Cell Res*. **100**, 276–280. (doi:10.1016/0014-4827(76)90148-8)
123. Seglen PO, Grinde B, Solheim AE. 1979 Inhibition of the lysosomal pathway of protein degradation in isolated rat hepatocytes by ammonia, methylamine, chloroquine and leupeptin. *Eur. J. Biochem*. **95**, 215–225. (doi:10.1111/j.1432-1033.1979.tb12956.x)
124. Preisinger C, Short B, De Corte V, Bruyneel E, Haas A, Kopajtich R, Gettemans J, Barr FA. 2004 YSK1 is activated by the golgi matrix protein GM130 and plays a role in cell migration through its substrate 14-3-3ζ. *J. Cell Biol*. **164**, 1009–1020. (doi:10.1083/jcb.200310061)
125. Reiter JF, Leroux MR. 2017 Genes and molecular pathways underpinning ciliopathies. *Nat. Rev. Mol. Cell Biol*. **18**, 533–547. (doi:10.1038/nrm.2017.60)
126. International Mouse Phenotype Consortium. *SIKE1*. See https://www.mousephenotype.org/data/genes/MGI:1913891 (accessed 15 July 2024).
127. Morin-Kensicki EM, Boone BN, Howell M, Stonebraker JR, Teed J, Alb JG, Magnuson TR, O'Neal W, Milgram SL. 2006 defects in yolk sac vasculogenesis, chorioallantoic fusion, and embryonic axis elongation in mice with targeted disruption of *Yap65* . *Mol. Cell. Biol*. **26**, 77–87. (doi:10.1128/MCB.26.1.77-87.2006)
128. Nishioka N *et al*. 2009 The hippo signaling pathway components lats and Yap pattern Tead4 activity to distinguish mouse trophectoderm from inner cell mass. *Dev. Cell* **16**, 398–410. (doi:10.1016/j.devcel.2009.02.003)
129. Aszodi A. 2016 *The cartilaginous growth plate*, (eds S Grassel, A Aszodi), pp. 83–113. Cham: Springer International Publishing. (doi:10.1007/978-3-319-29568-8_4)
130. Park TJ, Mitchell BJ, Abitua PB, Kintner C, Wallingford JB. 2008 Dishevelled controls apical docking and planar polarization of basal bodies in ciliated epithelial cells. *Nat. Genet*. **40**, 871–879. (doi:10.1038/ng.104)
131. Gupta GD *et al*. 2015 A dynamic protein interaction landscape of the human centrosome-cilium interface. *Cell* **163**, 1484–1499. (doi:10.1016/j.cell.2015.10.065)
132. Gheiratmand L, Coyaud E, Gupta GD, Laurent EM, Hasegan M, Prosser SL, Goncalves J, Raught B, Pelletier L. 2019 Spatial and proteomic profiling reveals centrosome-independent features of centriolar satellites. *EMBO J*. **38**, e101109. (doi:10.15252/embj.2018101109)

133. Quarantotti V, Chen JX, Tischer J, Gonzalez Tejedo C, Papachristou EK, D'Santos CS, Kilmartin JV, Miller ML, Gergely F. 2019 Centriolar satellites are acentriolar assemblies of centrosomal proteins. *EMBO J*. **38**, e101082. (doi:10.15252/embj.2018101082)
134. Kean MJ *et al*. 2011 Structure-function analysis of core STRIPAK proteins: a signaling complex implicated in golgi polarization. *J. Biol. Chem*. **286**, 25065–25075. (doi:10.1074/jbc.M110.214486)
135. Rusilowicz-Jones EV, Urbe S, Clague MJ. 2022 Protein degradation on the global scale. *Mol. Cell* **82**, 1414–1423. (doi:10.1016/j.molcel.2022.02.027)
136. Deng KQ *et al*. 2016 Suppressor of IKKε is an essential negative regulator of pathological cardiac hypertrophy. *Nat. Commun.* **7**, 11432. (doi:10.1038/ncomms11432)
137. Koca Y, Collu GM, Mlodzik M. 2022 Wnt-frizzled planar cell polarity signaling in the regulation of cell motility. *Curr. Top. Dev. Biol*. **150**, 255–297. (doi:10.1016/bs.ctdb.2022.03.006)
138. Davey CF, Moens CB. 2017 Planar cell polarity in moving cells: think globally, act locally. *Development* **144**, 187–200. (doi:10.1242/dev.122804)
139. Rack PG *et al*. 2014 Arhgap36-dependent activation of gli transcription factors. *Proc. Natl Acad. Sci. USA* **111**, 11061–11066. (doi:10.1073/pnas.1322362111)
140. Qiu LQ, Lai WS, Stumpo DJ, Blackshear PJ. 2016 Mouse embryonic fibroblast cell culture and stimulation. *Bio Protoc*. **6**, e1859. (doi:10.21769/BioProtoc.1859)
141. Addgene. 2024 SV40 1: pBSSVD2005 - Plasmid #21826. See https://www.addgene.org/21826/ (accessed 15 July 2024).
142. Addgene. plentiCRISPRv2sgEGFP- Plasmid #86153. See https://www.addgene.org/86153/ (accessed 15 July 2024).
143. Huang Y, Tejero R, Lee VK, Brusco C, Hannah T, Bertucci TB, et al. Plexin-B2 facilitates glioblastoma infiltration by modulating cell biomechanics. Commun Biol. 2021 Jan 29;**4**(1):145.
144. Addgene. LentiCRISPR v2 - Plasmid #52961. See https://www.addgene.org/52961/ (accessed 15 July 2024).
145. Sanjana NE, Shalem O, Zhang F. 2014 Improved vectors and genome-wide libraries for CRISPR screening. *Nat. Methods*. **11**, 783–784. (doi:10.1038/nmeth.3047)
146. VectorBuilder. *shRNA-SC*. See https://en.vectorbuilder.com/vector/VB221021-1240rmu.html (accessed 15 July 2024).
147. VectorBuilder. STRN3-shRNA#1. See https://en.vectorbuilder.com/vector/VB230413-1427xvn.html (accessed 15 July 2024).
148. VectorBuilder. *STRN3-shRNA#2*. See https://en.vectorbuilder.com/vector/VB230413-1430apw.html (accessed 15 July 2024).
149. VectorBuilder. *FGFR1OP2-shRNA#2*. See https://en.vectorbuilder.com/vector/VB230413-1350arz.html (accessed 15 July 2024).
150. VectorBuilder. FGFR1OP2-shRNA_all. See https://en.vectorbuilder.com/vector/VB230413-1351jve.html (accessed 15 July 2024).
151. VectorBuilder. FGFR1OP2-shRNA#1. See https://en.vectorbuilder.com/vector/VB230620-1373akk.html (accessed 15 July 2024).
152. VectorBuilder. FGFR1OP2-shRNA_custom#2. See https://en.vectorbuilder.com/vector/VB230620-1386uek.html (accessed 15 July 2024).
153. VectorBuilder. See https://en.vectorbuilder.com/vector/VB230913-1467ckj.html (accessed 15 July 2024).
154. VectorBuilder. See https://en.vectorbuilder.com/vector/VB230913-1480spv.html (accessed 15 July 2024).

155. Addgene. Lentivirus Production. See https://www.addgene.org/protocols/lentivirus-production/.
156. Addgene. Generating Stable Cell Lines. See https://www.addgene.org/protocols/generating-stable-cell-lines/ (accessed 2 July 2024).
157. Addgene. Isolating a Monoclonal Cell Population by Limiting Dilution. See https://www.addgene.org/protocols/limiting-dilution/ (accessed 2 July 2024).
158. Conner DA. 2000 Mouse embryo fibroblast (MEF) feeder cell preparation. In *Current protocols in molecular biology*, vol. **51**. (doi:10.1002/0471142727.mb2302s51)
159. Del Moral PM, Warburton D. 2010 Explant culture of mouse embryonic whole lung, isolated epithelium, or mesenchyme under chemically defined conditions as a system to evaluate the molecular mechanism of branching morphogenesis and cellular differentiation. *Methods Mol. Biol.* **633**, 71–79. (doi:10.1007/978-1-59745-019-5_5)
160. Jones M, Bellusci S. 2019 Imaging and Analysis of Mouse Embryonic Whole Lung, Isolated Tissue, and Lineage-Labelled Cell Culture. *Methods Mol. Biol.* **1940**, 109–127. (doi:10.1007/978-1-4939-9086-3_8)
161. Novus Biologicals. *Chromogenic Immunohistochemistry Staining Of Paraffin-Embedded Tissue*. See https://images.novusbio.com/design/chromogenicFFPE_protocol.pdf?_ga=2.64569322.459549045.1714614368-1449128987.1714614367 (accessed 15 July 2024).
162. Rigueur D, Lyons KM. 2014 Whole-mount skeletal staining. *Methods Mol. Biol.* **1130**, 113–121. (doi:10.1007/978-1-62703-989-5_9)
163. Das A, Fischer RS, Pan D, Waterman CM. 2016 YAP nuclear localization in the absence of cell-cell contact is mediated by a filamentous actin-dependent, myosin II- and phospho-YAP-independent pathway during extracellular matrix mechanosensing. *J. Biol. Chem.* **291**, 6096–6110. (doi:10.1074/jbc.M115.708313)
164. MD Anderson Cancer Center. 2024 *RPPA SPACE*. See https://bioinformatics.mdanderson.org/public-software/rppaspace/ (accessed 15 July 2024).
165. Shehwana H *et al*. 2022 RPPA SPACE: an R package for normalization and quantitation of reverse-phase protein array data. *Bioinformatics* **38**, 5131–5133. (doi:10.1093/bioinformatics/btac665)
166. Akbani R *et al*. 2014 A pan-cancer proteomic perspective on the cancer genome atlas. *Nat. Commun.* **5**, 3887. (doi:10.1038/ncomms4887)
167. Siwak DR, Li J, Akbani R, Liang H, Lu Y. 2019 Analytical platforms 3: processing samples via the RPPA pipeline to generate large-scale data for clinical studies. *Adv. Exp. Med. Biol.* **1188**, 113–147. (doi:10.1007/978-981-32-9755-5_7)
168. Patro R, Duggal G, Love MI, Irizarry RA, Kingsford C. 2017 Salmon provides fast and bias-aware quantification of transcript expression. *Nat. Methods* **14**, 417–419. (doi:10.1038/nmeth.4197)
169. Love MI, Huber W, Anders S. 2014 Moderated estimation of fold change and dispersion for RNA-seq data with deseq2. *Genome Biol.* **15**, 550. (doi:10.1186/s13059-014-0550-8)
170. Edgar R, Domrachev M, Lash AE. 2002 Gene expression omnibus: NCBI gene expression and hybridization array data repository. *Nucleic Acids Res.* **30**, 207–210. (doi:10.1093/nar/30.1.207)
171. Barrett T *et al*. 2013 NCBI GEO: archive for functional genomics data sets--update. *Nucleic Acids Res.* **41**, 991–995. (doi:10.1093/nar/gks1193)

172. Horzum U, Ozdil B, Pesen-Okvur D. Step-by-step quantitative analysis of focal adhesions. MethodsX. 2014;**1**:56–9.
173. Moores Cancer Center. Cell Cycle Analysis by DNA content (Propidium Iodide). See https://moorescancercenter.ucsd.edu/research/shared-resources/flow-cytometry/protocols.html#Cell-Cycle-Analysis-by-DNA-Cont (accessed 15 July 2024).
174. Chen JH, Ozanne SE, Hales CN. 2007 *Methods of cellular senescence induction using oxidative stress*, pp. 179–189.
175. GEO. 2024 *Analysis of gene expression in SLMAP3 knockout immortalized E14.5 mouse embryonic fibroblasts*. See https://www.ncbi.nlm.nih.gov/geo/query/acc.cgi?acc=GSE266611.

Figures Main Text

Figure 1. SLMAP3-/- mice display embryonic/perinatal lethality, with abnormalities in multiple organs

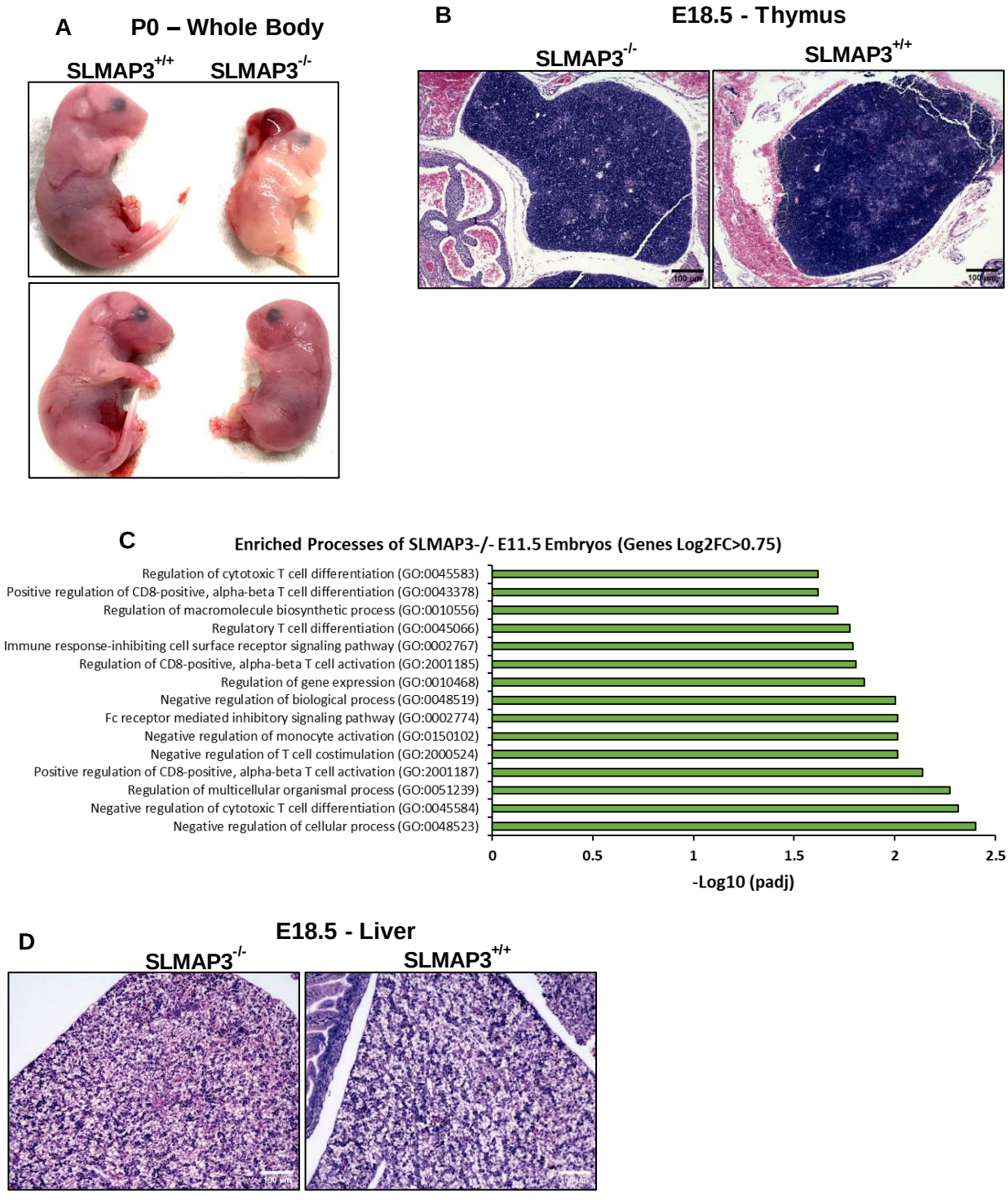

Figure 1. SLMAP3-/- mice display embryonic/perinatal lethality, with abnormalities in multiple organs

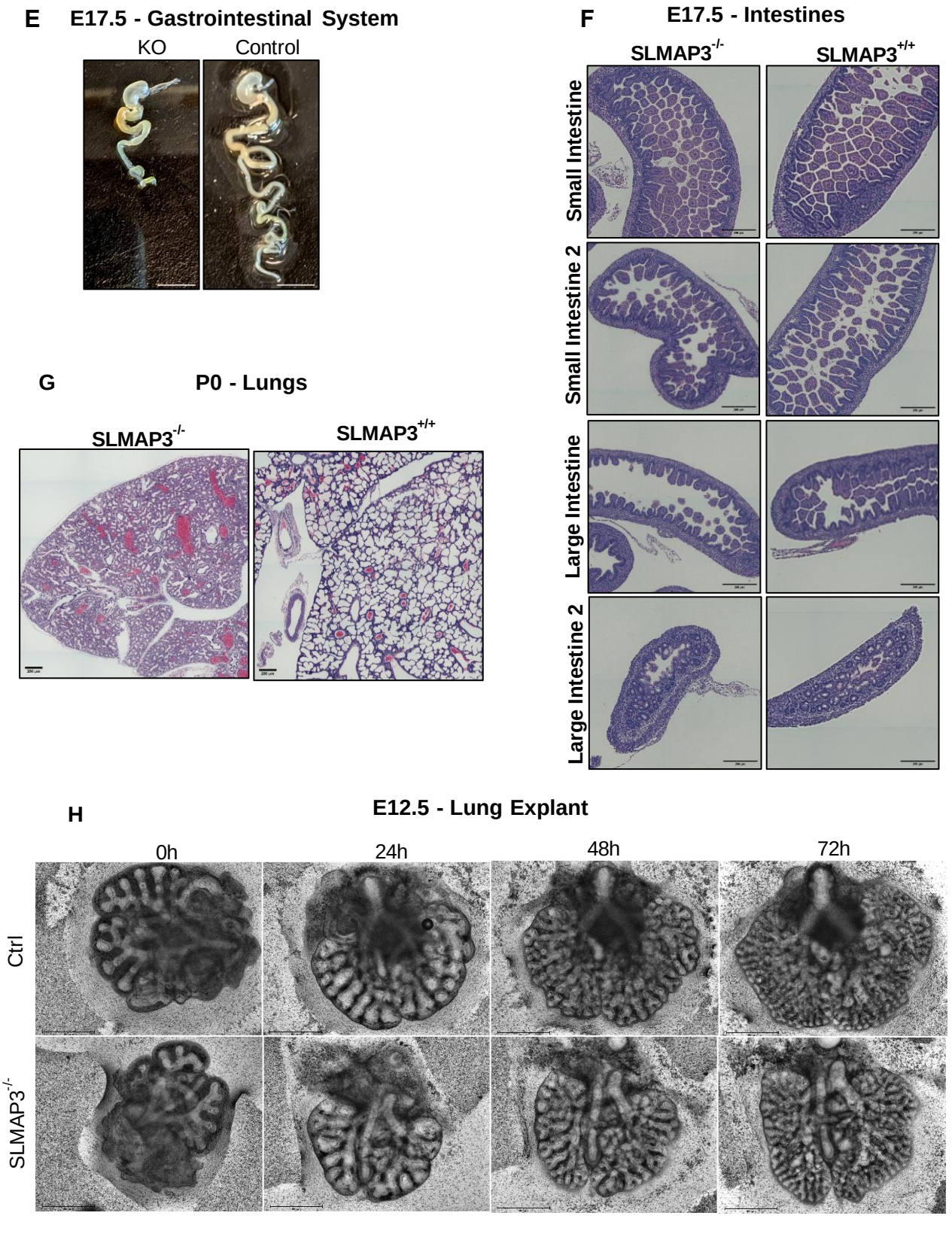

Figure 2. Loss of SLMAP3 results in organ structural defects

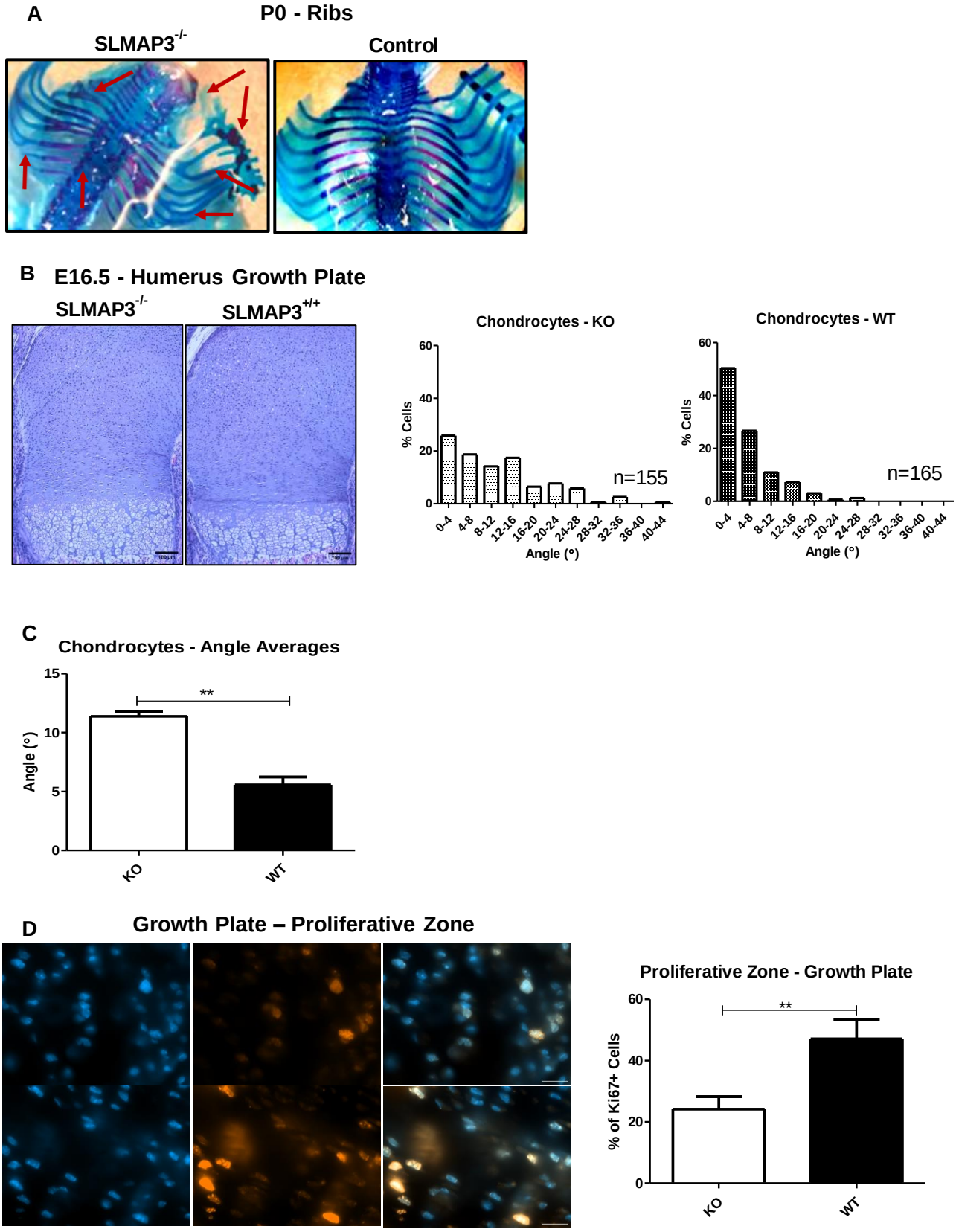

Figure 2. Loss of SLMAP3 results in organ structural defects

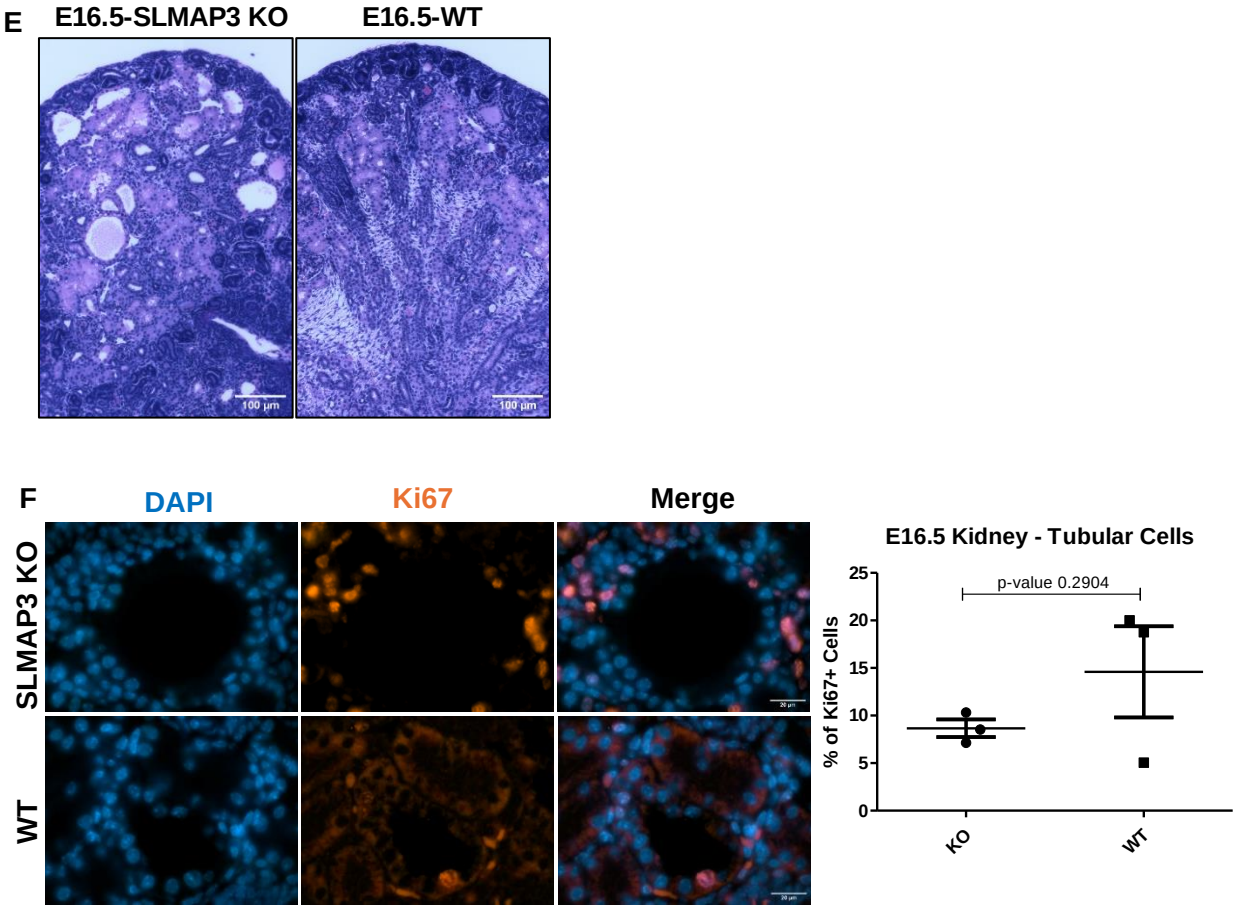

Figure 3. SLMAP3 functions independently of Hippo signaling during mouse embryogenesis

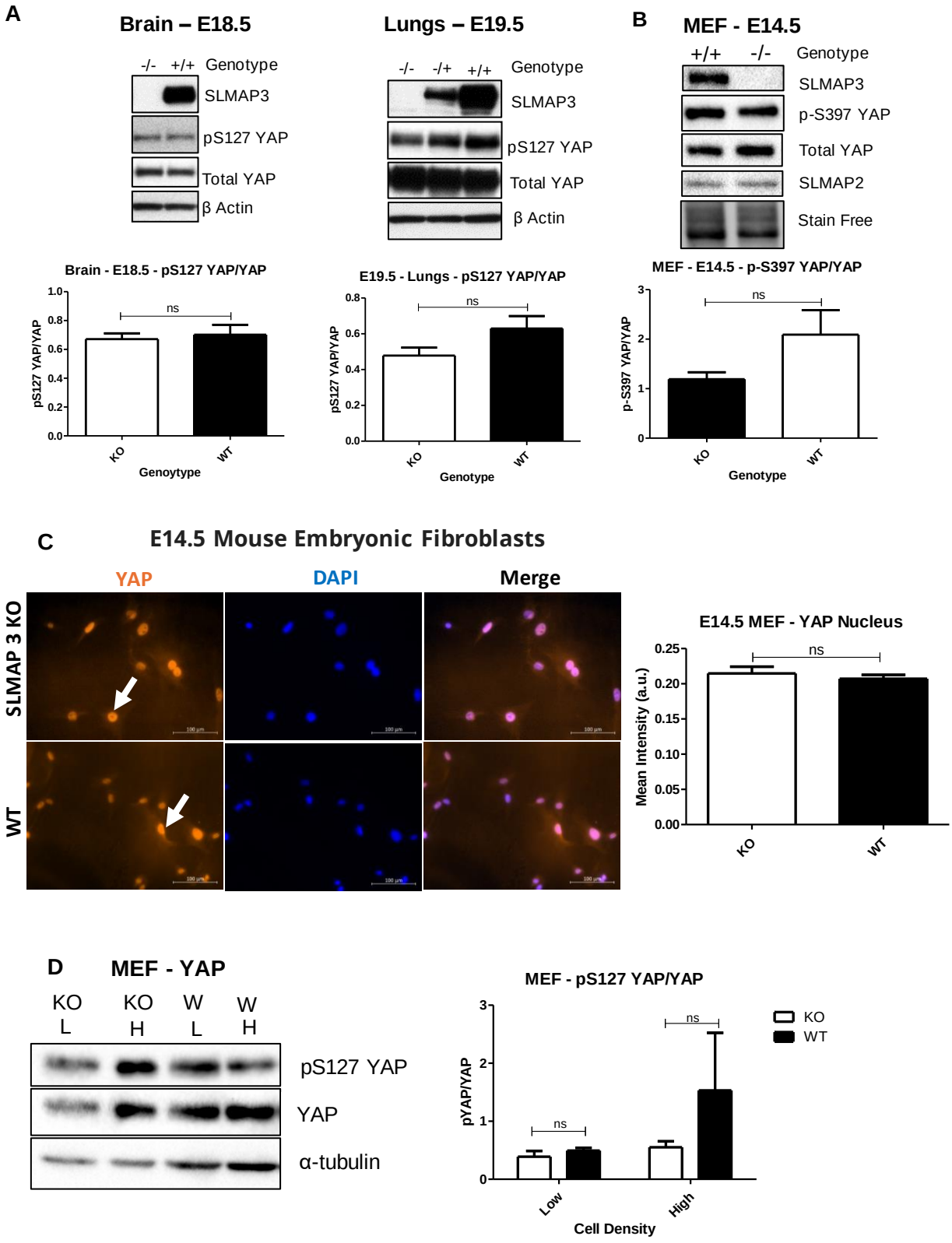

Figure 3. SLMAP3 functions independently of Hippo signaling during mouse embryogenesis

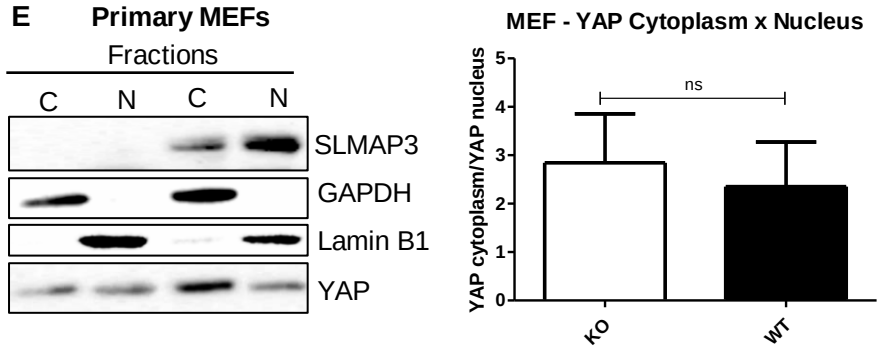

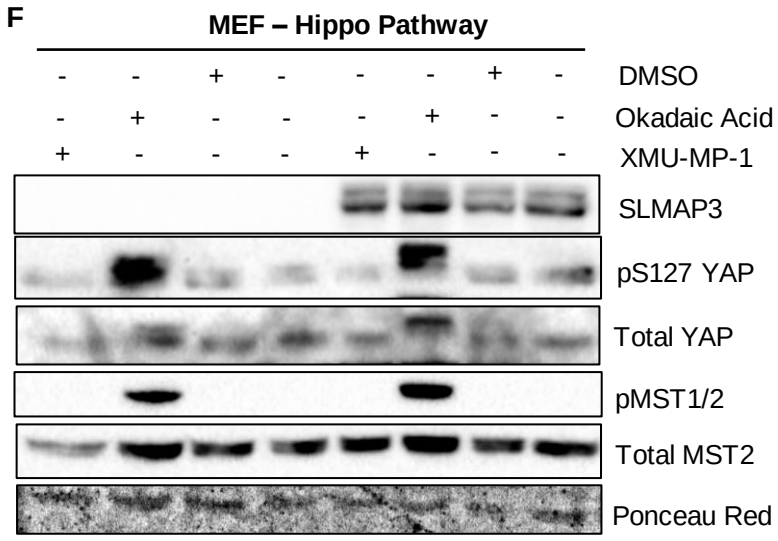

G

RNA-sequencing					
YAP Targets	MEF E14.5		Embryos E11.5		Function
	log2FC	Padj	log2FC	Padj	
Birc5	2.36E-06	0.99	4.60E-04	0.99	Anti-apoptotic
Ccn1	2.63E-06	0.99	-3.00E-02	0.81	Mitogen
Ccn2	9.60E-07	0.99	-8.00E-03	0.96	Growth-factor regulator
Myc	1.00E-06	0.99	-6.20E-04	0.99	Proto-oncogene

Figure 4. The knockout of SLMAP3 affects cell cycle in a cell specific manner

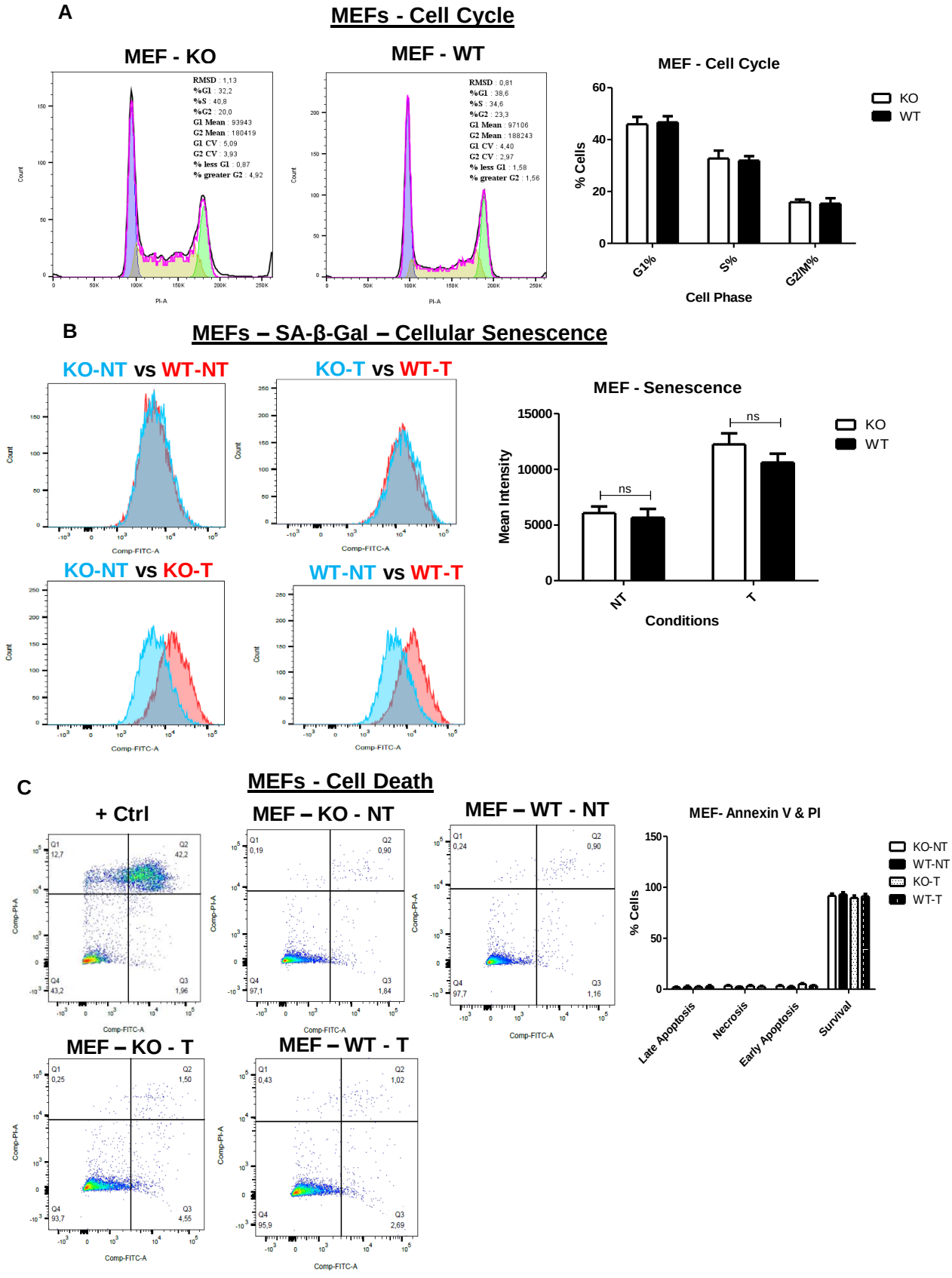

Figure 4. The knockout of SLMAP3 affects cell cycle in a cell specific manner

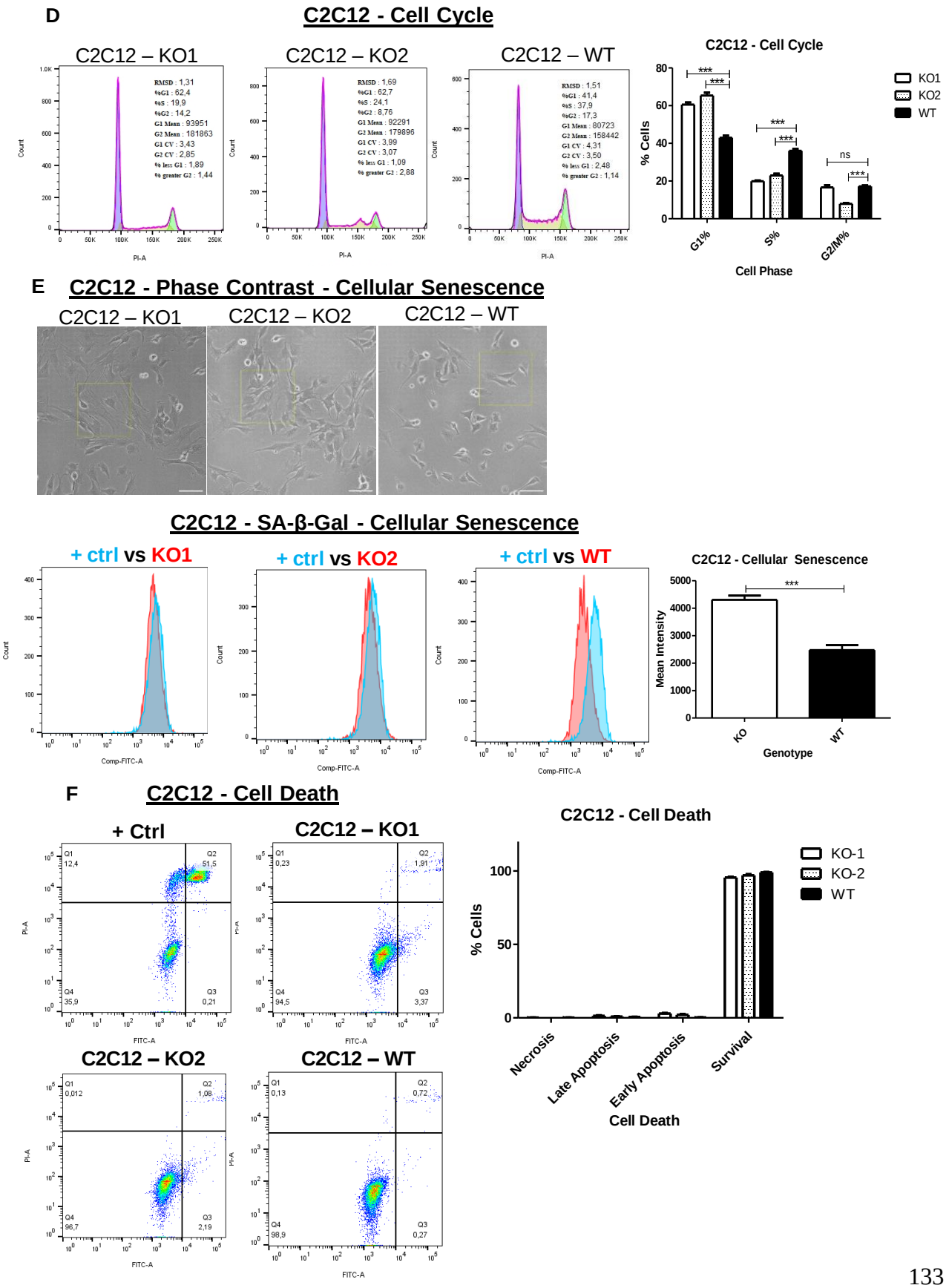

Figure 5. Loss of SLMAP3 impacts cell shape independent of changes in F-actin or focal adhesions

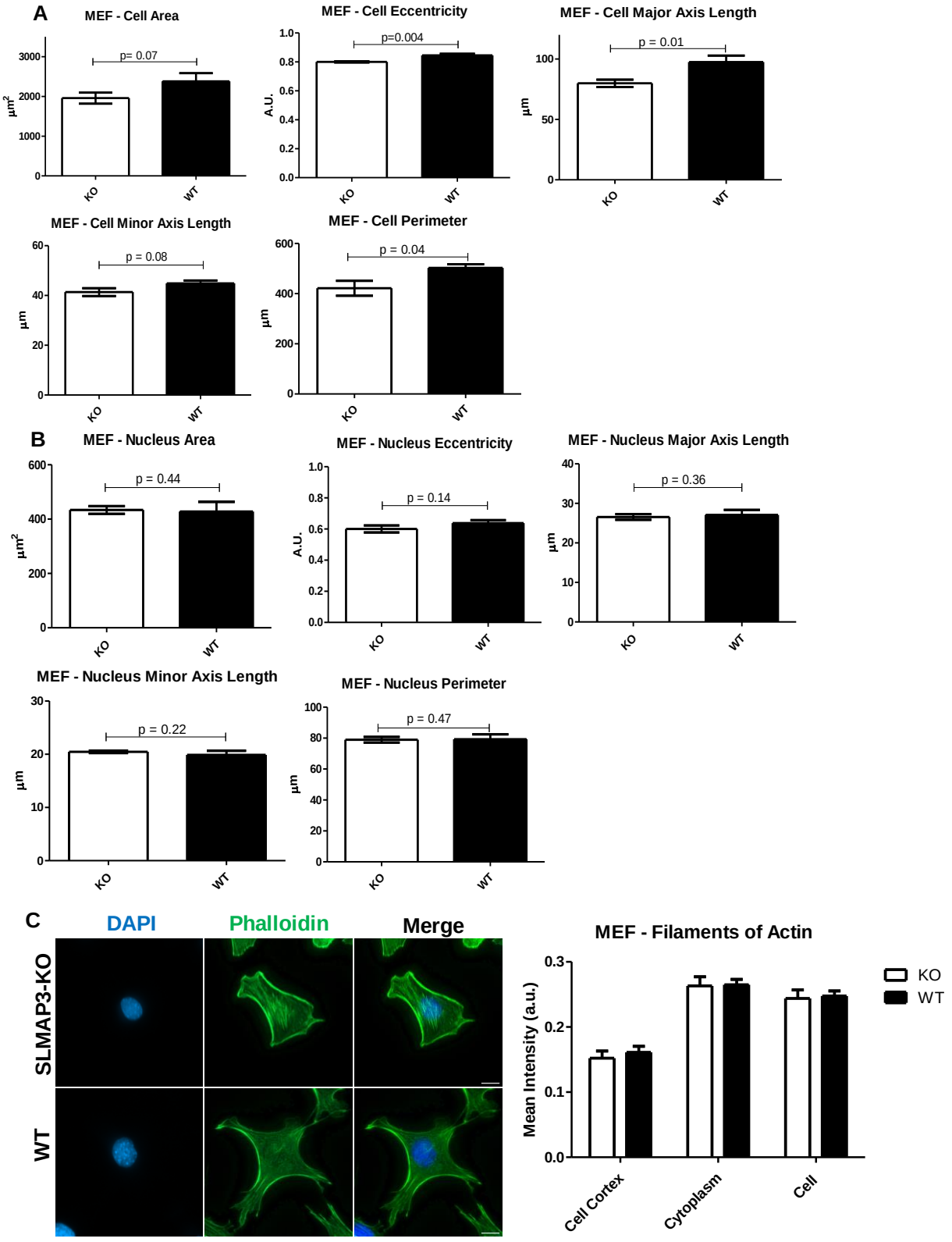

Figure 5. Loss of SLMAP3 impacts cell shape independent of changes in F-actin or focal adhesions

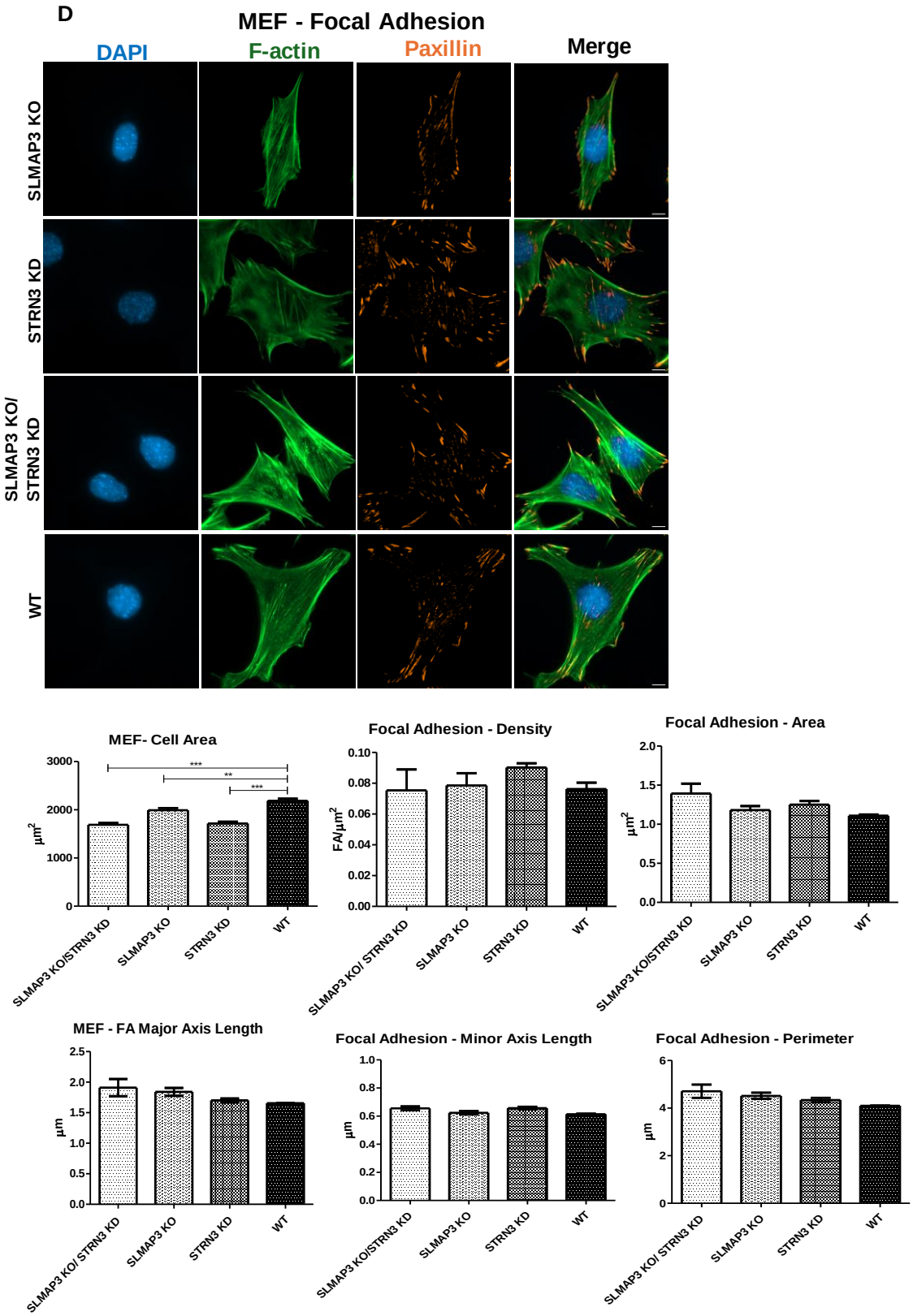

Figure 6. SLMAP3-/- MEFs do not present orientation defects

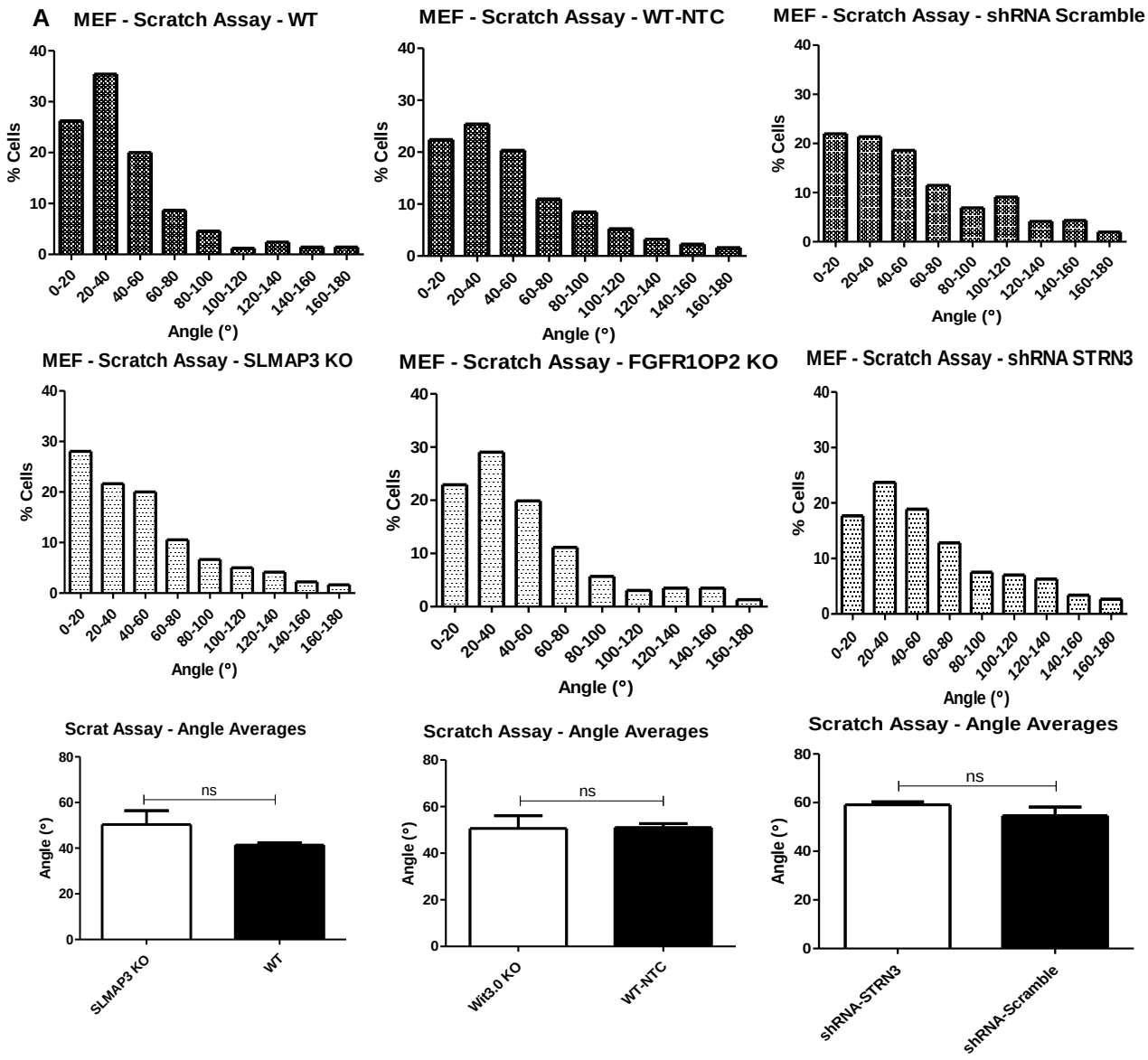

Figure 6. SLMAP3-/- MEFs do not present orientation defects

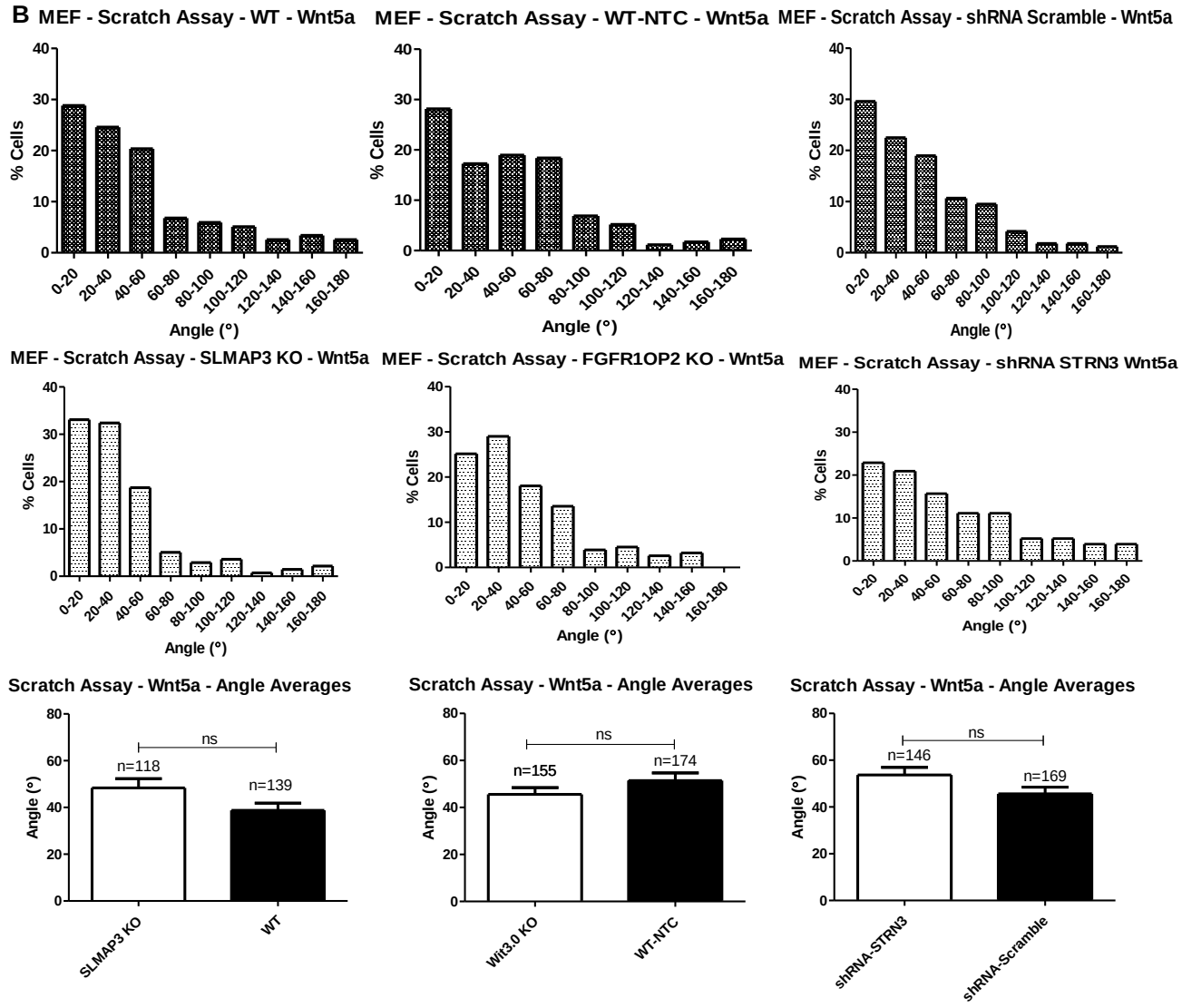

Figure 6. SLMAP3-/- MEFs do not present orientation defects

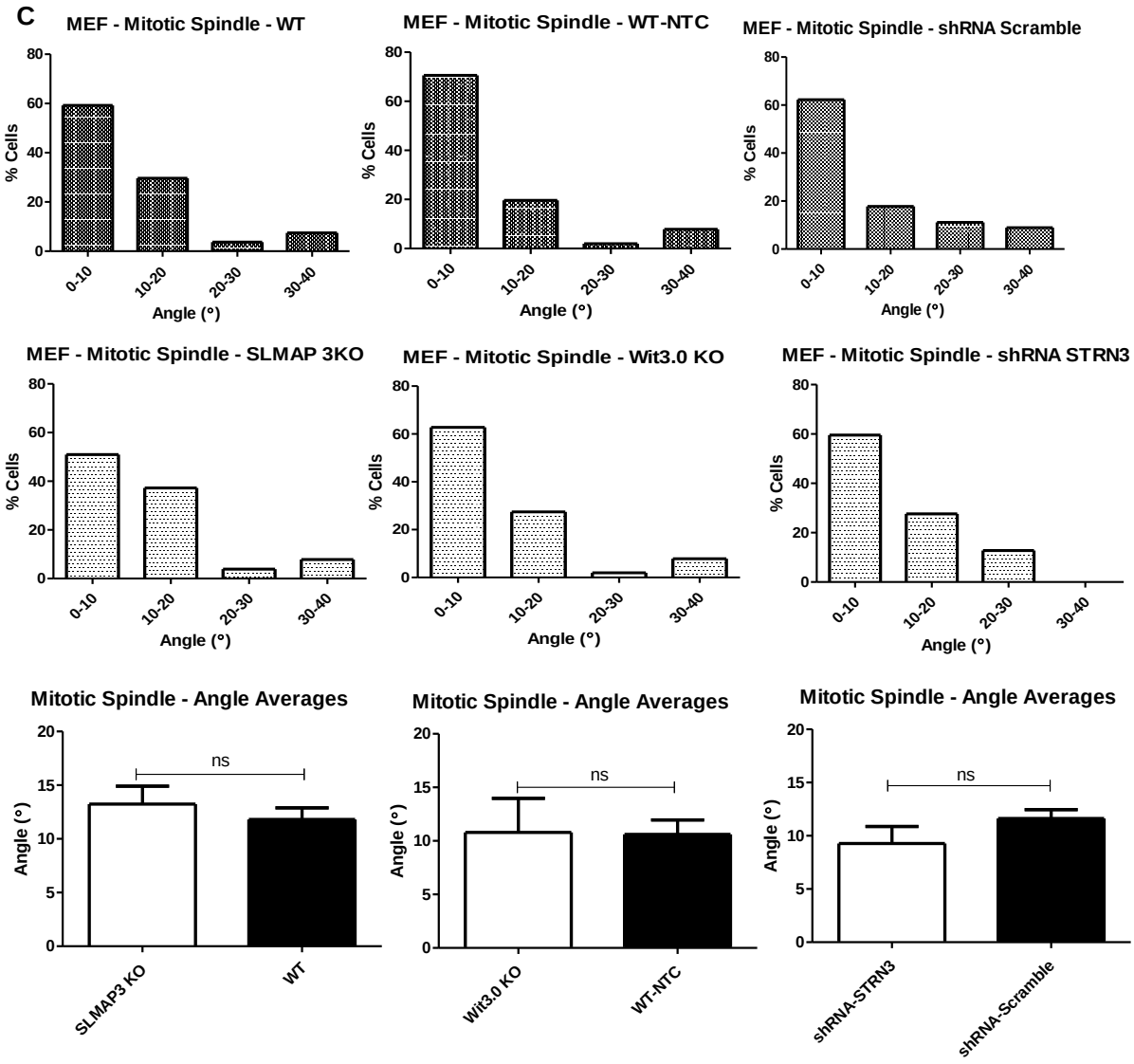

Figure 7. SLMAP3-/- MEFs do not present in defects in PCP or migration

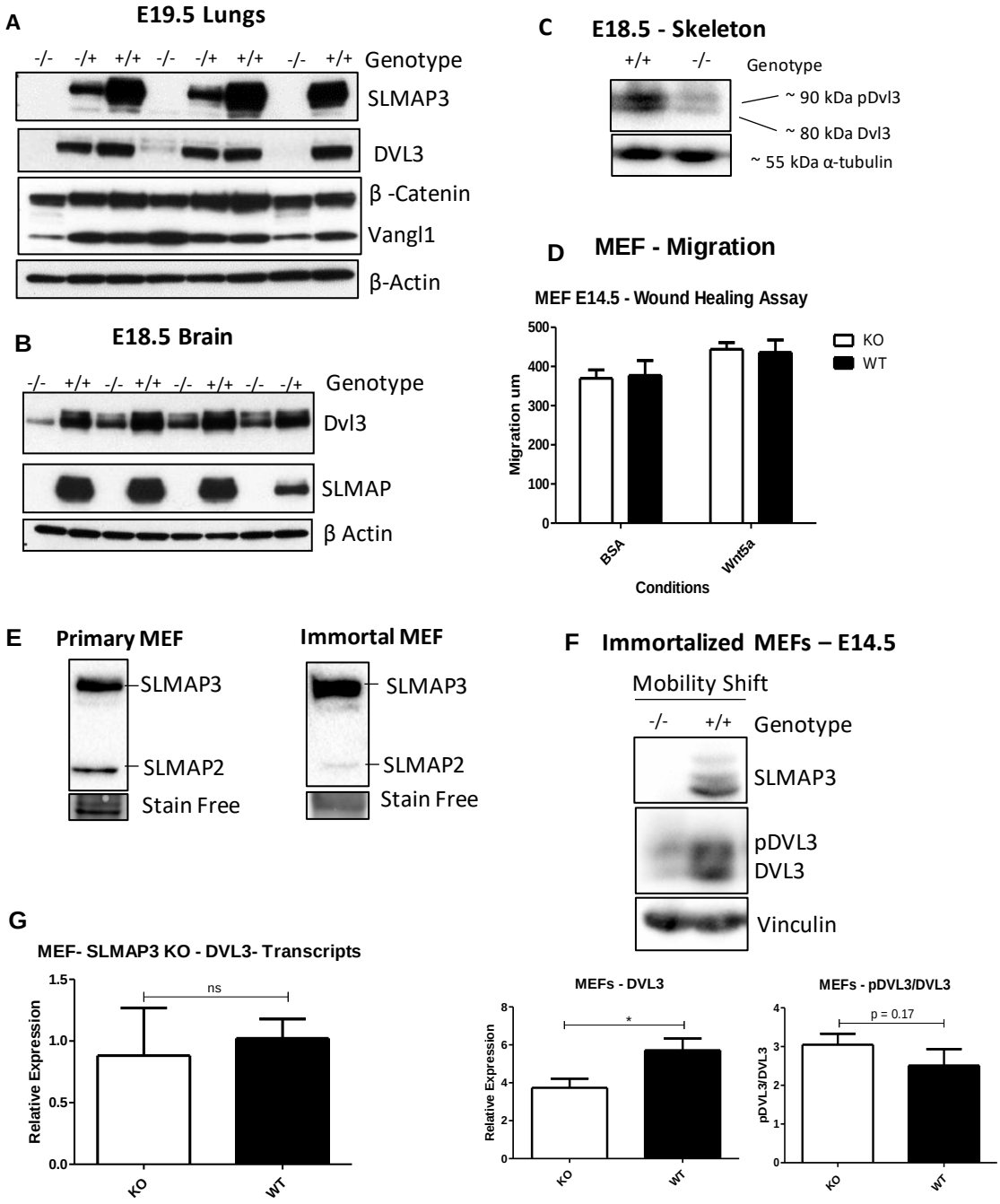

Figure 7. SLMAP3-/- MEFs do not present in defects in PCP or migration

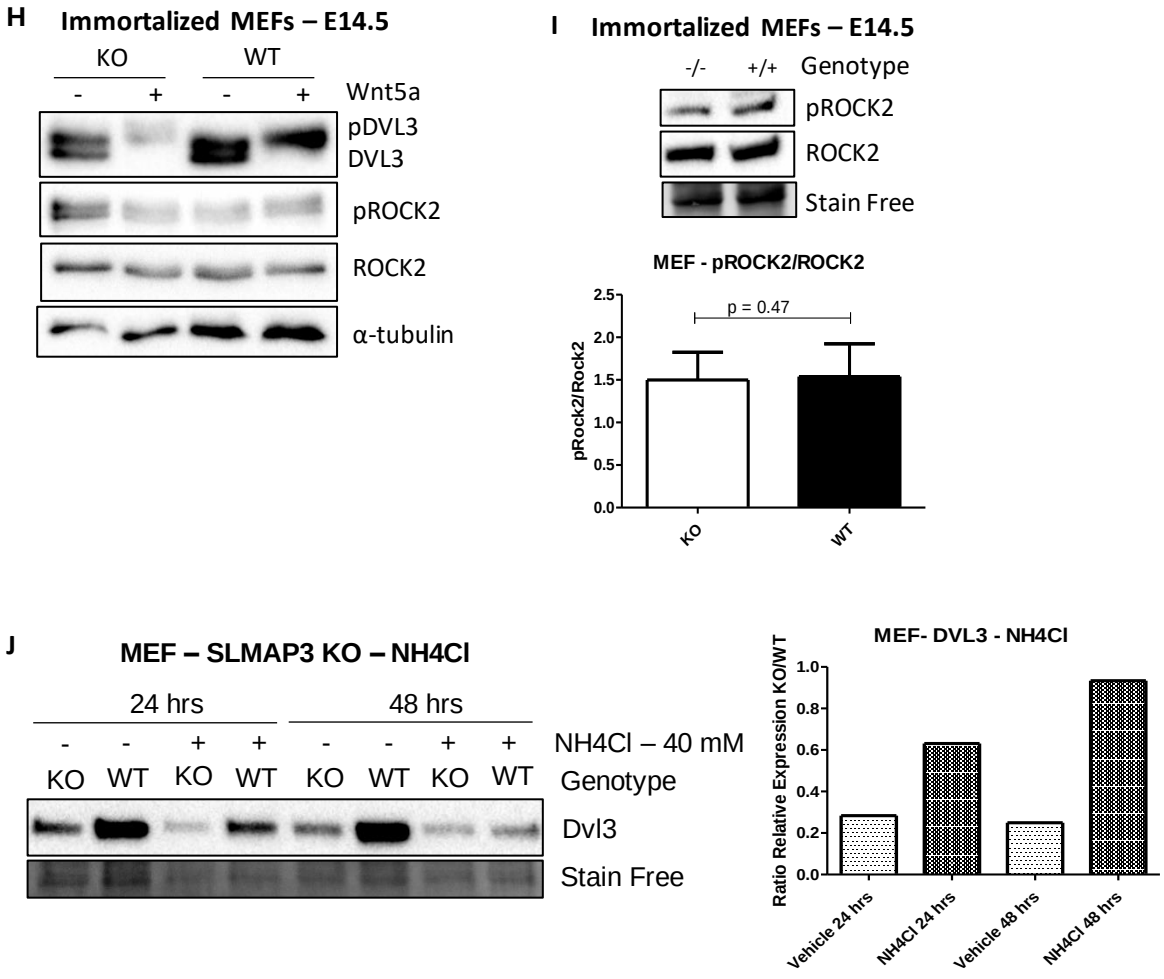

Figure 8. The knockout of SLMAP3 or FGFR1OP2/Wit3.0 results in defective primary cilia formation

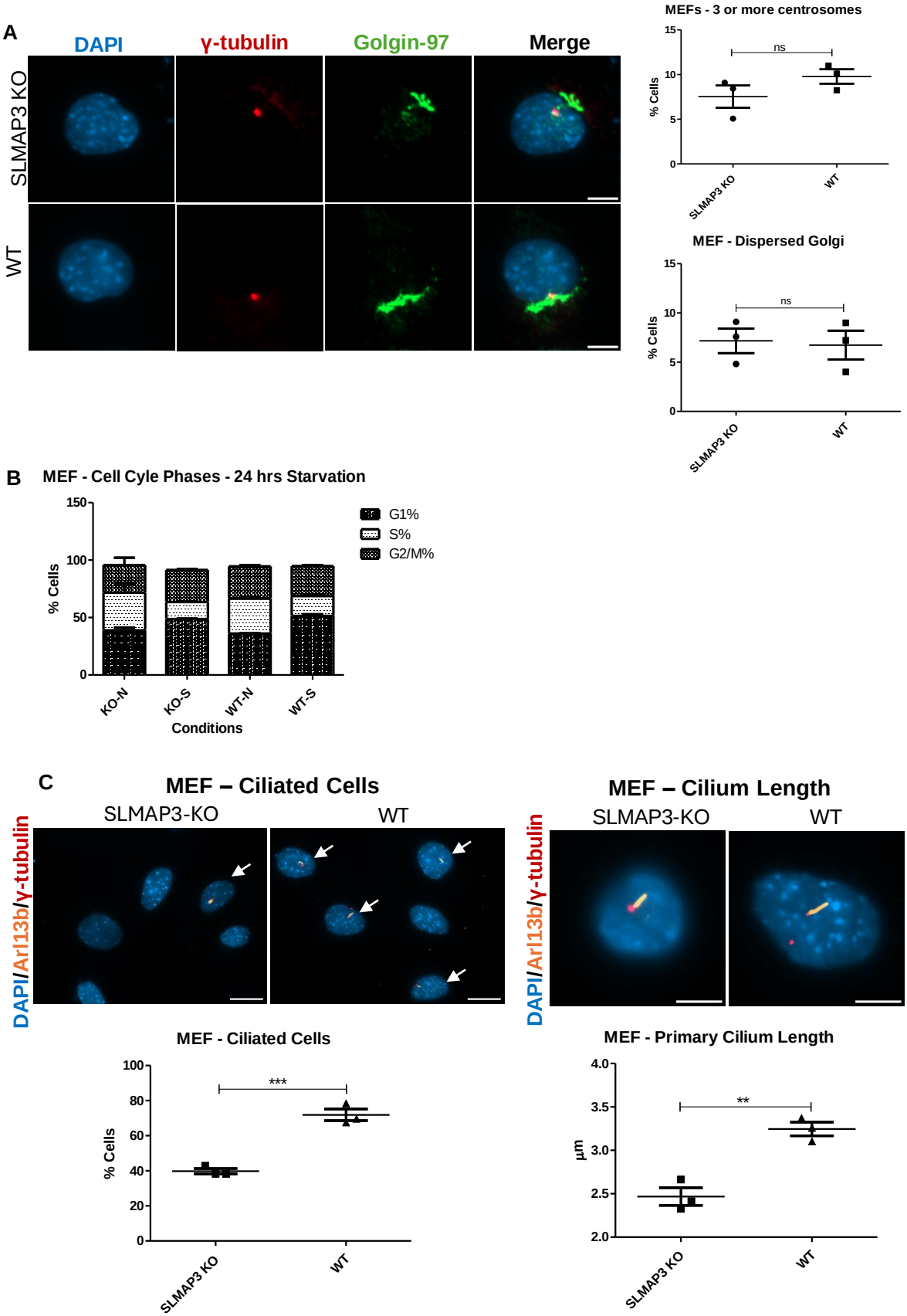

Figure 8. The knockout of SLMAP3 or FGFR1OP2/Wit3.0 results in defective primary cilia formation

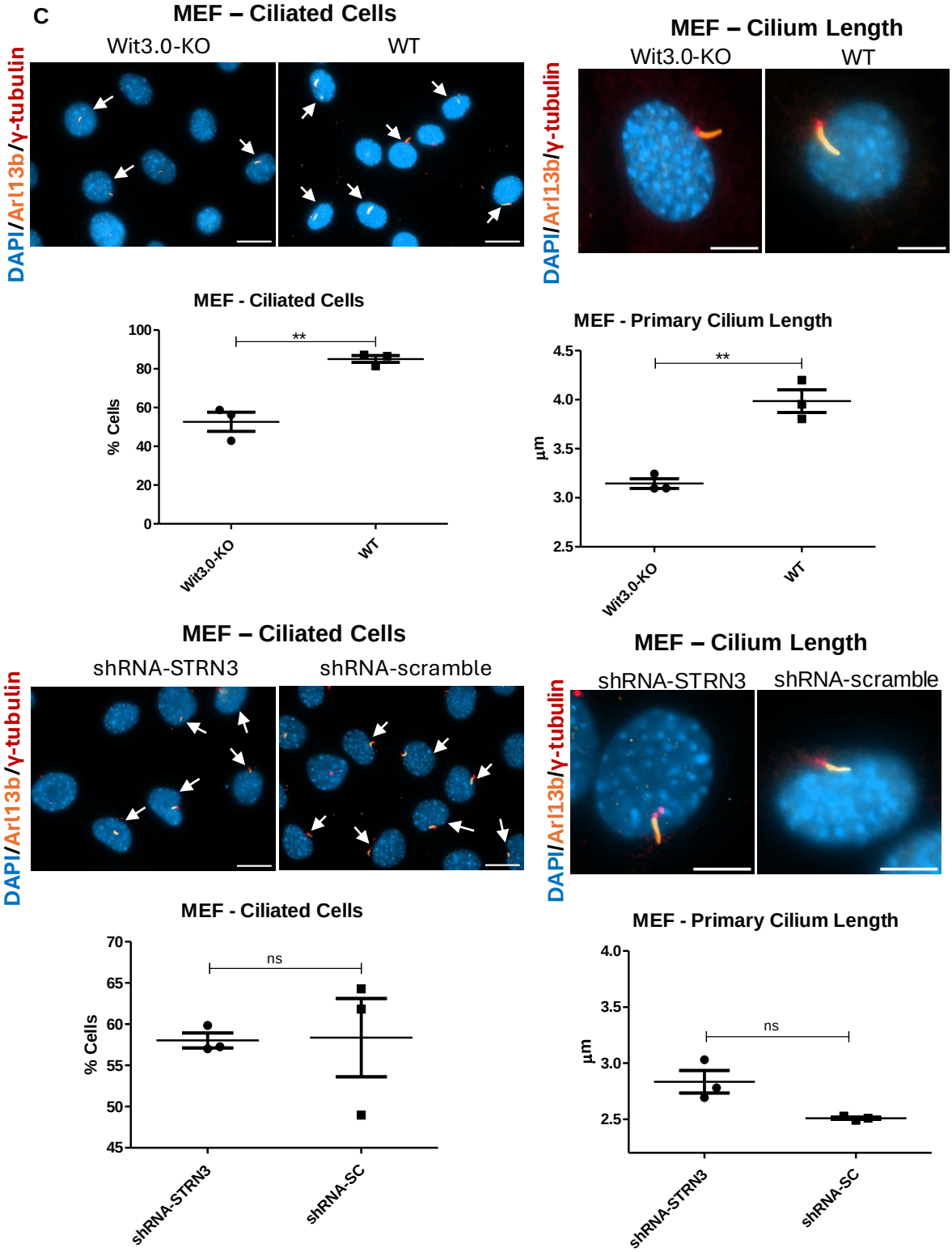

Figure 8. The knockout of SLMAP3 or FGFR1OP2/Wit3.0 results in defective primary cilia formation

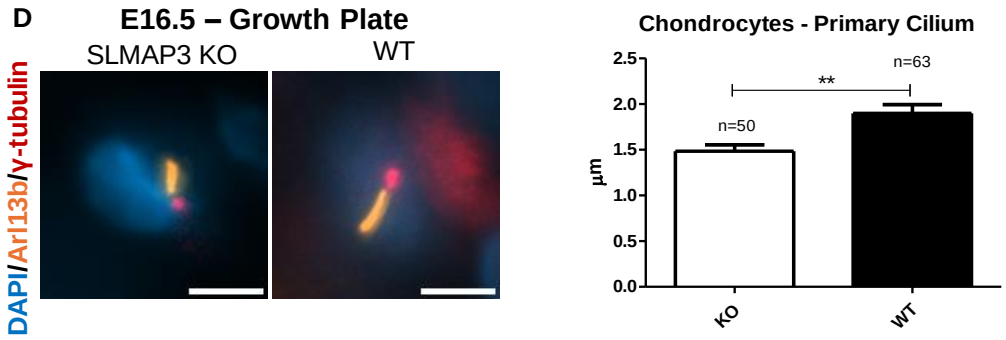

Figure 9. SLMAP3 is important for the protein stability of the STRIPAK members SIKE1 and FGFR1OP2

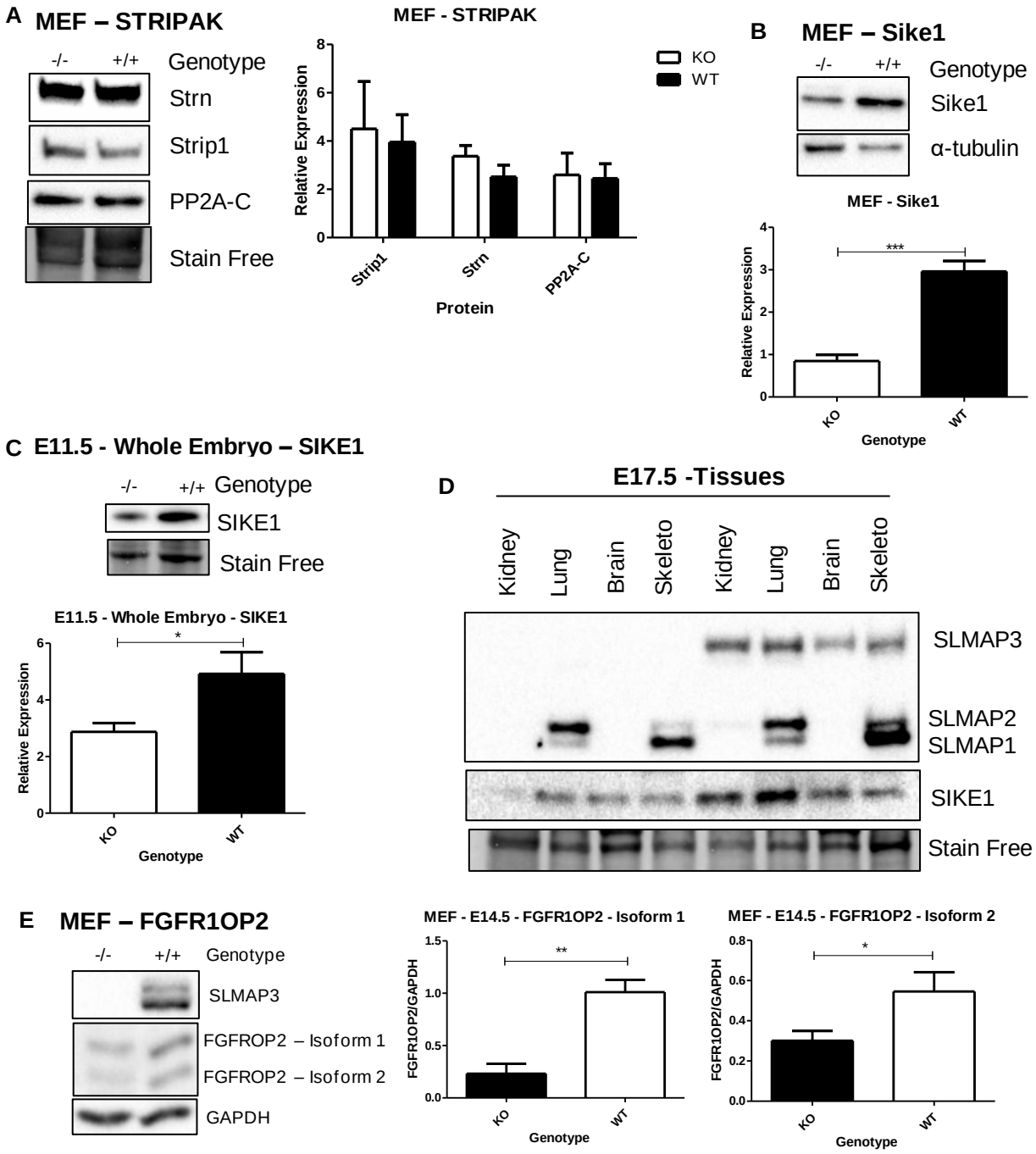

Figure 9. SLMAP3 is important for the protein stability of the STRIPAK members SIKE1 and FGFR1OP2

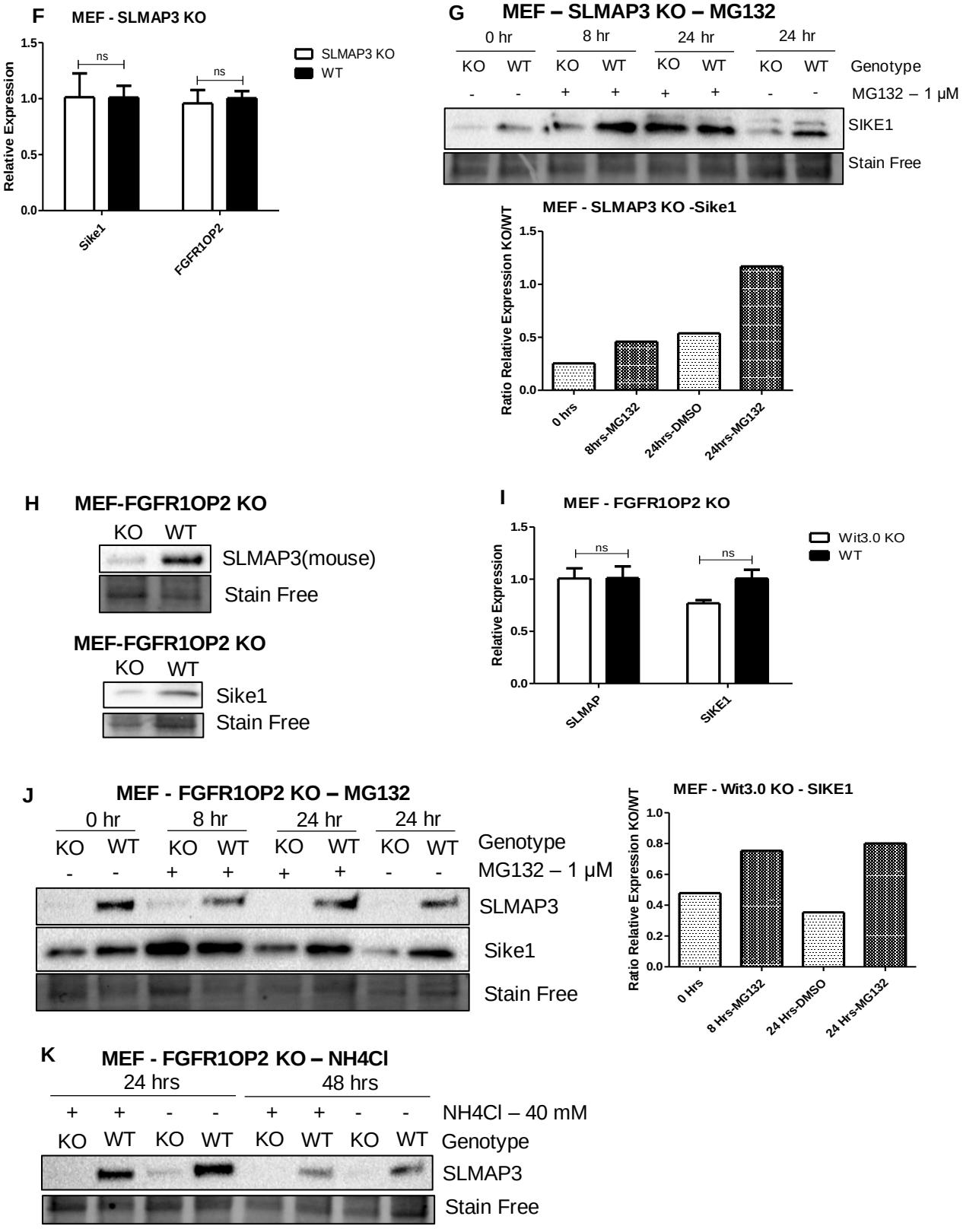

Figure 10. Proposed mechanisms of SLMAP3 for embryonic development and organogenesis

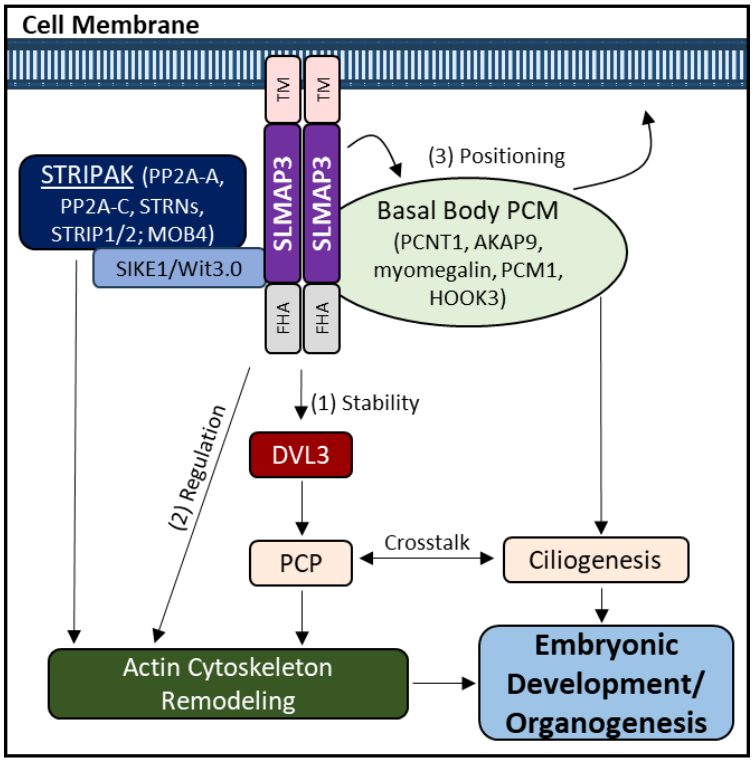

Supplemental Material 1

Supplementary Figure S1. Gene Expression in SLMAP3$^{-/-}$ MEFs

A

MEF – RNA-Seq		
Gene Name	**Log2FC**	**Padj**
Eng	-2.591000036	0.001294
Arhgap36	-2.339981561	0.008794
Slmap	-1.821444745	2.67E-40
Gm20655	-1.60544014	0.047293
Cdkn1a	-0.598646346	0.016705
Rpl27-ps3	2.97E-07	4.37E-08
Fbln1	0.677737896	0.015895
Tmem254b	0.820839371	0.047728
Mgst1	1.534564531	0.016705
St8sia4	3.794901067	0.015895
Gm21378	8.035925367	0.023277

B

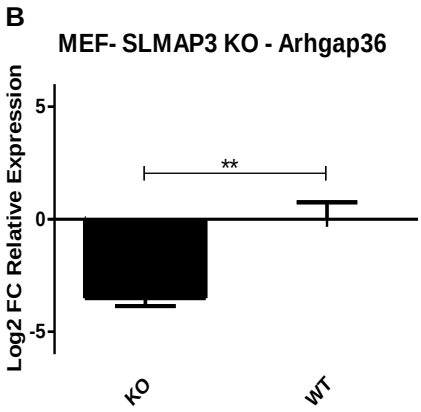

C

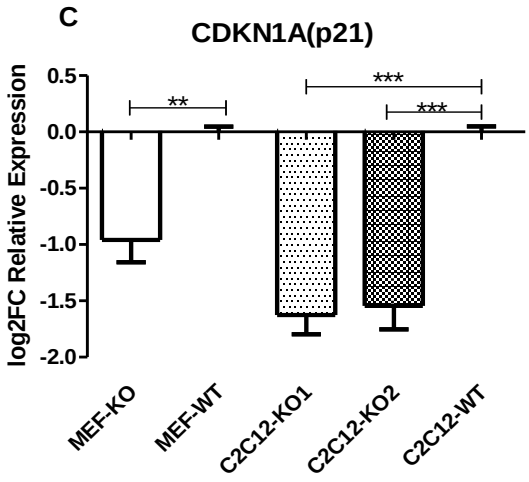

Supplementary Figure S2. Depletion of the Expression of SLMAP3, STRN3 and FGFR1OP2

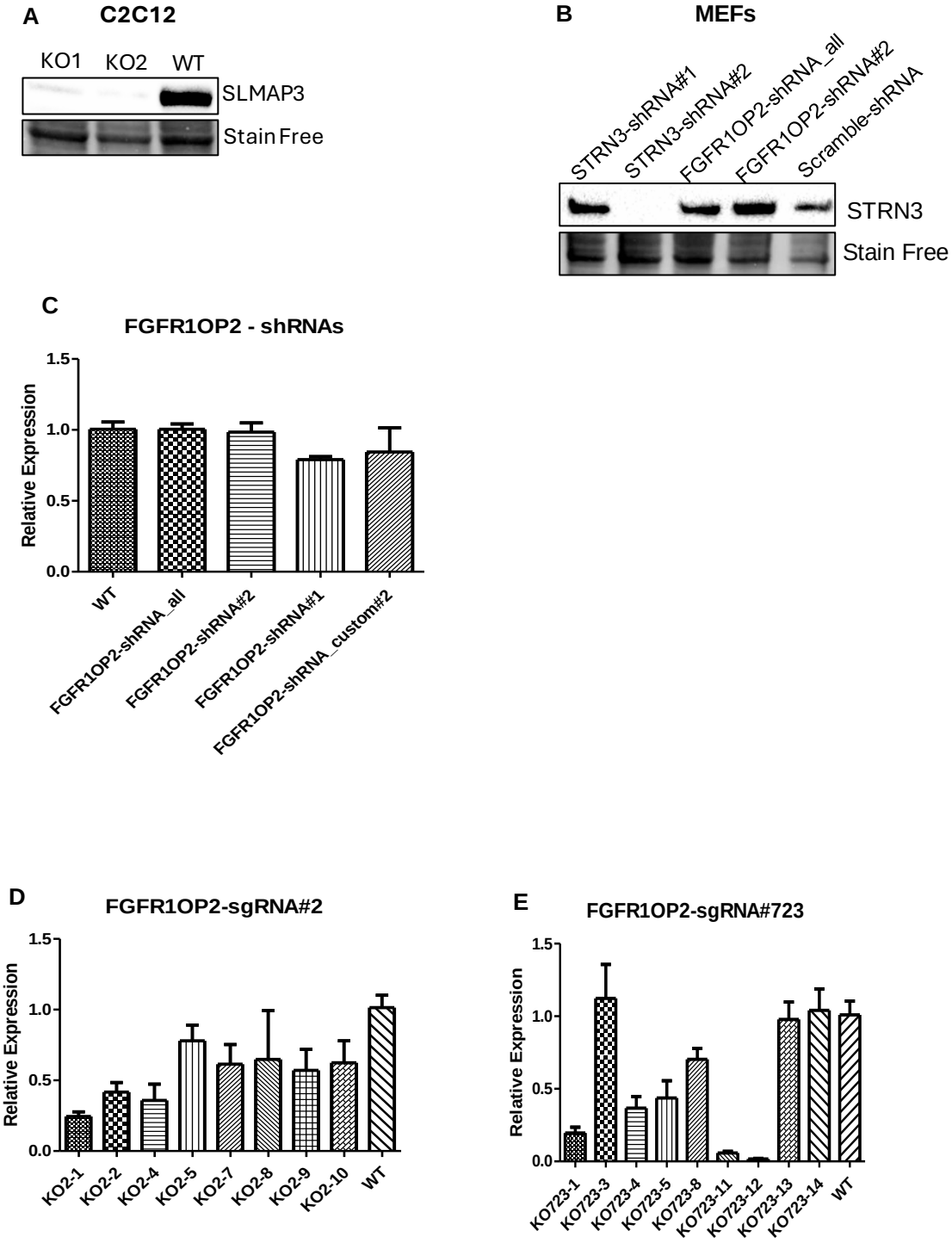

Supplementary Figure S3. SLMAP3$^{-/-}$ Primary MEFs do not present defects in PCP

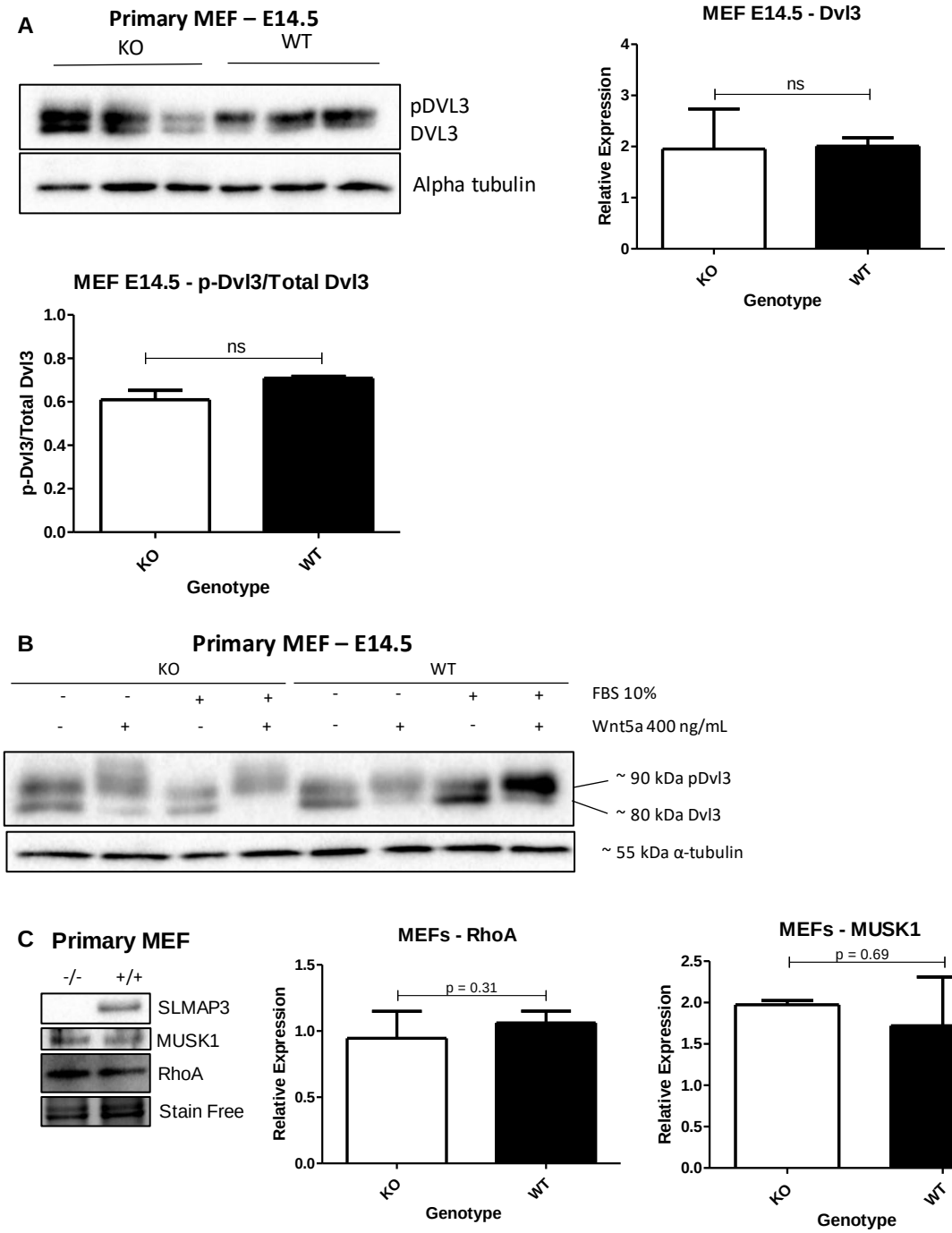

Supplementary Figure S3. SLMAP3$^{-/-}$ Primary MEFs do not present defects in PCP

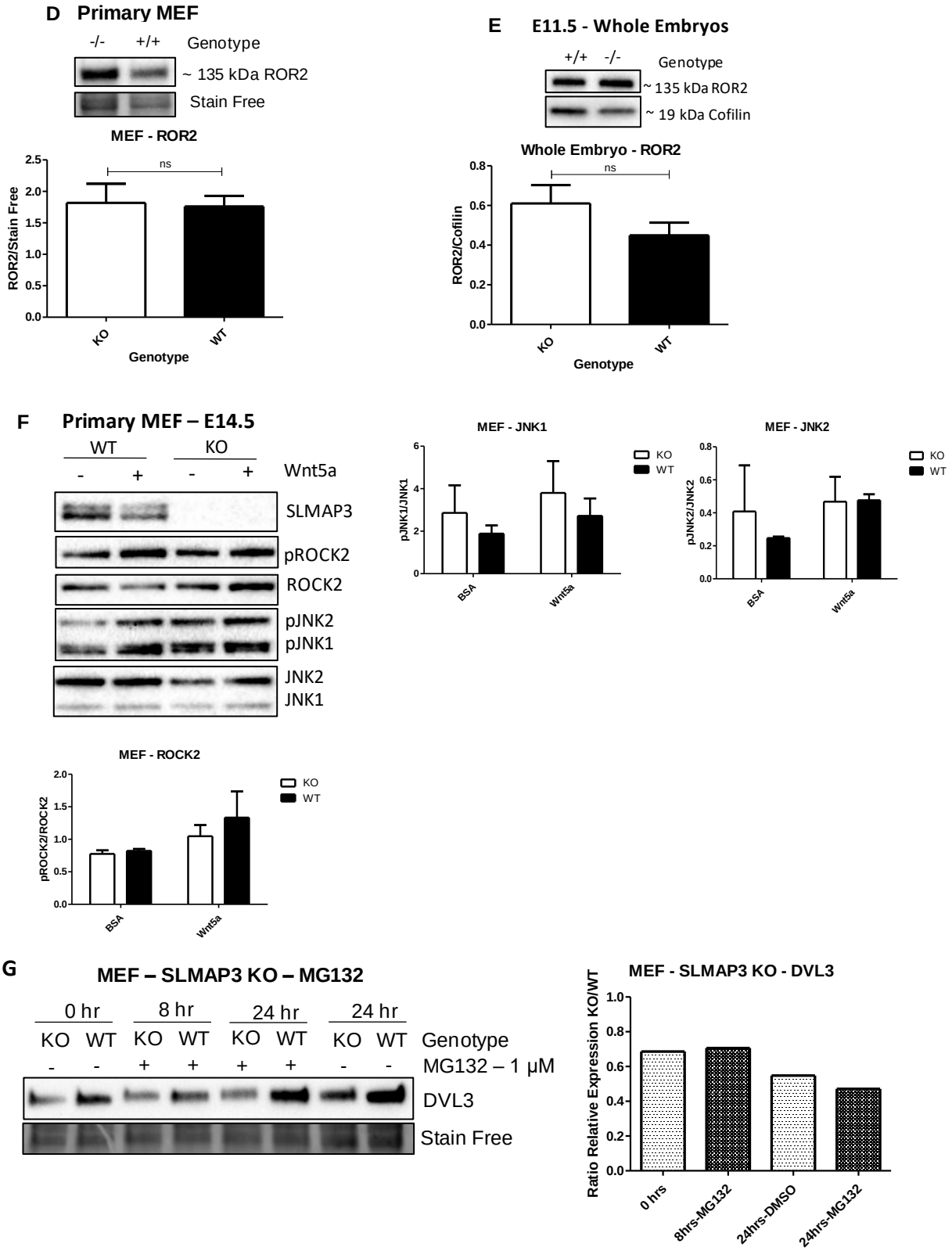

Chapter Five - SLMAP, Paralogs and Adaptors: Roles in Homeostasis, Physiology and Diseases

SLMAP, Paralogs and Adaptors: Roles in Homeostasis, Physiology and Diseases

Ana Paula Dias[1] and Balwant Tuana[1*]

[1]Deparment of Cellular and Molecular Medicine, University of Ottawa, Ottawa, K1H 8M5, Canada

*Correspondence: btuana@uottawa.ca

Abstract

SLMAP is a member of the evolutionary conserved STRIPAK complex, where it has been reported to negatively regulate Hippo signaling to induce the activity of the transcriptional coactivators YAP/TAZ, which leads to the expression of genes associated with growth and proliferation. Although this is the most known function of SLMAP, many other studies reported its involvement with different pathological conditions, including diabetic retinopathy, cancer, cardiac related disorders and defective embryonic development. Some of these functions are interconnected with its paralogs TRAF3IP3 and CCDC136, and with its adaptors SIKE1 and FGFR1OP2, which are also, with exception of CCDC136, STRIPAK members. Here we review the functions reported so far for these proteins to understand their roles in homeostasis, physiology and diseases. Although many studies investigated these proteins, a general and unifying role to explain the phenotypes associated with them *in vivo* remains missing.

1. Introduction

The sarcolemma associated protein (SLMAP) is a tail-anchored membrane protein first isolated by us[1]. Although its functions remain elusive, we know now that it is part to the evolutionary conserved striatin-interacting phosphatase and kinase (STRIPAK) complex[2–4], which has been described to negatively regulate Hippo pathway[5,6], to affect Golgi polarity[7], cytoskeleton[8] and other functions. SLMAP has two paralogs: CCDC136/NAG6 and TRAF3IP3/T3JAM, the latter also being a STRIPAK member. It also has two adaptors that are paralogs, SIKE1 and FGFR1OP2/Wit3.0, with SIKE1 being the protein responsible for the recruitment of SLMAP to the STRIPAK[9]. The global ablation of SLMAP in mice results in lethality[10–12], which is mirrored with the knockout of FGFR1OP2[13]. SLMAP has also been linked to numerous pathological conditions, including diabetic retinopathy, cancer, Brugada Syndrome and other cardiac related disorders. In the case of cancer, numerous studies reported the fusion of SLMAP and FGFR1OP2 with receptor tyrosine kinases. Cancer has also been linked to TRAF3IP3 and CCDC136, and TRAF3IP3 has additionally been associated with innate and adaptive immune functions. Regarding the innate response, TRAF3IP3 was shown to influence the activity of the kinase TBK1 by multiple mechanisms, which is an enzyme inhibited by SIKE1. Given the interconnected functions of SLMAP and its paralogs and adaptors, and considering that they comprise one of the "tentacles" of STRIPAK[14] (with exception of CCDC136), here we aim to describe their roles to gain insight into their functions in homeostasis, physiology and diseases. We also summarize the phenotypes and proposed mechanism in mice with the knockout of other STRIPAK members, and the roles of the counterpart STRIPAK members in different fungi species, which might be useful for the elucidation of SLMAP functions.

1.1. SLMAP Structure

The *slmap* gene, formerly known as slap, was first identified by our lab in a screening using cardiac cDNA library encoding proteins from sarcolemma[1]. With its cloning and further characterization, it was found that *slmap* gene encodes for multiple tail-anchored (TA) protein isoforms, with molecular weights of approximately 37 kDa, 45 kDa and 80-95 kDa, and which were called SLMAP1, SLMAP2 and SLMAP3, respectively[1,15–17]. In humans, *slmap* transcripts are organized into up to 25 exons (reference transcript Ensembl ENST00000671191.1). According to Ensembl database[18], exons 2 to 11 are always present in the largest isoforms, whereas exons 12 to 15 and 18 to 24 are alternatively spliced, generating a great variety of SLMAP3 isoforms. Exon 2 contains the start codon for SLMAP3 isoforms, whereas exon 17 has the start codon for SLMAP1 and SLMAP2, which differ in size due to the alternative splicing (**Figure 1**).

SLMAP3 is ubiquitously expressed, whereas SLMAP1 and SLMAP2 are expressed in a tissue and developmental stage specific manner[15,16]. All isoforms contain coiled-coil domains that are important for protein-protein interaction and self assembly[9,19]. The C-terminus region contain a transmembrane domain (TM), either TM1 or TM2, that are generated by the alternative splicing of exon 24 (**Figure 2A**)[15,16,20]. Both TM1 and TM2 direct SLMAP to ER and perinuclear membranes, but TM2 preferentially directs to mitochondria[20]. The N-terminus region of SLMAP3 isoforms was shown to be important to target the protein to the centrosomal microtubule organizing center (MTOC)[16]. It also contains a forkhead associated domain, which is known to bind to phosphothreonine residues[21,22].

1.2. The Structure and Homology of the SLMAP Paralogs and Adaptors

SLMAP3 has two known paralogs: TRAF3IP3/T3JAM and CCDC136/NAG6 (**Figure 2A**). Both TRAF3IP3 and CCDC136 have multiple coiled-coil domains along their structure, with a transmembrane domain in the C-terminus, but they lack the FHA domain. According to the sequences available on Uniprot, TRAF3IP3 has only one transmembrane domain, whereas CCDC136, similarly to SLMAP, has two that are exclusively present in the different isoforms.

The sequence alignment of SLMAP3 (Q14BN4-1) and TRAF3IP3 (Q9Y228-1) revels that 25% of SLMAP sequence has homology to TRAF3IP3, with 33.80% of amino acid identity. This is a region close to the N-terminus of both proteins **(Figure 2B**), and in SLMAP corresponds to the sequence required for interaction with SIKE1 and recruitment to STRIPAK[9]. As TRAF3IP3 is also a STRIPAK member, it is likely that this same region is important for its recruitment to the complex.

Regarding CCDC136 (Q96JN2-1), its sequence alignment with SLMAP3 shows that 35% of SLMAP sequence has homology to CCDC136, with identity of 33.33% of the amino acids. Differently from TRAF3IP3, this is a region close to the C-terminus of SLMAP and N-terminus of CCDC136 (**Figure 2C**). The homology sequence does not include the sequence necessary for the recruitment of SLMAP to STRIPAK, explaining why CCDC136 was never found to be part of this complex. The comparison of CCDC136 and TRAF3IP3 does not indicate any homologous sequence.

FGFR1OP2 (Q9NVK5-1) and SIKE1 (Q9BRV8-1) are coiled-coil proteins that are paralogs and members of STRIPAK. The blasting of these proteins shows that 94% of FGFR1OP2 has homology to SIKE1, with 43.50% of amino acid identity (**Figure 3**).

2. Functions

2.1. SLMAP and the STRIPAK Complex

SLMAP is a member of the STRIPAK complex, which was first identified in mammals by two affinity purification coupled to mass spectrometry studies[2,3]. It was confirmed with further proteomics, and now it is known to contain adaptor proteins, the subunits of the phosphatase PP2A and germinal center kinases (GCK) families II, III and IV[2,3,23–27]. Posterior studies characterized the organization of the complex[7,9,14,24,28–31]. The coiled-coil domains of four STRN proteins form the base, and on the top of it the adaptors Mob4 and STRIP proteins, one WD40 domain of the STRNs and the catalytic (C) and scaffold (A) subunits of the phosphatase PP2A interact holding the protein assembly together and forming the core of STRIPAK. The "tentacles" of STRN protein interact with the adaptors SIKE1 and CCM3, recruiting SLMAP and GCKIII, respectively (**Figure 4**). PP2A phosphatase has four families of regulatory B subunits, which is believed to create the variety of substrate recruitment and to target the phosphatase to different subcellular locations, and STRNs in the context of STRIPAK correspond to subunits B```[32].

STRIPAK was also detected in *Drosophila* in association with Hippo pathway members, wherein it was first proposed to be a negative regulator of this signaling axis[33]. The association of STRIPAK with Hippo was confirmed in mammals[25,26], and it was demonstrated both in human cells and *Drosophila* that SLMAP is responsible to recruit MST1/2 kinases to the STRIPAK, where they are dephosphorylated and inactivated, dampening the Hippo pathway[5,6]. Other STRIPAK functions reported include Golgi polarization[7], cytokinesis[23], regulation of cortical actomyosin[8] and cell transformation mediated by SV40 ST[34].

Although the negative regulation of Hippo signaling is one of the most reported functions of STRIPAK[5,6,9,27,33,35–38], it has been poorly reproduced *in vivo* in mammals. The knockout of STRIPAK members in mice results in phenotypes that cannot be explained, with very few exceptions, by disturbances in Hippo axis. The global ablation of SLMAP3 in our mice model results in defective organ formation, including fused skeleton, disoriented chondrocytes, short intestine, underdeveloped lungs, reduced body axis length, facial abnormalities and polycystic kidney, phenotypes that resemble defects in planar cell polarity, but without changes in YAP[12]. Considering that animal models manifest phenotypes that will most faithfully represent the cellular and molecular defects, and that these models are useful for clinical translation, we described the phenotypes exclusively on mice with the global knockout of all STRIPAK members and their proposed mechanisms in the **Table 1. Figure 5** summarizes the phenotypes and lethality with the knockout of each STRIPAK component. The phenotypes range from embryonic lethality, exemplified by gastrulation defects in some models, to viable animals but with changes in metabolism, blood cells and behavior, for example. The understanding of the pathophysiological mechanism in these models would shed light into therapeutic options for humans harboring mutations in these members. For more in-depth description of the molecular functions of each STRIPAK member we recommend the reviews[4,39–41].

STRIPAK is evolutionary conserved and was detected in *Saccharomyces cerevisiae* over two decades ago as the Far complex[42]. Although the repurposing of STRIPAK over the course of evolution has been suggested[43], the understanding of its mechanisms in lower eukaryotes remains invaluable, as functions of STRIPAK not described yet could still be conserved. Because of that, we summarized the functions of STRIPAK members in fungi species, which can be found in the tables **Table 2-8**. More details of STRIPAK functions in fungi can also be found in[44,45].

2.2. SLMAP and the Hippo Pathway

The Hippo pathway was originally discovered in *Drosophila*, and it is known to regulate cell fate, survival, proliferation and organ growth. The main components consist of the germinal center kinases II family members MST1/2 and their adaptor protein SAV1, which phosphorylates and activates the NDR kinases members LATS1/2 and their adaptor protein Mob1. The latter then phosphorylate the transcriptional coactivators YAP and TAZ. Their phosphorylation causes cytoplasmic sequestration by 14-3-3 and posterior proteasomal degradation[46]. Although MST1/2 were initially reported to be responsible for LATS1/2 activation, other kinases including members of the germinal center kinase IV family, TAO kinases, STK25 and MKK2 and MKK3 are known to phosphorylate LATS1/2[27,36–38,46,47]. The functions of Hippo pathway are exemplified by either the overexpression of Yki/YAP or mutation of Wts/LATS in the *Drosophila* wing disc, which results in massive growth of this structure[48,49]. In mouse, knockout of MST1/2 resulted in liver hypertrophy and hepatocellular carcinoma[50,51].

In the context of STRIPAK, SLMAP3 has been described as a negative regulator of Hippo signaling in human cells and *Drosophila*, by facilitating the dephosphorylation and inactivation of the germinal center kinases II MST1/2 by the phosphatase PP2A[3,5,6,9,26]. The FHA domain of SLMAP3 was shown to bind to phosphothreonine residues in the linker region of MST2, recruiting the kinase to STRIPAK, where PP2A dephosphorylates the phosphothreonine residue in its catalytic domain, suppressing the activity of MST2. The depletion of SLMAP led to increased phosphorylation and activation of MST1/2, in parallel to increased phosphorylation of YAP and its shift to the cytoplasm[5,6]. The inhibitory role of SLMAP-STRIPAK in Hippo signaling was further proposed to take place in cellular condensates, a process antagonized by condensates containing the Hippo inducers AMOT and KIBRA[52].

The negative regulation of Hippo by SLMAP is observed in the eye imaginal disc of *Drosophila*, a tissue that gives rises to the retinal progenitor cells or peripodial epithelium (PE). SLMAP was shown to favor the PE fate by allowing the translocation of YAP to the nucleus[53]. SLMAP was also found to be important for flight muscle morphogenesis in *Drosophila*, in a mechanism involving the repression of Hippo signaling[54]. The depletion of SLMAP in these studies were performed in a tissue specific manner, as the global ablation of SLMAP in *Drosophila* causes lethality prior to the end of pupal stage[6].

SLMAP3, together with its adaptor SIKE1, was also shown to positively regulate DNA damage repair via a non canonical Hippo signaling in human cells[55]. Mechanistically, upon DNA damage, the cGAS-STING senses cytoplasmic DNA, leading to the activation of TBK1. The active kinase interacts with SIKE and SLMAP3, stabilizing their association with STRIPAK. Consequently, MST1/2 kinases are recruited to the complex to be dephosphorylated and inactivated. This allows ZMYND8, a target to MST1/2, to be active and to be recruited to the sites of double strand break (DSB) to mediate DNA damage repair. Depletion of SLMAP, SIKE1 or TRAF3IP3 caused reduced DNA damage repair. In the context of gastric cancer, disruption of the recruitment of SIKE/SLMAP to the STRIPAK with the synthetic peptide SAIP-2, together with inhibitors of the DNA damage repair protein PARP, resulted in a strong synthetic lethality, with increased death of cancer cells[55].

A role of SLMAP in *Drosophila*, independent of Hippo pathway, has also been proposed, where it negatively regulates TAK1 by recruiting the kinase to the STRIPAK, where it undergoes dephosphorylation. This leads to JAK/STAT overactivation, which ultimately disrupts antiviral response[56]. In HEK-293FT, the suppression of SLMAP expression resulted in enhanced viral response, suggesting that it could be a conserved mechanism also present in mammals[56].

2.3. SLMAP in Skeletal Muscle

The functions of SLMAP were first related to skeletal myogenesis, where the overexpression of SLMAP3 in C2C12 myoblasts increased the expression of the differentiation markers myogenin (MyoG) and myosin heavy chain (MHC), but inhibited cell fusion[57]. Further indication of SLMAP importance for muscle development comes from the finding that its depletion in goat muscular satellite cells reduced the expression of the differentiation markers MyoG and Myosin7[58]. Recently, we have shown that these differentiation defects stem from abnormalities in the nuclear envelope of myoblasts, affecting the formation of microtubule organizing center (MTOC) in these organelles and impacting the myogenic program[11].

Another link between SLMAP3 and muscular function comes from the study by[59]. The authors generated transgenic Klhl31 knockout mice that at P10 days exhibited defective postnatal muscular growth, increased number of mitochondria, dilated SR, and abnormal Z-disc. The 6-week-old mice showed reduced forelimbs and hindlimbs strength. In the analysis of quadriceps lysate of these mice, SLMAP3 was the most upregulated protein. Klhl31 is part of Kelch proteins family[60], containing members known to function as substrate-specific adaptors of the E3 ubiquitin ligase Cullin E3[61]. A possible mechanism for the upregulation of SLMAP3 protein in the absence of Klhl31 could be reduced ubiquitin-mediated degradation of SLMAP3. However, the authors could not demonstrate protein-protein interaction between Klhl31 and SLMAP3. Although the mechanism of Klhl31 regulating SLMAP3 remains unknown, it highlights the importance of controlled SLMAP expression during muscle development.

2.4. SLMAP in the Heart

For the cardiac excitation-contraction (E-C) coupling, a strict control of intracellular Ca^{2+} is required. This control is performed by Ca^{2+} channels and transporters located at sarcolemma, transverse T-tubules and sarcoplasmic reticulum in cardiomyocytes[62,63]. Besides the control of cellular concentration of Ca^{2+}, the spatial organization of these structures is also important for (E-C) coupling[63]. SLMAP1 was demonstrated to localize at sarcolemma, transverse T-tubules and sarcoplasmic reticulum and to interact with α and β subunits of myosin heavy chain from the contraction apparatus of the heart, suggesting a possible role of this protein in the proper spatial organizing the (E-C) coupling structures[19]. The role of SLMAP in the heart is further evidenced by[64], where they showed that overexpression of SLMAP1 leads to vacuolated cardiomyocytes, with the presence of dilated SR and ER. Overexpression of SLMAP1 was also followed by reduced contractility and reduced responsiveness to adrenergic stimulus. Further investigation showed that the expression of proteins associated with calcium handling from the SR, including RyR2, SERCA, triadin and CSQ, were downregulated accompanied by reduced Ca^{2+} uptake, what could explain the less cardiac contractility. Therefore, besides participating in the E-C coupling in terms of spatial organization, SLMAP1 may also play a role in E-C coupling in terms of Ca^{2+} handling.

Regarding SLMAP3, we demonstrated that overexpression negatively affects cardiac function[65]. By analyzing cardiomyocytes from transgenic mice with postnatal cardiac specific overexpression of SLMAP3, we found decreased expression of SERCA, PLN and CSQ, proteins that participates in Ca^{2+} handling in SR. The heart of these transgenic mice also had reduced expression of Nav1.5, the sodium channel associated with Brugada Syndrome[66]. These alterations could explain the disturbances observed in the heart of the transgenic mice, including increased end-systolic volume and dysfunction in the atrioventricular conduction. On the other hand, it was also shown that overexpression of SLMAP3 coupled with adrenergic stimulus enhances rat

cardiomyocytes function by increasing intracellular Ca^{2+} and contraction rate[67]. These studies suggest that the controlled expression of SLMAP3 is important for proper heart physiology.

We have also generated a mouse model with the knockout of only SLMAP3 isoforms in postnatal hearts, which did not affect the expression of SLMAP1 or 2, and surprisingly no changes in organ function or structure were detected, even after the challenge with isoproterenol[17]. The cardiac SLMAP3 knockout prior heart development did not show severe phenotypes either, although hearts were smaller during embryonic development[68]. In contrast, the depletion of all SLMAP isoforms in rat neonatal cardiomyocytes reduced the rate of spontaneous contraction, which was still significantly reduced after the adrenergic stimulus[67]. The depletion of all SLMAP isoforms in rat cardiomyoblasts also reduced proliferation and induced cellular senescence[68]. These studies suggest a possible compensatory mechanism of SLMAP isoforms in the cardiac contractility and proliferation.

A partner of SLMAP in cardiac function is STRN, and their association was reviewed by[69]. STRN was demonstrated to regulate contraction rate in cardiomyocytes[70] and shown to interact with SLMP3 in these cells[67]. STRN also contains binding domains for Ca^{2+}-calmodulin[39,40], a regulator of the E-C coupling[71], and for caveolin, a component of the membrane domain caveolae known to harbor adrenergic receptors and to contribute to their signaling[72]. Proposed functions of STRN/SLMAP complex include their localization in the intercalated discs of cardiomyocyte, providing mechanical support and favoring electrical communication of cells during E-C coupling, and regulation of cellular flow of Ca^{2+} upon adrenergic stimulus by the localization in the T-tubule/sarcoplasmic reticulum junction and caveolae[69].

3. Diseases

3.1. SLMAP in Cardiac Disorders

Perhaps the most well-known pathological condition associated with SLMAP is Brugada Syndrome[73], a channelopathy that causes ventricular arrhythmia, leading to palpitations, syncope and sudden death[74]. Brugada Syndrome has been related to mutations in the *scn5a* gene, which encodes the α subunit of the cardiac Na^+ channel Nav1.5. However, mutations on this gene account for just 18% to 30% of the patients[66], and mutations in other genes that could affect sodium current could be responsible for the remaining cases[74]. Missense mutations in SLMAP were identified in individuals from Japan and Korea with Brugada Syndrome[73]. The expression of the SLMAP variants in rat cardiomyoblasts affected the cell surface availability of Nav1.5, which was reversed with depletion of the mutated proteins. Additionally, the SLMAP variants decreased the peak current density of sodium, suggesting a disturbance in the electrophysiology in the cardiomyoblasts. These two findings then provide foundation to explain the syndrome observed in the two subjects.

SLMAP was also found upregulated in the hypertrophic left ventricle of mice after thoracic aortic constriction, specially in the animals that developed congestive heart failure, which the authors associated with diastolic dysfunction[75]. However, the mechanistic involvement of SLMAP with this dysfunction was not further investigated.

Another condition related to SLMAP is dilated cardiomyopathy (DCM), in which its expression was found reduced in human patients[67]. SLMAP is not the only STRIPAK members linked to DCM, as deletion of STRN was associated with DCM in boxer dogs[76], and depleted SIKE1 was detected in patients with DCM and hypertrophic cardiomyopathy (HCM)[77]. In the case of SIKE1, it was shown in rodent cardiomyocytes that it plays a protective role against pathological hypertrophy, in a mechanism dependent on the inhibition of TBK1-AKT signaling[77]. Whether

SIKE1 can interact with SLMAP, STRN and TBK1, recruiting the TBK1 kinase to the STRIPAK, and whether the resulting assembly of proteins can play a role in DCM by affecting activation of AKT remains to be addressed.

3.2. SLMAP in Diabetes

Type 2 Diabetic Retinopathy has been linked to SLMAP. In a study with individuals from Qatari, a single-nucleotide polymorphism (SNP) of SLMAP (rs17058639C > T) was identified to be associated with increased risk and severity of retinopathy among patients with diabetes type 2[78]. The same variant was positively associated with retinopathy in diabetic Caucasian subjects[79]. However, this association did not reach statistical significance in type 2 diabetic patients from Egypt[80]. These studies suggest that the incidence of retinopathy in subjects harboring this mutation may vary across different populations.

A possible etiology of diabetic retinopathy is the impairment of retinal microvasculature, which causes the formation of microaneurysm and hemorrhage, leading to reduced blood supply and retinal damage[81]. In fact, in mouse model for diabetes type 2, SLMAP1 was found to be upregulated in the small mesenteric arteries, which exhibited high contractility and reduced relaxation[82]. The endothelial dysfunction with overexpression of SLMAP1 in HUVECs was also linked to disturbances in the expression of proteins associated with ER stress and autophagy, in a mechanism involving AMPK[83]. These endothelial abnormalities with overexpression of SLMAP could reflect the pathological mechanism behind retinopathies in subjects carrying SLMAP variants.

In another study, hyperglycemic mouse model for diabetes type 2 presented approximately 2-fold higher expression of SLMAP1 and SLMAP2 in adipose tissue when compared to normal glycemic mice. With the knockdown of SLMAP isoforms in adipocytes, the glucose uptake decreased to 61.7%, and the mechanism for this may involve with GLUT4 as SLMAP2 was demonstrated to interact with it[84]. This study suggests that another possible involvement of SLMAP in type 2 diabetes by glucose handling.

In diabetic cardiomyopathy mouse model, SLMAP was also found upregulated. Treatment of these animals with Glucagon-Like Peptide-1 Receptor Agonist (GLP-1RA), an agonist of the incretin hormone GLP-1 known to induce insulin secretion and that is used to treat type 2 diabetes[85], decreased SLMAP expression in the ventricular myocardium[86]. It was found that upon GLP-1RA treatment, the expression of miR-29b-3p increased and its targeting towards SLMAP was the reason for the reduced protein expression[86]. This study suggests that SLMAP may have a pathological role in the myocardium in diabetic cardiomyopathy.

3.3. SLMAP in Cancer

Overexpression of SLMAP was found in leiomyosarcomas (LMS), and it is a biomarker for the group 1 LMS, which has an improved disease-specific survival (DSS), and SLMAP expression correlates with better LMS prognosis[87–89]. Increased SLMAP expression was also observed in pulmonary sarcomatoid carcinoma, and it is part of the gene expression profile that differs from lung adenocarcinoma and lung squamous cell carcinoma[90].

Another feature of SLMAP in cancer is fusion with receptor tyrosine kinases. SLMAP was reported to be fused with ALK in lung adenocarcinoma[91], with FGFR2 in intrahepatic cholangiocarcinoma (ICC)[92], with ROS1 in non-small cell lung cancer[93], and with NTRK2 in ganglioglioma[94]. Additionally, SLMAP was found to be fused with the RTK downstream kinases RAF1 in spindle cell tumor[95,96] and BRAF in primary sarcoma[97]. In all these fused proteins, the

kinase domains were maintained, and so was the FHA domain of SLMAP, except for FGFR2 where the FHA domain was disrupted with the fusion. Although no mechanistic studies were conducted, it is likely that the coiled-coil domains of SLMAP favor the dimerization of the fused proteins, allowing the constitutive activation of these kinases. The FHA could also recruit substrates to the kinases, and the conserved region of SLMAP in these fused proteins ranging from amino acid 167 to 199 could recruit STRIPAK[9], adding an extra level of regulation of these kinases. Another study also reported the fusion of SLMAP with the transcriptional regulator EGR in prostate cancer, although the structural details of the fused protein was not provided[98].

4. SLMAP Paralogs

4.1. CCDC136/NAG6

CCDC136 is one of the SLMAP paralogs that displays coiled-coil and transmembrane domains. It was reported to be expressed in the testis[99] and in cone photoreceptor cells from the retina[100,101]. Its function remains mostly unknown, but it was found downregulated in gastric cancer[102], suggesting a tumor suppressor role. In accordance with this, higher expression of CCDC136 was associated with higher survival rate in patients with cervical cancer[103] and multiple myeloma[104]. Depletion of CCDC136 in the pancreatic cancer cell line PANC-1 also reduced cell proliferation[105]. The opposite however is also true, as higher expression of CCDC136 was associated with poorer survival of patients with colon cancer[106] and antibodies against it were detected in patients with asbestos related lung cancer[107]. CCDC136 might also have roles in cognitive functions, as SNPs in a locus containing *ccdc136* and its neighbour gene *flcn* were associated with reading disorders[108,109].

In sperms, CCDC136 was shown to be expressed in the acrosome and to be important for the formation of this organelle. Knockout mice are viable and females have normal pregnancy, but the males are infertile. This is due to sperm abnormalities, including reduced motility and increased number of round-headed sperms[99]. Smiley et al.[101] also disrupted CCDC136 expression in mice by gene trap strategy, but the resulting animals were fertile. This is probably because CCDC136 expression was not completely abolished, to what was attributed to the splicing out of the gene trap sequence.

A mechanistic role for CCDC136 has been proposed as an antagonist of Wnt canonical signaling[110]. In Zebrafish, CCDC136b, the corresponding ortholog, interacted with APC and increased its affinity for β-catenin, resulting in its degradation and reduced nuclear translocation. Further, the overexpression of CCDC136 in HEK-393T cells inhibited Wnt signaling[110].

4.2. TRAF3IP3/T3JAM

TRAF3IP3 is another of SLMAP paralog and a member of STRIPAK that contains coiled-coil and transmembrane domains. It is expressed specifically in immune system tissues, including bone marrow, spleen and thymus[111,112] and differently from SLMAP, the TRAF3IP3 knockout mice are viable and fertile[113]. It localizes in the Golgi, mitochondria, ER, perinuclear region and centriolar satellite[114–118].

TRAF3IP3 was first found to interact with TRAF3 to activate JNK signaling in T cells[111], and to induce JNK activation in HEK293T, PC-3 and Hela cells, accompanied by increased proliferation[119]. However, another study in thymocytes could not reproduce the interaction of TRAF3 and TRAF3IP3, and the knockout of TRAF3IP3 did not impair JNK activity [113]. Therefore, the link between TRAF3IP3 and JNK signaling remains controversial.

TRAF3IP3 was found upregulated in multiple cancers, including vascular cells from breast cancer[120], intrahepatic cholangiocarcinomas developed from cirrhotic livers[121], osteosarcoma, glioblastoma, plasmacytoma, melanoma, breast and gastric cancers[122], kidney renal clear cell carcinoma[123], glioma[124,125] and high-grade serous ovarian cancer[126]. A genetic variant of TRAF3IP3 was also proposed to be involved with B lymphoblastic leukemia[127]. A possible mechanism for the upregulation of TRAF3IP3 is reduced methylation in the promoter region of TRAF3IP3, as it was observed in kidney renal clear cell carcinoma[123].

Mechanistically, TRAF3IP3 could participate in cancer development by the Ras/Raf/MEK/ERK cascade, known to play important roles in carcinogenesis by promoting cell proliferation, migration, invasion, angiogenesis and extracellular matrix degradation[128]. In thymocytes and natural killer T (NKT) 2 cells, TRAF3IP3 was reported to recruit MEK to the Golgi to allow the MEK/ERK signaling activation[113,115]. Further, overexpression of TRAF3IP3 in glioma cells enhanced tumor progression and was associated with higher ERK activation[124]. However, in myeloid cells the knockout of TRAF3IP3 did not affect ERK signaling[129] and in regulatory T cells its depletion did not affect the MEK localization in the Golgi[130]. Therefore, the influence of TRAF3IP3 in MEK/ERK cascade might be cell specific.

TRAF3IP3 also plays roles in the innate immune system by regulating TBK1 in different ways. TBK1 is a central kinase in the innate response, receiving activating stimulus from TLRs-TRIF and the cytosolic nuclei acid responses RLR-MAVs (RNA) and cGAS-STING (DNA). Upon these stimuli, TBK1 activates IRF3 and IRF7 to induce the expression of cytokines[131]. In myeloid cells, TRAF3IP3 was shown to target TBK1 to ubiquitination, resulting in negative regulation of the antiviral response[129]. However, a positive regulation of TBK1 by TRAF3IP3 has also been reported, where TRAF3IP3 acted upstream to TBK1 by recruiting TRAF3 to the mitochondria to allow the interaction and activation with MAVs, which favored the antiviral defense mechanism [116]. In macrophages, TRAF3IP3 also functioned upstream to TBK1 by facilitating the translocation of TRL4 to lipid rafts, increasing the receptor response upon LPS stimulation[132]. The reasons for opposite findings on the regulation of TBK1 by TRAF3IP3 have not been addressed in the literature yet. Finally, TRAF3IP3 was found to interact with the 3C protease from enterovirus 71 (EV71), preventing the enzyme to enter the nucleus, showing that TRAF3IP3 also has innate response functions independently from TBK1 signaling[118].

An additional role of TRAF3IP3 is in the development of cells from immune system, including B cells, in a mechanism dependent on autophagy[112,133], of thymocytes, in a mechanism dependent on BRAF-MEK-ERK signaling[113], and of natural killer T 2 cells, also depending on ERK activation[115]. In regulatory T cells, TRAF3IP3 recruits PP2A to the lysosome to facilitate the dephosphorylation and inactivation of the mTORC1 component Raptor. In the absence of TRAF3IP3, there is a hyper glycolytic metabolism, affecting T reg function that leads to increased inflammation and enhanced antitumor T cell response in mice[130]. The importance of TRAF3IP3 to the immune system is further evidenced with the finding that genetic variants were found in Chinese patients with the autoimmune Graves diseases[134,135].

5. SLMAP Adaptors

5.1. SIKE

SIKE1 is a small coiled-coil protein with ubiquitous expression[136]. Although its function remains mostly unknown, it was reported to negatively regulate the innate immune response. It inhibits the paralog kinases IKKε and TBK1[137], and in the case of TBK1, by acting as a substrate[138]. The inhibition of these kinases by SIKE1 and upon TRL3 or viral stimulation with

VSV impaired IRF3 response, although the NF-κB signalling remained intact[137,138]. In accordance with these studies is the detection of overexpressed SIKE1 in B-cells infected with Hepatitis C virus, together with downregulation of heat shock protein Hsp90 that stabilizes TBK1, which were believed to contribute to the inhibition of the kinase. The consequence of this was reduced activation of IRF3 and impaired production of IFNβ, which allowed the evasion of Hepatitis C virus from the immune response and persistent of the infection in patients with chronic hepatitis C, with B-cells being the virus reservoir[139]. The role of SIKE1 as inhibitor of TBK1, and therefore an antagonist of antiviral response, was also confirmed in black carps[140].

Inhibition of TBK1 by SIKE1 was similarly observed in hearts, where it dampened the activation of AKT-mTOR signaling, a driver of pathological cardiac hypertrophy[77]. In the same study, the downregulation of SIKE1 in patients with human dilated cardiomyopathy and hypertrophic cardiomyopathy was reported, emphasizing its cardioprotective role[77].

SIKE1 was also shown to interact with the cytoskeleton proteins tubulin and α-actinin, which could be a mechanism to control cell mobility[141]. Indeed, knockout of SIKE1 in HAP1 and its depletion in mesenchymal stem cells from umbilical cord Wharton's jelly by miR-146a-5p reduced cell migration[141,142].

Despite these claims of SIKE1 roles, its global knockout in mice does not produce any phenotype and the animals are fertile[143]. It is possible that SIKE1 functions only under infection/cellular stress or has overlapping roles with its paralog FGFR1OP2.

5.2. FGFR1OP2/Wit3.0

Similarly to SIKE1, FGFR1OP2 is a ubiquitously expressed coiled-coil protein[144]. Despite being part of the STRIPAK and the knockout in mouse resulting in lethality[13], very little is known about how it can affect embryonic development. It has been demonstrated to be upregulated after tooth extraction and to enhance the wound closure of edentulous mucosa[145–147]. FGFR1OP2 was reported to associate with cytoskeleton, but not F-actin, and heterozygous fibroblasts FGFR1OP2$^{+/-}$ had reduced cell migration. Fibroblasts with upregulation of FGFR1OP2 were ruled out to be myofibroblasts that could contribute to the contraction of the wound. Therefore, its function in wound closure seems to be through the regulation of cytoskeleton of fibroblasts[147]. Further, the heterozygous fibroblasts FGFR1OP2$^{+/-}$ had altered cell morphology, which the authors described as disorganized cytoskeleton and loss of cell polarity[148].

FGFR1OP2 has also been linked to residual ridge resorption (RRR) of jawbone. Excessive RRR can happen post tooth extraction, although the cellular and molecular mechanisms for this are still not fully understood. It has been recently proposed that lymphocytes and fibroblasts from the oral mucosa barrier can enhance the activity of osteoclasts external to the jawbone, mainly induced by RANKL signaling, explaining the intense RRR[149]. SNPs of FGFR1OP2 have been detected in USA, Korean and Saudi individuals and associated with increased RRR[150–152] although the consequences of the variants to the expression and structure of FGFR1OP2 were not investigated. Still, with these studies it is conceivable that FGFR1OP2 might have direct or indirect roles in RANKL signaling in the edentulous mucosa.

FGFR1OP2 has been associated with cancer. Two patients with myeloproliferative syndrome presented fused FGFR1OP2-FGFR1 originated from a chromosomal translocation[153,154]. This same fusion was identified in KG-1 cell line derived from an acute myeloid leukemia, and its depletion was enough to induce apoptosis[155]. It is hypothesized that the coiled-coil domains in the N-terminus of FGFR1OP2 that is conserved in the fused protein keep FGFR1 dimerized and constitutively active, favoring the proliferation of the cells[153]. Further, it

was shown that HSP91 heat shock protein and its chaperon CDC37 are important to stabilize FGFR1OP2-FGFR1, protecting it from misfolding, ubiquitination, proteasomal degradation and keeping it in constantly active conformation[156]. A mouse model to study the FGFR1OP2-FGFR1 was also created, where animals transplanted with bone marrow cells carrying the sequence for the fused protein developed leukemia and lymphoma. The lymphoma cells had upregulation of Notch signaling, whereas the leukemia cells had abnormal expression of genes myeloid cell fate, all that could have contributed to the cancer development[157].

In the fused protein, it is possible that SLMAP could be recruited to further regulate FGFR1 activation. The first coiled-coil domain of SIKE1 in the N-terminus was shown to interact with SLMAP, with the requirement of the leucines at the positions 15, 19 and 36 (Uniprot Q9BRV8-1)[9]. This is a region with 67% homology with FGFR1OP2, which has these leucines conserved and is present in FGFR1OP2-FGFR1[153]. This is in line with the multiple reports of SLMAP fusions with receptor tyrosine kinases (see section SLMAP in cancer). Future studies investigating how FGFR1OP2 and SLMAP regulate RTK would contribute to the understanding of the overactivation of these receptors in neoplasias and their clinical manifestation.

6. Conclusion

Although Hippo pathway is the main signaling axis associated with SLMAP, here we revised other described functions for it, its paralogs (TRAF3IP3 and CCDC136) and adaptors (SIKE1 and FGFR1OP2). Even though some of their functions might be interconnected, as in cancer and regulation of TBK1, a unifying and general mechanism involving them to explain the phenotypes observed in mice models carrying mutations or having the knockout of these genes remains missing. A systematic investigation of their functions and validation *in vivo* in mammal organisms will clarify the clinical manifestation of individuals harboring mutations in these genes and will open opportunities for therapeutic strategies.

Authors Contributions

A.P.D.: project conceptualization, investigation, data visualization and manuscript writing;
B.T.: project conceptualization, supervision, manuscript review and funding acquisition.

Acknowledgments

This project was funded with the grant 220996-151999 from the Canadian Institute of Health Research (CIHR) to Dr. Balwant Tuana.

Declaration of Interests

The authors declare no competing interests.

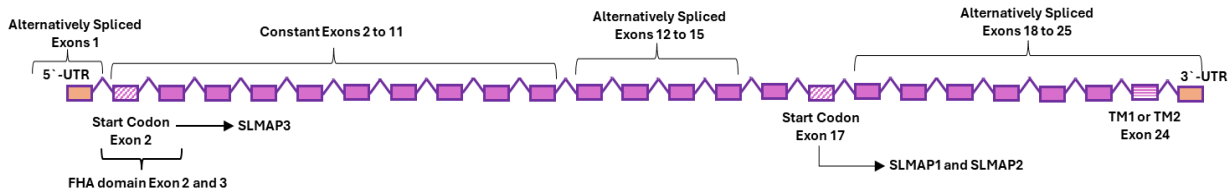

Figure 1. SLMAP transcript organization. Exon 2 contains the start codon for SLMAP3 isoforms. Exon 17 has the start codon for SLMAP1 and 2, which differ in size due to the alternative splicing of exons 18 to 24. Exons 2 to 11 are constant in all SLMAP3 isoforms. Exons 2 and 3 encode for the FHA domain, where exon 24 encode for either of the TM domains.

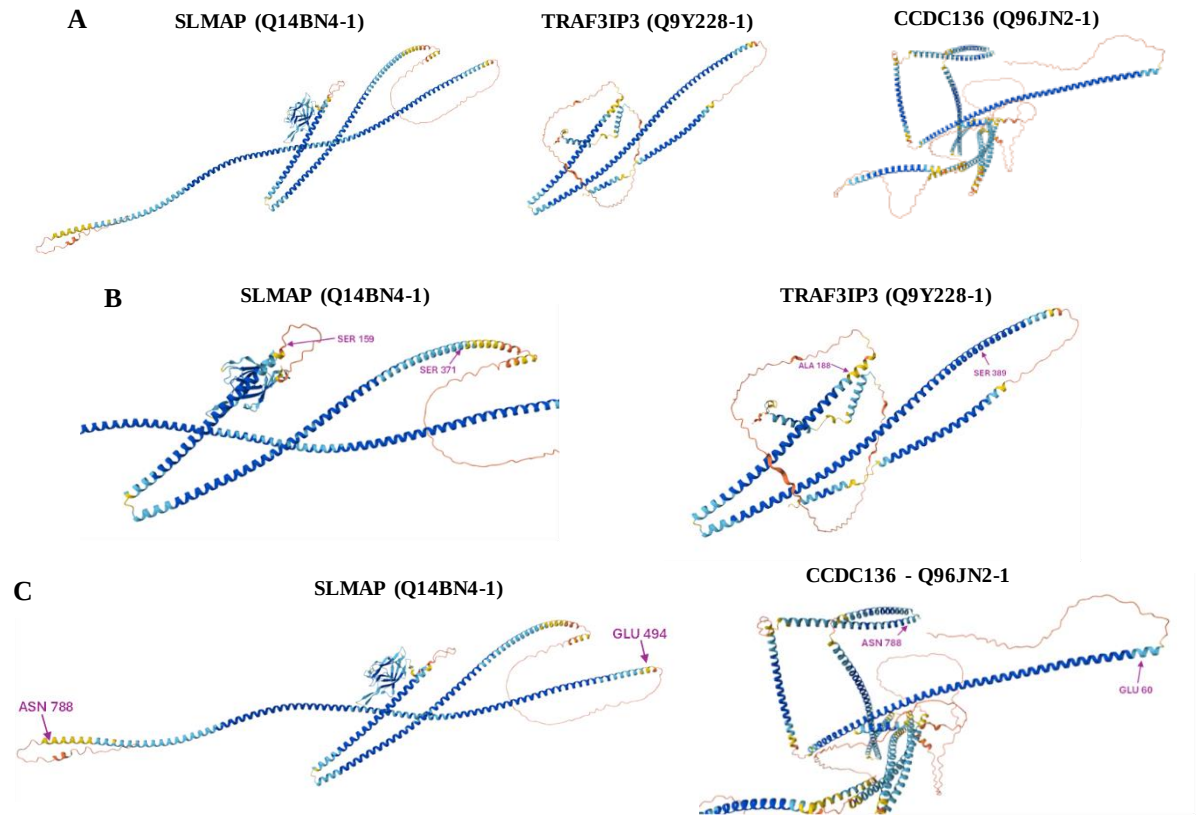

Figure 2. SLMAP Paralogs. A) Structures of SLMAP (Q14BN4-1), TRAF3IP3 (Q9Y228-1) and CCDC136 (Q96JN2-1) from AlphaFold2. B) Comparison of the homologous region between SLMAP (Ser159 to Ser371) and TRAF3IP3 (Ala188 and Ser389). C) Comparison of the homologous region between SLMAP (Glu494 to Asn788) and CCDC136 (Glu60 and Asn788).

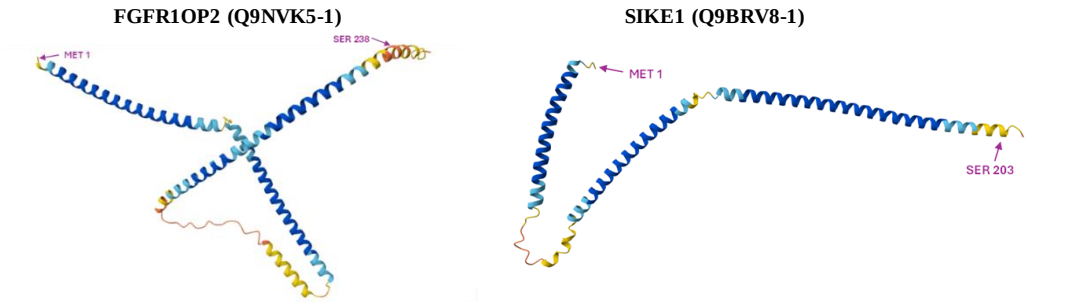

Figure 3. SLMAP Adaptors. Structures of FGFR1OP2 (Q9NVK5-1) and SIKE1 (Q9BRV8-1) from AlphaFold2 and the homologous region between FGFR1OP2 (Met1 to Ser238) and SIKE1 (Met1 to Ser203).

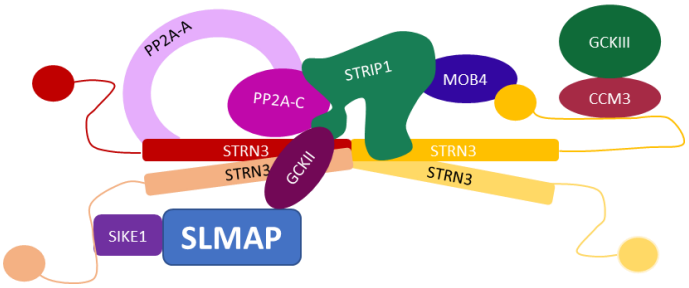

Figure 4. STRIPAK. The STRIPAK complex based on the structure and model proposed[14].

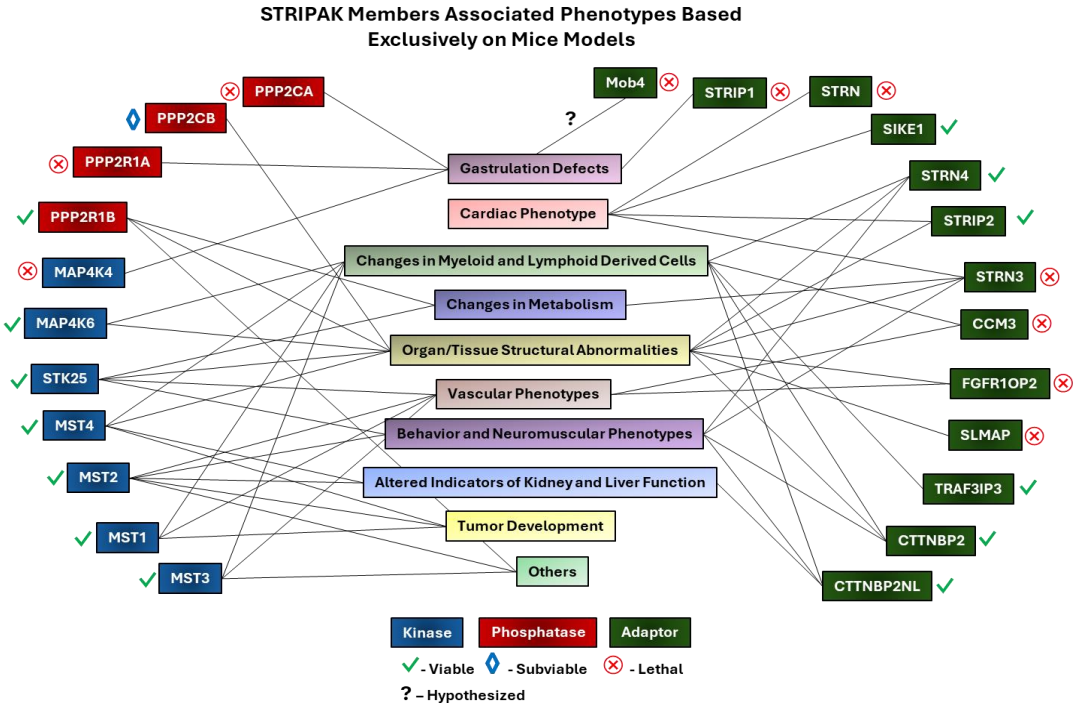

Figure 5. Phenotypes in mice associated with the knockout of STRIPAK members. The detailed description of each knockout is available at Table 1. For Mob4, a mechanism for the embryonic lethality with its knockout has not been proposed yet, but considering that the lethality is prior organogenesis and the phenotypes caused with the knockout out STRIP1, PPP2CA, PPP2R1A and MAP4K4, our hypothesis is that it is involved with gastrulation defects.

Table 1. Phenotypes of the Global Knockout of STRIPAK Members in Mice

STRIPAK Member	Viability	Phenotype	Proposed Mechanism
PP2A-C/PPP2CA	Lethal	Development until post implantation, but without mesoderm formation after gastrulation, and with degenerated endoderm and ectoderm[158,159].	PPP2CA might be required for cell fate determination[158]; the embryonic lethality could a result from defects in cell adhesion caused by impaired targeting of E-cad and β-catenin to the plasma membrane[160,161].
PP2A-C/PPP2CB	Subviable	No abnormal phenotype, and animals were fertile[159]; preweaning lethality with incomplete penetrance, and the heterozygous animals have abnormal thickness of retina and cornea[162].	Not described.
PP2A-A/PPP2R1A	Lethal	Embryonic lethality before E10.5[163]; gastrulation defects at E6.5, with failure in the formation of primitive streak and mesoderm and abnormal embryonic patterning[164].	Impaired Wnt and Nodal signaling[164].
PP2A-A/PPP2R1B	Viable	Male infertility, increased fasting circulating glucose level and abnormal tooth morphology[165].	Not described.
STRN	Lethal	Phenotypes of the homozygous mutants are not described. The heterozygous mutants present higher blood pressure with higher salt diet[166]. Heterozygous mice are also less predisposed to cardiac hypertrophy upon angiotensin II stimulation[167].	Higher blood pressure due enhanced mineralocorticoid receptor activation[166]. Depletion of STRN protects heart against hypertrophy due compromised response to angiotensin II[167].
STRN3/SG2NA	Lethal	No generation of node, and death before organogenesis[168]. Another knockout grows at least until E15.5, but has reduced body size, cardiac septal defect and fetal oedema[169,170]. The heterozygous mutants exhibit abnormal behavior, abnormal circulating glucose level, decreased thigmotaxis and increased vertical activity[170]. The specific knockout in gastric mucosa protects against gastric cancer induced by the carcinogen N-methyl-N`-nitro-N-nitrosoguanidine (MNNG)[31].	The mechanism for the phenotypes in the global knockout mouse are not described. The protection against gastric cancer is due reduced YAP activity[31].
STRN4/Zinedin	Viable	Homozygous mutants have no spontaneous movement; heterozygous animals have abnormal retina, decreased corpuscular hemoglobin, altered behavior and decreased thigmotaxis[171].	Not described.

STRIP1/FAM40A	Lethal	No mesoderm cell migration, being accumulated in the primitive streak. No formation of somites[172].	Abnormal focal adhesion, reduced cell migration and changes in the F-actin cytoskeleton[172].
STRIP2/FAM40B/Myoscape	Viable	Abnormal pancreas and seminal vesicle morphology [173]. Impairment of cardiac contractility[174].	STRIP2 regulates the targeting of L-type calcium channels to plasma membrane and affects calcium currents[174].
MOB4/phocein	Lethal	Embryonic lethality prior to organogenesis (E9.5)[175].	Not described.
CCM3/TFAR15/PDC10	Lethal	Embryos are smaller, pale, die at E8-8.5 and have vasculogenesis and hematopoiesis defects. The knockout in endothelial cells causes angiogenesis defects, disruption of vascular integrity, venous enlargement and death by E13.5 due hemorrhage caused by venous rupture[176,177].	CCM3 functions with GCKIIIs for endothelial lumen formation[177], and CCM3 facilitates VEGFR2 signaling[176].
SIKE1	Viable	No phenotypes[143], but The specific knockout in the heart predisposes animals to cardiac hypertrophy and heart failure after cardiac pressure overload[77].	SIKE1 is an inhibitor of TBK1, and its knockout facilitates the TBK1-AKT signaling that induces cardiac hypertrophy[77].
FGFR1OP2/Wit3.0	Lethal	Homozygous mutants display abnormal craniofacial, tail, placenta, limb and blood vessel morphologies; abnormal placenta vasculature, cleft palate, edema and growth retardation. Heterozygous exhibit cataract, microphthalmia, persistence of hyaloid vascular system and abnormal retina, skin, placenta and vitreous body morphologies[13].	Not described.
SLMAP/SLAP	Lethal	Cleft palate; abnormal head, embryo size, limb and tail morphologies[10]. Delayed development; edema; abnormal head, limbs, and embryo size; polycystic kidney; open neural tube; short bowel; fused bones and cartilages from sternum and ribs[12].	Planar cell polarity defects[12].
TRAF3IP3/T3JAM	Viable	Decreased mean corpuscular volume and mean corpuscular hemoglobin; reduced leukocyte cell number[178]. The animals are viable and fertile, and although the total number of thymocytes is not reduced, the number of some cell subtypes are altered[117].	Defective recruitment of MEK to the Golgi apparatus, downregulating the BRAF-MEK-ERK axis and affecting T cell development[117].

CTTNBP2	Viable	Increased memory CD4-positive, CD25-positive, alpha-beta regulatory T cell number; increased plasma cell number, increased grip strength, decreased transitional stage T1 B cell number[179]; Cttnbp2 deficiency impairs the formation of dendritic spines and neuronal activation, reduces zinc level in the brain, affects the distribution of synaptic proteins and influences autism-like behaviours[180].	Affects the synaptic expression of NMDAR-SHANK signaling members and zinc-regulated autism-associated genes[180].
CTTNBP2NL	Viable	Decreased mean corpuscular hemoglobin, increased blood urea nitrogen level, decreased grip strength and increased startle reflex[181].	Not described.
MST3/STK24	Viable	No gross phenotype but increased neutrophil degranulation[182]. Mice with constitutive MST3 KO and postnatally STK25 KO in endothelial cells (DKO) develop cavernomas[183]. Hypomorphic MST3 mutated mice develops hypernatremia, hypokalemia and hypertension due dysregulation of ENaC channels from the nephron[184].	STK24 supresses exocytosis by competing with UNC13D C2B domain, impairing UNC13D ability to tether granules to plasma membrane[182]. MST3 negatively regulates ENaC channels[184].
MST4/STK26/MASK	Viable	Abnormal adrenal gland, kidney, and vertebral arch; decreased mean platelet volume, circulating creatinine level and monocytes number[185]. MST4 deletion favors gastric tumor development upon the treatment with the carcinogen N-methyl-N`-nitro-N-nitrosoguanidine (MNNG)[186]. The knockout mice do not have any metabolic phenotype, even with high-fat or methionine–choline-deficient diets[187].	Gastric cancer development due increased YAP activation[186].
STK25/SOK1/YSK1	Viable	No neuronal phenotypes with constitutive KO, but the acute depletion of STK25 causes abnormal neuronal migration[188]. Mice exhibit hepatomegaly at around 11 months of age[36]. The KO protects the mice against metabolic dysregulation in high-fat diet, including liver steatosis lipid accumulation in muscle[189]. They also have reduced kidney steatosis development[190] and protection against atherosclerosis induced with PCSK9 mutation[191]. Mice with constitutive MST3 KO and	Disturbance in the LBK1-STRAD-GM130 axis, which controls neuronal positioning[188]. STK25 is a negative regulator of insulin and glucose homeostasis[189]. STK25 contributes to renal lipid accumulation[190]. The hepatomegaly is due increased YAP activation[36].

		postnatally STK25 KO in endothelial cells (DKO) develop cavernomas[183].	
MST1/STK4/KRS2	Viable (DKO MST1/2 lethal)	MST1 KO mice are normal[192–197], but with altered number of lymphocytes[194–197]. The DKO MST1/2 results in embryonic lethality and developmental delay. Although the three germ layers and extraembryonic tissues are formed, the embryos and yolk sac are pale[192,193,195]. The postanal MST1/2 DKO induces the formation of liver tumor[193].	The lymphopenia in MST1 KO mice was attributed to reduced egression of cells from the thymus, defective cell adhesion to peripheral lymphoid organs and abnormal lymphocyte trafficking due to defective to chemotaxis[194–197]. MST1/2 are important for placenta development, primitive hematopoiesis and vascular patterning, independent of LATS and YAP, explaining the embryonic lethality in the DKO[192]. The liver tumor in postnatal DKO is caused by higher YAP activity[193].
MST2/STK3/KRS1	Viable (DKO MST1/2 lethal)	MST2 KO mice are viable, with no defects in the immune system cells or development[192,195], but exhibit abnormal gait, tremors, increased circulating creatinine level, increased circulating levels of alanine and aspartate transaminases[198]. The DKO MST1/2 results in embryonic lethality and developmental delay. Although the three germ layers and extraembryonic tissues are formed, the embryos and yolk sac are pale[192,193,195]. The postanal MST1/2 DKO induces the formation of liver tumor[193].	The mechanism for the phenotypes in MST2 KO are not described. MST1/2 are important for placenta development, primitive hematopoiesis and vascular patterning, independent of LATS and YAP, explaining the embryonic lethality in the DKO[192]. The liver tumor in postnatal DKO is caused by higher YAP activity[193].
MAP4K4/NIK	Lethal	Death at E9.5-E10.5. Failure of mesodermal precursor cells to migrate from the primitive streak, resulting in posteriorly truncated embryos and impaired somitogenesis (cell non-autonomous phenotype). The presomitic cells exhibit failure to differentiate into dermomyotome (cell autonomous phenotype)[199].	NICK/NCK might form a complex with phosphorylated p130Cas and is required for segmentation of presomitic mesoderm into somites[199].

MAP4K6/MINK	Viable	Abnormal skin, tooth and sternum morphologies; enlarged kidney and lymph nodes; small uterus; microphthalmia[200]. Longer bleeding time, reduced thrombus formation and less platelet spreading on fibrinogen[201].	In platelet, the mechanism is reduced dense-granule secretion and disturbance of MAPK signaling, which impaired platelet activation[201].

Table 2. STRIPAK in *Saccharomyces cerevisiae*

Mammal Counterpart	***Saccharomyces cerevisiae***	**Functions**
SLMAP	VPS64/FAR9	Involved in the carboxypeptidase Y pathway and secretion of mature alpha factor; important for vacuole morphology[202]; important for cell cycle arrest in response to pheromone[42]; antagonizes TORC2[203]; required to caspase-10-induced cell death [204]; negatively regulates Atg32, antagonizing mitophagy[205,206]; required to control gluconeogenesis after glucose depletion[207].
SLMAP	FAR10	Important for cell cycle arrest in response to pheromone[42]; required to caspase-10-induced cell death[204]; important for the dephosphorylation of Atg32, antagonizing mitophagy[206].
STRIP	YNL127W/FAR11	Important for carboxypeptidase Y pathway[202]; important for cell cycle arrest in response to pheromone[42]; antagonizes TORC2[208]; required to caspase-10-induced cell death[204]; negatively regulates Atg32, antagonizing mitophagy[205,206]; required to control gluconeogenesis after glucose depletion[207].
SIKE1/FGFR1OP2	Far3/Far7	Important for cell cycle arrest in response to pheromone[42]; required to caspase-10-induced cell death [204]; negatively regulates Atg32, antagonizing mitophagy[205,206].
STRN	Far8	Important for cell cycle arrest in response to pheromone[42]; required to caspase-10-induced cell death[204]; negatively regulates Atg32, antagonizing mitophagy[205,206]; required to control gluconeogenesis after glucose depletion[207].
PP2A-A	Tpd3	Antagonizes TORC2[208].
PP2A-C	Pph21	Antagonizes TORC2[208]; Required to caspase-10-induced cell death[204].
PP2A like phosphatase	Ppg1	Negatively regulates Atg32, antagonizing mitophagy[205,206]; required to assembly the Far complex and to control gluconeogenesis after glucose depletion[207].

Table 3. STRIPAK in *Schizosaccharomyces pombe*

Mammal Counterpart	***Schizosaccharomyces pombe***	**Functions**
SLMAP	Csc1p	Required to the asymmetry of SIN members during cytokinesis[209]. Anchors the SIP complex to the spindle pole body via its FHA domain, which inhibits SIN[210].
STRIP	Csc2p	Required to the asymmetry of SIN members during cytokinesis[209].
SIKE1/FGFR1OP2	Csc4p	Required to the asymmetry of SIN members during cytokinesis[209].
STRN	Csc3p	Required to the asymmetry of SIN members during cytokinesis[209].
PP2A-A	Paa1p	Required to the asymmetry of SIN members during cytokinesis[209].
PP2A-C	Ppa3p	Required to the asymmetry of SIN members during cytokinesis[209].

Table 4. STRIPAK in *Neurospora crassa*

Mammal Counterpart	*Neurospora crassa*	Functions
SLMAP	Ham-4	Required for vegetative but not sexual hyphal fusion; mutants cause defective meiosis and abnormally shaped ascopore[211]; not needed for the nuclear accumulation of MAK-1[212].
STRIP	Ham-2	Required for vegetative but not sexual hyphal fusion; mutants cause defective meiosis and abnormally shaped ascopore[211,213]; required for cell fusion[214]; important for the nuclear accumulation of MAK-1[212].
STRN	Ham-3	Required for vegetative but not sexual hyphal fusion; mutants cause defective meiosis and abnormally shaped ascopore[211]; required for cell fusion[214]; needed for the nuclear accumulation of MAK-1[212].
Mob4	Mob3/phocein	Required for vegetative hyphal and germling fusion[215]; required for cell fusion[214]; important for the nuclear accumulation of MAK-1, in a mechanism that depends on Mob3 phosphorylation by MAK-2[212].
PP2A-C	PPG-1	Required for cell fusion[214]; not needed for the nuclear accumulation of MAK-1[212].
PP2A-A	PP2A-A	Essential for viability[212].

Table 5. STRIPAK in *Fusarium graminearum*

Mammal Counterpart	*Fusarium graminearum*	Functions
STRN	FgFSR1/Ham3	The mutant has reduced growth and is more sensitive to stress; important for deoxynivalenol (DON) production; required for proper sexual and asexual development; important for virulence; the mutant reduced Mgv1 phosphorylation and nuclear localization; interacted with TAP42 (TOR effector)[216,217].
STRIP	Ham2	The mutant has reduced growth and is more sensitive to stress; important for deoxynivalenol (DON) production; required for proper sexual and asexual development; important for virulence; the mutant reduced Mgv1 phosphorylation and nuclear localization; interacted with TAP42 (TOR effector)[216]
SLMAP	Ham4	The mutant has reduced growth and is more sensitive to stress; important for deoxynivalenol (DON) production; required for proper sexual and asexual development; important for virulence; the mutant reduced Mgv1 phosphorylation and nuclear localization; associated with TAP42 (TOR effector)[216].
Mob3	Mob3	The mutant has reduced growth and is more sensitive to stress; important for deoxynivalenol (DON) production; required for proper sexual and asexual development; important for virulence; the mutant reduced Mgv1 phosphorylation and nuclear localization; associated with TAP42 (TOR effector)[216].
PP2A-A	PP2Aa	Associated with TAP42 (TOR effector)[216].
PP2A-C	Ppg1	The mutant has reduced growth and is more sensitive to stress; important for deoxynivalenol (DON) production; required for proper sexual and asexual development; important for virulence; the mutant reduced Mgv1 phosphorylation and nuclear localization; interacted with TAP42 (TOR effector)[216,217].

Table 6. STRIPAK in *Aspergillus nidulans*

Mammal Counterpart	*Aspergillus nidulans*	Functions
SLMAP	SipD	Required for growth and sexual development; important for stress response; important for secondary metabolite production[218].
STRIP	SipC	Required for growth and sexual development; important for stress response; important for secondary metabolite production[218].
SIKE1/FGFR1OP2	SipB	Required for growth and sexual development; important for stress response; important for secondary metabolite production[218].
STRN	StrA	Required for sexual development[218,219]; required for growth; important for stress response; important for secondary metabolite production; required for Mpk8 activation phosphorylation; restrict the translocation of MpkC to the nucleus in the absence of stress[218].
Mob4	SipA	The mutant results in excessive growth and abnormal sexual development; excessive growth during stress; important for secondary metabolite production[218].
PP2A-C	SipE/PpgA	Required for growth and sexual development; important for stress response; important for secondary metabolite production[218].
PP2A-A	SipF	Essential for the viability[218].

Table 7. STRIPAK in *Sordaria macrospora*

Mammal Counterpart	*Sordaria macrospora*	Functions
SLMAP	PRO45	Required for sexual propagation and hyphal fusion[220].
STRIP	PRO22	Required for ascogonial septum formation[221]; mutations cause defects in sexual development and cell fusion[222]; important for vegetative growth[223]; controls the phosphorylation status of CLA4[224], GUL1[225], SmKIN3 and DBF2[226].
SIKE1/FGFR1OP2	SCL1	Required for cell fusion, vegetative growth and sexual development[227].
STRN	PRO11	Required for cell differentiation[228]; important for vegetative growth[227]; required for fertility and mutants cause sexual abnormalities and defective cell fusion[222,227–229]; controls the phosphorylation status of CLA4[224], GUL1[225], SmKIN3 and DBF2[226].
Mob4	SmMOB3	Required for sexual development and cell fusion[229].
PP2A-A	SmPP2AA	Member of the STRIPAK in *Sordaria macrospora*[222].
GCKIII	SmKIN3	Mutations lead to increased aerial hyphae formation and enhanced protoplast regeneration[230]; required for sexual development, hyphal fusion and septation[230,231]
GCKIII	SmKIN24	Mutations causes hyperseptation and sterility[230].
PP2A-C	PP2Ac1	Required for sexual development, hyphal fusion and vegetative growth[223]; controls the phosphorylation status of CLA4[224], GUL1[225], SmKIN3 and DBF2[226].

Table 8. STRIPAK in other species

Mammal Counterpart	***Duddingtonia flagrans***	**Functions**
STRIP	SipC	Required for vegetative growth, septation and asexual development; important to determine the fate of trap cells[232].
Mammal Counterpart	***Fusarium pseudograminearum***	**Functions**
STRN	FpHam-3	Mutation causes reduced growth rate, defects in hyphal fusion and conidiation; also results in increased sensitive for cell membrane, cell wall and oxidative stress responses, and decreased in virulence[233].
STRIP	FpHam-2	Mutation causes reduced growth rate, defects in hyphal fusion and conidiation; also results in increased sensitive for cell membrane, cell wall and oxidative stress responses, and decreased in virulence[233].
SLMAP	FpHam-4	Mutation causes reduced growth rate, defects in hyphal fusion and conidiation; also results in increased sensitive for cell membrane, cell wall and oxidative stress responses, and decreased in virulence[233].
Mammal Counterpart	***Fusarium virguliforme***	**Functions**
STRN	FvSTR1	Important for virulence, asexual development, and production of secondary metabolites[234].
Mammal Counterpart	***Colletotrichum graminicola***	**Functions**
STRN	Str1	The mutant exhibits impaired virulence, growth, hyphal fusion, and defective sexual development[235].
Mammal Counterpart	***Magnaporthe oryzae***	**Functions**
PP2A-C	MoPPG1	Required for hyphal growth and proper formation of conidia; mutation impairs the virulence, which is probably associated with reduced expression of the Rho GTPases MgCDC42, MgRHO3 and MgRAC1[236].
Mammal Counterpart	***Epichloe festucae***	**Functions**
Mob3	MobC	Important for hyphal fusion and symbiosis with *Lolium perenne*[237].
Mammal Counterpart	***Fusarium verticillioides***	**Functions**
STRN	FSR1	Important for sexual fertility and fungal virulence[217,238].
STRIP	FvStp1	Important for virulence[238].

7. References

1. Wigle, J. T. *et al.* Molecular Cloning, Expression, and Chromosomal Assignment of Sarcolemmal-associated Proteins. *Journal of Biological Chemistry* **272**, 32384–32392 (1997).
2. Glatter, T., Wepf, A., Aebersold, R. & Gstaiger, M. An integrated workflow for charting the human interaction proteome: insights into the PP2A system. *Mol Syst Biol* **5**, (2009).
3. Goudreault, M. *et al.* A PP2A phosphatase high density interaction network identifies a novel striatin-interacting phosphatase and kinase complex linked to the cerebral cavernous malformation 3 (CCM3) protein. *Molecular and Cellular Proteomics* **8**, 157–171 (2009).
4. Kück, U., Radchenko, D. & Teichert, I. STRIPAK, a highly conserved signaling complex, controls multiple eukaryotic cellular and developmental processes and is linked with human diseases. *Biol Chem* **400**, 1005–1022 (2019).
5. Bae, S. J. *et al.* SAV1 promotes Hippo kinase activation through antagonizing the PP2A phosphatase STRIPAK. *Elife* **6**, (2017).
6. Zheng, Y. *et al.* Homeostatic Control of Hpo/MST Kinase Activity through Autophosphorylation-Dependent Recruitment of the STRIPAK PP2A Phosphatase Complex. *Cell Rep* **21**, 3612–3623 (2017).
7. Kean, M. J. *et al.* Structure-function analysis of core STRIPAK proteins: A signaling complex implicated in Golgi polarization. *Journal of Biological Chemistry* **286**, 25065–25075 (2011).
8. Madsen, C. D. *et al.* STRIPAK components determine mode of cancer cell migration and metastasis. *Nat Cell Biol* **17**, 68–80 (2015).
9. Tang, Y. *et al.* Architecture, substructures, and dynamic assembly of STRIPAK complexes in Hippo signaling. *Cell Discov* **5**, (2019).
10. International Mouse Phenotype Consortium. SLMAP. https://www.mousephenotype.org/data/genes/MGI:1933549.
11. Dias, A. P., Rehmani, T., Salih, M. & Tuana, B. Tail Anchored Membrane Protein SLMAP3 is Essential for Targeting Centrosomal Proteins to the Nuclear Envelope in Skeletal Myogenesis. *Open Biol* **14**, 240094 (2024).
12. Dias, A. P., Rehmani, T., Applin, B. D., Salih, M. & Tuana, B. SLMAP3 is crucial for organogenesis through mechanisms involving primary cilia formation - Submitted. *Open Biol* **14**, 240206. (2024).
13. International Mouse Phenotype Consortium. FGFR1OP2. https://www.mousephenotype.org/data/genes/MGI:1914779.
14. Jeong, B. C. *et al.* Cryo-EM structure of the Hippo signaling integrator human STRIPAK. *Nat Struct Mol Biol* **28**, 290–299 (2021).
15. Wielowieyski, P. A. *et al.* Alternative splicing, expression, and genomic structure of the 3′ region of the gene encoding the sarcolemmal-associated proteins (SLAPs) defines a novel class of coiled-coil tail-anchored membrane proteins. *Journal of Biological Chemistry* **275**, 38474–38481 (2000).
16. Guzzo, R. M., Sevinc, S., Salih, M. & Tuana, B. S. A novel isoform of sarcolemmal membrane-associated protein (SLMAP) is a component of the microtubule organizing centre. *J Cell Sci* **117**, 2271–2281 (2004).
17. Rehmani, T., Mlynarova, J., Byers, J., Salih, M. & Tuana, B. S. Specific Deletion of the FHA Domain Containing SLMAP3 Isoform in Postnatal Myocardium Has No Impact on Structure or Function. *Cardiogenetics* **11**, 164–184 (2021).

18. Ensembl. Human SLMAP Transcripts. https://grch37.ensembl.org/Homo_sapiens/Transcript/Exons?db=core;g=ENSG00000163681;r=3:57741177-57914895;t=ENST00000295951.
19. Guzzo, R. M., Salih, M., Moore, E. D. & Tuana, B. S. Molecular properties of cardiac tail-anchored membrane protein SLMAP are consistent with structural role in arrangement of excitation-contraction coupling apparatus. *American Journal of Physiology-Heart and Circulatory Physiology* **288**, H1810–H1819 (2005).
20. Byers, J. T., Guzzo, R. M., Salih, M. & Tuana, B. S. Hydrophobic profiles of the tail anchors in SLMAP dictate subcellular targeting. *BMC Cell Biol* **10**, (2009).
21. Durocher, D. *et al*. The Molecular Basis of FHA Domain:Phosphopeptide Binding Specificity and Implications for Phospho-Dependent Signaling Mechanisms. *Mol Cell* **6**, 1169–1182 (2000).
22. Durocher, D. & Jackson, S. P. The FHA domain. *FEBS Lett* **513**, 58–66 (2002).
23. Hyodo, T. *et al*. Misshapen-like kinase 1 (MINK1) is a novel component of striatin-interacting phosphatase and kinase (STRIPAK) and is required for the completion of cytokinesis. *Journal of Biological Chemistry* **287**, 25019–25029 (2012).
24. Herzog, F. *et al*. Structural Probing of a Protein Phosphatase 2A Network by Chemical Cross-Linking and Mass Spectrometry. *Science (1979)* **337**, 1348–1352 (2012).
25. Hauri, S. *et al*. Interaction proteome of human Hippo signaling: Modular control of the co-activator YAP1. *Mol Syst Biol* **9**, (2013).
26. Couzens, A. L. *et al*. Protein Interaction Network of the Mammalian Hippo Pathway Reveals Mechanisms of Kinase-Phosphatase Interactions. *Sci Signal* **6**, (2013).
27. Seo, G. *et al*. MAP4K Interactome Reveals STRN4 as a Key STRIPAK Complex Component in Hippo Pathway Regulation. *Cell Rep* **32**, (2020).
28. Ceccarelli, D. F. *et al*. CCM3/PDCD10 heterodimerizes with germinal center kinase III (GCKIII) proteins using a mechanism analogous to CCM3 homodimerization. *Journal of Biological Chemistry* **286**, 25056–25064 (2011).
29. Gordon, J. *et al*. Protein phosphatase 2a (PP2A) binds within the oligomerization domain of striatin and regulates the phosphorylation and activation of the mammalian Ste20-Like kinase Mst3. *BMC Biochem* **12**, 54 (2011).
30. Huang, W., Leonard, D. & Taylor, D. J. Pack a STRIPAK with hubs inside a hub. *Nat Struct Mol Biol* **28**, 232–233 (2021).
31. Tang, Y. *et al*. Selective Inhibition of STRN3-Containing PP2A Phosphatase Restores Hippo Tumor-Suppressor Activity in Gastric Cancer. *Cancer Cell* **38**, 115-128.e9 (2020).
32. Fowle, H., Zhao, Z. & Graña, X. PP2A holoenzymes, substrate specificity driving cellular functions and deregulation in cancer. in *Advances in Cancer Research* vol. 144 55–93 (Academic Press Inc., 2019).
33. Ribeiro, P. S. *et al*. Combined Functional Genomic and Proteomic Approaches Identify a PP2A Complex as a Negative Regulator of Hippo Signaling. *Mol Cell* **39**, 521–534 (2010).
34. Kim, J. W. *et al*. STRIPAK directs PP2A activity toward MAP4K4 to promote oncogenic transformation of human cells. *Elife* **9**, (2020).
35. Chen, R., Xie, R., Meng, Z., Ma, S. & Guan, K. L. STRIPAK integrates upstream signals to initiate the Hippo kinase cascade. *Nat Cell Biol* **21**, 1565–1577 (2019).
36. Lim, S. *et al*. Identification of the kinase STK25 as an upstream activator of LATS signaling. *Nat Commun* **10**, (2019).

37. Meng, Z. *et al*. MAP4K family kinases act in parallel to MST1/2 to activate LATS1/2 in the Hippo pathway. *Nat Commun* **6**, (2015).
38. Zheng, Y. *et al*. Identification of Happyhour/MAP4K as Alternative Hpo/Mst-like Kinases in the Hippo Kinase Cascade. *Dev Cell* **34**, 642–655 (2015).
39. Hwang, J. & Pallas, D. C. STRIPAK complexes: Structure, biological function, and involvement in human diseases. *Int J Biochem Cell Biol* **47**, 118–148 (2014).
40. Shi, Z., Jiao, S. & Zhou, Z. STRIPAK complexes in cell signaling and cancer. *Oncogene* **35**, 4549–4557 (2016).
41. Li, A. X., Martin, T. A., Lane, J. & Jiang, W. G. Cellular Impacts of Striatins and the STRIPAK Complex and Their Roles in the Development and Metastasis in Clinical Cancers (Review). *Cancers (Basel)* **16**, 76 (2023).
42. Kemp, H. A. & Sprague, G. F. Far3 and Five Interacting Proteins Prevent Premature Recovery from Pheromone Arrest in the Budding Yeast Saccharomyces cerevisiae . *Mol Cell Biol* **23**, 1750–1763 (2003).
43. Frost, A. *et al*. Functional repurposing revealed by comparing S. pombe and S. cerevisiae genetic interactions. *Cell* **149**, 1339–1352 (2012).
44. Kück, U., Beier, A. M. & Teichert, I. The composition and function of the striatin-interacting phosphatases and kinases (STRIPAK) complex in fungi. *Fungal Genetics and Biology* **90**, 31–38 (2016).
45. Kück, U. & Stein, V. STRIPAK, a Key Regulator of Fungal Development, Operates as a Multifunctional Signaling Hub. *Journal of Fungi* **7**, 443 (2021).
46. Ma, S., Meng, Z., Chen, R. & Guan, K.-L. The Hippo Pathway: Biology and Pathophysiology. *Annu Rev Biochem* **88**, 577–604 (2019).
47. Lu, J. *et al*. MEKK2 and MEKK3 orchestrate multiple signals to regulate Hippo pathway. *Journal of Biological Chemistry* **296**, 100400 (2021).
48. Huang, J., Wu, S., Barrera, J., Matthews, K. & Pan, D. The Hippo signaling pathway coordinately regulates cell proliferation and apoptosis by inactivating Yorkie, the Drosophila homolog of YAP. *Cell* **122**, 421–434 (2005).
49. Justice, R. W., Zilian, O., Woods, D. F., Noll, M. & Bryant, P. J. The Drosophila tumor suppressor gene warts encodes a homolog of human myotonic dystrophy kinase and is required for the control of cell shape and proliferation. *Genes Dev* **9**, 534–546 (1995).
50. Song, H. *et al*. Mammalian Mst1 and Mst2 kinases play essential roles in organ size control and tumor suppression. *Proc Natl Acad Sci U S A* **107**, 1431–1436 (2010).
51. Zhou, D. *et al*. Mst1 and Mst2 Maintain Hepatocyte Quiescence and Suppress Hepatocellular Carcinoma Development through Inactivation of the Yap1 Oncogene. *Cancer Cell* **16**, 425–438 (2009).
52. Wang, L. *et al*. Multiphase coalescence mediates Hippo pathway activation. *Cell* **185**, 4376-4393.e18 (2022).
53. Neal, S. J., Zhou, Q. & Pignoni, F. STRIPAK–PP2A regulates Hippo-Yorkie signaling to suppress retinal fate in the Drosophila eye disc peripodial epithelium. *J Cell Sci* **133**, (2020).
54. Kaya-çopur, A. *et al*. The hippo pathway controls myofibril assembly and muscle fiber growth by regulating sarcomeric gene expression. *Elife* **10**, 1–34 (2021).
55. An, L. *et al*. Combinatorial targeting of Hippo-STRIPAK and PARP elicits synthetic lethality in gastrointestinal cancers. *Journal of Clinical Investigation* **132**, (2022).

56. Shen, R. *et al.* A dRASSF-STRIPAK-Imd-JAK/STAT axis controls antiviral immune response in Drosophila. *Cell Rep* **40**, (2022).
57. Guzzo, R. M., Wigle, J., Salih, M., Moore, E. D. & Tuana, B. S. Regulated expression and temporal induction of the tail-anchored sarcolemmal-membrane-associated protein is critical for myoblast fusion. *Biochemical Journal* **381**, 599–608 (2004).
58. Zheng, Q. *et al.* Identification of transition factors in myotube formation from proteome and transcriptome analyses. *J Integr Agric* **22**, 3135–3147 (2023).
59. Papizan, J. B. *et al.* Deficiency in Kelch protein Klhl31 causes congenital myopathy in mice. in *Journal of Clinical Investigation* vol. 127 3730–3740 (American Society for Clinical Investigation, 2017).
60. Yu, W. *et al.* A novel human BTB-kelch protein KLHL31, strongly expressed in muscle and heart, inhibits transcriptional activities of TRE and SRE. *Mol Cells* **26**, 443–53 (2008).
61. Gupta, V. A. & Beggs, A. H. Kelch proteins: emerging roles in skeletal muscle development and diseases. *Skelet Muscle* **4**, 11 (2014).
62. Bers, D. M. Cardiac excitation–contraction coupling. *Nature* **415**, 198–205 (2002).
63. Eisner, D. A., Caldwell, J. L., Kistamás, K. & Trafford, A. W. Calcium and Excitation-Contraction Coupling in the Heart. *Circ Res* **121**, 181–195 (2017).
64. Nader, M. *et al.* Tail-anchored membrane protein SLMAP is a novel regulator of cardiac function at the sarcoplasmic reticulum. *American Journal of Physiology-Heart and Circulatory Physiology* **302**, H1138–H1145 (2012).
65. Mlynarova, J. *et al.* SLMAP3 isoform modulates cardiac gene expression and function. *PLoS One* **14**, (2019).
66. Benito, B., Brugada, R., Brugada, J. & Brugada, P. Brugada Syndrome. *Prog Cardiovasc Dis* **51**, 1–22 (2008).
67. Nader, M. *et al.* SLMAP-3 is downregulated in human dilated ventricles and its overexpression promotes cardiomyocyte response to adrenergic stimuli by increasing intracellular calcium. *Can J Physiol Pharmacol* **97**, 623–630 (2019).
68. Rehmani, T., Dias, A. P., Kamal, M., Salih, M. & Tuana, B. S. Deletion of Sarcolemmal Membrane-Associated Protein Isoform 3 (SLMAP3) in Cardiac Progenitors Delays Embryonic Growth of Myocardium without Affecting Hippo Pathway. *Int J Mol Sci* **25**, 2888 (2024).
69. Nader, M. The SLMAP/Striatin complex: An emerging regulator of normal and abnormal cardiac excitation-contraction coupling. *Eur J Pharmacol* **858**, 172491 (2019).
70. Nader, M. *et al.* Cardiac striatin interacts with caveolin-3 and calmodulin in a calcium sensitive manner and regulates cardiomyocyte spontaneous contraction rate. *Can J Physiol Pharmacol* **95**, 1306–1312 (2017).
71. Yang, Y. *et al.* Innate immune and proinflammatory signals activate the Hippo pathway via a Tak1-STRIPAK-Tao axis. *Nat Commun* **15**, (2024).
72. Steinberg, S. beta(2)-Adrenergic receptor signaling complexes in cardiomyocyte caveolae/lipid rafts. *J Mol Cell Cardiol* **37**, 407–415 (2004).
73. Ishikawa, T. *et al.* A Novel Disease Gene for Brugada Syndrome. *Circ Arrhythm Electrophysiol* **5**, 1098–1107 (2012).
74. Li, K. H. C. *et al.* Brugada syndrome: A comprehensive review of pathophysiological mechanisms and risk stratification strategies. *Int J Cardiol Heart Vasc* **26**, 100468 (2020).

75. Prévilon, M. *et al*. Comparative differential proteomic profiles of nonfailing and failing hearts after in vivo thoracic aortic constriction in mice overexpressing FKBP12.6. *Physiol Rep* **1**, (2013).
76. Meurs, K. M. *et al*. Association of dilated cardiomyopathy with the striatin mutation genotype in boxer dogs. *J Vet Intern Med* **27**, 1437–1440 (2013).
77. Deng, K. Q. *et al*. Suppressor of IKKIε is an essential negative regulator of pathological cardiac hypertrophy. *Nat Commun* **7**, (2016).
78. Upadhyay, R. *et al*. Role of SLMAP genetic variants in susceptibility of diabetes and diabetic retinopathy in Qatari population. *J Transl Med* **13**, (2015).
79. Pearce, E. *et al*. Intraretinal Microvascular Abnormalities and Venous Beading Have Different Genetic Profiles in Caucasian Patients with Non-Proliferative Diabetic Retinopathy. *Vision* **7**, 18 (2023).
80. Mohamed Farhan, H., Nassar, M., Hassan Ahmed, M., Abougabal, K. & Abd Elazim Taha, N. An association between the sarcolemmal membrane-associated protein gene and microvascular endothelial diabetic retinopathy in patients with type 2 diabetes mellitus: A preliminary case control study. *Diabetes and Metabolic Syndrome: Clinical Research and Reviews* **16**, (2022).
81. Wang, W. & Lo, A. C. Y. Diabetic Retinopathy: Pathophysiology and Treatments. *Int J Mol Sci* **19**, 1816 (2018).
82. Ding, H. *et al*. Endothelial dysfunction in Type 2 diabetes correlates with deregulated expression of the tail-anchored membrane protein SLMAP. *American Journal of Physiology-Heart and Circulatory Physiology* **289**, H206–H211 (2005).
83. Lakshmanan, A. P., Samuel, S. M., Triggle, C., Tuana, B. S. & Ding, H. A role for Sarcolemmal Membrane-Associated Protein (SLMAP) in mediating autophagy in endothelial cells through an AMPK-dependent mechanism. *The FASEB Journal* **30**, (2016).
84. Chen, X. & Ding, H. Increased Expression of the Tail-Anchored Membrane Protein SLMAP in Adipose Tissue from Type 2 Tally Ho Diabetic Mice. *Exp Diabetes Res* **2011**, 1–10 (2011).
85. Logan Collins; Ryan A. Costello. Glucagon-Like Peptide-1 Receptor Agonists. *StatPearls* https://www.ncbi.nlm.nih.gov/books/NBK551568/#:~:text=Glucagon%2Dlike%20peptide%2D1%20(,options%20for%20these%20endocrine%20diseases. (2024).
86. Fang, P. *et al*. Glucagon-Like Peptide-1 Receptor Agonist Protects Against Diabetic Cardiomyopathy by Modulating microRNA-29b-3p/SLMAP. *Drug Des Devel Ther* **17**, 791–806 (2023).
87. Beck, A. H. *et al*. Discovery of molecular subtypes in leiomyosarcoma through integrative molecular profiling. *Oncogene* **29**, 845–854 (2010).
88. An, Y. *et al*. Distinct molecular subtypes of uterine leiomyosarcoma respond differently to chemotherapy treatment. *BMC Cancer* **17**, 639 (2017).
89. Mills, A. M. *et al*. Expression of Subtype-Specific Group 1 Leiomyosarcoma Markers in a Wide Variety of Sarcomas by Gene Expression Analysis and Immunohistochemistry. *American Journal of Surgical Pathology* **35**, 583–589 (2011).
90. Alì, G. *et al*. Whole transcriptome targeted gene quantification provides new insights on pulmonary sarcomatoid carcinomas. *Sci Rep* **9**, (2019).
91. Pagan, C. *et al*. Targeting SLMAP-ALK-a novel gene fusion in lung adenocarcinoma. *Cold Spring Harb Mol Case Stud* **5**, (2019).

92. Kongpetch, S. *et al*. Lack of Targetable FGFR2 Fusions in Endemic Fluke-Associated Cholangiocarcinoma. *JCO Glob Oncol* **6**, 628–638 (2020).
93. Park, S. *et al*. Characteristics and Outcome of ROS1-Positive Non–Small Cell Lung Cancer Patients in Routine Clinical Practice. *Journal of Thoracic Oncology* **13**, 1373–1382 (2018).
94. Qaddoumi, I. *et al*. Genetic alterations in uncommon low-grade neuroepithelial tumors: BRAF, FGFR1, and MYB mutations occur at high frequency and align with morphology. *Acta Neuropathol* **131**, 833–845 (2016).
95. Suurmeijer, A. J. H. *et al*. A novel group of spindle cell tumors defined by S100 and CD34 co-expression shows recurrent fusions involving RAF1, BRAF, and NTRK1/2 genes. *Genes Chromosomes Cancer* **57**, 611–621 (2018).
96. Cordier, F. *et al*. RAF1-rearranged Spindle Cell Mesenchymal Tumor With Calcification and Heterotopic Ossification: A Case Report and Review of Literature. *Int J Surg Pathol* **32**, 133–139 (2024).
97. Zhou, P., Liu, W., Zheng, J., Zhang, H. & Luo, J. Case report: Primary sarcoma of the mandible with a novel SLMAP-BRAF fusion. *Front Oncol* **14**, (2024).
98. Suh, J. *et al*. Targeted next-generation sequencing for locally advanced prostate cancer in the Korean population. *Investig Clin Urol* **61**, 127–135 (2020).
99. Geng, Q. *et al*. A Novel Testis-Specific Gene, Ccdc136, Is Required for Acrosome Formation and Fertilization in Mice. *Reproductive Sciences* **23**, 1387–1396 (2016).
100. Brooks, M. J., Rajasimha, H. K., Roger, J. E. & Swaroop, A. Next-generation sequencing facilitates quantitative analysis of wild-type and Nrl(-/-) retinal transcriptomes. *Mol Vis* **17**, 3034–54 (2011).
101. Smiley, S. *et al*. Establishment of a cone photoreceptor transplantation platform based on a novel cone-GFP reporter mouse line. *Sci Rep* **6**, 22867 (2016).
102. Zhang, X.-M. *et al*. Expression of tumor related gene NAG6 in gastric cancer and restriction fragment length polymorphism analysis. *World J Gastroenterol* **10**, 1361 (2004).
103. Xie, F. *et al*. An 8-gene signature predicts the prognosis of cervical cancer following radiotherapy. *Mol Med Rep* **20**, 2990–3002 (2019).
104. Nylund, P. *et al*. PVT1 interacts with polycomb repressive complex 2 to suppress genomic regions with pro-apoptotic and tumour suppressor functions in multiple myeloma. *Haematologica* **109**, 567–577 (2024).
105. Bakke, J. *et al*. Genome-wide CRISPR screen reveals PSMA6 to be an essential gene in pancreatic cancer cells. *BMC Cancer* **19**, (2019).
106. Lu, J. & Chen, Q. Transcriptome-based identification of molecular markers related to the development and prognosis of Colon cancer. *Nucleosides Nucleotides Nucleic Acids* **40**, 1114–1124 (2021).
107. Yasuda, M. *et al*. Identification of a tumour associated antigen in lung cancer patients with asbestos exposure. *Anticancer Res* **30**, 2631–9 (2010).
108. Gialluisi, A. *et al*. Genome-wide screening for DNA variants associated with reading and language traits. *Genes Brain Behav* **13**, 686–701 (2014).
109. Adams, A. K. *et al*. Enrichment of putatively damaging rare variants in the DYX2 locus and the reading-related genes CCDC136 and FLNC. *Hum Genet* **136**, 1395–1405 (2017).
110. Wei, S., Shang, H., Cao, Y. & Wang, Q. The coiled-coil domain containing protein Ccdc136b antagonizes maternal Wnt/β-catenin activity during zebrafish dorsoventral axial patterning. *Journal of Genetics and Genomics* **43**, 431–438 (2016).

111. Dadgostar, H., Doyle, S. E., Shahangian, A., Garcia, D. E. & Cheng, G. T3JAM, a novel protein that specifically interacts with TRAF3 and promotes the activation of JNK. *FEBS Lett* **553**, 403–407 (2003).
112. Peng, S. *et al.* TRAF3IP3, a novel autophagy up-regulated gene, is involved in marginal zone B lymphocyte development and survival. *Clin Exp Immunol* **182**, 57–68 (2015).
113. Zou, Q. *et al.* T cell development involves TRAF3IP3-mediated ERK signaling in the Golgi. *Journal of Experimental Medicine* **212**, 1323–1336 (2015).
114. Quarantotti, V. *et al.* Centriolar satellites are acentriolar assemblies of centrosomal proteins. *EMBO J* **38**, (2019).
115. Zhang, X. *et al.* TRAF3IP3 at the trans-Golgi network regulates NKT2 maturation via the MEK/ERK signaling pathway. *Cell Mol Immunol* **17**, 395–406 (2020).
116. Zhu, W. *et al.* TRAF3IP3 mediates the recruitment of TRAF3 to MAVS for antiviral innate immunity. *EMBO J* **38**, (2019).
117. Zou, Q. *et al.* T cell development involves TRAF3IP3-mediated ERK signaling in the Golgi. *Journal of Experimental Medicine* **212**, 1323–1336 (2015).
118. Li, H. *et al.* TRAF3IP3 Is Cleaved by EV71 3C Protease and Exhibits Antiviral Activity. *Front Microbiol* **13**, (2022).
119. Ma, X. *et al.* Identification of five human novel genes associated with cell proliferation by cell-based screening from an expressed cDNA ORF library. *Life Sci* **81**, 1141–1151 (2007).
120. Bhati, R. *et al.* Molecular characterization of human breast tumor vascular cells. *American Journal of Pathology* **172**, 1381–1390 (2008).
121. Le Faouder, J. *et al.* Proteomic Landscape of Cholangiocarcinomas Reveals Three Different Subgroups According to Their Localization and the Aspect of Non-Tumor Liver. *Proteomics Clin Appl* **13**, (2019).
122. Nasarre, P., Bonilla, I. V., Metcalf, J. S., Hilliard, E. G. & Klauber-Demore, N. TRAF3-interacting protein 3, a new oncotarget, promotes tumor growth in melanoma. *Melanoma Res* **28**, 185–194 (2018).
123. Xie, R., Wen, F. & Qin, Y. The Dysregulation and Prognostic Analysis of STRIPAK Complex Across Cancers. *Front Cell Dev Biol* **8**, (2020).
124. Lin, Q. *et al.* TRAF3IP3 promotes glioma progression through the ERK signaling pathway. *Front Oncol* **12**, (2022).
125. Yang, G., Tang, S., Zhang, J. & Qin, L. High TRAF3IP3 Level Predicts Poor Prognosis of Patients with Gliomas. *World Neurosurg* **148**, e436–e449 (2021).
126. Liu, H. *et al.* Characterization of candidate factors associated with the metastasis and progression of high-grade serous ovarian cancer. *Chin Med J (Engl)* **136**, 2974–2982 (2023).
127. Pommert, L. *et al.* Novel germline TRAF3IP3 mutation in a dyad with familial acute B lymphoblastic leukemia. *Cancer Rep* **4**, (2021).
128. Guo, Y.-J. *et al.* ERK/MAPK signalling pathway and tumorigenesis. *Exp Ther Med* **19**, 1997–2007 (2020).
129. Deng, M. *et al.* TRAF3IP3 negatively regulates cytosolic RNA induced anti-viral signaling by promoting TBK1 K48 ubiquitination. *Nat Commun* **11**, 2193 (2020).
130. Yu, X. *et al.* Metabolic control of regulatory T cell stability and function by TRAF3IP3 at the lysosome. *Journal of Experimental Medicine* **215**, 2463–2476 (2018).
131. Zhou, R., Zhang, Q. & Xu, P. TBK1, a central kinase in innate immune sensing of nucleic acids and beyond. *Acta Biochim Biophys Sin (Shanghai)* **52**, 757–767 (2020).

132. Li, Y. *et al*. TRAF3-interacting JNK-activating modulator promotes inflammation by stimulating translocation of Toll-like receptor 4 to lipid rafts. *Journal of Biological Chemistry* **294**, 2744–2756 (2019).
133. Boada-Romero, E. *et al*. TMEM59 defines a novel ATG16L1-binding motif that promotes local activation of LC3. *EMBO Journal* **32**, 566–582 (2013).
134. Hu, Z. *et al*. Screening of Graves' disease susceptibility genes by whole exome sequencing in a three-generation family. *BMC Med Genomics* **14**, (2021).
135. Li, W. *et al*. The variants in PTPRB, TRAF3IP3, and DISC1 genes were associated with Graves' disease in the Chinese population. *Medicine (United States)* **101**, E31501 (2022).
136. The Human Protein Atlas. SIKE1. https://www.proteinatlas.org/ENSG00000052723-SIKE1/tissue.
137. Huang, J. *et al*. SIKE is an IKKε/TBK1-associated suppressor of TLR3- and virus-triggered IRF-3 activation pathways. *EMBO Journal* **24**, 4018–4028 (2005).
138. Marion, J. D. *et al*. Mechanism of endogenous regulation of the type i interferon response by suppressor of IkB kinase (SIKE), a novel substrate of TANK-binding kinase 1 (TBK1). *Journal of Biological Chemistry* **288**, 18612–18623 (2013).
139. Ito, M. *et al*. Peripheral B Cells May Serve as a Reservoir for Persistent Hepatitis C Virus Infection. *J Innate Immun* **2**, 607–617 (2010).
140. Li, J., Yan, C., Liu, J., Yan, J. & Feng, H. SIKE of black carp is a substrate of TBK1 and suppresses TBK1-mediated antiviral signaling. *Dev Comp Immunol* **90**, 157–164 (2019).
141. Sonnenschein, H. A. *et al*. Suppressor of IKKepsilon forms direct interactions with cytoskeletal proteins, tubulin and α-actinin, linking innate immunity to the cytoskeleton. *FEBS Open Bio* **8**, 1064–1082 (2018).
142. Hsieh, J. Y. *et al*. MiR-146a-5p circuitry uncouples cell proliferation and migration, but not differentiation, in human mesenchymal stem cells. *Nucleic Acids Res* **41**, 9753–9763 (2013).
143. International Mouse Phenotype Consortium. SIKE1. https://www.mousephenotype.org/data/genes/MGI:1913891.
144. The Human Protein Atlas. FGFR1OP2. https://www.proteinatlas.org/ENSG00000111790-FGFR1OP2/tissue.
145. Sukotjo, C., Abanmy, A. A., Ogawa, T. & Nishimura, I. Molecular Cloning of Wound Inducible Transcript (wit 3.0) Differentially Expressed in Edentulous Oral Mucosa Undergoing Tooth Extraction Wound-healing. *J Dent Res* **81**, 229–235 (2002).
146. Sukotjo, C. *et al*. Oral Fibroblast Expression of wound-inducible transcript 3.0 (wit3.0) Accelerates the Collagen Gel Contraction in Vitro. *Journal of Biological Chemistry* **278**, 51527–51534 (2003).
147. Lin, A., Hokugo, A., Choi, J. & Nishimura, I. Small cytoskeleton-associated molecule, fibroblast growth factor receptor 1 oncogene partner 2/wound inducible transcript-3.0 (FGFR1OP2/wit3.0), facilitates fibroblast-driven wound closure. *American Journal of Pathology* **176**, 108–121 (2010).
148. Cheng, W. & Nishimura, I. High Throughput Screening of Biologically Functional Small Molecules for Modulating the Expression of FGFR1OP2/wit3.0 in Fibroblasts. *J Calif Dent Assoc* **40**, 929–937 (2012).
149. Kondo, T., Kanayama, K., Egusa, H. & Nishimura, I. Current perspectives of residual ridge resorption: Pathological activation of oral barrier osteoclasts. *J Prosthodont Res* **67**, JPR_D_21_00333 (2023).

150. Suwanwela, J. *et al*. A Genetic Association Study of Single Nucleotide Polymorphisms in FGFR1OP2/wit3.0 and Long-Term Atrophy of Edentulous Mandible. *PLoS One* **6**, e16204 (2011).
151. Kim, J. H., Oh, M. Y., Paek, J. & Lee, J. Association between FGFR1OP2/wit3.0 Polymorphisms and Residual Ridge Resorption of Mandible in Korean Population. *PLoS One* **7**, e42734 (2012).
152. Alzain, S. *et al*. Significant association of a single nucleotide polymorphism in the upstream region of FGFR1OP2/wit3.0 gene with residual ridge resorption of mandible in Saudis. *BIOCELL* **44**, 55–62 (2020).
153. Grand, E. K. *et al*. Identification of a Novel Gene, FGFR1OP2, Fused to FGFR1 in 8p11 Myeloproliferative Syndrome. *Genes Chromosomes Cancer* **40**, 78–83 (2004).
154. Onozawa, M. *et al*. The 8p11 myeloproliferative syndrome owing to rare FGFR1OP2-FGFR1 fusion. *Eur J Haematol* **86**, 347–349 (2011).
155. Gu, T.-L. *et al*. Phosphotyrosine profiling identifies the KG-1 cell line as a model for the study of FGFR1 fusions in acute myeloid leukemia. *Blood* **108**, 4202–4204 (2006).
156. Jin, Y., Zhen, Y., Haugsten, E. M. & Wiedlocha, A. The driver of malignancy in KG-1a leukemic cells, FGFR1OP2–FGFR1, encodes an HSP90 addicted oncoprotein. *Cell Signal* **23**, 1758–1766 (2011).
157. Qin, H., Wu, Q., Cowell, J. K. & Ren, M. FGFR1OP2-FGFR1 induced myeloid leukemia and T-cell lymphoma in a mouse model. *Haematologica* **101**, e91–e94 (2016).
158. Götz, J., Probst, A., Ehler, E., Hemmings, B. & Kues, W. Delayed embryonic lethality in mice lacking protein phosphatase 2A catalytic subunit Cα. *Proceedings of the National Academy of Sciences* **95**, 12370–12375 (1998).
159. Gu, P., Qi, X., Zhou, Y., Wang, Y. & Gao, X. Generation of Ppp2Ca and Ppp2Cb conditional null alleles in mouse. *genesis* **50**, 429–436 (2012).
160. Zolnierowicz, S. Type 2A protein phosphatase, the complex regulator of numerous signaling pathways. *Biochem Pharmacol* **60**, 1225–1235 (2000).
161. Zolnierowicz, S. & Bollen, M. Protein phosphorylation and protein phosphatasesDe Panne, Belgium, September 19–24, 1999. *EMBO J* **19**, 483–488 (2000).
162. International Mouse Phenotype Consortium. Ppp2cb. https://www.mousephenotype.org/data/genes/MGI:1321161.
163. Ruediger, R., Ruiz, J. & Walter, G. Human Cancer-Associated Mutations in the Aα Subunit of Protein Phosphatase 2A Increase Lung Cancer Incidence in Aα Knock-In and Knockout Mice. *Mol Cell Biol* **31**, 3832–3844 (2011).
164. Lange, L. *et al*. Patterning and gastrulation defects caused by the *tw18* lethal are due to loss of *Ppp2r1a*. *Biol Open* **6**, 752–764 (2017).
165. International Mouse Phenotype Consortium. Ppp2r1b. https://www.mousephenotype.org/data/genes/MGI:1920949.
166. Garza, A. E. *et al*. Variants in Striatin Gene Are Associated With Salt-Sensitive Blood Pressure in Mice and Humans. *Hypertension* **65**, 211–217 (2015).
167. Cull, J. J. *et al*. Striatin plays a major role in angiotensin II-induced cardiomyocyte and cardiac hypertrophy in mice *in vivo*. *Clin Sci* **138**, 573–597 (2024).
168. Mager Lab. Strn3. https://websites.umass.edu/jmager/strn3/.
169. Dickinson, M. E. *et al*. High-throughput discovery of novel developmental phenotypes. *Nature* **537**, 508–514 (2016).

170. International Mouse Phenotype Consortium. Strn3. https://www.mousephenotype.org/data/genes/MGI:2151064.
171. International Mouse Phenotype Consortium. Strn4. https://www.mousephenotype.org/data/genes/MGI:2142346.
172. Bazzi, H., Soroka, E., Alcorn, H. L., Anderson, K. V. & Hogan, B. L. M. STRIP1, a core component of STRIPAK complexes, is essential for normal mesoderm migration in the mouse embryo. *Proc Natl Acad Sci U S A* **114**, E10928–E10936 (2017).
173. International Mouse Phenotype Consortium. Strip2. https://www.mousephenotype.org/data/genes/MGI:2444363.
174. Eden, M. *et al.* Myoscape controls cardiac calcium cycling and contractility via regulation of L-type calcium channel surface expression. *Nat Commun* **7**, 11317 (2016).
175. International Mouse Phenotype Consortium. Mob4. https://www.mousephenotype.org/data/genes/MGI:104899.
176. He, Y. *et al.* Stabilization of VEGFR2 Signaling by Cerebral Cavernous Malformation 3 Is Critical for Vascular Development. *Sci Signal* **3**, (2010).
177. Chan, A. C. *et al.* Mutations in 2 distinct genetic pathways result in cerebral cavernous malformations in mice. *Journal of Clinical Investigation* **121**, 1871–1881 (2011).
178. International Mouse Phenotype Consortium. Traf3ip3. https://www.mousephenotype.org/data/genes/MGI:2441706.
179. International Mouse Phenotype Consortium. Cttnbp2 . https://www.mousephenotype.org/data/genes/MGI:1353467.
180. Shih, P.-Y. *et al.* CTTNBP2 Controls Synaptic Expression of Zinc-Related Autism-Associated Proteins and Regulates Synapse Formation and Autism-like Behaviors. *Cell Rep* **31**, 107700 (2020).
181. International Mouse Phenotype Consortium. Cttnbp2nl. https://www.mousephenotype.org/data/genes/MGI:1933137.
182. Zhang, Y. *et al.* A Network of Interactions Enables CCM3 and STK24 to Coordinate UNC13D-Driven Vesicle Exocytosis in Neutrophils. *Dev Cell* **27**, 215–226 (2013).
183. Sartages, M. *et al.* GCKIII (Germinal Center Kinase III) Kinases STK24 and STK25 (Serine/Threonine Kinase 24 and 25) Inhibit Cavernoma Development. *Stroke* **53**, 976–986 (2022).
184. Lu, T.-J. *et al.* MST3 is involved in ENaC-mediated hypertension. *American Journal of Physiology-Renal Physiology* **317**, F30–F42 (2019).
185. International Mouse Phenotype Consortium. Stk26. https://www.mousephenotype.org/data/genes/MGI:1917665.
186. An, L. *et al.* MST4 kinase suppresses gastric tumorigenesis by limiting YAP activation via a non-canonical pathway. *Journal of Experimental Medicine* **217**, (2020).
187. Caputo, M. *et al.* Genetic Ablation of STE20-Type Kinase MST4 Does Not Alleviate Diet-Induced MASLD Susceptibility in Mice. *Int J Mol Sci* **25**, 2446 (2024).
188. Matsuki, T., Chen, J. & Howell, B. W. Acute inactivation of the serine-threonine kinase Stk25 disrupts neuronal migration. *Neural Dev* **8**, 21 (2013).
189. Amrutkar, M. *et al.* Genetic Disruption of Protein Kinase STK25 Ameliorates Metabolic Defects in a Diet-Induced Type 2 Diabetes Model. *Diabetes* **64**, 2791–2804 (2015).
190. Cansby, E. *et al.* Depletion of protein kinase STK25 ameliorates renal lipotoxicity and protects against diabetic kidney disease. *JCI Insight* **5**, (2020).

191. Cansby, E. *et al.* STK25 Regulates Cardiovascular Disease Progression in a Mouse Model of Hypercholesterolemia. *Arterioscler Thromb Vasc Biol* **38**, 1723–1737 (2018).
192. Oh, S. *et al.* Crucial Role for Mst1 and Mst2 Kinases in Early Embryonic Development of the Mouse. *Mol Cell Biol* **29**, 6309–6320 (2009).
193. Song, H. *et al.* Mammalian Mst1 and Mst2 kinases play essential roles in organ size control and tumor suppression. *Proceedings of the National Academy of Sciences* **107**, 1431–1436 (2010).
194. Zhou, D. *et al.* The Nore1B/Mst1 complex restrains antigen receptor-induced proliferation of naïve T cells. *Proceedings of the National Academy of Sciences* **105**, 20321–20326 (2008).
195. Zhou, D. *et al.* Mst1 and Mst2 Maintain Hepatocyte Quiescence and Suppress Hepatocellular Carcinoma Development through Inactivation of the Yap1 Oncogene. *Cancer Cell* **16**, 425–438 (2009).
196. Katagiri, K. *et al.* Mst1 controls lymphocyte trafficking and interstitial motility within lymph nodes. *EMBO J* **28**, 1319–1331 (2009).
197. Dong, Y. *et al.* A Cell-Intrinsic Role for *Mst1* in Regulating Thymocyte Egress. *The Journal of Immunology* **183**, 3865–3872 (2009).
198. International Mouse Phenotype Consortium. Stk3. https://www.mousephenotype.org/data/genes/MGI:1928487.
199. Xue, Y. *et al.* Mesodermal patterning defect in mice lacking the Ste20 NCK interacting kinase (NIK). *Development* **128**, 1559–1572 (2001).
200. International Mouse Phenotype Consortium. MINK. https://www.mousephenotype.org/data/genes/MGI:1355329.
201. Yue, M. *et al.* Misshapen/NIK-related kinase (MINK1) is involved in platelet function, hemostasis, and thrombus formation. *Blood* **127**, 927–937 (2016).
202. Bonangelino, C. J., Chavez, E. M. & Bonifacino, J. S. Genomic Screen for Vacuolar Protein Sorting Genes in Saccharomyces cerevisiae. *Mol Biol Cell* **13**, 2486–2501 (2002).
203. Pracheil, T. & Liu, Z. Tiered assembly of the yeast Far3-7-8-9-10-11 complex at the endoplasmic reticulum. *Journal of Biological Chemistry* **288**, 16986–16997 (2013).
204. Lisa-Santamari, P., Jiménez, A. & Revuelta, J. L. The protein Factor-arrest 11 (Far11) is essential for the toxicity of human caspase-10 in yeast and participates in the regulation of autophagy and the DNA damage signaling. *Journal of Biological Chemistry* **287**, 29636–29647 (2012).
205. Furukawa, K. *et al.* The PP2A-like Protein Phosphatase Ppg1 and the Far Complex Cooperatively Counteract CK2-Mediated Phosphorylation of Atg32 to Inhibit Mitophagy. *Cell Rep* **23**, 3579–3590 (2018).
206. Innokentev, A. *et al.* Association and dissociation between the mitochondrial far complex and atg32 regulate mitophagy. *Elife* **9**, 1–27 (2020).
207. Niphadkar, S., Karinje, L. & Laxman, S. The PP2A-like phosphatase Ppg1 mediates assembly of the Far complex to balance gluconeogenic outputs and enables adaptation to glucose depletion. *PLoS Genet* **20**, e1011202 (2024).
208. Pracheil, T., Thornton, J. & Liu, Z. TORC2 signaling is antagonized by protein phosphatase 2A and the far complex in saccharomyces cerevisiae. *Genetics* **190**, 1325–1339 (2012).
209. Singh, N. S. *et al.* SIN-inhibitory phosphatase complex promotes Cdc11p dephosphorylation and propagates SIN asymmetry in fission yeast. *Current Biology* **21**, 1968–1978 (2011).

210. Willet, A. H., Ren, L., Turner, L. A. & Gould, K. L. Transient PP2A SIP complex localization to mitotic SPBs for SIN inhibition is mediated solely by the Csc1 FHA domain. *Mol Biol Cell* **35**, (2024).
211. Simonin, A. R., Rasmussen, C. G., Yang, M. & Glass, N. L. Genes encoding a striatin-like protein (ham-3) and a forkhead associated protein (ham-4) are required for hyphal fusion in Neurospora crassa. *Fungal Genetics and Biology* **47**, 855–868 (2010).
212. Dettmann, A. *et al.* HAM-2 and HAM-3 are central for the assembly of the NeurosporaSTRIPAK complex at the nuclear envelope and regulate nuclear accumulation of the MAP kinase MAK-1 in a MAK-2-dependent manner. *Mol Microbiol* **90**, 796–812 (2013).
213. Xiang, Q., Rasmussen, C. & Glass, N. L. The *ham-2* Locus, Encoding a Putative Transmembrane Protein, Is Required for Hyphal Fusion in *Neurospora crassa*. *Genetics* **160**, 169–180 (2002).
214. Fu, C. *et al.* Identification and characterization of genes required for cell-to-cell fusion in neurospora crassa. *Eukaryot Cell* **10**, 1100–1109 (2011).
215. Maerz, S. *et al.* Two NDR kinase-MOB complexes function as distinct modules during septum formation and tip extension in Neurospora crassa. *Mol Microbiol* **74**, 707–723 (2009).
216. Chen, A. *et al.* The STRIPAK complex orchestrates cell wall integrity signalling to govern the fungal development and virulence of Fusarium graminearum. *Mol Plant Pathol* **24**, 1139–1153 (2023).
217. Shim, W.-B. *et al. FSR1* Is Essential for Virulence and Female Fertility in *Fusarium verticillioides* and *F. graminearum*. *Molecular Plant-Microbe Interactions* **19**, 725–733 (2006).
218. Elramli, N. *et al.* Assembly of a heptameric STRIPAK complex is required for coordination of light-dependent multicellular fungal development with secondary metabolism in aspergillus nidulans. *PLoS Genet* **15**, (2019).
219. Wang, C. L., Shim, W. B. & Shaw, B. D. Aspergillus nidulans striatin (StrA) mediates sexual development and localizes to the endoplasmic reticulum. *Fungal Genetics and Biology* **47**, 789–799 (2010).
220. Nordzieke, S. *et al.* A fungal sarcolemmal membrane-associated protein (SLMAP) homolog plays a fundamental role in development and localizes to the nuclear envelope, endoplasmic reticulum, and mitochondria. *Eukaryot Cell* **14**, 345–358 (2015).
221. Bloemendal, S. *et al.* A Mutant Defective in Sexual Development Produces Aseptate Ascogonia. *Eukaryot Cell* **9**, 1856–1866 (2010).
222. Bloemendal, S. *et al.* A homologue of the human STRIPAK complex controls sexual development in fungi. *Mol Microbiol* **84**, 310–323 (2012).
223. Beier, A., Teichert, I., Krisp, C., Wolters, D. A. & Kück, U. Catalytic Subunit 1 of Protein Phosphatase 2A Is a Subunit of the STRIPAK Complex and Governs Fungal Sexual Development. *mBio* **7**, (2016).
224. Märker, R., Blank-Landeshammer, B., Beier-Rosberger, A., Sickmann, A. & Kück, U. Phosphoproteomic analysis of STRIPAK mutants identifies a conserved serine phosphorylation site in PAK kinase CLA4 to be important in fungal sexual development and polarized growth. *Mol Microbiol* **113**, 1053–1069 (2020).
225. Stein, V. *et al.* The STRIPAK signaling complex regulates dephosphorylation of GUL1, an RNA-binding protein that shuttles on endosomes. *PLoS Genet* **16**, (2020).

226. Stein, V., Blank-Landeshammer, B., Märker, R., Sickmann, A. & Kück, U. Targeted Quantification of Phosphorylation Sites Identifies STRIPAK-Dependent Phosphorylation of the Hippo Pathway-Related Kinase SmKIN3. *mBio* **12**, (2021).
227. J. Reschka, E., Nordzieke, S., Valerius, O., Braus, G. H. & Pöggeler, S. A novel STRIPAK complex component mediates hyphal fusion and fruiting-body development in filamentous fungi. *Mol Microbiol* **110**, 513–532 (2018).
228. Pöggeler, S. & Kück, U. A WD40 Repeat Protein Regulates Fungal Cell Differentiation and Can Be Replaced Functionally by the Mammalian Homologue Striatin. *Eukaryot Cell* **3**, 232–240 (2004).
229. Bernhards, Y. & Pöggeler, S. The phocein homologue SmMOB3 is essential for vegetative cell fusion and sexual development in the filamentous ascomycete Sordaria macrospora. *Curr Genet* **57**, 133–149 (2011).
230. Frey, S., Reschka, E. J. & Pöggeler, S. Germinal center kinases SmKIN3 and SmKIN24 are associated with the Sordaria macrospora striatin-interacting phosphatase and kinase (STRIPAK) complex. *PLoS One* **10**, (2015).
231. Radchenko, D., Teichert, I., Pöggeler, S. & Kück, U. A hippo pathway-related GCK controls both sexual and vegetative developmental processes in the Fungus Sordaria macrospora. *Genetics* **210**, 137–153 (2018).
232. Wernet, V., Wäckerle, J. & Fischer, R. The STRIPAK component SipC is involved in morphology and cell-fate determination in the nematode-trapping fungus Duddingtonia flagrans. *Genetics* **220**, (2022).
233. Chen, L. *et al*. A potential hyphal fusion protein complex with an important role in development and virulence interacts with autophagy related proteins in Fusarium pseudograminearum. *J Integr Agric* (2023) doi:10.1016/j.jia.2023.09.005.
234. Islam, K. T., Bond, J. P. & Fakhoury, A. M. FvSTR1, a striatin orthologue in Fusarium virguliforme, is required for asexual development and virulence. *Appl Microbiol Biotechnol* **101**, 6431–6445 (2017).
235. Wang, C. L., Shim, W. B. & Shaw, B. D. The Colletotrichum graminicola striatin orthologue Str1 is necessary for anastomosis and is a virulence factor. *Mol Plant Pathol* **17**, 931–942 (2016).
236. Du, Y. *et al*. A serine/threonine-protein phosphatase PP2A catalytic subunit is essential for asexual development and plant infection in Magnaporthe oryzae. *Curr Genet* **59**, 33–41 (2013).
237. Green, K. A., Becker, Y., Fitzsimons, H. L. & Scott, B. An epichloë festucae homologue of MOB3, a component of the stripak complex, is required for the establishment of a mutualistic symbiotic interaction with Lolium perenne. *Mol Plant Pathol* **17**, 1480–1492 (2016).
238. Zhang, H., Mukherjee, M., Kim, J. E., Yu, W. & Shim, W. B. Fsr1, a striatin homologue, forms an endomembrane-associated complex that regulates virulence in the maize pathogen Fusarium verticillioides. *Mol Plant Pathol* **19**, 812–826 (2018).

Chapter Six – General Discussion and Conclusion

6.1. General Discussion

6.1.1. SLMAP is involved with cardiac cell size and proliferation independent of Hippo

SLMAP3 is a member of the STRIPAK complex[17,18], and initial reports suggested that it is an inhibitor of Hippo pathway by recruiting the kinases MST1/2 to the STRIPAK, where they are dephosphorylated and inactivated, leading to the nuclear translocation of the transcriptional co-activators YAP/TAZ to induce the expression of genes associated with proliferation[28,29]. At the same time, cardiac functions have been proposed for SLMAP, including the organization of the excitation-contraction (E-C) coupling structures[9] and calcium handling[119–121]. SLMAP was also linked to the cardiac channelopathy Brugada Syndrome[122]. To investigate the *in vivo* role of SLMAP3, we generated a mouse model with the specific knockout in cardiac progenitor cells using Nkx2.5-Cre/Flox system, which becomes active around E8.0[123]. The construct designed was to generate a knockout of SLMAP3 specifically by floxing exon 3, while the smaller SLMAP1 and SLMAP2 that are predicted to have start codons at exon 16[124] would not be affected.

We observed that during early embryogenesis, from E9.5 to E16.5, the SLMAP3$^{-/-}$ hearts are smaller, cardiomyocytes have reduced size and the hearts present delayed septation, although postnatally they are comparable to the WTs. There was no changes in hypertrophic program but we observed an increased expression of SLMAP1/2 isoforms relative to SLMAP3 from E9.5 to P0, which may compensate for the lack of SLMAP3 during postnatal development. Indeed, depletion of all SLMAP isoforms in H9C2 cardiomyoblasts reduced cellular proliferation accompanied by cellular senescence. Although we thought that the smaller hearts could be due to an enhanced Hippo signaling, no changes in this pathway were detected in the SLMAP3 depleted hearts or H9C2 cells depleted of SLMAPs, suggesting that the role of SLMAP during cardiac development is independent of this signaling.

6.1.2. SLMAP3 is important to organize MTOC at the NE for myogenesis

We generated a mouse model with the global knockout of SLMAP3 using the CMV-Cre/Flox system that presented embryonic/neonatal lethality and stunted growth characteristics. Based on the literature, we expected an enhanced Hippo signaling that could explain the phenotypes observed, but we did not find any changes in this pathway. Thus, to elucidate potential mechanisms for these abnormalities, we conducted a RNA-seq analysis with samples from E11.5 embryo and found that the top genes downregulated were associated with skeletal muscle development. To investigate this further, we used CRISPR/Cas9 to generate C2C12 myoblasts null for SLMAP3. Consistently with our RNA-seq date, the differentiation markers MyoD, MyoG and MHC, and myoblast fusion were all markedly reduced due to SLMAP3 loss. At the same time, our immunoprecipitation followed by mass spectrometry (IP-MS) analysis identified SLMAP3 interaction with centrosomal proteins, including AKAP9, pericentrin, Kinesin-1 subunits and PCM1. This was consistent with our previous finding that SLMAP3 is a centrosomal component[5], a function that might be evolutionary conserved[12].

Considering the differentiation defects in SLMAP3$^{-/-}$ myoblasts and its association with the centrosome, we hypothesized that the shift of the MTOC from the centrosome to the nuclear envelope of differentiating myoblasts could be impaired in the absence of SLMAP3, and this could be linked to the differentiation defects. Suppression of AKAP6 and Kinesin-1 leads to defective differentiation and myotube formation[69,125], and SLMAP3 could have a function similar to them. Indeed, we observed that the recruitment of pericentrin, AKAP6 and Kif5b, the heavy subunit of Kinesin-1, to the nuclear envelope of MHC+ SLMAP3$^{-/-}$ myoblasts was reduced. In addition, the protein expression of AKAP6 and Kif5b was not changing, indicating that their absence in the nuclear envelope is due to defective recruitment rather than reduced expression. Further,

microtubule nucleation assay in differentiated myoblasts showed reduced microtubule formation in the nuclear envelope of cells lacking SLMAP3.

A consequence of defective MTOC formation in the nuclear envelope during myogenesis is aberrant positioning of the nuclei[66–68,71,126,127]. Indeed, nuclear clustering in the myofibers of SLMAP3$^{-/-}$ embryos was observed, accompanied by reduced distance between nuclei. The pericentrin staining in the nuclear envelope in SLMAP3$^{-/-}$ muscle *in vivo* was also decreased, in accordance with our findings in cultured myoblasts.

6.1.3. Regulated expression of SLMAP3 is required for nuclear envelope organization in myoblasts

Another phenotype in C2C12 cells lacking SLMAP3 was cellular senescence, which was similar to what we observed in H9C2 cardiomyoblasts. C2C12 myoblasts were found to express only SLMAP3 isoform, and we used two different sgRNA to target exon 3, with the knockout mediated by Cas9, whereas in H9C2 cells we used two different shRNAs targeting sequences corresponding to the C-terminus regions of SLMAP to deplete all three isoforms expressed by these cells. The cellular senescence observed was specific for myoblasts, since MEFs isolated from SLMAP3$^{-/-}$ embryos and NE-4C cells with SLMAP depletion with the same shRNAs used in H9C2[128] did not exhibit any changes in cell cycle dynamics.

Given that SLMAP also localizes in the nuclear envelope[11] and considering the defective MTOC formation in this structure in myoblasts lacking SLMAP3, we believe that the senescence observed may be due to the disturbances in the nuclear envelope. Mutations in Lamin A/C can impact the mechanical properties of the NE, and influence chromatin structure and stability, which can trigger the cellular senescence response[129,130]. Indeed, we found subtle changes in Lamin A/C,

Nesprin-1 (a LINC member) and Lamin B1 in SLMAP3$^{-/-}$ C2C12 cells. Also, in our previous study with overexpression of SLMAP3 in NIH-3T3, cells showed reduced proliferation with increased peak of cells in G2/M phase in the cell cycle assay with propidium iodide staining[5]. Now we know that such an increase was probably due to multinucleated cells, since the overexpression of SLMAP3 in C2C12 cells disrupts the nuclear structure (**Figure 1**).

Another consequence of disturbances in the nuclear envelope is changes in the heterochromatin, which ultimately leads to changes in gene expression. This is exemplified with mutations in Lamin that affect muscle differentiation[131–135]. It is plausible that the disturbances in the nuclear envelope of myoblasts lacking SLMAP3 could potentially explain the defective myogenic program through heterochromatin dynamics, although this requires further investigation. Future studies addressing the distribution of SLMAP3 in the nuclear envelope and how it may impact its structure leading to cellular senescence and changes in gene expression in myoblasts would contribute to the understanding of SLMAP3 functions in a tissue specific fashion. It would be interesting to investigate if SLMAP3 is present in the inner nuclear envelope membrane by assessing possible interactions with chromatin and/or with LEM domain containing proteins, such as emerin, LAP2 and LEMD1, which are also C-terminus transmembrane proteins and regulate heterochromatin, genome stability and gene expression in cooperation with lamins[136].

6.1.4. SLMAP3 has functions involving PCP and primary cilium

Although we observed defective formation of the MTOC in the nuclear envelope of SLMAP3$^{-/-}$ myoblasts, our microtubule nucleation assay in undifferentiated cells did not indicate any reduction in microtubule formation from the centrosome. We also performed the same experiments in MEFs derived from SLMAP3$^{-/-}$ embryos and did not find any changes. In these

MEFs we did not find an increase in the number of centrosomes either, which is contrary to what was reported in SLMAP depleted HeLa cells[21].

A detailed analysis of the phenotypes in SLMAP3$^{-/-}$ embryos revealed that besides the smaller size, they presented reduced limbs and tails, abnormal face morphology and in some cases craniorachischisis. The animals that are born alive display cyanosis and respiratory distress, ultimately leading to their death. Histological analysis showed that this is due to underdeveloped lungs, with impaired alveolar sacs formation. Further, we found that these animals have fused skeleton, disoriented chondrocytes, short intestines and polycystic kidneys. All these phenotypes together are indicative of defects in PCP. Indeed, we identified a significant reduction in protein expression of DVL3, which is a PCP member. This was intriguing, since disturbances of primary cilium components impacts the expression of DVL proteins[109–112].

Although we could not detect changes in PCP pathway in SLMAP3$^{-/-}$ MEFs by assessing activation of DVL3, ROCK2 and JNK1/2 upon Wnt5a treatment, nor did we see changes in cell orientation during migration and cell division, we did detect reduced primary cilium length and decreased number of ciliated MEFs lacking SLMAP3. Interestingly, we found that MEFs depleted of FGFR1OP2 showed reduced protein levels of SLMAP3, and decrease in primary cilium length and reduced number of ciliated cells, without changes in polarization during migration or cell division, similar to what we observed with SLMAP3 depletion. Although the measurement of number of ciliated cells in tissues is challenging, we detected a small but significant change in primary cilium length of SLMAP3$^{-/-}$ chondrocytes. Further, MEFs analyzed were isolated from E14.5 SLMAP3$^{-/-}$ embryos, thus being representative of sampling in these mice. It is worth noting that depletion of the SLMAP paralog TRAF3IP3 in lymphocytes also reduced the number of

ciliated cells [107]. Altogether, these findings suggest that SLMAP3 could have functions in the primary cilium, explaining the phenotypes observed in SLMAP3$^{-/-}$ embryos.

An interesting finding in both SLMAP3$^{-/-}$ embryos and MEFs was depleted protein levels of DVL3, but without changes in its activation status, as observed in mobility shift assays of DVL3 from lysates of cells treated with Wnt5a. Interestingly, we found that DVL3 was being specifically degraded by the lysosomal pathway, but it does not interact with SLMAP3, so it seems that SLMAP3 protects DVL3 from lysosomal degradation by an indirect mechanism. Mutations in DVL3 are associated with Robinow Syndrome, a condition characterized by short limbs, broad and prominent forehead, orbital hypertelorism, depressed nose and ambiguous genitalia [137,138], phenotypes that are like those observed in SLMAP3$^{-/-}$ mice. However, heterozygous DVL3$^{+/-}$ mice are viable[139], so the sole depletion of DVL3 in SLMAP3$^{-/-}$ animals might not be enough to explain the phenotypes observed. Nonetheless, it provides a lead for future investigation on how SLMAP3 may function with PCP components.

Overall, we showed that SLMAP3 is crucial for organ development, acting at the level of PCP/primary cilium. Therefore, it could be considered as a biomarker candidate for abnormal embryonic development when its expression is compromised. Genetic analysis such as mining of sequencing data from patients with phenotypes similar to what we observed in our SLMAP3$^{-/-}$ mice may link SLMAP to human developmental disorders.

6.1.5. SIKE1 and FGFR1OP2/Wit3.0 are adaptors of SLMAP3

SIKE1 and FGFR1OP2 are paralog proteins with functions poorly understood. SIKE1 was shown to interact with STRN3 to bridge SLMAP3 to the STRIPAK[10]. We observed in a previous

study that depletion of SLMAP3 or SIKE1 decreased the protein levels of each other[10]. In fact, every tissue we analyzed with depleted SLMAP3 had reduced SIKE1 proteins, which was not due to transcriptional mechanisms, but we found that SLMAP3 is important for SIKE1 stability by preventing its degradation through the proteosome. Surprisingly, the knockout of SIKE1 results in viable animals[43]. Then we wondered about the relationship of SLMAP3 with FGFR1OP2, as the latter could compensate for the lack of SIKE1 during the embryonic development. The functions of FGFR1OP2 are even less known than of SIKE1, as it has been mainly associated with oral wound closure[46–48] and myeloproliferative syndrome due a fusion with FGFR1 receptor[49–51]. Still, the knockout of FGFR1OP2 in mice causes lethality, with phenotypes resembling the ones observed in SLMA3$^{-/-}$ animals, such as reduced body size, short limbs and tails and abnormal cell morphology[45]. FGFR1OP2$^{-/-}$ also reduces protein levels of SLMAP3, suggesting that it is important for its stability, although we could not identify the mechanism for that. These findings suggest that FGFR1OP2 is as important for embryogenesis as is SLMAP3, and they should be considered together in future studies when addressing the links between SLMAP3 and PCP/primary cilium/MTOC.

6.1.6. SLMAP3 regulates cell morphology by mechanisms that differ from STRIPAK components

One of the changes that we observed in SLMAP3$^{-/-}$ MEFs was in cell morphology, with cells appearing rounder and with reduced axis length. *In vivo*, changes in cell morphology were also noted in SLMAP3$^{-/-}$ cardiomyocytes from Nkx2.5-Cre mice. STRIPAK has been associated with cytoskeleton by regulating ERM (ezrin, radixin and moesin), proteins that connect the cell cortex to the F-actin cytoskeleton, which helps to dictate cell shape [140]. MST3/4 and MAP4K4

were shown to induce the phosphorylation and activation of ERM[31,141–143], with STRIP1 and STRN3 antagonizing MST3/4 in this function[31]. STRIPAK is also involved with focal adhesion (FA) regulation, as it was the case for MAP4K4[143,144], CCM3 [145] and STRIP1[146], which ultimately leads to changes in cell morphology. We have assessed the cortical F-actin and FAs in SLMAP3$^{-/-}$ MEFs, however we could not find significant differences, suggesting that SLMAP3 might regulate the cytoskeleton by mechanisms different than the ones proposed for STRIPAK.

The changes in cell morphology in SLMAP3$^{-/-}$ could be linked to primary cilium and the PCP transducers regulating F-actin cytoskeleton. Kidney epithelial cystic cells from a patient with mutation in *pkd1*, gene that encodes for the ciliary protein PC1, displayed reduced number of ciliated cells and cilium length, and actin cytoskeleton abnormalities. Authors attributed this partially to an increased activity of RhoA in the centrosome due to reduced recruitment of Arhgap35 to this organelle, leading to enhanced actin polymerization[147]. Another example was MEFs with the knockout of the ciliary protein NHPH2/inversin, which resulted in smaller cells and rounder shape[148]. These cells fail to form lamellipodia, although filopodia is not affected, and have increased activity of the small GTPases Rhoa, Rac1 and CCDC42, while the targeting of Rhoa and Rac1 was reduced at the migratory leading edge, which could explain the cell morphology changes[148]. Finally, the centrosome itself could regulate F-actin cytoskeleton, as it has been proposed to be an actin-organizing center[149]. Future studies investigating the activities of RhoA, Rac1 and CCDC42 globally and in distinct regions, such as the centrosome or cell periphery, in SLMAP3 deficiency would shed light into possible mechanism of how it can impact the cytoskeleton.

6.1.7. Additional functions of SLMAP3

Although in this project we used knockout mice models to investigate SLMAP3 functions, it is worth noting that SLMAP3 has been linked to pathological conditions other than defective embryogenesis, including diabetes, cancer and cardiac related disorders. Patients with diabetic retinopathy were found to carry single nucleotide polymorphism in SLMAP[150,151]; SLMAP has been linked to glucose handling[152] and found upregulated in a mouse model with diabetic cardiomyopathy [153]. In cancer, SLMAP was found fused with receptor tyrosine kinases[154–157], and so was its interactor FGFR1OP2[49–51]. The SLMAP paralogs TRAF3IP3/T3JAM and CCDC136/NAG6 have also been associated with cancer[158–169]. Upregulation of SLMAP was detected in hypertrophic ventricle of mice that were induced to develop congestive heart failure[170], though its expression was found reduced in patients with dilated cardiomyopathy[121]. Further, a SLMAP variant was linked to Brugada syndrome[122]. These studies point to additional roles of SLMAP not involved in development.

Another possible function of SLMAP3 might involve the regulation of TBK1 kinase. The first investigations of SIKE1 described it as an inhibitor of this kinase[39,40], and TRAF3IP3/T3JAM was shown to regulate TBK1 by different mechanisms[171–173]. In fact, recently it was reported that activation of TBK1 leads to increased association of SLMAP3 and SIKE1 to the STRIPAK[174]. Future studies addressing this association of SLMAP3 with TBK1 in the context of cardiac hypertrophy[41], innate immune response[171–173] and DNA damage[174] will contribute to the elucidation of not only its function, but also of SIKE1 and TRAF3IP3.

6.1.8. Models of SLMAP3 functions in organogenesis

The ability of SLMAP3 to target subcellular organelles including the NE, and to reside in the versatile signaling complex STRIPAK suggest that it may serve to connect events at membranes with gene programming in the nucleus, as exemplified in developing muscle. The localization of SLMAP3 in the centrosome and my findings that it impacts the MTOC, PCP and primary cilia to govern organogenesis is modeled in **Figure 2**.

6.2. Conclusion

I investigated the *in vivo* functions of SLMAP3 using mice and primary cell culture and found that is critical for embryonic development and organogenesis. I found no changes in Hippo signaling, but discovered that SLMAP3 is crucial for the formation of NE-MTOC, which is required for the differentiation of myoblasts and myofiber development. Further, my data indicates that SLMAP3 impact PCP components, primary cilium and cell dynamics to guide embryonic development and organogenesis.

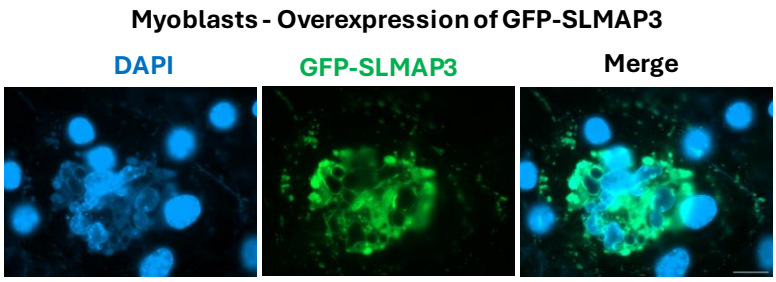

Figure 1. Ectopic expression of GFP-SLMAP3 in C2C12 myoblasts for 72 hours. The excess of SLMAP3 in myoblasts disrupts the nucleus. Scale bar 20 µm.

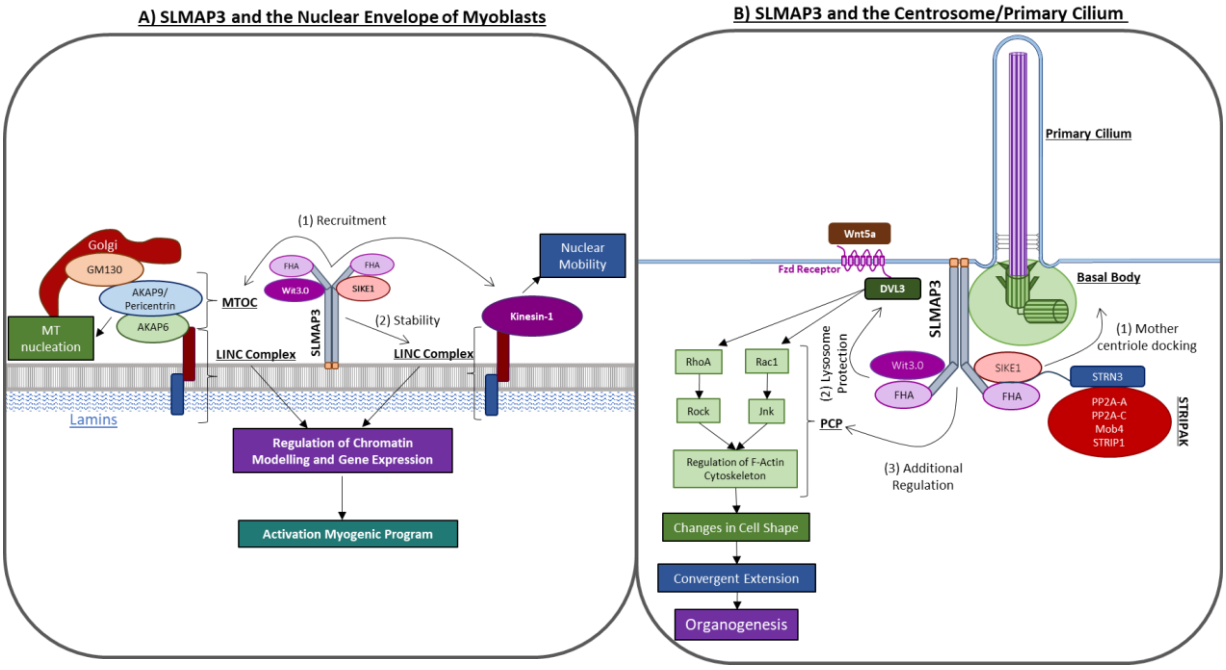

Figure 2. Proposed mechanisms for SLMAP3 action during organogenesis. **A)** In differentiating myoblasts, (1) SLMAP3 is required for the recruitment of MTOC proteins, such as pericentrin, and AKAP6 and Kinesin-1. The MTOC in the nuclear envelope allows the nucleation of microtubules (MTs), and Kinesin-1 can use those as rail to allow nuclear trafficking. (2) Depletion or overexpression of SLMAP3 disrupts the nuclear envelope, which can impair the myogenic program. Model designed considering[62,66,70,71]. **B)** In the centrosome, (1) SLMAP3 could serve in docking of the mother centriole to the cell surface to allow primary cilium formation. (2) SLMAP3 also protects DVL3 from lysosomal degradation. (3) SLMAP3 could have additional mechanisms to affect PCP. All these processes, with a possible involvement of STRIPAK, lead to the modelling of F-actin cytoskeleton and polarization, allowing cells to engage in convergent extension for organogenesis. Model designed considering[10,89,90,110,112,148,175].

Chapter Seven – References

7. References

1. Dias, A. P., Rehmani, T., Salih, M. & Tuana, B. Tail Anchored Membrane Protein SLMAP3 is Essential for Targeting Centrosomal Proteins to the Nuclear Envelope in Skeletal Myogenesis. *Open Biol* **14**, 240094 (2024).
2. Dias, A. P., Rehmani, T., Applin, B. D., Salih, M. & Tuana, B. SLMAP3 is crucial for organogenesis through mechanisms involving primary cilia formation - Submitted. *Open Biol* **14**, 240206 (2024). (doi:10.1098/rsob.240206)
3. Rehmani, T., Dias, A. P., Kamal, M., Salih, M. & Tuana, B. S. Deletion of Sarcolemmal Membrane-Associated Protein Isoform 3 (SLMAP3) in Cardiac Progenitors Delays Embryonic Growth of Myocardium without Affecting Hippo Pathway. *Int J Mol Sci* **25**, 2888 (2024).
4. Dias, A. P. & Tuana, B. SLMAP, Paralogs and Adaptors: Roles in Homeostasis, Physiology and Diseases. (2024).
5. Guzzo, R. M., Sevinc, S., Salih, M. & Tuana, B. S. A novel isoform of sarcolemmal membrane-associated protein (SLMAP) is a component of the microtubule organizing centre. *J Cell Sci* **117**, 2271–2281 (2004).
6. Wigle, J. T. *et al.* Molecular Cloning, Expression, and Chromosomal Assignment of Sarcolemmal-associated Proteins. *Journal of Biological Chemistry* **272**, 32384–32392 (1997).
7. Wielowieyski, P. A. *et al.* Alternative splicing, expression, and genomic structure of the 3′ region of the gene encoding the sarcolemmal-associated proteins (SLAPs) defines a novel class of coiled-coil tail-anchored membrane proteins. *Journal of Biological Chemistry* **275**, 38474–38481 (2000).
8. Rehmani, T., Mlynarova, J., Byers, J., Salih, M. & Tuana, B. S. Specific Deletion of the FHA Domain Containing SLMAP3 Isoform in Postnatal Myocardium Has No Impact on Structure or Function. *Cardiogenetics* **11**, 164–184 (2021).
9. Guzzo, R. M., Salih, M., Moore, E. D. & Tuana, B. S. Molecular properties of cardiac tail-anchored membrane protein SLMAP are consistent with structural role in arrangement of excitation-contraction coupling apparatus. *American Journal of Physiology-Heart and Circulatory Physiology* **288**, H1810–H1819 (2005).
10. Tang, Y. *et al.* Architecture, substructures, and dynamic assembly of STRIPAK complexes in Hippo signaling. *Cell Discov* **5**, (2019).
11. Byers, J. T., Guzzo, R. M., Salih, M. & Tuana, B. S. Hydrophobic profiles of the tail anchors in SLMAP dictate subcellular targeting. *BMC Cell Biol* **10**, (2009).
12. Willet, A. H., Ren, L., Turner, L. A. & Gould, K. L. Transient PP2A SIP complex localization to mitotic SPBs for SIN inhibition is mediated solely by the Csc1 FHA domain. *Mol Biol Cell* **35**, (2024).
13. Durocher, D. *et al.* The Molecular Basis of FHA Domain:Phosphopeptide Binding Specificity and Implications for Phospho-Dependent Signaling Mechanisms. *Mol Cell* **6**, 1169–1182 (2000).
14. Durocher, D. & Jackson, S. P. The FHA domain. *FEBS Lett* **513**, 58–66 (2002).
15. SMART. http://smart.embl-heidelberg.de/help/smart_about.shtml.
16. Schultz, J., Copley, R. R., Doerks, T., Ponting, C. P. & Bork, P. SMART: a web-based tool for the study of genetically mobile domains. *Nucleic Acids Res* **28**, 231–4 (2000).

17. Goudreault, M. *et al.* A PP2A phosphatase high density interaction network identifies a novel striatin-interacting phosphatase and kinase complex linked to the cerebral cavernous malformation 3 (CCM3) protein. *Molecular and Cellular Proteomics* **8**, 157–171 (2009).
18. Glatter, T., Wepf, A., Aebersold, R. & Gstaiger, M. An integrated workflow for charting the human interaction proteome: insights into the PP2A system. *Mol Syst Biol* **5**, (2009).
19. Kemp, H. A. & Sprague, G. F. Far3 and Five Interacting Proteins Prevent Premature Recovery from Pheromone Arrest in the Budding Yeast Saccharomyces cerevisiae . *Mol Cell Biol* **23**, 1750–1763 (2003).
20. Kück, U., Radchenko, D. & Teichert, I. STRIPAK, a highly conserved signaling complex, controls multiple eukaryotic cellular and developmental processes and is linked with human diseases. *Biol Chem* **400**, 1005–1022 (2019).
21. Frost, A. *et al.* Functional repurposing revealed by comparing S. pombe and S. cerevisiae genetic interactions. *Cell* **149**, 1339–1352 (2012).
22. Hyodo, T. *et al.* Misshapen-like kinase 1 (MINK1) is a novel component of striatin-interacting phosphatase and kinase (STRIPAK) and is required for the completion of cytokinesis. *Journal of Biological Chemistry* **287**, 25019–25029 (2012).
23. Herzog, F. *et al.* Structural Probing of a Protein Phosphatase 2A Network by Chemical Cross-Linking and Mass Spectrometry. *Science (1979)* **337**, 1348–1352 (2012).
24. Hauri, S. *et al.* Interaction proteome of human Hippo signaling: Modular control of the co-activator YAP1. *Mol Syst Biol* **9**, (2013).
25. Couzens, A. L. *et al.* Protein Interaction Network of the Mammalian Hippo Pathway Reveals Mechanisms of Kinase-Phosphatase Interactions. *Sci Signal* **6**, (2013).
26. Seo, G. *et al.* MAP4K Interactome Reveals STRN4 as a Key STRIPAK Complex Component in Hippo Pathway Regulation. *Cell Rep* **32**, (2020).
27. Ribeiro, P. S. *et al.* Combined Functional Genomic and Proteomic Approaches Identify a PP2A Complex as a Negative Regulator of Hippo Signaling. *Mol Cell* **39**, 521–534 (2010).
28. Zheng, Y. *et al.* Homeostatic Control of Hpo/MST Kinase Activity through Autophosphorylation-Dependent Recruitment of the STRIPAK PP2A Phosphatase Complex. *Cell Rep* **21**, 3612–3623 (2017).
29. Bae, S. J. *et al.* SAV1 promotes Hippo kinase activation through antagonizing the PP2A phosphatase STRIPAK. *Elife* **6**, (2017).
30. Kean, M. J. *et al.* Structure-function analysis of core STRIPAK proteins: A signaling complex implicated in Golgi polarization. *Journal of Biological Chemistry* **286**, 25065–25075 (2011).
31. Madsen, C. D. *et al.* STRIPAK components determine mode of cancer cell migration and metastasis. *Nat Cell Biol* **17**, 68–80 (2015).
32. Ma, S., Meng, Z., Chen, R. & Guan, K.-L. The Hippo Pathway: Biology and Pathophysiology. *Annu Rev Biochem* **88**, 577–604 (2019).
33. Huang, J., Wu, S., Barrera, J., Matthews, K. & Pan, D. The Hippo signaling pathway coordinately regulates cell proliferation and apoptosis by inactivating Yorkie, the Drosophila homolog of YAP. *Cell* **122**, 421–434 (2005).
34. Justice, R. W., Zilian, O., Woods, D. F., Noll, M. & Bryant, P. J. The Drosophila tumor suppressor gene warts encodes a homolog of human myotonic dystrophy kinase and is required for the control of cell shape and proliferation. *Genes Dev* **9**, 534–546 (1995).
35. Song, H. *et al.* Mammalian Mst1 and Mst2 kinases play essential roles in organ size control and tumor suppression. *Proc Natl Acad Sci U S A* **107**, 1431–1436 (2010).

36. Zhou, D. *et al*. Mst1 and Mst2 Maintain Hepatocyte Quiescence and Suppress Hepatocellular Carcinoma Development through Inactivation of the Yap1 Oncogene. *Cancer Cell* **16**, 425–438 (2009).
37. Neal, S. J., Zhou, Q. & Pignoni, F. STRIPAK–PP2A regulates Hippo-Yorkie signaling to suppress retinal fate in the Drosophila eye disc peripodial epithelium. *J Cell Sci* **133**, (2020).
38. Kaya-çopur, A. *et al*. The hippo pathway controls myofibril assembly and muscle fiber growth by regulating sarcomeric gene expression. *Elife* **10**, 1–34 (2021).
39. Huang, J. *et al*. SIKE is an IKKε/TBK1-associated suppressor of TLR3- and virus-triggered IRF-3 activation pathways. *EMBO Journal* **24**, 4018–4028 (2005).
40. Marion, J. D. *et al*. Mechanism of endogenous regulation of the type i interferon response by suppressor of IkB kinase (SIKE), a novel substrate of TANK-binding kinase 1 (TBK1). *Journal of Biological Chemistry* **288**, 18612–18623 (2013).
41. Deng, K. Q. *et al*. Suppressor of IKKIε is an essential negative regulator of pathological cardiac hypertrophy. *Nat Commun* **7**, (2016).
42. The Human Protein Atlas. SIKE1. https://www.proteinatlas.org/ENSG00000052723-SIKE1/tissue.
43. International Mouse Phenotype Consortium. SIKE1. https://www.mousephenotype.org/data/genes/MGI:1913891.
44. The Human Protein Atlas. FGFR1OP2. https://www.proteinatlas.org/ENSG00000111790-FGFR1OP2/tissue.
45. International Mouse Phenotype Consortium. FGFR1OP2. https://www.mousephenotype.org/data/genes/MGI:1914779.
46. Sukotjo, C., Abanmy, A. A., Ogawa, T. & Nishimura, I. Molecular Cloning of Wound Inducible Transcript (wit 3.0) Differentially Expressed in Edentulous Oral Mucosa Undergoing Tooth Extraction Wound-healing. *J Dent Res* **81**, 229–235 (2002).
47. Sukotjo, C. *et al*. Oral Fibroblast Expression of wound-inducible transcript 3.0 (wit3.0) Accelerates the Collagen Gel Contraction in Vitro. *Journal of Biological Chemistry* **278**, 51527–51534 (2003).
48. Lin, A., Hokugo, A., Choi, J. & Nishimura, I. Small cytoskeleton-associated molecule, fibroblast growth factor receptor 1 oncogene partner 2/wound inducible transcript-3.0 (FGFR1OP2/wit3.0), facilitates fibroblast-driven wound closure. *American Journal of Pathology* **176**, 108–121 (2010).
49. Grand, E. K. *et al*. Identification of a Novel Gene, FGFR1OP2, Fused to FGFR1 in 8p11 Myeloproliferative Syndrome. *Genes Chromosomes Cancer* **40**, 78–83 (2004).
50. Onozawa, M. *et al*. The 8p11 myeloproliferative syndrome owing to rare FGFR1OP2-FGFR1 fusion. *Eur J Haematol* **86**, 347–349 (2011).
51. Gu, T.-L. *et al*. Phosphotyrosine profiling identifies the KG-1 cell line as a model for the study of FGFR1 fusions in acute myeloid leukemia. *Blood* **108**, 4202–4204 (2006).
52. Sanchez, A. D. & Feldman, J. L. Microtubule-organizing centers: from the centrosome to non-centrosomal sites. *Curr Opin Cell Biol* **44**, 93–101 (2017).
53. Lüders, J. Nucleating microtubules in neurons: Challenges and solutions. *Dev Neurobiol* **81**, 273–283 (2021).
54. Ralston, E. Changes in architecture of the Golgi complex and other subcellular organelles during myogenesis. *J Cell Biol* **120**, 399–409 (1993).
55. Tassin, A. M., Maro, B. & Bornens, M. Fate of microtubule-organizing centers during myogenesis in vitro. *J Cell Biol* **100**, 35–46 (1985).

56. Tassin, A. M., Paintrand, M., Berger, E. G. & Bornens, M. The Golgi apparatus remains associated with microtubule organizing centers during myogenesis. *J Cell Biol* **101**, 630–638 (1985).
57. Bugnard, E., Zaal, K. J. M. & Ralston, E. Reorganization of microtubule nucleation during muscle differentiation. *Cell Motil Cytoskeleton* **60**, 1–13 (2005).
58. Becker, R., Leone, M. & Engel, F. Microtubule Organization in Striated Muscle Cells. *Cells* **9**, 1395 (2020).
59. Starr, D. A. Muscle Development: Nucleating Microtubules at the Nuclear Envelope. *Current Biology* **27**, R1071–R1073 (2017).
60. Bonne, G., Leturcq, F. & Ben Yaou, R. *Emery-Dreifuss Muscular Dystrophy*. (1993).
61. Heller, S. A., Shih, R., Kalra, R. & Kang, P. B. Emery-Dreifuss muscular dystrophy. *Muscle Nerve* **61**, 436–448 (2020).
62. Méjat, A. LINC complexes in health and disease. *Nucleus* **1**, 40–52 (2010).
63. Storey, E. C., Holt, I., Morris, G. E. & Fuller, H. R. Muscle cell differentiation and development pathway defects in Emery-Dreifuss muscular dystrophy. *Neuromuscular Disorders* **30**, 443–456 (2020).
64. Reumers, S. F. I. *et al.* Clinical, genetic, and histological features of centronuclear myopathy in the Netherlands. *Clin Genet* **100**, 692–702 (2021).
65. Espigat-Georger, A., Dyachuk, V., Chemin, C., Emorine, L. & Merdes, A. Nuclear alignment in myotubes requires centrosome proteins recruited by nesprin-1. *J Cell Sci* **129**, 4227–4237 (2016).
66. Gimpel, P. *et al.* Nesprin-1α-Dependent Microtubule Nucleation from the Nuclear Envelope via Akap450 Is Necessary for Nuclear Positioning in Muscle Cells. *Current Biology* **27**, 2999-3009.e9 (2017).
67. Wilson, M. H. & Holzbaur, E. L. F. Nesprins anchor kinesin-1 motors to the nucleus to drive nuclear distribution in muscle cells. *Development* **142**, 218–228 (2015).
68. Wilson, M. H. & Holzbaur, E. L. F. Opposing microtubule motors drive robust nuclear dynamics in developing muscle cells. *J Cell Sci* **125**, 4158–4169 (2012).
69. Zhou, C. *et al.* Novel nesprin-1 mutations associated with dilated cardiomyopathy cause nuclear envelope disruption and defects in myogenesis. *Hum Mol Genet* **26**, 2258–2276 (2017).
70. Vergarajauregui, S. *et al.* AKAP6 orchestrates the nuclear envelope microtubule-organizing center by linking golgi and nucleus via AKAP9. *Elife* **9**, (2020).
71. Becker, R. *et al.* Myogenin controls via AKAP6 non-centrosomal microtubule-organizing center formation at the nuclear envelope. *Elife* **10**, (2021).
72. Pare, G. C., Easlick, J. L., Mislow, J. M., McNally, E. M. & Kapiloff, M. S. Nesprin-1α contributes to the targeting of mAKAP to the cardiac myocyte nuclear envelope. *Exp Cell Res* **303**, 388–399 (2005).
73. Takahashi, M., Yamagiwa, A., Nishimura, T., Mukai, H. & Ono, Y. Centrosomal Proteins CG-NAP and Kendrin Provide Microtubule Nucleation Sites by Anchoring γ-Tubulin Ring Complex. *Mol Biol Cell* **13**, 3235–3245 (2002).
74. Srsen, V., Fant, X., Heald, R., Rabouille, C. & Merdes, A. Centrosome proteins form an insoluble perinuclear matrix during muscle cell differentiation. *BMC Cell Biol* **10**, 28 (2009).

75. Odabasi, E., Batman, U. & Firat-Karalar, E. N. Unraveling the mysteries of centriolar satellites: time to rewrite the textbooks about the centrosome/cilium complex. *Mol Biol Cell* **31**, 866–872 (2020).
76. Lu, Z., Joseph, D., Bugnard, E., Zaal, K. J. M. & Ralston, E. Golgi Complex Reorganization during Muscle Differentiation: Visualization in Living Cells and Mechanism. *Mol Biol Cell* **12**, 795–808 (2001).
77. Zaal, K. J. M. *et al*. Who Needs Microtubules? Myogenic Reorganization of MTOC, Golgi Complex and ER Exit Sites Persists Despite Lack of Normal Microtubule Tracks. *PLoS One* **6**, e29057 (2011).
78. Giacomello, E., Ronchi, P. & Pepperkok, R. GM130 and p115 play a key role in the organisation of the early secretory pathway during skeletal muscle differentiation. *J Cell Sci* **132**, (2019).
79. Oddoux, S. *et al*. Microtubules that form the stationary lattice of muscle fibers are dynamic and nucleated at Golgi elements. *Journal of Cell Biology* **203**, 205–213 (2013).
80. Ide, K., Muko, M. & Hayashi, K. The Golgi apparatus is the main microtubule-organizing center in differentiating skeletal muscle cells. *Histochem Cell Biol* **156**, 273–281 (2021).
81. Devenport, D. The cell biology of planar cell polarity. *Journal of Cell Biology* **207**, 171–179 (2014).
82. Butler, M. T. & Wallingford, J. B. Planar cell polarity in development and disease. *Nat Rev Mol Cell Biol* **18**, 375–388 (2017).
83. Hayes, M., Naito, M., Daulat, A., Angers, S. & Ciruna, B. Ptk7 promotes non-canonical Wnt/PCP-mediated morphogenesis and inhibits Wnt/β-catenin-dependent cell fate decisions during vertebrate development. *Development* **140**, 1807–1818 (2013).
84. Minami, Y., Oishi, I., Endo, M. & Nishita, M. Ror-family receptor tyrosine kinases in noncanonical Wnt signaling: Their implications in developmental morphogenesis and human diseases. *Developmental Dynamics* **239**, 1–15 (2010).
85. Courbard, J.-R., Djiane, A., Wu, J. & Mlodzik, M. The apical/basal-polarity determinant Scribble cooperates with the PCP core factor Stbm/Vang and functions as one of its effectors. *Dev Biol* **333**, 67–77 (2009).
86. Sutherland, A., Keller, R. & Lesko, A. Convergent extension in mammalian morphogenesis. *Semin Cell Dev Biol* **100**, 199–211 (2020).
87. Shwartz, Y., Farkas, Z., Stern, T., Aszódi, A. & Zelzer, E. Muscle contraction controls skeletal morphogenesis through regulation of chondrocyte convergent extension. *Dev Biol* **370**, 154–163 (2012).
88. Yamada, M. *et al*. Ror2 is required for midgut elongation during mouse development. *Developmental Dynamics* **239**, 941–953 (2010).
89. Pataki, C. A., Couchman, J. R. & Brábek, J. Wnt Signaling Cascades and the Roles of Syndecan Proteoglycans. *Journal of Histochemistry & Cytochemistry* **63**, 465–480 (2015).
90. Huang, S., Hirota, Y. & Sawamoto, K. Various facets of vertebrate cilia: motility, signaling, and role in adult neurogenesis. *Proceedings of the Japan Academy, Series B* **85**, 324–336 (2009).
91. Robinson, A. *et al*. Mutations in the planar cell polarity genes CELSR1 and SCRIB are associated with the severe neural tube defect craniorachischisis. *Hum Mutat* **33**, 440–447 (2012).

92. Harris, M. J. & Juriloff, D. M. Mouse mutants with neural tube closure defects and their role in understanding human neural tube defects. *Birth Defects Res A Clin Mol Teratol* **79**, 187–210 (2007).
93. Yates, L. L. *et al.* The planar cell polarity gene Vangl2 is required for mammalian kidney-branching morphogenesis and glomerular maturation. *Hum Mol Genet* **19**, 4663–4676 (2010).
94. Yates, L. L. *et al.* The PCP genes Celsr1 and Vangl2 are required for normal lung branching morphogenesis. *Hum Mol Genet* **19**, 2251–2267 (2010).
95. Brzóska, H. Ł. *et al.* Planar cell polarity genes Celsr1 and Vangl2 are necessary for kidney growth, differentiation, and rostrocaudal patterning. *Kidney Int* **90**, 1274–1284 (2016).
96. Yamaguchi, T. P., Bradley, A., McMahon, A. P. & Jones, S. A Wnt5a pathway underlies outgrowth of multiple structures in the vertebrate embryo. *Development* **126**, 1211–1223 (1999).
97. Li, C., Xiao, J., Hormi, K., Borok, Z. & Minoo, P. Wnt5a Participates in Distal Lung Morphogenesis. *Dev Biol* **248**, 68–81 (2002).
98. Cervantes, S., Yamaguchi, T. P. & Hebrok, M. Wnt5a is essential for intestinal elongation in mice. *Dev Biol* **326**, 285–294 (2009).
99. Nomi, M. *et al.* Loss of mRor1 Enhances the Heart and Skeletal Abnormalities in mRor2 -Deficient Mice: Redundant and Pleiotropic Functions of mRor1 and mRor2 Receptor Tyrosine Kinases. *Mol Cell Biol* **21**, 8329–8335 (2001).
100. Schwabe, G. C. *et al.* Ror2 knockout mouse as a model for the developmental pathology of autosomal recessive Robinow syndrome. *Developmental Dynamics* **229**, 400–410 (2004).
101. Irigoin, F. & L. Badano, J. Keeping the Balance Between Proliferation and Differentiation:The Primary Cilium. *Curr Genomics* **12**, 285–297 (2011).
102. Garcia, G. & Reiter, J. F. A primer on the mouse basal body. *Cilia* **5**, 17 (2016).
103. Kumar, D. & Reiter, J. How the centriole builds its cilium: of mothers, daughters, and the acquisition of appendages. *Curr Opin Struct Biol* **66**, 41–48 (2021).
104. Anvarian, Z., Mykytyn, K., Mukhopadhyay, S., Pedersen, L. B. & Christensen, S. T. Cellular signalling by primary cilia in development, organ function and disease. *Nat Rev Nephrol* **15**, 199–219 (2019).
105. Mill, P., Christensen, S. T. & Pedersen, L. B. Primary cilia as dynamic and diverse signalling hubs in development and disease. *Nat Rev Genet* **24**, 421–441 (2023).
106. Prosser, S. L. & Pelletier, L. Centriolar satellite biogenesis and function in vertebrate cells. *J Cell Sci* **133**, (2020).
107. Quarantotti, V. *et al.* Centriolar satellites are acentriolar assemblies of centrosomal proteins. *EMBO J* **38**, (2019).
108. Reiter, J. F. & Leroux, M. R. Genes and molecular pathways underpinning ciliopathies. *Nat Rev Mol Cell Biol* **18**, 533–547 (2017).
109. Simons, M. *et al.* Inversin, the gene product mutated in nephronophthisis type II, functions as a molecular switch between Wnt signaling pathways. *Nat Genet* **37**, 537–543 (2005).
110. Burcklé, C. *et al.* Control of the Wnt pathways by nephrocystin-4 is required for morphogenesis of the zebrafish pronephros. *Hum Mol Genet* **20**, 2611–2627 (2011).
111. Gerdes, J. M. *et al.* Disruption of the basal body compromises proteasomal function and perturbs intracellular Wnt response. *Nat Genet* **39**, 1350–1360 (2007).
112. Mahuzier, A. *et al.* Dishevelled stabilization by the ciliopathy protein Rpgrip1l is essential for planar cell polarity. *Journal of Cell Biology* **198**, 927–940 (2012).

113. Wallingford, J. B. & Mitchell, B. Strange as it may seem: the many links between Wnt signaling, planar cell polarity, and cilia: Figure 1. *Genes Dev* **25**, 201–213 (2011).
114. Corbit, K. C. *et al*. Kif3a constrains β-catenin-dependent Wnt signalling through dual ciliary and non-ciliary mechanisms. *Nat Cell Biol* **10**, 70–76 (2008).
115. Jones, C. *et al*. Ciliary proteins link basal body polarization to planar cell polarity regulation. *Nat Genet* **40**, 69–77 (2008).
116. Ross, A. J. *et al*. Disruption of Bardet-Biedl syndrome ciliary proteins perturbs planar cell polarity in vertebrates. *Nat Genet* **37**, 1135–1140 (2005).
117. Boutin, C. *et al*. A dual role for planar cell polarity genes in ciliated cells. *Proceedings of the National Academy of Sciences* **111**, (2014).
118. Park, T. J., Mitchell, B. J., Abitua, P. B., Kintner, C. & Wallingford, J. B. Dishevelled controls apical docking and planar polarization of basal bodies in ciliated epithelial cells. *Nat Genet* **40**, 871–879 (2008).
119. Nader, M. *et al*. Tail-anchored membrane protein SLMAP is a novel regulator of cardiac function at the sarcoplasmic reticulum. *American Journal of Physiology-Heart and Circulatory Physiology* **302**, H1138–H1145 (2012).
120. Mlynarova, J. *et al*. SLMAP3 isoform modulates cardiac gene expression and function. *PLoS One* **14**, (2019).
121. Nader, M. *et al*. SLMAP-3 is downregulated in human dilated ventricles and its overexpression promotes cardiomyocyte response to adrenergic stimuli by increasing intracellular calcium. *Can J Physiol Pharmacol* **97**, 623–630 (2019).
122. Ishikawa, T. *et al*. A Novel Disease Gene for Brugada Syndrome. *Circ Arrhythm Electrophysiol* **5**, 1098–1107 (2012).
123. Stanley, E. G. *et al*. Efficient Cre-mediated deletion in cardiac progenitor cells conferred by a 3'UTR-ires-Cre allele of the homeobox gene Nkx2-5. *Int J Dev Biol* **46**, 431–9 (2002).
124. Ensembl. Human SLMAP Transcripts. https://grch37.ensembl.org/Homo_sapiens/Transcript/Exons?db=core;g=ENSG00000163681;r=3:57741177-57914895;t=ENST00000295951.
125. Lee, S.-W. *et al*. AKAP6 inhibition impairs myoblast differentiation and muscle regeneration: Positive loop between AKAP6 and myogenin. *Sci Rep* **5**, 16523 (2015).
126. Metzger, T. *et al*. MAP and kinesin-dependent nuclear positioning is required for skeletal muscle function. *Nature* **484**, 120–124 (2012).
127. Wang, Z. *et al*. Kif5b controls the localization of myofibril components for their assembly and linkage to the myotendinous junctions. *Development* **140**, 617–626 (2013).
128. Rehmani, T., Dias, A. P., Salih, M. & Tuana, B. SLMAP3 is essential for neurulation through mechanisms involving cytoskeletal elements, ABP, and PCP. *Life Sci Alliance* **7**, e202302545 (2024).
129. Vidak, S. & Foisner, R. Molecular insights into the premature aging disease progeria. *Histochem Cell Biol* **145**, 401–417 (2016).
130. Barateau, A. *et al*. A Novel Lamin A Mutant Responsible for Congenital Muscular Dystrophy Causes Distinct Abnormalities of the Cell Nucleus. *PLoS One* **12**, e0169189 (2017).
131. Favreau, C., Higuet, D., Courvalin, J.-C. & Buendia, B. Expression of a Mutant Lamin A That Causes Emery-Dreifuss Muscular Dystrophy Inhibits In Vitro Differentiation of C2C12 Myoblasts. *Mol Cell Biol* **24**, 1481–1492 (2004).

132. Frock, R. L. *et al*. Lamin A/C and emerin are critical for skeletal muscle satellite cell differentiation. *Genes Dev* **20**, 486–500 (2006).
133. Markiewicz, E., Ledran, M. & Hutchison, C. J. Remodelling of the nuclear lamina and nucleoskeleton is required for skeletal muscle differentiation in vitro. *J Cell Sci* **118**, 409–420 (2005).
134. Bertrand, A. T. *et al*. Lamin A/C Assembly Defects in LMNA-Congenital Muscular Dystrophy Is Responsible for the Increased Severity of the Disease Compared with Emery–Dreifuss Muscular Dystrophy. *Cells* **9**, 844 (2020).
135. Kandert, S., Wehnert, M., Müller, C. R., Buendia, B. & Dabauvalle, M.-C. Impaired nuclear functions lead to increased senescence and inefficient differentiation in human myoblasts with a dominant p.R545C mutation in the LMNA gene. *Eur J Cell Biol* **88**, 593–608 (2009).
136. Barton, L. J., Soshnev, A. A. & Geyer, P. K. Networking in the nucleus: a spotlight on LEM-domain proteins. *Curr Opin Cell Biol* **34**, 1–8 (2015).
137. Patton, M. A. Robinow syndrome. *J Med Genet* **39**, 305–310 (2002).
138. Robinow, M. A Newly Recognized Dwarfing Syndrome. *Arch Pediatr Adolesc Med* **117**, 645 (1969).
139. Etheridge, S. L. *et al*. Murine Dishevelled 3 Functions in Redundant Pathways with Dishevelled 1 and 2 in Normal Cardiac Outflow Tract, Cochlea, and Neural Tube Development. *PLoS Genet* **4**, e1000259 (2008).
140. Fehon, R. G., McClatchey, A. I. & Bretscher, A. Organizing the cell cortex: the role of ERM proteins. *Nat Rev Mol Cell Biol* **11**, 276–287 (2010).
141. Baumgartner, M. *et al*. The Nck-interacting kinase phosphorylates ERM proteins for formation of lamellipodium by growth factors. *Proceedings of the National Academy of Sciences* **103**, 13391–13396 (2006).
142. Fidalgo, M. *et al*. Adaptor Protein Cerebral Cavernous Malformation 3 (CCM3) Mediates Phosphorylation of the Cytoskeletal Proteins Ezrin/Radixin/Moesin by Mammalian Ste20-4 to Protect Cells from Oxidative Stress. *Journal of Biological Chemistry* **287**, 11556–11565 (2012).
143. Vitorino, P. *et al*. MAP4K4 regulates integrin-FERM binding to control endothelial cell motility. *Nature* **519**, 425–430 (2015).
144. Yue, J. *et al*. Microtubules Regulate Focal Adhesion Dynamics through MAP4K4. *Dev Cell* **31**, 572–585 (2014).
145. Wang, S. *et al*. CCM3 is a gatekeeper in focal adhesions regulating mechanotransduction and YAP/TAZ signalling. *Nat Cell Biol* **23**, 758–770 (2021).
146. Bazzi, H., Soroka, E., Alcorn, H. L., Anderson, K. V. & Hogan, B. L. M. STRIP1, a core component of STRIPAK complexes, is essential for normal mesoderm migration in the mouse embryo. *Proc Natl Acad Sci U S A* **114**, E10928–E10936 (2017).
147. Streets, A. J., Prosseda, P. P. & Ong, A. C. M. Polycystin-1 regulates ARHGAP35-dependent centrosomal RhoA activation and ROCK signaling. *JCI Insight* **5**, (2020).
148. Veland, I. R. *et al*. Inversin/Nephrocystin-2 Is Required for Fibroblast Polarity and Directional Cell Migration. *PLoS One* **8**, e60193 (2013).
149. Farina, F. *et al*. The centrosome is an actin-organizing centre. *Nat Cell Biol* **18**, 65–75 (2016).
150. Upadhyay, R. *et al*. Role of SLMAP genetic variants in susceptibility of diabetes and diabetic retinopathy in Qatari population. *J Transl Med* **13**, (2015).

151. Pearce, E. *et al*. Intraretinal Microvascular Abnormalities and Venous Beading Have Different Genetic Profiles in Caucasian Patients with Non-Proliferative Diabetic Retinopathy. *Vision* **7**, 18 (2023).
152. Chen, X. & Ding, H. Increased Expression of the Tail-Anchored Membrane Protein SLMAP in Adipose Tissue from Type 2 Tally Ho Diabetic Mice. *Exp Diabetes Res* **2011**, 1–10 (2011).
153. Fang, P. *et al*. Glucagon-Like Peptide-1 Receptor Agonist Protects Against Diabetic Cardiomyopathy by Modulating microRNA-29b-3p/SLMAP. *Drug Des Devel Ther* **17**, 791–806 (2023).
154. Pagan, C. *et al*. Targeting SLMAP-ALK-a novel gene fusion in lung adenocarcinoma. *Cold Spring Harb Mol Case Stud* **5**, (2019).
155. Kongpetch, S. *et al*. Lack of Targetable FGFR2 Fusions in Endemic Fluke-Associated Cholangiocarcinoma. *JCO Glob Oncol* **6**, 628–638 (2020).
156. Park, S. *et al*. Characteristics and Outcome of ROS1-Positive Non–Small Cell Lung Cancer Patients in Routine Clinical Practice. *Journal of Thoracic Oncology* **13**, 1373–1382 (2018).
157. Qaddoumi, I. *et al*. Genetic alterations in uncommon low-grade neuroepithelial tumors: BRAF, FGFR1, and MYB mutations occur at high frequency and align with morphology. *Acta Neuropathol* **131**, 833–845 (2016).
158. Bhati, R. *et al*. Molecular characterization of human breast tumor vascular cells. *American Journal of Pathology* **172**, 1381–1390 (2008).
159. Le Faouder, J. *et al*. Proteomic Landscape of Cholangiocarcinomas Reveals Three Different Subgroups According to Their Localization and the Aspect of Non-Tumor Liver. *Proteomics Clin Appl* **13**, (2019).
160. Nasarre, P., Bonilla, I. V., Metcalf, J. S., Hilliard, E. G. & Klauber-Demore, N. TRAF3-interacting protein 3, a new oncotarget, promotes tumor growth in melanoma. *Melanoma Res* **28**, 185–194 (2018).
161. Xie, R., Wen, F. & Qin, Y. The Dysregulation and Prognostic Analysis of STRIPAK Complex Across Cancers. *Front Cell Dev Biol* **8**, (2020).
162. Lin, Q. *et al*. TRAF3IP3 promotes glioma progression through the ERK signaling pathway. *Front Oncol* **12**, (2022).
163. Yang, G., Tang, S., Zhang, J. & Qin, L. High TRAF3IP3 Level Predicts Poor Prognosis of Patients with Gliomas. *World Neurosurg* **148**, e436–e449 (2021).
164. Liu, H. *et al*. Characterization of candidate factors associated with the metastasis and progression of high-grade serous ovarian cancer. *Chin Med J (Engl)* **136**, 2974–2982 (2023).
165. Pommert, L. *et al*. Novel germline TRAF3IP3 mutation in a dyad with familial acute B lymphoblastic leukemia. *Cancer Rep* **4**, (2021).
166. Zhang, X.-M. *et al*. Expression of tumor related gene NAG6 in gastric cancer and restriction fragment length polymorphism analysis. *World J Gastroenterol* **10**, 1361 (2004).
167. Xie, F. *et al*. An 8-gene signature predicts the prognosis of cervical cancer following radiotherapy. *Mol Med Rep* **20**, 2990–3002 (2019).
168. Nylund, P. *et al*. PVT1 interacts with polycomb repressive complex 2 to suppress genomic regions with pro-apoptotic and tumour suppressor functions in multiple myeloma. *Haematologica* **109**, 567–577 (2024).

169. Lu, J. & Chen, Q. Transcriptome-based identification of molecular markers related to the development and prognosis of Colon cancer. *Nucleosides Nucleotides Nucleic Acids* **40**, 1114–1124 (2021).
170. Prévilon, M. *et al.* Comparative differential proteomic profiles of nonfailing and failing hearts after in vivo thoracic aortic constriction in mice overexpressing FKBP12.6. *Physiol Rep* **1**, (2013).
171. Deng, M. *et al.* TRAF3IP3 negatively regulates cytosolic RNA induced anti-viral signaling by promoting TBK1 K48 ubiquitination. *Nat Commun* **11**, 2193 (2020).
172. Zhu, W. *et al.* TRAF3IP3 mediates the recruitment of TRAF3 to MAVS for antiviral innate immunity. *EMBO J* **38**, (2019).
173. Li, Y. *et al.* TRAF3-interacting JNK-activating modulator promotes inflammation by stimulating translocation of Toll-like receptor 4 to lipid rafts. *Journal of Biological Chemistry* **294**, 2744–2756 (2019).
174. An, L. *et al.* Combinatorial targeting of Hippo-STRIPAK and PARP elicits synthetic lethality in gastrointestinal cancers. *Journal of Clinical Investigation* **132**, (2022).
175. Jeong, B. C. *et al.* Cryo-EM structure of the Hippo signaling integrator human STRIPAK. *Nat Struct Mol Biol* **28**, 290–299 (2021).